Mechanism of SspH1: A Bacterial Effector Ubiquitin Ligase Hijacks the Eukaryotic Ubiquitylation Pathway

Matthew J. Cook

A dissertation

submitted in partial fulfillment of the

requirements for the degree of

Doctor of Philosophy

University of Washington

2018

Reading Committee:

Peter S Brzovic, Chair

Suzanne Hoppins

Ning Zheng

Program Authorized to Offer Degree:

Biochemistry

University of Washington

Abstract

Mechanism of SspH1: A Bacterial Effector Ubiquitin Ligase

Hijacks the Eukaryotic Ubiquitylation Pathway

Matthew J. Cook

Chair of the Supervisory Committee:

Peter S Brzovic

Department of Biochemistry

Bacterial effector proteins promote the pathogenicity of bacteria by interacting with host cell proteins and modulating signaling pathways in the host cell. Some bacterial effectors hijack the eukaryotic ubiquitylation pathway to promote pathogenicity, despite the absence of the pathway in prokaryotes. One family of bacterial effectors, the IpaH-SspH family of E3 ligases, are unrelated in sequence or structure to eukaryotic E3s. This work elucidates key aspects in the structure and mechanism of one member of the IpaH-SspH family from *Salmonella typhimurium*, SspH1. Biophysical and biochemical methods were used to examine the structure of SspH1 in solution and the interactions between SspH1 and components of the eukaryotic ubiquitylation pathway, with an emphasis on the mechanisms of ubiquitin transfer from the E2 active site to the SspH1 active site, and from the SspH1 active site to substrate. Important results of this work include 1) a

reanalysis of existing crystal structures of IpaH-SspH1 E3 domains leading to a new way of characterizing the structural organization of the SspH1 E3 domain, revealing two independent subdomains. 2) Identification of the E2~Ub conjugate binding region and how E2~Ub engages SspH1 in a productive complex. 3) Generation of a chemically stable mimic of SspH1~Ub allowing for structural characterization of the second stage of Ub transfer, from SspH1~Ub to substrate. 4) Development of a model in which E2~Ub not only is involved in the transfer of Ub to the SspH1 active site, but also drives the transfer of Ub from the SspH1 active site to substrate.

Table of Contents

List of Figures

List of Tables

Acknowledgments

I would like to thank my mentors, Peter S. Brzovic and Rachel E. Klevit for allowing me to perform research in their lab, and for their invaluable support and expertise, as well as all of the other members of the lab for advice and helpful discussions. I would also like to thank Miklos Guttman in the Department of Medicinal Chemistry at the University of Washington for his generous help in performing HDX-MS and SAXS experiments. Finally, I would like to thank the administrators in the Department of Biochemistry, especially graduate program coordinator Erin Kirschner, for their guidance and support. My research and training was supported with funding from the Hurd Fellowship, Schultz travel fellowship, and the Molecular Biophysics Training Grant (T32GM826827).

Introduction

Bacterial Effector Proteins and Pathogenesis

To survive and replicate within a host cell, bacterial pathogens must evade or prevent innate immune responses and redirect cellular resources for their own use. Pathogenic bacteria have evolved many strategies to achieve the goals of survival and replication in a hostile environment, with one of the most important being the evolution of various types of secretion systems used to introduce effector proteins directly into host cells. Gram-negative pathogens such as *Salmonella* and *Shigella* utilize a Type III Secretion System (T3SS) to introduce a suite of bacterial effector proteins directly into the cytosol of the target cell. The T3SS is a large, needle-like macromolecular complex that forms a channel between the bacterium and the cytosol of a neighboring cell, allowing the bacterium to secrete a variety of different effector proteins to effect changes in the host favorable for pathogenesis. Different *bacterial effector proteins* serve numerous functions necessary for pathogenesis including facilitating entry of a bacterium into the host cell, dampening the host innate immune response, and generating an environmental niche inside the host favorable for survival and replication of the bacterium [(1)]. For enteropathogenic gram-negative bacteria such as *Salmonella* or *Shigella*, the target cells are often human intestinal epithelial cells or macrophages.

When a *Salmonella* or *Shigella* bacterium initially encounters the outer membrane of a host cell, the first wave of bacterial effector proteins are introduced, targeting the host actin cytoskeleton to induce membrane ruffling in which the invading bacterium enters the cell via micropinocytosis. Encapsulated within a phagocytic vesicle, the bacterium must now prevent fusion with the lysosome to avoid intracellular digestion. *Shigella* solves this problem by escaping

the phagosome into the host cytoplasm. In contrast, *Salmonella* reshapes the phagosome and host cytoskeleton into a different cellular compartment called the *Salmonella*-containing vacuole (SCV). SCVs are networked, tubular membrane-enclosed structures that isolate *Salmonella* from the cytoplasm of the host cell.

To effect these changes in the host environment, *Salmonella* and *Shigella* release as many as 40-60 different types of effector proteins via the T3SS. In many cases, a T3SS-secreted protein contains an N-terminal peptide motif that directs the protein to the T3SS apparatus. In other cases, specific bacterial chaperones deliver the effector protein to the T3SS for secretion. Upon engaging the effector protein, an ATPase that is part of the T3SS unfolds the protein and threads it into the pore of the secretion system. The protein is pumped through the pore using ATP until it exits the T3SS, where it refolds and interacts with host proteins. *Salmonella* secretes effector proteins via the T3SS both before and after entry into the host cell. Many secreted bacterial effectors target eukaryotic signaling systems such as the NF-κB inflammation pathway, endocytic trafficking, and cytoskeleton regulation. To accomplish this, effectors can function as kinases, phosphatases or proteases that target specific host proteins. Interestingly, a variety of bacterial effectors secreted by the T3SS have been shown to interact with and exploit the eukaryotic ubiquitin-proteasome system, despite the absence of these pathways in prokaryotes [2, 3, 4]. Though prokaryotes lack the ubiquitin-proteasome system, some species of pathogenic bacteria have evolved proteins that utilize the system in eukaryotic cells to effect cellular changes that promote pathogenicity. A major goal of this research is to understand the molecular details of one of the mechanisms in which pathogenic bacteria hijack eukaryotic ubiquitylation pathways.

Ubiquitylation

Ubiquitylation is a eukaryotic post-translational modification in which the small, 76-residue protein ubiquitin (Ub) is covalently attached to a protein. Like phosphorylation, ubiquitylation enables diverse and reversible regulation of nearly every eukaryotic signaling pathway through the modification of their constituent proteins. Unlike phosphorylation, which is performed by kinases and removed by phosphatases, ubiquitin is added to a protein via the successive actions of three classes of enzymes (**Fig 1**): E1 ubiquitin activating enzymes, E2 ubiquitin conjugating enzymes, and E3 ubiquitin ligases [(5)]. A forth class of enzyme, deubiquitylases (DUBs), catalyze the removal of Ub modifications. Covalent modification of a target protein by Ub involves the synthesis of a covalent linkage between the C-terminal carboxyl group of Ub and (most often) the primary amino group of a lysine side chain or polypeptide N-terminus. Modification of a protein by a single Ub molecule, *monoubiquitylation*, can alter the tertiary or quaternary structure of the modified protein due to the presence of the new molecular surface provided by Ub. This, in turn, can affect protein activity, function, or cellular localization. Proteins may also be *multi-monoubiquitylated* (monoubiquitylated at different positions simultaneously) which may further change a protein's function or localization. Ub itself contains seven lysine residues and an N-terminus that may also serve as targets for ubiquitylation. When a Ub molecule on a monoubiquitylated or multi-monoubiquitylated protein is a target for ubiquitylation, poly-Ubiquitin (poly-Ub) chains are formed on the modified protein. *Poly-Ubiquitylation* serves a variety of different functions depending on the type of linkage between individual Ub molecules in the poly-Ub chain. Some well-characterized poly-Ub chains include those formed through Ub lysine residue 11 (K11 chains), residue 48 (K48 chains), or residue 63 (K63 chains) [(6)]. K48 and K11 chains are recognized by the 26S proteasome and provide a signal

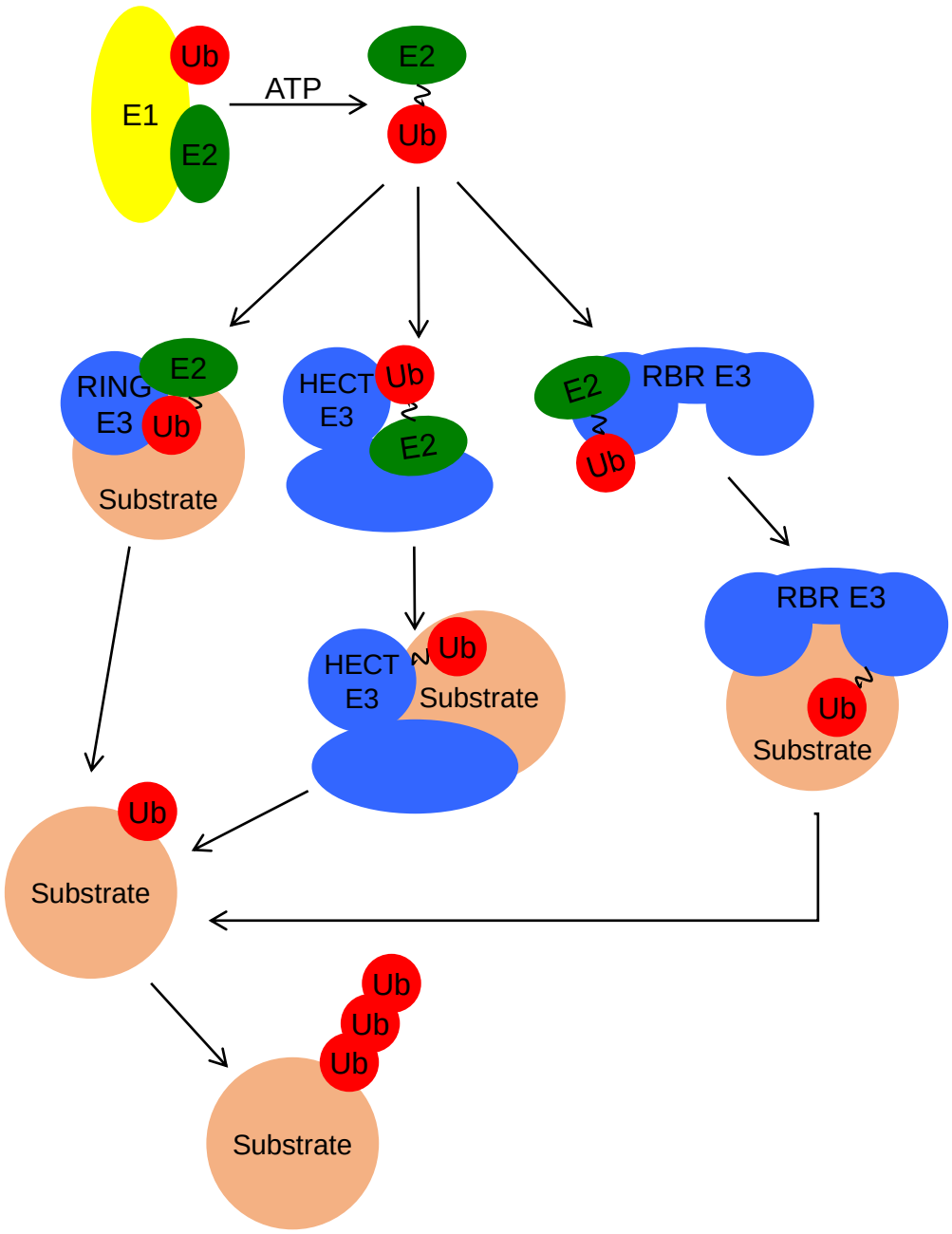

Figure 1. Ubiquitin (Ub) modification is achieved through the successive actions of three classes of enzymes: ubiquitin activating enzyme (E1), ubiquitin conjugating enzyme (E2), and ubiquitin ligase (E3). There are three classes of eukaryotic E3: RINGs, which bind E2~Ub in a conformation that promotes aminolysis to a substrate lysine, HECTs, which bind E2~Ub on the C-lobe in a conformation that promotes transthiolation to the active site Cys on the N-lobe, and RBRs, which bind E2~Ub on a RING domain in a conformation that promotes transthiolation to the active site Cys on a separate pseudo-RING domain. HECTs and RBRs ubiquitylate substrate via an obligate E3~Ub intermediate. Successive rounds of ubiquitylation create polyubiquitin chains on a substrate protein.

for the modified protein to be degraded [7]. K63 chains can serve as scaffolds that bring together signaling proteins that activate DNA repair or NF-κB inflammatory pathways [7]. The functions of other poly-Ub chain architectures, including branched or mixed-linkage chains, are not well understood. The diversity in morphologies of possible poly-Ub chains and the high degree to which their formation is regulated is reflected by the large number of ubiquitylation enzymes encoded in the human genome. For humans, 2 E1s, ~40 E2s, > 600 E3s, and ~100 DUBs are encoded in the genome [8]. For comparison, ~500 kinases and ~200 phosphatases are encoded in the human genome [9].

Activation of Ub by E1

Since the process of ubiquitylation results in the energetically unfavorable formation of an isopeptide bond between the C-terminal carboxyl group of Ub and another protein, the first step of ubiquitylation is to chemically activate Ub to bridge the activation energy gap. The first step of ubiquitylation is activation of the C-terminus of Ub in an ATP-dependent mechanism by an E1 ubiquitin activating enzyme. First, Ub, ATP, and a Mg^{2+} ion bind E1, and E1 catalyzes acyl adenylation of the C-terminal carboxylate group of Ub with a release of pyrophosphate. An E1 active site cysteine then nucleophilically attacks the adenylated C-terminus of the Ub molecule in an acyl substitution reaction, resulting in formation of a thioester bond between the sulfhydryl group of the active site cysteine and the C-terminal carboxylate group of Ub with release of AMP. Two functional E1 genes for Ub are encoded in the human genome. Other ubiquitin-like modifiers, such as SUMO, NEDD8, or ISG15 utilize different E1s.

Transfer of Ub from E1 to E2

After activation, the E1 holds Ub at its active site in a complex called the E1-ubiquitin conjugate, or E1~Ub (in this case, use of '~' refers to a reactive thioester bond). The next step is transfer of Ub from the E1~Ub to an active site cysteine on an E2 ubiquitin conjugating enzyme (**Fig 1**). There are about 40 E2s encoded by the human genome, and all share a conserved ubiquitin-conjugating (Ubc) domain that is critical for activity [(10)]. The Ubc domain contains the active site cysteine and is the domain that mediates transfer of Ub from E1~Ub. Ub transfer proceeds through an energetically neutral transthiolation reaction in which the Ubc domain of the E2 binds E1~Ub and induces a conformational change that allows the E2 active site cysteine to nucleophilically attack the E1~Ub thioester bond, resulting in transfer of the C-terminal carboxylate group of Ub from the sulfhydryl group of the E1 active site cysteine to that of the E2 active site cysteine. The resulting species is called the E2-ubiquitin conjugate, or E2~Ub. The E2~Ub conjugate may now pair with an E3 to mediate ubiquitin transfer to a substrate protein.

Families of E2s and their activity

The diversity provided by the number of E2s encoded by the human genome enables a cell to fine-tune regulation of ubiquitylation [(5)]. E2s vary considerably in their reactivity: they may be active only with certain classes of E3s or specialized for catalyzing monoubiquitylation or specific types of poly-Ubiquitin chain architectures. Structurally, E2s like Ube2D3 may consist of only a topologically conserved Ubc domain as shown in **Fig 2A** or may possess N- and/or C-terminal extensions that modulate reactivity or enable protein-protein interactions. Though often disordered, the sequences of these extensions vary considerably in sequence and length and may also include structured domains.

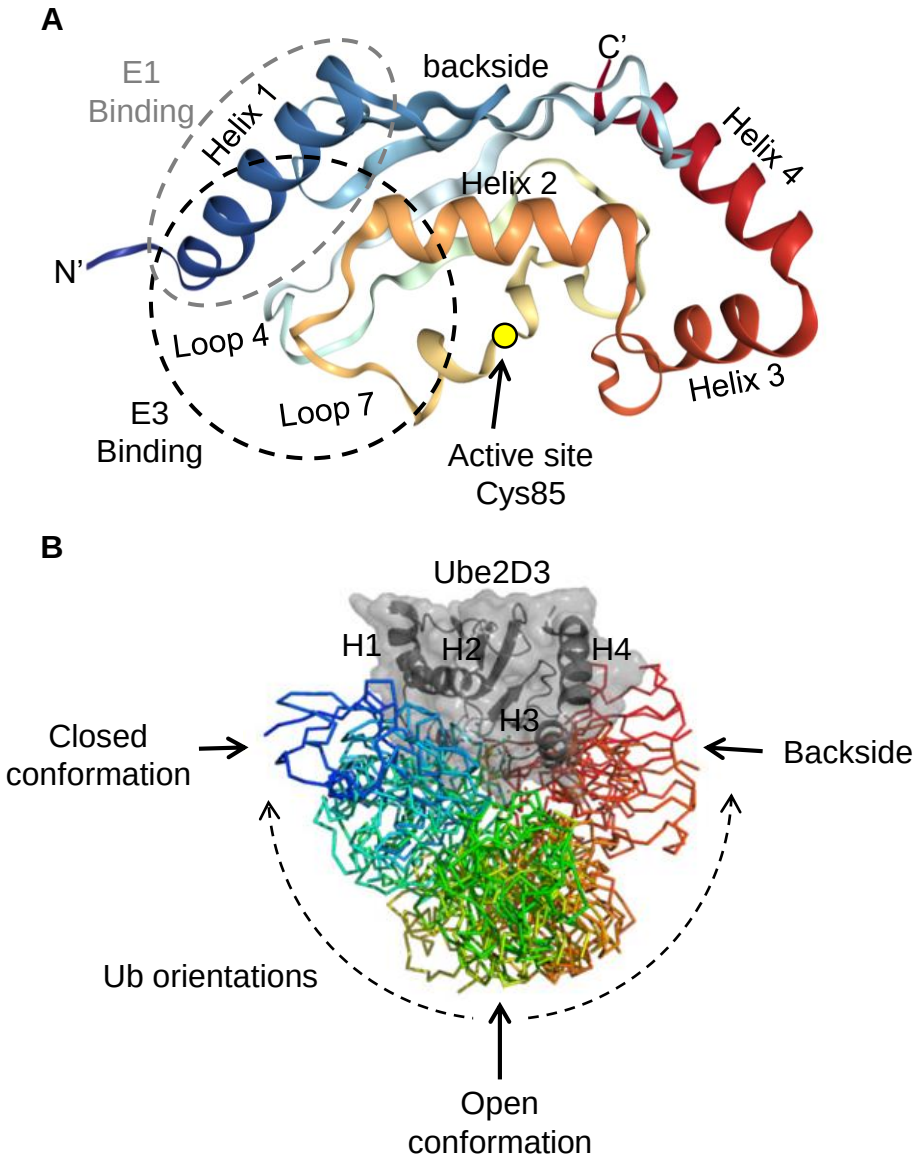

Figure 2. (A) Structure of Ube2D3 (PDB 1X23) colored Blue (N-term) to Red (C-term) . Important features include: the E1 and E3 binding surfaces, the hydrophobic "backside" beta-sheet surface, and the active site Cys85 (yellow sphere) that forms a thioester bond with the ubiquitin carboxy terminus. Adapted from Figure 2 in Wenzel *et al.* (2011). **(B)** Conformations between the E2 and Ub subunits in Ube2D3~Ub modeled from SAXS curves. Ub spends some time loosely bound to helix 2 (the closed conformation) or the backside of the Ube2D3, with most of its time spent in an open conformation. Adapted with permission from Pruneda, J.N., Stoll, K.E., Bolton, L.J., Brzovic, P.S., Klevit, R.E. (2011) Ubiquitin in motion: structural studies of the ubiquitin-conjugating enzyme~ubiquitin conjugate. *Biochemistry*. **50(10)**, 1624-1633. Copyright 2011 American Chemical Society.

Three E2s used in this work, Ube2D3, Ube2E3 and Ube2L3 differ in their structure and reactivity, and their interactions with human E3s have been well-characterized. These E2s have varying biochemical activities with the bacterial proteins studied in this work, and the differences in activity were important to elucidating one of the mechanisms in which pathogenic bacteria hijack the eukaryotic ubiquitylation system. The Ube2D family in humans is known as a promiscuous family of E2s because they can form a diverse set of poly-Ub chain architectures and are catalytically active with most E3s *in vitro,* including members from each class of E3 [11]. Members of the Ube2D family lack extensions, and atomic structures are available of Ube2D members alone or in complex with E3s and/or substrates. The molecular details of Ube2D surfaces involved in protein-protein interactions are well known and are highlighted in **Fig 2A**. Important surfaces include Helix 1, which is involved in E1 and E3 interactions, Loops 4 and 7, which are involved in E3 interactions, the 'backside' β-sheet, which noncovalently binds Ub, and the active site Cys, which forms a thioester intermediate with the C-terminus of Ub [5, 11]. Other than the noncovalent Ub-binding backside, the functions of these structural features are also conserved for other E2s [5].

Members of the Ube2E family possess a Ubc domain highly homologous to that of Ube2D, but additionally possess an unstructured ~60-residue N-terminal extension of unknown function. Ube2E E2s have been shown to specifically catalyze monoubiquitylation with eukaryotic E3s *in vitro* [12]. This catalytic restriction is imparted by the backside of the Ube2E Ubc domain, which does not bind Ub as in the Ube2D family [12]. Ube2L3 is an E2 specialized for transthiolation reactions with E3s harboring an active site cysteine. It consists of a Ubc domain with no extensions but is not highly homologous to that of Ube2D and does not bind Ub through its backside. [5].

Though the topology of the Ubc domain and the regions mediating interactions with E1 and E3 are conserved across the various E2 families, they still possess great diversity in catalytic function.

Transfer of Ub from E2 to Substrate

An E2~Ub pairs with an E3 ubiquitin ligase to transfer Ub to substrate (**Fig 1**). The human genome encodes over 600 E3s, which can be organized into 3 classes based on their structure and mechanism [(10)]. "RING" (*Really Interesting New Gene*) or "U-BOX" E3s bind E2~Ub and a substrate protein and promote the transfer of Ub directly from E2 to substrate [(13)]. RING and U-BOX domains are small (generally < 80 residues) and are structurally homologous to each other, but RINGs coordinate two Zn^{2+} ions to maintain their tertiary structure [(14)]. "HECT" (*Homologous to E6-AP Carboxy-Terminus*) and "RBR" (*RING-Between-RING*) E3s are larger, (~400-500 residues for their catalytic domains) and possess an active site cysteine that is required to form a thioester intermediate with the C-terminus of Ub prior to transfer of Ub to substrate [(15, 16, 17, 18, 19)]. HECT and RBR E3s therefore utilize a 2-step Ub transfer mechanism in which Ub must be transferred to the E3 active site prior to being transferred to substrate, while RING/U-BOX E3s utilize a 1-step Ub transfer mechanism in which Ub is transferred directly from E2 to substrate.

Structural conformations of E2~Ub

Canonical RING/U-BOX type E3s bind E2~Ub and catalyze aminolysis via a conserved RING domain (**Fig 3A**) [(14)]. HECT domains are not homologous to RINGs and the E3 domains of these enzymes consist of an N-terminal lobe which binds E2~Ub and a C-terminal lobe which harbors the active site cysteine (**Fig 3B**) [(17)]. RBR E3s have a catalytic core consisting of an E2~Ub binding domain (RING1), a Ub transfer domain harboring an active site cysteine (RING2), and a

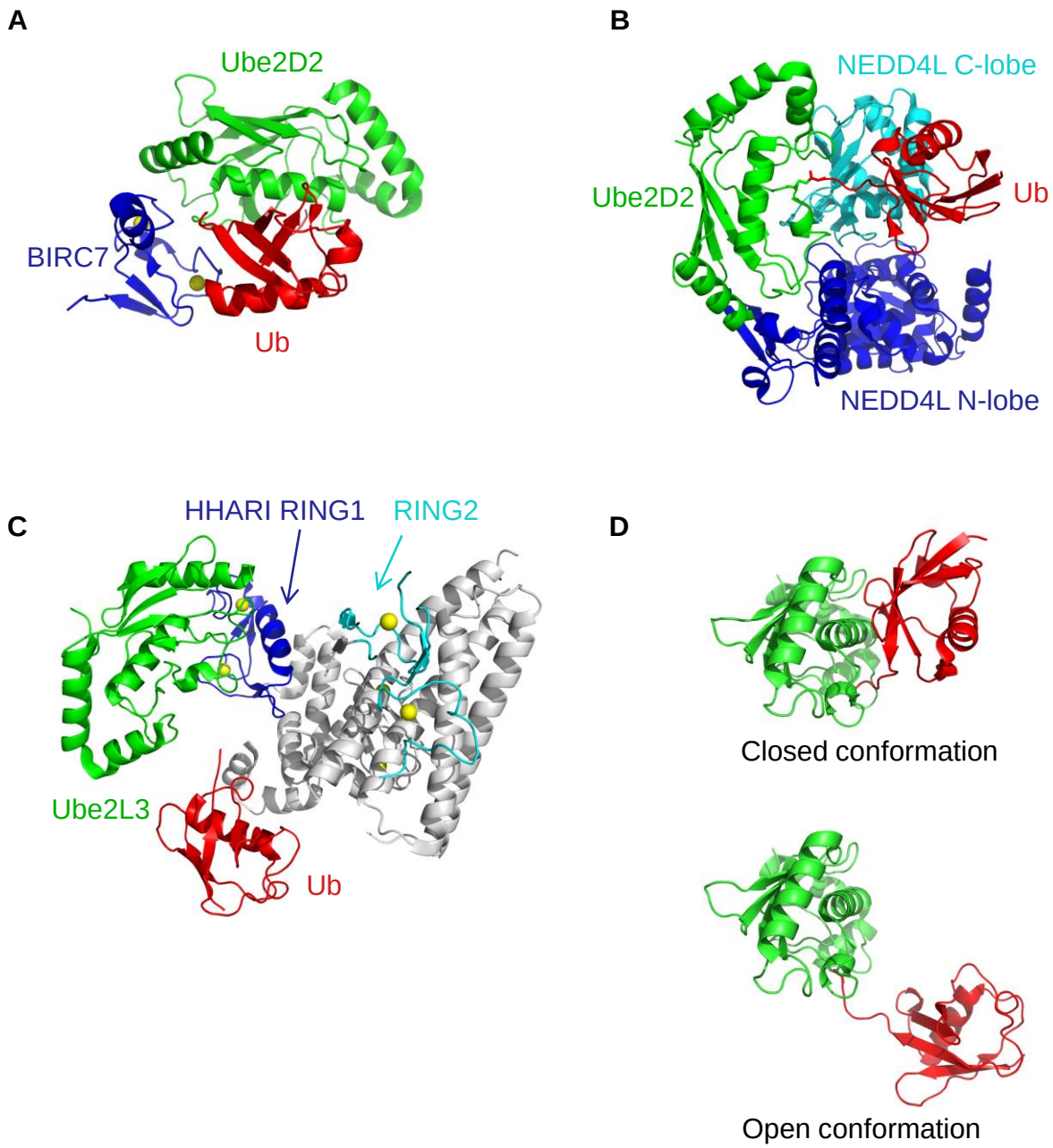

Figure 3. Structures of each class of eukaryotic E3s in complex with E2~Ub: **(A)** RING type E3 BIRC7 bound to Ube2D2~Ub (PDB 4AUQ) **(B)** HECT type E3 NEDD4L bound to Ube2D2~Ub (PDB 3JW0) **(C)** RBR type E3 HHARI bound to UbeL3~Ub (PDB 5UDH). **(D)** The conformation of E2~Ub when bound to an E3 differs depending on the class of E3. RINGs bind E2~Ub in a lysine-reactive closed conformation (top panel), while HECTs and RBRs bind E2~Ub in an open conformation (bottom panel).

linker domain connecting them (**Fig 3C**). The E2~Ub conjugate binding and transfer domains of RBRs are homologous to RING domains [18, 19], but engage E2~Ub in a different conformation than canonical RING domains. For all classes of E3s, the orientation in which the E3 engages an E2~Ub determines the reactivity of the E2~Ub conjugate thioester bond. RING/U-BOX E3s bind E2~Ub in an orientation that promotes aminolysis by a substrate lysine side chain while HECT/RBR E3s bind E2~Ub in an orientation that inhibits aminolysis to promote energetically-neutral transthiolation between cysteine active sites.

The relative orientation of subunits of the E2~Ub conjugate, defined by the torsion angles of residues residing in the C-terminus of Ub and the active site of the E2, are important in determining reactivity. Studies on the conformations of two well-characterized human E2s, Ube2D3 and Ube2L3, have been useful in elucidating the connection between E2~Ub conformations and reactivity. Pruneda *et al*. (2011) showed that, free in solution, E2 and Ub subunits in Ube2D3~Ub adopt an ensemble of conformations. The primary conformation is an 'open' conformation, with little contact between domains other than the thioester bond tethering them together. Other less populated conformations include Ub loosely bound to either helix 2 of the E2 (the 'closed' conformation) or towards the backside beta-sheet region of the E2 near the active site (**Fig 2B,3D**) [20]. Upon binding to a RING/U-BOX type E3, the Ube2D3~Ub conformation is preferentially shifted to the closed conformation, and results in increased lysine reactivity of the E2~Ub conjugate [21, 20]. This closed conformation was confirmed in the structure of the RING E3 Birc7 bound to Ube2D2~Ub (**Fig 3A**) [14].

In contrast, Dove *et al.* (2016) showed that, for Ube2D3~Ub, upon binding to an RBR type E3, the E2~Ub conjugate conformation was preferentially shifted to an "open" conformation in which Ub was neither bound to helix 2 nor the backside of the E2. This conformation was

associated with a decrease in lysine reactivity so as to promote transthiolation of the C-terminus of Ub to the active site cysteine of the RBR [22]. Dove *et al.* (2016, 2017) further showed that, unlike Ube2D3~Ub, free Ube2L3~Ub in solution preferentially adopts a closed-like conformation, though it is not lysine-reactive [22, 23]. However, similarly to Ube2D3~Ub, Ube2L3~Ub adopts an open conformation upon binding to an RBR type E3 (**Fig 3C**) [23]. This open conformation is also observed in structures of Ube2D2~Ub bound to the HECT type E3 NEDD4L (**Fig 3B**), which also promote transthiolation of the C-terminus of Ub to the active site cysteine of the E3 [17]. While the chemical environment of the E2 active site plays a large role in governing the reactivity of the E2, from these studies it is clear the conformation of the E2~Ub conjugate when bound to an E3 is also critical to understanding ubiquitylation mechanisms.

IpaH-SspH Family of Bacterial Effector E3 Ligases

Despite the absence of Ub signaling in prokaryotes, pathogenic bacteria have evolved effector proteins capable of hijacking, exploiting, or disabling host cell Ub signaling pathways. Considering the numerous important roles of Ub signaling pathways in the eukaryotic cell, they present a prime target for manipulation by bacterial effector proteins. Some of these bacterial effectors mimic eukaryotic ubiquitylating enzymes [24, 25, 26]. NleL in *E. coli* [27] and SopA in *Salmonella typhimurium* [28] mimic HECT-type E3 ligases. NleG in *E. coli* [29], LubX in *Legionella pneumophilia* [30], and AvrPtoB in *Pseudomonas syringae* [31] mimic RING/U-BOX-type E3 ligases. Some bacterial effectors can post-translationally modify host ubiquitylating enzymes. OspI in *Shigella* [32] deamidates glutamine side chains on the E2 Ubc13, and the Cif family of effectors in *E. coli* [33] deamidate glutamine side chains on Ub and NEDD8. Remarkably, some

genera of bacteria have also evolved E3s that are completely unrelated to their eukaryotic counterparts in sequence or structure.

Members of the SspH and IpaH families of T3SS-secreted bacterial effector E3s, whose ubiquitin ligase activity was discovered by Rohde *et al* in 2007, define a new class of ubiquitin ligases that function in a eukaryotic host cell. These enzymes form an obligate thioester with the C-terminus of Ub via an active site cysteine, which classifies SspH/IpaH E3s as E3s with a HECT-type mechanism [34, 35, 36, 37]. SspH and IpaH enzymes are found in *Salmonella* and *Shigella*, respectively, with other members of the SspH/IpaH family widely distributed in gram-negative pathogens that utilize a T3SS. Members of this family have in the past been called "Novel E3 Ligases" (NELs) or "Bacterial E3 Ligases" (BELs), however other families of unrelated E3s have also previously been given the NEL nomenclature, and some bacterial species secrete E3 ligases that are not related to SspH or IpaH. Here, the family will be referred to as the IpaH-SspH family.

Although members of the IpaH-SspH family exist in other bacterial genera, the best characterized in terms of structure, biochemical activity, or cellular effects are the three SspH family members in *Salmonella* (SspH1, SspH2, SlrP) and the ~10 members of the IpaH family in *Shigella* (including IpaH3, IpaH4, IpaH1.4, IpaH4.5, IpaH7.8, and IpaH9.8). They all have a similar shared domain architecture consisting of three regions (**Fig 4A**): **1)** A highly variable ~100-150 residue N-terminal region required for secretion by the T3SS [38, 39]. **2)** A ~250-300 residue leucine rich repeat (LRR) domain that mediates substrate binding. **3)** A highly conserved ~300 residue catalytic E3 domain that harbors the catalytic cysteine required for Ub transfer. There are currently crystal structures available for various domains of IpaH1.4 [36], IpaH3 [35], IpaH4 (PDB: 5KH1), IpaH9.8 [40, 41], SspH1 [42], SspH2 [37], and SlrP [43]. Comparison between the structures has revealed that the LRR and E3 domains can adopt quite different conformations relative to each

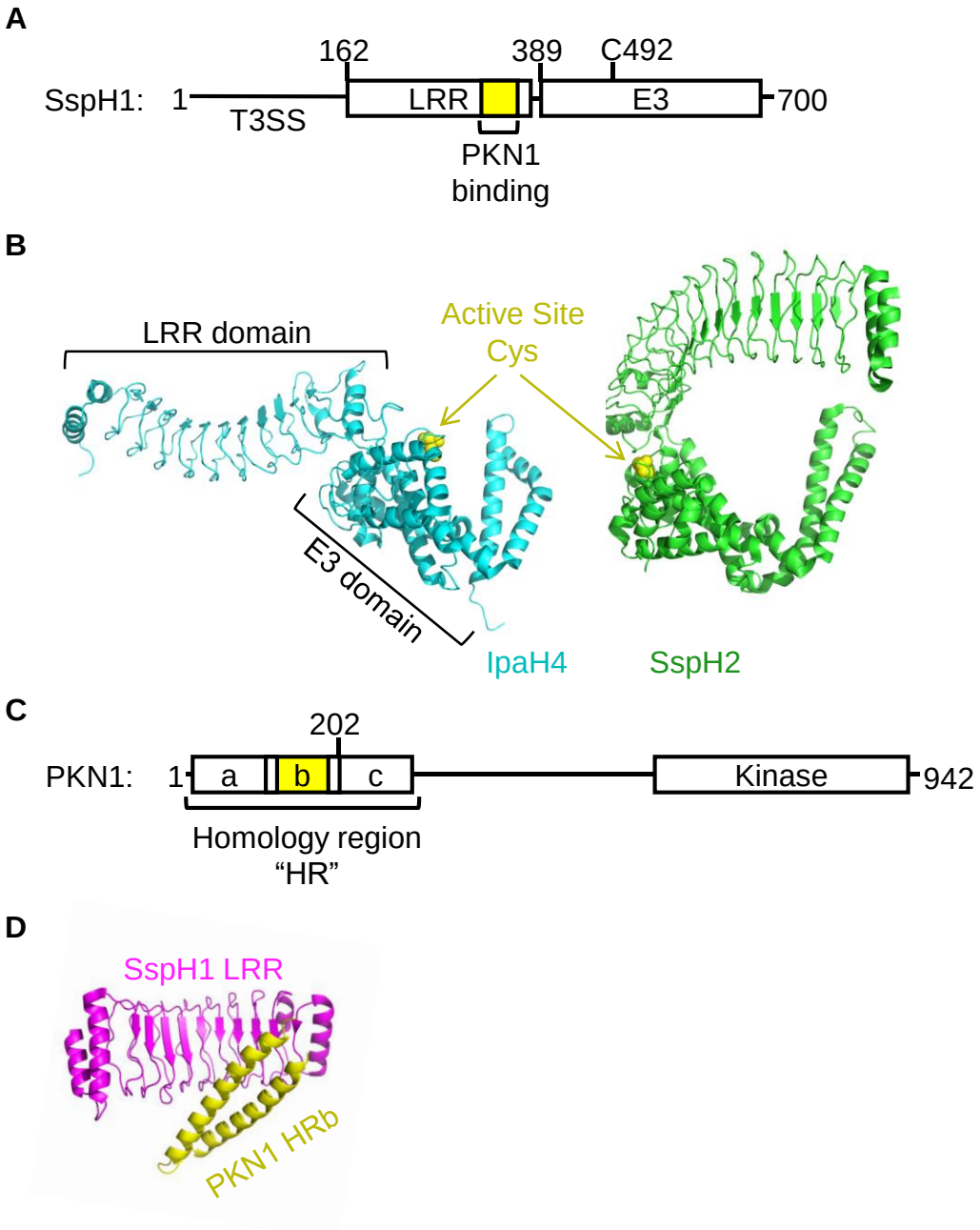

Figure 4. (A) Domain architecture of SspH1. SspH1 consists of an N-terminal T3SS targeting sequence, a leucine-rich repeat (LRR) substrate-binding domain, and a C-terminal E3 ubiquitin ligase domain. The region of the LRR that binds a fragment of PKN1 HRb region is highlighted in yellow. **(B)** Structures of IpaH4 (PDB 5KH1) and SspH2 (PDB 3G06). The LRR and E3 domains can occupy very different conformations relative to each other. **(C)** Domain architecture of PKN1. PKN1 consists of an N-terminal HR region consisting of 3 helical repeat domains, 'a', 'b' and 'c', and a C-terminal kinase domain. The fragment of PKN1 that binds the LRR of SspH1 is highlighted in yellow. Both 'a' and 'b' HR regions get ubiquitylated by SspH1 *in vitro*. **(D)** Structure of PKN1 HRb bound to the LRR domain of SspH1 (PDB 4NKG).

other (**Fig 4B**). Founded on the assumption that the observed crystal structures represent the most prevalent states in solution, it has been proposed that both observed conformations are autoinhibited conformations based on observations that full-length IpaH-SspH E3s fail to synthesize unanchored poly-Ub chains, unlike the isolated E3 domains [42, 44]. While these structures have provided structural insights of IpaH-SspH LRR and E3 domains and interactions with substrate, they lack any information regarding the conformational state in solution, how these enzymes interact with E2~Ub or Ub, or how the various domains coordinate to facilitate Ub transfer.

Interactions between IpaH-SspH E3s and host proteins

There are few confirmed substrates for members of the IpaH-SspH family, and little is known about the consequences of specific changes in signaling pathways affected by these enzymes *in vivo*. Several studies have identified substrates through yeast two-hybrid or proteomic mass-spectrometry approaches [45, 46, 47]. Studies verifying candidate substrates *in vitro* have shown that IpaH-SspH family members preferentially build K48 chains that direct their substrates to be degraded by the proteasome [48, 49]. It has also been shown in cell-culture assays that members from the IpaH-SspH family dampen host innate immune signaling pathways [49, 50]. Therefore, a likely role for IpaH-SspH effectors in bacterial pathogenesis is to hijack a host cell's ubiquitylation machinery to destroy signaling molecules upstream of host innate immune response pathways.

IpaH-SspH E3s have been shown to exclusively use E2s from the Ube2D family for Ub transfer [34, 49, 51]. As described previously, Ube2D is a promiscuous family of E2s capable of being used by each of the 3 classes of eukaryotic E3s. The topology of IpaH-SspH E3 catalytic domains differs greatly from RING, HECT and RBR E3s, so the location of the E2~Ub conjugate binding

site cannot be determined by simple inspection. Levin *et al.* (2010) used NMR to show that the E3 domain of SspH2 binds a surface of Ube2D3~Ub that is distinct from that recognized by eukaryotic E3s [48], suggesting that IpaH-SspH E3s may be binding E2~Ub in a conformation different from those observed in eukaryotic complexes.

SspH1: A experimental model for the IpaH-SspH family

To gain further insight into the functions and mechanisms of IpaH-SspH enzymes, this work focuses on one member of the IpaH-SspH family, SspH1. SspH1 is secreted by *Salmonella typhimurium* during infection of human intestinal epithelial cells and macrophages. After translocation into a host cell by the T3SS, SspH1 is transported to the nucleus through an unknown mechanism [45]. The biological effects of SspH1 include inhibition of NF-κB and androgen receptor (AR)-dependent gene expression [42, 45]. One confirmed substrate has been identified for SspH1, the Ser/Thr kinase PKN1. PKN1 has a domain architecture consisting of a C-terminal kinase domain, and an N-terminal HR domain composed of three helical repeats (HRa, HRb, and HRc) that mediate protein-protein interactions and regulate the activity of the kinase domain (**Fig 4C**). PKN1 is involved in a multitude of biological processes including: cytoskeletal regulation [52], cell migration [53], and AR-dependent transcription [54, 55]. PKN1 can be activated by binding Rho GTPases via its HR repeat domains [56, 57]. *In vitro*, SspH1 builds K48 chains on the HR domains of PKN1 [42]. In cell culture assays, PKN1 is degraded by the proteasome upon introduction of SspH1 into the host cell [42]. A crystal structure is available of the PKN1 HRb domain bound to the LRR domain of SspH1 (**Fig 4D**), and disruption of the interface revealed in the structure prevents SspH1-PKN1 complex formation and ubiquitylation of PKN1 by SspH1 [42].

SspH1 represents a good experimental model for investigating Ub transfer reactions for several reasons: **1)** SspH1 expresses well and is monomeric in solution. Several members of the IpaH-SspH family have been reported to function as dimers [49, 43]. As described herein, SspH1, has been shown experimentally to be a monomer on its own and in complex with substrate, and thus is a simpler system to use for investigating the structural details of its ubiquitin transfer mechanism. **2)** SspH1 has a confirmed substrate, PKN1. To date, PKN1 is the only putative IpaH-SspH effector substrate that has been shown to ubiquitylated and degraded by the proteasome. *In vitro*, only the PKN1 HRb repeat (< 100 residues) is required for efficient Ub modification, making it a tractable system for studying Ub transfer in detail. **3)** SspH1 is inactive in absence of substrate [34]. The isolated catalytic domain of IpaH-SspH enzymes exhibits intrinsic poly-Ub chain-building activity; when expressed alone, they rapidly build unanchored K48 chains. In the absence of substrate, IpaH-SspH family members containing both LRR and E3 domains have been shown to be autoinhibited in their poly-Ub chain building ability. The autoinhibitory effect of the LRR is relieved upon substrate binding. Some IpaH-SspH family members retain residual poly-Ub chain-building activity in the absence of substrate, which can complicate the interpretation of *in vitro* ubiquitylation assays. SspH1 has no such residual activity, allowing for clear results in *in vitro* assays.

Objectives

The objective of this work is to describe the structure and ubiquitin transfer mechanism of IpaH-SspH E3s, using SspH1 from *Salmonella* as a model system for the family. This entails defining the structure and dynamics of SspH1 in solution, the interaction between SspH1 and its interacting partners in the eukaryotic ubiquitin signaling pathway, and the mechanism of Ub

transfer. The main steps in the Ub transfer mechanism required for SspH1-mediated modification of PKN1 are (**Fig 5**): **1)** SspH1 binding to PKN1, **2)** SspH1 binding to E2~Ub, **3)** transfer of Ub to the active site of SspH1, forming an obligate SspH1~Ub intermediate, **4)** transfer of Ub from SspH1~Ub to PKN1, and **5)** synthesis of a K48-linked poly-Ub chain. I will describe the methods used to generate key protein complexes that are crucial to this transfer process and what they reveal about the mechanism of Ub transfer.

Significance

As antibiotic resistance continues to be a growing problem worldwide, it is necessary to understand bacterial pathogenesis and the factors that contribute to the infectivity and lethality of pathogenic bacteria. Members of the IpaH-SspH family are found exclusively in pathogenic, gram-negative bacteria, so understanding their structure and mechanism may reveal new opportunities for the development of antibiotic therapeutics. An understanding of how IpaH-SspH family members interact with the eukaryotic ubiquitylation pathway will also provide knowledge of the general chemical processes of Ub transfer, particularly with respect to the ability of an E2~Ub to transfer Ub to a set of structurally diverse set of E3s. Understanding general mechanisms of Ub transfer is important because it is critical to many eukaryotic signaling pathways, and the lessons gleaned from understanding how SspH1 engages E2~Ub and substrate during Ub transfer may reveal new insights into the mechanisms used by eukaryotic E3s.

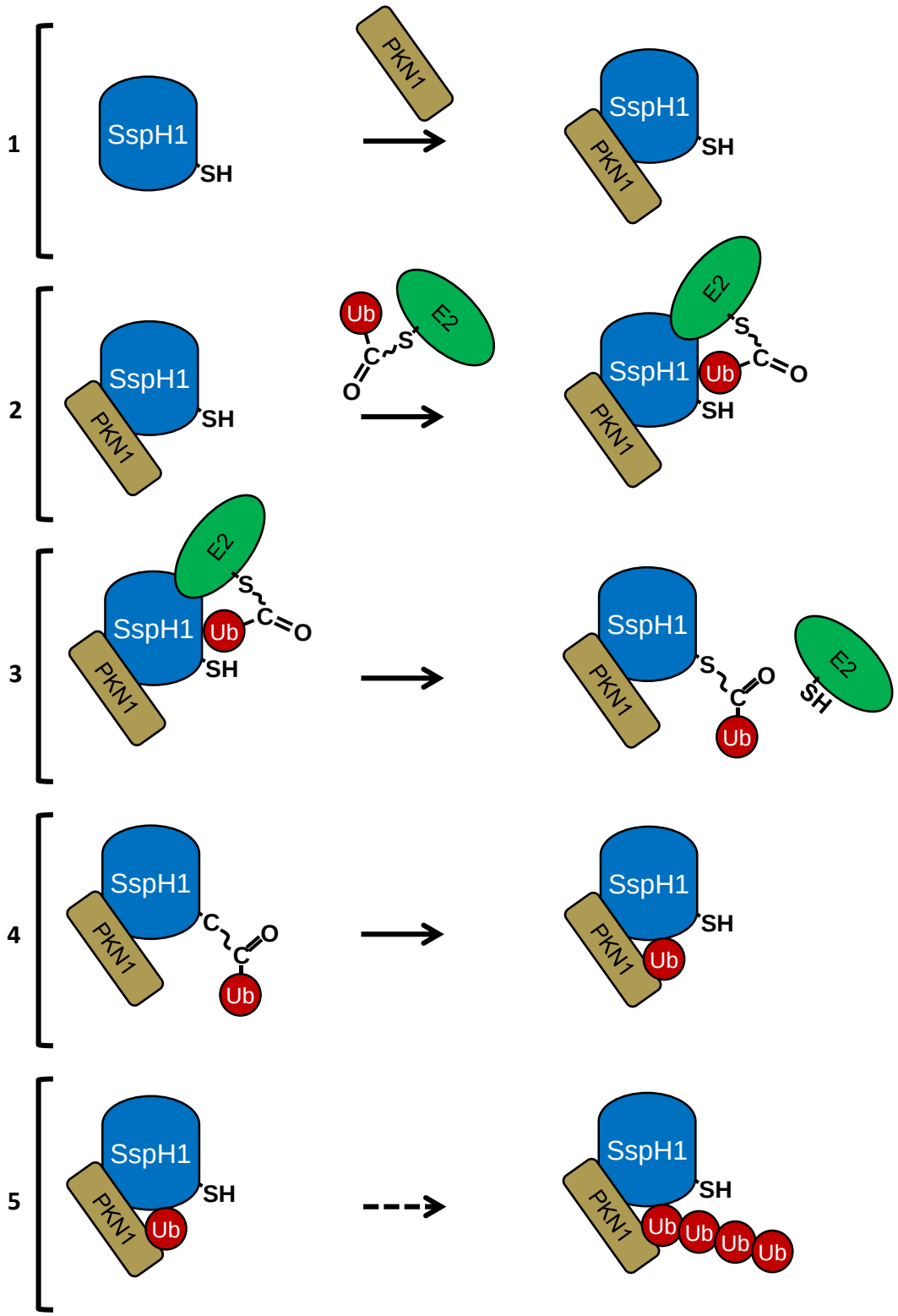

Figure 5. Stages of SspH1 Ub transfer mechanism (1) SspH1 binds PKN1. (2) SspH1 binds E2~Ub. (3) Ub transferred from E2 to SspH1 active site Cys. (4) Ub transferred from SspH1 to PKN1 Lys. (5) Extension of K48-linked polyubiquitin chains on PKN1.

Methods

Protein constructs and purification

Plasmids for proteins used in this work were generated through common molecular biology techniques of DNA amplification via polymerase chain reaction (PCR), restriction enzyme double-digestion, and T4 DNA ligation. For purification, DNA sequences were subcloned into pET-derived expression vectors possessing an IPTG-inducible *lac*-operon expression system. DNA sequences for the proteins used in this work were originally obtained from existing plasmids in the laboratory, bought from AddGene, synthesized from Genewiz, or were gifts from collaborators. DNA sequences for point mutations or HA- or FLAG-tag sequences for use in Western Blots were introduced using the QuickChange PCR site-directed mutagenesis protocol (Stratgene/Agilent) using primers purchased from Integrated DNA Technologies and confirmed via Sanger sequencing (Genewiz).

An outline of protein expression procedure is provided here, followed by details pertaining to specific proteins. Expression plasmids were electroporated into *E. coli* BL21(DE3) cells grown in LB media or isotopically-supplemented minimal growth media such as MOPS or M9 media (for NMR studies). Cells were grown to an OD_{600}=0.6-0.8 at 37°C and expression was induced with IPTG at 16°C for 16-24 hours. Cells were harvested by centrifugation, suspended in buffer, and lysed by French press. Lysed cells were clarified by centrifugation. For proteins containing hexahistidine tags, clarified supernatant was separated by immobilized Ni^{2+}chromatography. For non-ubiquitin proteins lacking tags, clarified supernatant was separated by cation-exchange chromatography via a progressive salt gradient. For ubiquitin, clarified lysate was incubated in ice-cold perchloric acid to precipitate non-ubiquitin proteins (taking advantage of the high stability

of ubiquitin) and clarified by centrifugation. Twice-clarified ubiquitin supernatant was dialyzed against buffer and separated by cation-exchange chromatography via a progressive salt gradient. For all proteins, a final separation step was performed by size exclusion chromatography using SDX-75 resin (GE). Final protein purity was assessed by SDS-PAGE to an estimated visual purity of >90%, concentrated by centrifugal filtration, and frozen. Mutant protein constructs were purified similarly to wildtype proteins.

The E1s used in this work, human E1 (hE1) and wheat E1 (wE1) were cloned into pET expression vectors in-frame with a hexahistidine tag and expressed in *E. coli.* BL21 cells. Purification proceeded by immobilized Affi-Gel (BioRad)-conjugated ubiquitin chromatography and gel filtration over 125 mL SDX-75 resin (GE) into 25 mM sodium phosphate, 150 mM sodium chloride, 1 mM dithiothreitol, pH 7.0 buffer. E1s were concentrated to 10 or 40 μM, aliquoted, flash frozen in liquid nitrogen, and stored at -80°C until use.

The E2s used in this work, (Ube2D3, Ube2E3, and Ube2L3), and ubiquitin were cloned into pET expression vectors, expressed in *E. coli* BL21 cells, and purified by cation-exchange chromatography over a 5mL SP HiTrap column (GE) using a 0-1M NaCl gradient in 25mM MOPS (3-(*N*-morpholino)propanesulfonic acid) buffer, followed by gel filtration over 125mL, 80mL, or 24mL SDX-75 resin (GE) into 25 mM sodium phosphate, 150 mM sodium chloride, pH 7.0 buffer. For ubiquitin, 50mM sodium acetate, pH 4.5 buffer was used for the cation-exchange step using a 0-1M NaCl gradient. E2s were concentrated to 100 μM or ~1 mM aliquots, flash frozen in liquid nitrogen, and stored at -80°C until use. Ubiquitin was concentrated to 3mM and frozen at -20°C until use.

The E3s and substrate used in this work, SspH1, SspH2, and IpaH4.5, and SspH1 substrate PKN1 (all combinations of HR domains alone and together), were cloned into pET expression

vectors in-frame with an N-terminal hexahistidine tag and thrombin or TEV protease site and expressed in *E. coli.* BL21 cells. Proteins were purified by immobilized Ni^{2+} chromatography over 5mL NiNTA resin (Thermo Fisher), or a 5mL HisTrap column (GE) in 20mM Tris, 150mM NaCl pH 7.6 buffer, with elution buffer supplemented with 500mM imidazole, followed by gel filtration over 125mL, 80mL, or 24mL SDX-75 resin (GE) into 25 mM sodium phosphate, 150 mM sodium chloride, pH 7.0 buffer. Hexahistidine tags were cleaved by thrombin or TEV protease where indicated. E3s or PKN1 were concentrated to 100 μM or ~1 mM, flash frozen in liquid nitrogen, and stored at -80°C until use.

Biochemical Assays

In vitro assays are particularly useful in the study of ubiquitinating enzymes because the ubiquitin post-translational modification has a high molecular weight (8.5 kDa) compared to other PTMs and is a highly stable modification due to the covalent attachment of ubiquitin to substrate via an isopeptide bond. The depletion of free Ub, substrate, or the formation of higher molecular weight poly-Ub chains can be monitored by SDS-PAGE. In a ubiquitylation assay, various components of the ubiquitylation pathway (E1, E2, E3, or substrate) are recombinantly purified and mixed together to initiate an isolated ubiquitylation pathway *in vitro*. The products of ubiquitylation assays can then be resolved by molecular weight when run on SDS-PAGE in reducing or nonreducing conditions. Under nonreducing conditions, thioester intermediates can be detected for E1~Ub, E2~Ub, or E3~Ub. Under reducing conditions, thioester intermediates are not observed. Useful comparisons can be made between assays run under reducing or non-reducing SDS-PAGE, such as the amount of ubiquitin held in thioester conjugates versus poly-Ub chains for different E2 or E3 mutants.

There are two major types of SDS-PAGE resolved ubiquitylation assays presented in this work: **1)** a multiple turnover assay, involving all components of the ubiquitylation system (E1, E2 and E3) along with ATP and Mg^{2+}, such that multiple turnovers of Ub activation are possible, and **2)** E2~Ub single turnover assays utilizing purified E2~Ub as the source of activated Ub. These assays lack E1 and ATP so that Ub cannot be reactivated. Generally, E2~Ub single turnover assays are used to assess the ability of an E3 to catalyze the removal of Ub from E2, while multiple turnover ubiquitylation assays are used to assess the ability of an E3 to form unanchored poly-Ub chains or modify a substrate with mono- or poly-ubiquitin.

E2~Ub multiple turnover reactions

Both human and wheat E1s are used as ubiquitin activating enzymes for ubiquitylation reactions involving the E2 Ube2D3, while hE1 is used as the E1 for reactions involving the E2s Ube2E3 or Ube2L3. Compared to hE1, wE1 is more stable, is recombinantly expressed in higher yields in *E. coli*, and transfers ubiquitin to E2s of the Ube2D family just as effectively as hE1. Thus, for ubiquitylation assays involving Ube2D3, wE1 is the preferred E1. However, wE1 does not transfer ubiquitin as effectively to Ube2E3 or Ube2L3, so hE1 is the preferred E1 in ubiquitylation reactions involving these E2s.

After mixing together the protein components with Mg^{2+} required for E1-mediated ubiquitin activation, the multiple turnover ubiquitylation reaction is initiated by addition of a large excess of ATP (~2.5-5mM). Once the reaction is initiated, Ub can be activated and covalently attached to a substrate or poly-Ub chain via formation of an isopeptide bond. Throughout the course of the ubiquitylation reaction, the C-terminus of ubiquitin forms transient, reactive thioester bonds with active site cysteines on the E1, E2 or E3; in these complexes there is a chance that a

solvent water molecule will hydrolyze the thioester ubiquitin conjugate, resulting in a nonproductive reaction. In multiple turnover ubiquitylation reactions, these 'lost' ubiquitin molecules can be reactivated by E1 and ATP in the reaction mixture. The large excess of ATP in the reaction allows multiple turnover ubiquitylation assays to persist until free ubiquitin is depleted.

Typical concentrations of proteins and cofactors used in a multiple turnover ubiquitylation assays in this work are: 1 μM E1, 2-5 μM E2, 2-5 μM E3, 2-5 μM substrate, 50-100 μM ubiquitin, 5 mM ATP, and 5 mM $MgCl_2$. Typical buffer conditions of multiple turnover ubiquitylation assays are: 25 mM sodium phosphate, 150 mM sodium chloride, 1mM TCEP (tris(2-carboxyethyl)phosphine), pH 7.0, 25-37°C. TCEP is a reducing agent used to prevent oxidation of active site cysteines, but does not interfere with ubiquitin transfer.

E2~Ub single turnover reactions

Instead of mixing all the components of the ubiquitylation reaction together, an E2~Ub single turnover assay separates the reaction into two stages: **1)** E1 activation of ubiquitin and transfer to E2 forming the E2~Ub conjugate. **2)** Interaction of an E2~Ub with an E3 and transfer of ubiquitin from E2 to E3; substrate may also be included. After step 1, E2~Ub is purified away from E1, free E2, free Ub, and excess ATP/Mg^{2+} by gel filtration and used as the source of activated ubiquitin in a second reaction with E3 and substrate. In the second step, E1, free ubiquitin, ATP, and $MgCl_2$ are absent, so ubiquitin cannot be reactivated and is either incorporated into substrate or a ubiquitin chain or is hydrolyzed from E2~Ub or E3~Ub by solvent water molecules to free ubiquitin when the reaction is complete. The absence of E1 in the second step also prevents catalysis of the reverse reaction, E2~Ub → E2 + Ub

In an E2~Ub single turnover reaction there are typically three or more experimental conditions, and the rate of disappearance of the E2~Ub conjugate band (*i.e.* the amount of activated ubiquitin) is monitored over time and compared between conditions. One condition, a negative control, is always E2~Ub alone, so that the basal amount of ubiquitin hydrolyzed from E2 due to solvent molecules over the course of the reaction can be determined. A second condition, inclusion of E3 with or without substrate, is compared to E2~Ub alone to determine how effective the E3 is in catalyzing transfer of ubiquitin to E3 or substrate. Other conditions often include mutations in E3 or E2 to assess the functional role of specific residues in E2-to-E3 ubiquitin transfer.

Separating the overall reaction into two stages places the focus of the E2~Ub conjugate single turnover assay on the E2 transfer step and eliminates experimental complications that could result from the presence of E1, ATP, or $MgCl_2$ in the reaction. It also prevents free ubiquitin molecules from being reactivated, ensuring each ubiquitin can only be used once, approximating a single-turnover type of reaction. However, a lack of ubiquitin regeneration can mean hydrolysis can compete with substrate resulting in fewer substrate modifications than in multiple turnover ubiquitylation assays.

Nuclear Magnetic Resonance Spectroscopy

Nuclear magnetic resonance (NMR) spectroscopy is a physical technique used to study the atomic structure of molecules, including biological molecules such as proteins. The technique is dependent on indirectly measuring properties of the nuclear magnetic moments of nuclei. Nuclear magnetic moment is a manifestation of nuclear spin angular momentum, the physical origins of which are beyond the scope of this work. NMR spectroscopy of proteins is a highly important field of study, as it is one of only three experimental techniques capable of determining high resolution

atomic structures of proteins, along with X-ray crystallography and electron microscopy. Of these techniques, only NMR spectroscopy is capable of precise structural studies in the solution state, allowing for ensemble structure determination of intrinsically disordered proteins or structurally ambiguous "fuzzy" complexes. NMR spectroscopy can additionally provide thermodynamic and kinetic information about protein complex formation. In the work presented here, NMR spectroscopy is used extensively to identify interfaces of protein-protein complexes, and to probe dynamic changes in enzyme structure during catalysis.

History and Theory

Nuclear magnetic resonance, the absorption of electromagnetic radiation by a nucleus when placed in a magnetic field, was first reported by Isidor Rabi in 1938 for a molecular beam of lithium chloride in a vacuum [(58)]. NMR in liquid and solid states was then demonstrated by two groups in 1946, in liquid water by Felix Bloch and solid paraffin by Edward Purcell [(59, 60, 61, 62)]. Bloch's 1946 papers extensively explained the theoretical basis of NMR in bulk condensed phase nuclei, and in the 72 years since the publication of the Bloch equations, the field of NMR has expanded tremendously.

NMR spectroscopic studies of proteins began in 1957 with the proton spectrum of ribonuclease by Martin Saunders, and it quickly became apparent that the proton NMR spectrum of proteins are more complicated than the sum of the spectra of their constituent amino acids [(63)]. The location of the NMR line for a proton in an amino acid is dependent on the covalent structure of the residue as well as the chemical environment of surrounding residues and solvent molecules [(64)]. The change in the location of any given NMR line relative to a reference compound (*e.g.* tetramethylsilane) is known as the *chemical shift* of a proton [(64)]. Since the core of most proteins

exclude solvent, the chemical shift of a proton in a residue on the surface of the protein will experience a different chemical shift than that of a proton in an identical residue in the core of the protein [65]. Thus, the structured nature of folded proteins means identical residues residing within the same polypeptide chain may be distinguished by differences in their chemical environment [65]. Changes in the NMR spectrum can result from changes in protein structure, buffer conditions, and formation of protein-protein complexes. Residues directly involved in a protein-protein interface will experience a particularly large change in chemical environment due to replacement of surrounding solvent molecules with another polypeptide. Therefore, NMR is an excellent method for identifying protein-protein interfaces, or changes in protein structure resulting from formation of a complex.

Since the first NMR spectrum of ribonuclease in 1957, a huge number advances have been made in the application of NMR spectroscopy to the study of proteins. These advances have occurred to overcome two major hurdles in the study of proteins by NMR spectroscopy: low signal-to-noise and spectral complexity [65]. Three advances in particular have been fundamental. **1)** the innovation of pulsed Fourier transform NMR spectroscopy reported in 1966 by Richard Ernst and Weston Anderson, which unified the various fields of NMR methodologies and allowed spectra to be obtained much faster [66]. In pulsed Fourier-transform NMR, the magnetic moments of all nuclei of a particular type (usually ^{1}H, ^{13}C, or ^{15}N, in protein systems) begin aligned with an external magnetic field, and a short, hard pulse of energy in the radio frequency is applied perpendicularly to the direction of the external magnetic field (the Z-axis). The hard pulse rotates the magnetic moment of the nuclei perpendicular to the magnetic field, into the XY-plane. When the hard pulse is stopped, the magnetic moments of the nuclei precess around the Z-axis as they return to align with the external magnetic field. The precessing magnetic moments are recorded as

an oscillating signal called a free-induction decay (FID). The rate at which nuclei precess as they return to alignment with the external magnetic field is dependent on the local chemical environment of the nuclei, and Fourier transformation of the collected FID gives the various precession frequencies [64]. **2)** The use of Nuclear Overhauser effects (NOE) due to dipolar interactions between nuclei to measure through-space distances between nuclei [64, 65, 67]. **3)** Multi-dimensional NMR spectroscopy, first proposed by Jean Jeener in 1971 and experimentally reported by Ernst's lab in 1976, which allows for the interpretation of complex protein spectra by separating overlapped NMR lines along additional dimensions [68, 69]. The development of multi-dimensional NMR spectroscopy was dependent on the advancement of pulsed Fourier transform NMR spectroscopy, and, importantly for biological NMR spectroscopy, allows for heteronuclear *coherence* transfer between spin systems of different nuclear species (primarily ^{1}H, ^{15}N, and ^{13}C) [65]. Formally, *coherence* is the persistent correlation of phase relationships between spin systems after removal of an external radio frequency field, and it is a fundamental concept in the field of NMR spectroscopy [70]. Coherence transfer is an important method of transferring magnetization through bonds to obtain correlations between nuclei and is the basis for the most commonly used NMR spectroscopic experiment used in this work, the ^{1}H,^{15}N-TROSY [70].

^{1}H,^{15}N-TROSY

The primary NMR spectroscopic experiment used in this work is a multi-dimensional experiment called ^{1}H,^{15}N-TROSY. The ^{1}H,^{15}N-TROSY experiment produces spectra similar to the classic 2D HSQC (heteronuclear single quantum coherence) experiment and correlates the spins of two bonded ^{1}H and ^{15}N nuclei into two different frequency dimensions, one for ^{15}N (typically along the y-axis) and one for ^{1}H (typically along the x-axis) [70]. The TROSY (transverse relaxation

optimized spectroscopy) principle, selects the component of the multiplet (spin-splitting) resonance with the lowest *transverse relaxation* rate, resulting in better resolution and sensitivity for large macromolecules [70]. Transverse relaxation is a phenomenon associated with the loss of coherence (decoherence) between spin systems and is a major contributor to the low sensitivity observed for NMR spectroscopic studies of proteins [70]. Selecting the component of the resonance with the lowest transverse relaxation rate in a $^{1}H,^{15}N$-TROSY experiment allows for clearer interpretation of spectra of larger proteins or complexes (> 30kDa).

The result of an $^{1}H,^{15}N$-TROSY experiment is a set of free-induction decay curves (FIDs) representing the NMR signal generated by nuclear spins precessing around an external magnetic field [70]. The set of FIDs are then Fourier transformed in two dimensions, and, due to coherence between bonded ^{1}H and ^{15}N nuclei, the resulting Fourier transform is a two-dimensional spectrum with each peak in the spectrum representing a ^{1}H-^{15}N bond [64]. Before and after application of the Fourier Transform to the set of FIDs, layers of data processing are applied to improve sensitivity, resolution, and to correct for artifacts and solvent effects [71]. These methods include extrapolation, apodization, phase correction, linear prediction, and normalization of the spectrum to a reference chemical so that NMR spectra across various magnetic field strengths can be compared. It is critical to ensure that each of these processing steps are performed in identical fashion when making quantitative comparisons between experiments [71].

The location of each peak in the resulting spectrum of an $^{1}H,^{15}N$-TROSY experiment represents the *chemical space* of the corresponding ^{1}H-^{15}N bond. For a protein, each amide group in the polypeptide chain, as well as the N-H bonds in tryptophan, asparagine, glutamine, arginine and lysine side chains can give rise to a peak in the NMR spectrum. In practice, peaks resulting from arginine and lysine side chains are usually only visible in experiments performed at low pH

or in cases where a buried or hydrogen-bonded side chain lowers the apparent pKa of the side chain guanidine or amino group [70]. The TROSY effect strongly suppresses the signal from peaks arising from asparagine and glutamine side chains, so most peaks in a $^{1}H,^{15}N$-TROSY spectrum represent a backbone amide group [70]. While the inherent location of peaks arising from particular residue types in the spectrum do follow some broad trends, it is generally not possible to assign each peak in the $^{1}H,^{15}N$-TROSY spectrum to a particular residue using the $^{1}H,^{15}N$-TROSY spectrum alone. A series of more complicated three-dimensional NMR experiments correlating ^{1}H, ^{15}N, and ^{13}C bonds are required to assign each peak in the spectrum to its corresponding residue [65, 72].

The ability to observe an NMR signal is inversely proportional to the molecular weight of the species being studied [70]. This limits the study of proteins using traditional NMR methods to molecular weights of less than ~50 kDa. The proteins or complexes studied in this work are above 50 kDa, so several recent in advancements in NMR technology and sample preparation were used extensively. NMR signal is proportional to external magnetic field strength, so higher-field strength magnets allow for the study of larger proteins; the experiments in this work used magnets with magnetic field strengths of 500, 600, and 800 Mhz in units of proton Larmor frequency (corresponding to 11.7, 14.1, and 18.8 Tesla, the traditional unit for magnetic field strength) [70]. Other technological improvements, such as cryogenically cooling spectroscopic equipment to reduce thermal noise, have also led to improved signal-to-noise for large proteins; the 600 and 800 Mhz magnets used in this work were used in conjugation with cryogenically-cooled detection probes [70]. Replacement of all but the amide protons in a protein with deuterium, a process called deuteration, can also lead to higher signal due to a reduction in transverse relaxation rates [70]. The transverse relaxation rate for a nucleus is proportional to the surrounding dipole magnetic field

resulting from the magnetic dipole moments of nearby nuclei [70]. Deuterons have a much weaker magnetic dipole moment than protons due to the presence of a neutron, so deuterating a protein decreases the overall dipole magnetic field of the protein, and thus decreases the transverse relaxation rates for nuclei in the protein [70]. In this work, deuteration coupled with a high-field strength 800 MHz magnet with cryoprobe were essential for performing $^{1}H,^{15}N$-TROSY experiments of ^{15}N-Ub conjugated to the SspH1 active site.

Paramagnetic Spin Labels

Paramagnetic spin labels such as TEMPO (2,2,6,6-Tetramethylpiperidin 1-oxyl) or MTSL (*S*-(1-oxyl-2,2,5,5-tetramethyl-2,5-dihydro-1H-pyrrol-3-yl) methyl methansulfono-thioate) are small nitroxide-based molecules that can be covalently attached to a protein, often via iodoacetamide or maleamide linkages to free sulfhydryl groups of cysteine side chains. Spin labels such as these carry a large magnetic dipole moment due to the presence of an unpaired electron on the nitroxide radical. The large magnetic dipole moment greatly increases the local dipole magnetic field such that nuclei close to the spin label (within ~10-20 Å) undergo a large increase in transverse relaxation rate. For nuclei very close to the spin label, the increase in transverse relaxation rate is so great that the NMR lines resulting from those nuclei broaden out completely, and the corresponding peaks in the $^{1}H,^{15}N$-TROSY spectrum are lost.

Addition of sodium ascorbate to a spin-labelled sample chemically reduces the nitroxide radical on the spin label to hydroxylamine. This reduction decreases the magnetic dipole moment of the spin label, resulting in a decreased local dipole magnetic field, and an increase in transverse relaxation rates of nearby nuclei. The increase in transverse relaxation rate strengthens the NMR signal of surrounding nuclei, so peaks in the resultant NMR spectrum that would have otherwise

been lost due to the paramagnetic spin label effects now reappear. Therefore, comparing the NMR spectrum of a spin-labelled sample before and after addition of sodium ascorbate will reveal which residues in the protein are in close proximity to the spin label. Spin labels were used in this work to identify protein-protein interactions and specific orientations between SspH1 and E2~Ub, as well as SspH1~Ub and PKN1.

NMR Sample preparation

The NMR effect is dependent on nuclei possessing the property of nuclear spin. Nuclei with odd mass numbers have half-integral spin quantum numbers, nuclei with even mass numbers and an even atomic number have no spin quantum number, and nuclei with even mass numbers and an odd atomic number have integral spin quantum numbers. Nuclei with spin quantum numbers greater than ½ also possess an electric quadrupole moment, which decreases the lifetime of the magnetic state of the nuclei. [(70)]. Thus, for protein NMR spectroscopy, relevant nuclei include ^{1}H, ^{13}C, ^{15}N, and in specialized cases ^{31}P (as previously described, ^{2}H nuclei, which have an integral spin quantum number, are also relevant for reasons related to transverse relaxation). The natural abundance of ^{1}H is 99.99%, while the natural abundance of ^{13}C is 1.07%, and for ^{15}N it is only 0.37% [(70)]. Because the 1D proton NMR spectrum of most proteins suffer from spectral crowding, and the abundance of ^{13}C and ^{15}N in natural proteins is too low given the current state of NMR spectroscopic technology, natural proteins and proteins expressed recombinantly in traditional growth mediums are unsuitable for NMR spectroscopic studies.

To introduce NMR-suitable nuclei into proteins, proteins must be recombinantly expressed in media supplemented with isotopically-labelled metabolites as the only source of the desired nucleus. In this work, ^{15}N was incorporated into proteins by supplementing a minimal MOPS or

M9-based growth medium with $^{15}NH_4Cl$ as the only source of nitrogen to uniformly label the protein with ^{15}N. To introduce ^{13}C into a protein, a minimal MOPS or M9-based growth media can be supplemented with ^{13}C-glucose as the only carbon source. Incorporating ^{2}H is more difficult, as there are many sources of protons that can incorporate into a protein. In this work, $^{2}H^{15}N$-labelled ubiquitin was expressed in a deuterium oxide-based minimal MOPS or M9-based growth media supplemented with $^{15}NH_4Cl$, but *not* with ^{2}H-glucose; this gives a total deuteration estimated to be ~80-85%, which was suitable for obtaining an NHSQC-TROSY spectrum of ubiquitin conjugated to the active site of SspH1.

NMR samples were prepared by diluting concentrated stock protein to a concentration of 100-200μM in 25mM sodium phosphate, 150mM sodium chloride, pH 7 aqueous buffer supplemented with 10% deuterium oxide. D_2O in the sample is used as in internal reference that the NMR spectrometer uses to compensate for magnetic field drift throughout the course of an experiment. Final sample volumes were 500μL and were transferred to a 5mM-diameter borosilicate glass tube. NMR experiments were performed at 25°C.

Hydrogen-Deuterium Exchange Mass Spectrometry (HDX-MS)

Hydrogen-deuterium exchange labelling of proteins followed by mass spectrometry is a method for probing the structure and conformation of proteins in solution. The first HDX-MS experiment, reported in 1991 by Katta and Chait, was used to study conformational changes in ubiquitin induced by addition of methanol to an aqueous acidic solution of ubiquitin [(73)]. For a polypeptide, labile hydrogens readily accessible to solvent, such as those on the peptide backbone amide group, may exchange with deuterium when introduced to deuterated solvent [(73)]. The rate of hydrogen-deuterium exchange (HDX) is dependent on chemical group, accessibility to solvent,

and solvent pH (or pD, for a deuterated solvent) [73]. Amide proton exchange can occur via base- or acid-catalysis mechanisms by solvent D_2O. Base catalysis is favorable at high pH while acid-catalysis is favorable at low pH; the overall minimal rate of catalysis occurs at pH 2.5. For a folded protein, exchangeable hydrogens may be buried in the core of the protein with less accessibility to solvent or may be involved in secondary structure-forming hydrogen-bond or salt-bridge interactions. Thus, the rate of HDX for exchangeable hydrogens in a folded protein may differ by several orders of magnitude [73]. If the exchange rates of labile hydrogens in a protein can be determined experimentally, they can be used to probe structural properties of the protein. NMR spectroscopy can be used to precisely determine HDX rates for exchangeable hydrogens for each residue, but the method is limited to studies of proteins small enough to be investigated by NMR (< 50-60 kDa). Additionally, current NMR technology is incapable of investigating HDX at short time points (<5 minutes), making accurate determinations of fast-exchanging hydrogens difficult. Modern mass spectrometry techniques are sensitive enough to detect the mass difference between hydrogen and deuterium, can be used for a wide range of protein sizes, can investigate HDX at short times points (down to 1-3 seconds), and over the last 20 years have been gaining in popularity as a technique for indirectly measuring the HDX rates of exchangeable hydrogens in a protein [74].

In this work, HDX-MS was used to probe for potential structural changes in SspH1 as it advances through its catalytic cycle. Eight constructs of SspH1 were chosen to investigate structural changes in either the E3 domain or the full-length protein resulting from the presence of the LRR domain, the N-terminal T3SS targeting sequence, addition of PKN1, and Ub tethered to the active site. The constructs were: **1)** SspH1 E3 domain, **2)** SspH1 E3-Ub domain, **3)** Full-length SspH1, **4)** Full-length SspH1-Ub, **5)** SspH1 LRR-E3 **6)** SspH1 LRR-E3-Ub, **7)** SspH1 LRR-E3 in complex with PKN1 HRb, and **8)** SspH1 LRR-E3-Ub in complex with PKN1 HRb. Here, “LRR-

E3" denotes a construct of SspH containing only LRR and E3 domains and lacking the first 161 residues required for targeting to the T3SS. "-Ub" denotes ubiquitin covalently linked to the SspH1 active site mutation C492K via an isopeptide bond. A first round of HDX experiments was performed with hexahistidine-tagged constructs **1**, **2**, **3**, **4**, and a second round of experiments was performed with tag-cleaved constructs **1**, **2**, **5**, **6**, **7**, **8**. Each round was performed using different mass spectrometers and slightly different experimental conditions; thus, quantitative comparisons are only made between constructs investigated within the same round of HDX experiments. Though experimental conditions and instrumentation varied slightly between rounds, the experimental procedures were similar.

The workflow for HDX-MS experiments was performed as follows: **1)** 200 μL of 1 mg/mL of each sample was incubated in deuteration buffer (25mM sodium phosphate, 150mM NaCl, 1mM DTT pH 7.0, 90% D_2O) for varying amounts of time at room temperature (~20°C). Samples were incubated for 3 seconds, 1 minute, 30 minutes, and 20 hours. An undeuterated sample was prepared by incubation in non-deuterated buffer (25mM sodium phosphate, 150mM NaCl, 1mM DTT pH 7.0). A fully-deuterated sample was prepared by incubation in deuteration buffer supplemented with 4M guanidine hydrochloride and incubation at 100°C for 30 minutes. **2)** The hydrogen-deuterium exchange process was quenched by addition of 200μL of deuteration buffer containing 0.1% TFA, dropping the pH of samples to 2.5, and rapidly flash frozen in liquid nitrogen. Hydrogen-deuterium exchange rates are minimal at pH 2.5, so addition of acidic quench buffer to samples followed by flash freezing effectively stops the exchange reactions. **3)** Quenched samples were digested with pepsin to produce small peptides (~6-30 residues in length). Pepsin is a nonspecific protease active at pH 2.5. Digestion in quenched conditions allows samples to be cleaved into fragments amenable for mass spectrometry while preventing any further HD-

exchange during processing. For the first round of experiments, the digestion step occurred immediately after the quenching step. Quenched samples were digested with 3 mg/mL pepsin on ice for 5 minutes and then flash frozen in liquid nitrogen. For the second round, samples were quenched and flash frozen, then were thawed and digested on a home-made immobilized pepsin column (supplied by Miklos Guttman in the Department of Medicinal Chemistry at the University of Washington) at 2°C immediately prior to liquid chromatography-mass spectrometry. **4)** Digested peptides were separated by reverse-phase liquid chromatography (LC) on a C18 peptide column in-line with the mass spectrometer using a gradient of 0.1% formic acid, 5% acetonitrile, 0.02% trifluoroacetic acid, pH 2.5 to 0.1% formic acid, 100% acetonitrile at 2°C. For the second round, digestion over an immobilized pepsin column was performed in-line with the C18 column. **5)** Mass spectra of separated peptides were obtained by time-of-flight mass spectrometry (TOF-MS). For the first round, a Waters Synapt G1 was used for mass spectrometry, and for the second round, a Waters Synapt G2 was used for mass spectrometry. For the second round, ion-mobility spectrometry (IMS) was performed prior to TOF-MS in a drift cell prior to the quadrupole in the TOF-mass spectrometer. IMS provides an additional step of peptide separation to reduce spectral overlap in the mass spectrum.

The above steps were performed for each undeuterated, fully-deuterated, and variable-time incubated samples. For Round 2 experiments, duplicates of each variable time-incubated samples were collected. Additionally, MS/MS spectra of undeuterated protein were collected for each sample during each round for peptide identification. Overall, 84 HDX-LC-MS runs were performed for downstream data analysis.

MS/MS Peptide Identification

For each undeuterated sample, MS/MS was performed to identify peptides for analysis. For Round 1, peptide search within the MS/MS data was performed using the online server Protein Prospector [75] developed and hosted by the University of California San Francisco Mass Spectrometry Facility. For Round 2, peptide search within the MS/MS data was performed using ProteinLynx Global SERVER (PLGS) [76] developed by, and licensed from, the Waters Corporation, available through the Mass Spectrometry Center in the Department of Medicinal Chemistry at the University of Washington. Putative peptides identified from automated analysis were subsequently manually inspected and validated using MassLynx and DriftScope (Waters).

HDX Data Processing

Processing of HDX data was performed using HXExpress [77, 78]. The workflow for data processing was performed as follows: **1)** for each validated peptide, two parameters (for Round 1) or three parameters (for Round 2) of each peptide were catalogued for data extraction. These parameters include: mass-to-charge ratio, retention time from the liquid chromatography step, and drift time from the ion mobility step (for Round 2). These parameters were used to automatically extract mass spectral distributions for each peptide from either the Waters Coroporation's MassLynx software (for Round 1 experiments) or from raw mass spectra data files (for Round 2 experiments) (**Fig 1A**).

2) A binomial curve was fit to a mass spectral distribution to obtain a center of mass for each experimental condition of every catalogued peptide in each sample (**Fig 1B**). Though spectral overlap is minimized by liquid chromatography and ion mobility separation, convolution of mass spectral distributions resulting from different peptides with similar mass-to-charge ratios, retention

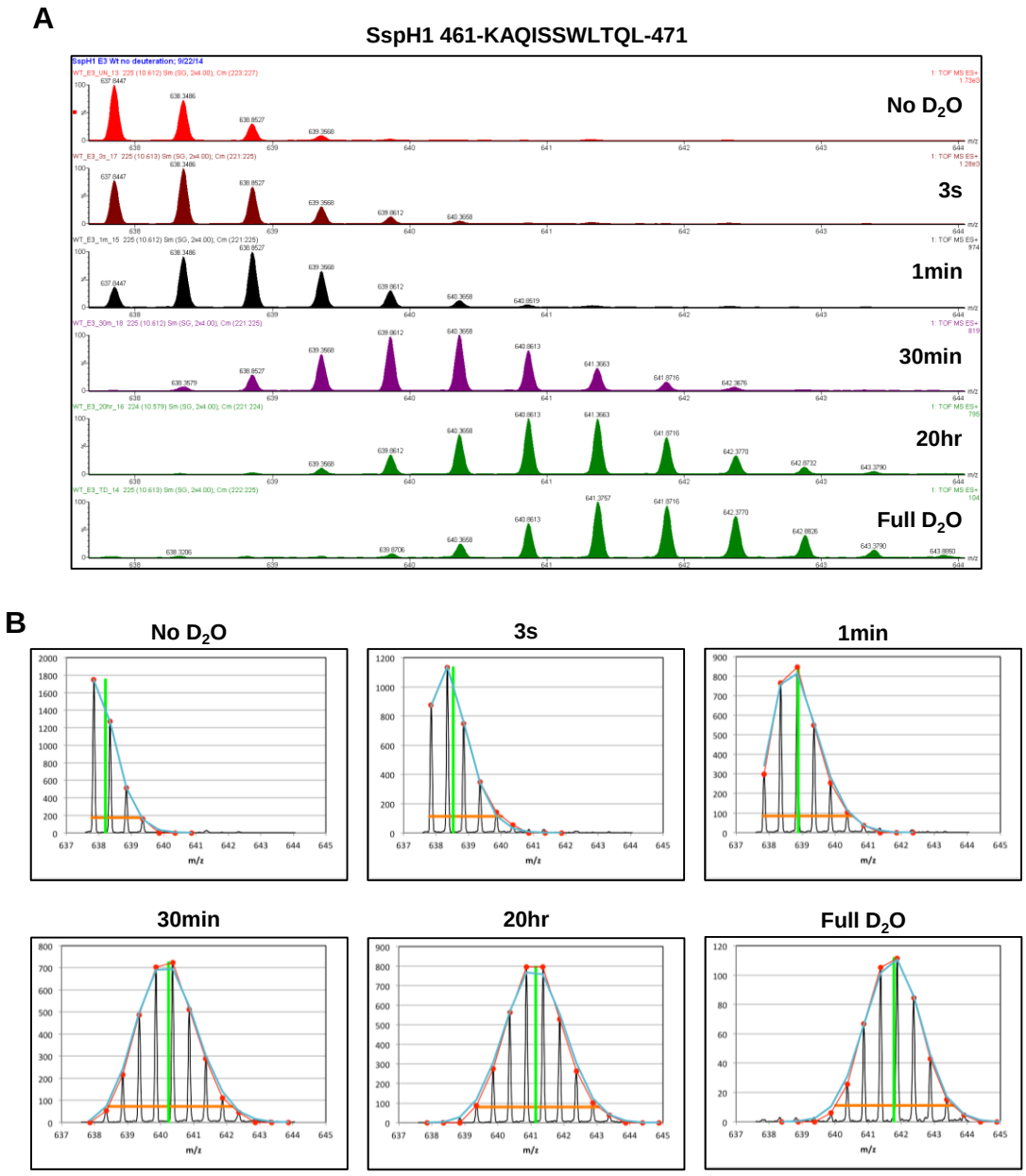

Figure 1. LC HDX-MS data processing scheme. **(A)** Peptide mass spectra distributions correlating to that of SspH1 461-471 "KAQISSWLTQL" arising after pepsin digestion following incubation in deuterated buffer for 3 sec, 1 min, 30 min, 20 hours. **(B)** A binomial distribution was fit for each mass envelope, the mean of the distribution was used to calculate percent deuteration and plotted in **(C)**.

times, and drift times may still occur in some instances. In some cases, the overlap in distributions is so severe that the individual distributions cannot be deconvoluted. In most cases, overlapped distributions do not occur, or can be deconvoluted during binomial fitting.

3) Deuterium uptake curves were plotted as a function of time (**Fig 1C**). Plots were visualized on a logarithmic x-axis due to the large range in sampled time points (3 seconds to 20 hours). Given the results from step 2, there are three ways of representing deuterium uptake curves as a function of $\log_{10}$(time): peptide mass, relative deuteration and fractional deuteration. Peptide mass, m_i, is simply the center of mass for each sampled timepoint. Relative deuteration is ($m_i - m_0$), where m_0 is the center of mass of the undeuterated peptide. Fractional deuteration is [($m_i - m_0$) / ($m_{100} - m_0$)], where m_{100} is the center of mass of the fully deuterated peptide. Calculating fractional deuteration is the ideal method for accounting for experimental differences occurring between samples and correcting for *back exchange*. Back exchange occurs from HDX after quenching, during the digestion and liquid chromatography steps, when deuterated buffer is not present. Results from Round 1 were calculated using fractional deuteration.

Results from Round 2 were calculated using relative deuteration because extensive back exchange during preparation of fully deuterated samples gave extremely broad mass distributions with characteristics similar to a mixture of undeuterated and fully deuterated peptides, which prevented binomial fitting. Generation of fully deuterated samples is not trivial due to the presence of high concentrations of denaturant used to unfold proteins in the sample [(78)] Here, 4M GndCl was necessary to fully denature ubiquitin tethered to the active site of SspH1, and each of three separately-prepared fully deuterated samples for each construct in Round 2 gave similarly poor results. The primary experimental difference between Rounds 1 and 2 that could lead to increased back exchange was use of an immobilized pepsin column during Round 2. It is possible that, due

to the unfolded nature of the fully deuterated samples giving all exchangeable hydrogens a very fast exchange rate, back exchange occurred rapidly on the pepsin column. In contrast, during Round 1, pepsin digestion was performed on ice during quenching. However, because each of the samples in Round 2 was performed under identical experimental conditions within a 72-hour time period, and two replicates were obtained for each time point, relative deuteration was suitable for downstream analysis.

Butterfly Plots

The results of data processing give an individual deuterium uptake curves for each peptide per protein construct. One way of comparing all the deuterium uptake curves between two constructs or different complexes is to create a *butterfly plot*. A butterfly plot is created by plotting (1 – Fractional Deuteration) for one construct (*e.*g. wildtype) and (Fractional Deuteration – 1) for another (*e.g.* mutant). These values are calculated for each sampled timepoint per peptide shared between the two compared constructs and plotted as a function of mean peptide residue number. Differences in the butterfly plots are highlighted in a *summation plot*, shown below the butterfly plot. A summation plot is created by summing the butterfly plot values calculated for each construct and plotting as a function of mean peptide residue number. For peptides with identical deuterium uptake curves between constructs, [(1 – Fractional Deuteration) + (Fractional Deuteration - 1)] sum to zero, and no peak is observed in the difference graph. For peptides with different deuterium uptake curves, the summation plot value does not sum to zero, and a peak in the difference graph is observed. A difference in deuterium uptake for a peptide indicates a change in its structure, so butterfly plots and corresponding summation plots can be used to identify regions of a protein with structural differences between two constructs.

Butterfly plots were used to visualize potentially interesting pairwise comparisons between SspH1 constructs, with an emphasis on structural changes that occur in the E3 domain. A potentially interesting pairwise comparison is defined as a comparison between two SspH1 constructs in which there is only one major difference between the constructs: e.g. presence or absence of LRR domain, substrate, or Ub conjugated to the active site. For Round 1 experiments, four SspH1 constructs were analyzed, leading to 4 potentially interesting pairwise comparisons: **1)** SspH1 E3 vs SspH1 E3-Ub, **2)** full length SspH1 vs full length SspH1-Ub, **3)** SspH1 E3 vs full length SspH1, and **4)** SspH1 E3-Ub vs full length SspH1-Ub. For Round 2 experiments, six SspH1 constructs were analyzed, leading to seven potentially interesting pairwise comparisons: **1)** SspH1 E3 vs SspH1 E3-Ub, **2)** SspH1 LRR-E3 vs SspH1 LRR-E3-Ub, **3)** SspH1 LRR-E3:PKN1 vs SspH1 LRR-E3-Ub:PKN1, **4)** SspH1 E3 vs SspH1 LRR-E3, **5)** SspH1 LRR-E3 vs SspH1 LRR-E3:PKN1, **6)** SspH1 E3-Ub vs SspH1 LRR-E3-Ub and **7)** SspH1 LRR-E3-Ub vs SspH1 LRR-E3-Ub:PKN1. While each of these comparisons can be made, there is redundancy in the relevant structural information obtained from each, and a method of comparing more than two constructs at a time is desired.

Protection Factors

One relatively new method for quantitatively comparing deuterium uptake curves between two constructs is to calculate the *protection factor* for each peptide shared between the constructs. Protection factors quantitate the change in HDX rate constant from one experimental condition to another [(79)]. For a single exchangeable site, the protection factor from condition 1 to condition 2 is given by: $PF_{C1\rightarrow C2} = \frac{k_{ex,C1}}{k_{ex,C2}}$, where k_{ex} is the exchange rate for the exchangeable site [(79)]. To analytically calculate protection factors, k_{ex} must be determined for each exchangeable site in the

protein. HDX mass spectrometry cannot resolve single exchangeable sites, making a calculation of k_{ex} underdetermined and analytical calculation of protection factors impossible. Walters (2017) demonstrated a theoretical basis for an empirical determination of protection factors for HDX data obtained from mass spectrometry. The rationale behind this method is briefly outlined below.

Deuterium exchange, *d*, for a single exchangeable site can described by a monoexponential equation: $d = f(t) = 1 - e^{-k_{ex}t}$. By inversion, the amount of time, *t*, required to reach a particular value of d can be shown to be: $t = f^{-1}(d) = \ln(1-d)/-k_{ex}$. Importantly, the quotient of the functions $f^{-1}(d)$ for a single exchange site under two conditions can be shown to be equivalent to the protection factor:

$$\frac{f_{C2}^{-1}(d)}{f_{C1}^{-1}(d)} = \frac{\ln(1-d)/-k_{ex,C2}}{\ln(1-d)/-k_{ex,C1}} = \frac{k_{ex,C1}}{k_{ex,C2}} = PF_{C1\rightarrow C2}$$

Therefore, if $\frac{f_{C2}^{-1}(d)}{f_{C1}^{-1}(d)}$ can be determined, $PF_{C1\rightarrow C2}$ can be calculated. For a group of *N* rate constants measured together:

$$f(t) = N - \sum_{i=1}^{N} e^{-k_i t}$$

This means that $\frac{f_{C2}^{-1}(d)}{f_{C1}^{-1}(d)}$ now varies with *d* and cannot be solved analytically as $f^{-1}(d)$ cannot be solved for multiple exponentials analytically. However, Walters (2017) showed that the average protection factor for a group of *N* rate constants measured together is approximate to the geometric mean of $\frac{f_{C2}^{-1}(d)}{f_{C1}^{-1}(d)}$:

$$\langle PF_{C1\rightarrow C2} \rangle \approx GM\left[\frac{f_{C2}^{-1}(\boldsymbol{d})}{f_{C1}^{-1}(\boldsymbol{d})}\right]$$

The geometric mean for a series of *n* values is $(\prod_{i=1}^{n} x_i)^{1/n}$. The relationship between the average protection factor and the geometric mean of $\frac{f_{C2}^{-1}(d)}{f_{C1}^{-1}(d)}$ cannot be proven analytically but can be

demonstrated empirically. To show this, the steps required to calculate $GM\left[\frac{f_{C2}^{-1}(\boldsymbol{d})}{f_{C1}^{-1}(\boldsymbol{d})}\right]$ will first be described. Then, several examples will be used to empirically demonstrate the relationship.

The steps for empirically calculating $\langle PF_{C1\rightarrow C2}\rangle$ are as follows: **1)** within the range of deuterium uptake values shared between two conditions (e.g. points on the y-axis of the HDX plot shared between two curves), *d*, ten points are chosen for each observed unit of deuterium exchanged. This gives a list, *d'*, of *m* points in the deuterium uptake curves shared between two conditions. **2)** For each point, d_i', the time it would take for the point to be observed, $f_{Ci}^{-1}(d_i')$, is calculated from the experimental data by log-linear interpolation. **3)** Finally, the empirical averaged protection factor is given by:

$$\langle PF_{C1\rightarrow C2}\rangle_{empirical} = \left(\prod_{i=1}^{m} f_{C2}^{-1}(d_i')/f_{C1}^{-1}(d_i')\right)^{1/m}$$

In order to apply this new methodology to HDX data for SspH1, it was necessary to develop a custom Python script. To demonstrate that the program was implemented correctly, the examples presented in Walters (2017) were replicated. First, a hypothetical peptide with 3 exchangeable sites that exchange at different rates with k_{ex} = 0.1, 0.2, 0.3 was plotted using the equation $f(t) = 3 - e^{-0.1t} - e^{-0.2t} - e^{-0.3t}$ (**Fig 2A**, left panel, blue curve). The geometric mean of these exchange rates, 0.39, was calculated to plot a monoexponential function, $g(t) = 3(1 - e^{-0.39t})$, according to the methodology presented in 79 (**Fig 2A**, left panel, orange curve). 5 sampled deuterium points were chosen, *d* = 0.5, 1.0, 1.5, 2.0, 2.5 (**Fig 2A**, left panel, open circles) and $g^{-1}(d)/f^{-1}(d)$ was plotted (**Fig 2A**, right panel, open circles). The protection factor, or geometric mean of $g^{-1}(d)/f^{-1}(d)$, is 1 (**Fig 2A**, right panel, dotted line). This demonstrates that the method works for a trivial case, as the two curves represent the same set of data, and thus should give a protection factor of 1. The results obtained were identical to those reported in Walters (2017) (**Fig 2B**).

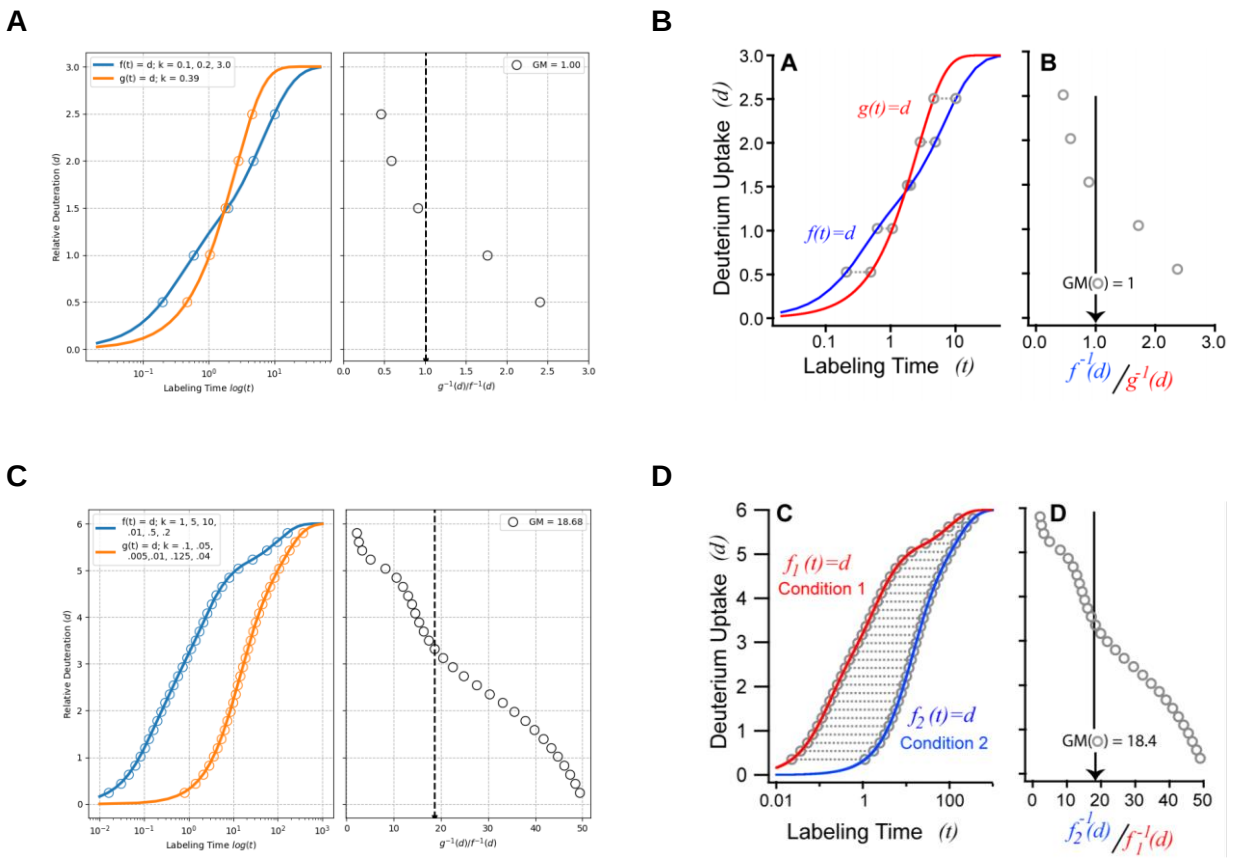

Figure 2. Calculation of Protection Factor (PF) reproducing the results from Walters (2017). **(A)** Left panel: plot of group of three 3 exchangeable groups with k_{ex} = 0.1, 0.2, 0.3 (blue curve) and a monoexponential with k = 0.39, the geometric mean of k_{exs}. 5 points were sampled at d = 0.5, 1.0, 1.5, 2.0, 2.5 (open circles). Right panel: $g^{-1}(d)/f^{-1}(d)$ for the 5 sampled points, and their geometric mean (dotted line), giving PF = 1.0 **(B)** Figure 1A,B from Walters (2017). **(C)** Left panel: deuterium uptake curves for a hypothetical 5-residue peptide with $k_{ex,C1}$ = 1, 5, 10, 0.01, 0.5, 0.2 (blue curve) and $k_{ex,C2}$ = 0.1, 0.05, 0.005, 0.01, 0.125, 0.04 (orange curve). 30 even distributed points within the range of shared values of d between the two conditions were chosen (open circles). Right panel: $g^{-1}(d)/f^{-1}(d)$ for the 30 sampled points, and their geometric mean (dotted line), giving PF = 18.68. **(D)** Figure 1C,D from Walters (2017). For the hypothetical peptide in **(C,D)**, the ideal answer is the geometric mean (GM) of $k_{ex,C1}/k_{ex,C2}$ = GM(10 + 100 + 2000 + 1 + 4 + 5] = 18.49. Figures B and D are adapted with permission from Walters, B.T. (2017) Empirical method to accurately determine peptide-averaged protection factors from hydrogen exchange MS data. *Anal. Chem.* **89(2)**, 1049-1053. Copyright 2016 American Chemical Society.

A more complicated example from Walters (2017) is shown in (**Fig 2C,D**). Here, a hypothetical 5-residue peptide is simulated in two different environments, with $k_{ex,C1}$ = 1, 5, 10, 0.01, 0.5, 0.2 (**Fig 2C**, *f(t)* - blue curve) and $k_{ex,C2}$ = 0.1, 0.05, 0.005, 0.01, 0.125, 0.04 (**Fig 2C**, *g(t)* - orange curve). A set of 30 evenly distributed sampled deuterium uptake points within the range of shared deuterium uptake values between the two conditions was chosen (**Fig 2C**, open circles), and $g^{-1}(d)/f^{-1}(d)$ was calculated for each sampled point (**Fig 2C**, open circles). The protection factor between the two hypothetical conditions, or geometric mean of $g^{-1}(d)/f^{-1}(d)$, was calculated to be 18.68 (**Fig 2C**, dotted line). The results from Walters (2017) gave a protection factor of 18.4 (**Fig 2D**). In this example, the ideal answer can be calculated because k_{ex} is known for each exchangeable site under each condition. For each site, the value of $k_{ex,C1}/k_{ex,C2}$ is 10, 100, 2000, 1, 4, 5. The geometric mean of these values, and thus the ideal protection factor, is 18.49. The estimated results found here and in Walters (2017) are close to the ideal answer. The discrepancy between the estimated results comes from the difference in choice of sampled deuterium uptake points. Walters (2017) did not detail how points were sampled, so a best approximation was made here in replicating the results.

The algorithm outlined above was used to calculate pairwise protection factors for HDX Round 2 results. Analysis of the results showed some problems in the naïve implementation of the algorithm outlined in Walters (2017) when applied to real data. Ideally, the slope of deuterium uptake curves is always positive. However, real data occasionally show small dips in deuterium uptake curves at low or high time points due to noise. The naïve implementation of the algorithm in cases of dips leads to incorrect choices in sampling points for the calculation of $g^{-1}(d)/f^{-1}(d)$, and thus to incorrect calculations of protection factors (**Fig 3A,B**). These errors can be easily fixed by eliminating dips when choosing sampled deuterium uptake points (**Fig 3C,D**). Once protection

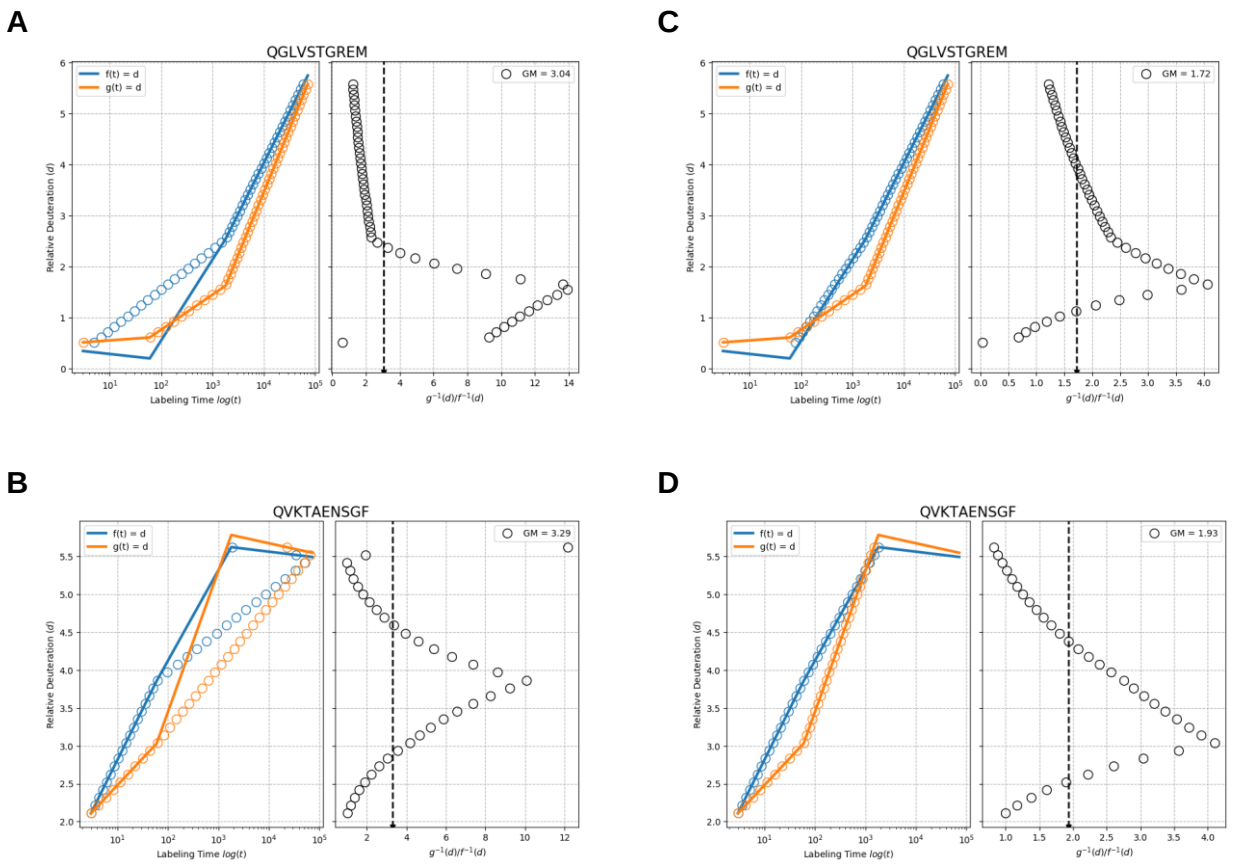

Figure 3. Correcting errors in algorithm for calculating protections factors. A naïve implementation of the algorithm outlined in Walters (2017) incorrectly samples points for calculating $g^{-1}(d)/f^{-1}(d)$ in cases of dips at **(A)** early and **(B)** late timepoints arising from noise. Errors in sampling are fixed by flattening dips when choosing points **(C,D)**. Improper sampling leads to incorrect protection factor calculations (3.04 in **(A)** vs 1.72 in **(B)**; 3.29 in **(C)** vs 1.93 in **(D)**).

factors are calculated, they can be plotted as a function of mean peptide residue number. Since more than one protection factor can be easily visualized, these plots can show more than one pairwise comparison at a time, and thus lead to easier simultaneous interpretation of structural changes that occur in a protein under varying conditions. The source code for calculating protection factors is provided as **Appendix I**.

SAXS

Small-angle X-ray scattering (SAXS) is a biophysical technique for determining low resolution structures in solution, and is often helpful for understanding the conformation of multi-domain proteins in solution. SAXS theory was developed by André Guinier in the 1930s and began to be applied to proteins in the 1950s [80]. Compared to other techniques for studying protein structure, SAXS has advantages in speed of data collection and processing but is limited in the information it provides. In a SAXS experiment, X-rays are scattered by a monodisperse sample of particles (proteins) and the intensity of the scattered waves is recorded by a detector [81]. The momentum transfer, q, of scattered waves is governed by the equation $q = {4\pi sin\theta}/{\lambda}$, where θ is the scattering angle and λ is the wavelength of generated x-rays [81]. Since λ is constant and θ is small (< 3° in most cases), q is essentially a function of scattering angle [81]. The result of a SAXS experiment is an intensity curve, $I(q)$, plotted as a function of q. From the SAXS curve, several parameters of the particle can be calculated, including molecular weight, radius of gyration (R_g), maximum particle dimension (D_{max}), and hydrated volume (V_p) [81]. The SAXS curve can also be used to generate low resolution (>2nm) *ab initio* models of the particle [81].

Crystal structures of SspH2 and IpaH4 show very different conformations of LRR and E3 domains relative to each other, but it is not clear which of these conformations, if any,

predominates in solution. To understand the conformational states of the LRR and E3 domains in solution for SspH1, and to probe how addition of PKN1 or Ub at the active site alter the conformational state, SAXS experiments were performed on various constructs of SspH1 alone or in complex with its substrate, PKN1, to obtain the parameters R_g, D_{max}, and V_p, and to generate *ab initio* models using a variety of software packages and online servers.

Sample Preparation and Data Collection

SAXS experiments were performed for the following SspH1 constructs: **1)** SspH1 E3 C492K (10 mg/mL), **2)** SspH1 E3 C492K-Ub (10 mg/mL), **3)** SspH1 LRR-E3 C492K (10 mg/mL), **4)** SspH1 LRR-E3 C492K-Ub (10 mg/mL), **5)** SspH1 LRR-E3 C492K:PKN1 HRb (10 mg/mL complex), **6)** SspH1 LRR-E3 C492K-Ub:PKN1 HRb (10 mg/mL complex). Hexahistidine tags were cleaved from SspH1 constructs. For samples 5 and 6, a 2X molar concentration of PKN1 was included to ensure all SspH1 molecules were in complex with substrate. Samples were prepared in 25mM sodium phosphate, 150mM NaCl, 1mM DTT, pH 7 buffer, and frozen on dry ice. After shipment to Stanford Synchrotron Radiation Lightsource (SSRL), samples were thawed and injected onto a Superose 6 gel filtration column equilibrated with 20mM HEPES, 150mM NaCl, 1mM DTT, pH 7 buffer in-line with SSRL Beamline 4-2. Intensities of scattered X-rays were detected with a Pilatus3 X 1M detector. Data collected at the peak of the eluted SspH1 peak off of gel filtration were used for downstream data analysis.

Data Analysis

Data was analyzed using the ATSAS software package developed by the European Molecular Biology Laboratory [82, 83]. The top 5 SAXS curves by intensity were buffer-subtracted

and merged [80]. R_g was calculated by Guinier approximation, which states that for small values of q, $I(q) = I(0)e^{-q^2R_g^2/3}$ [81]. A linear fit of $\ln[I(q)]$ vs q^2 at the low q region yielded a slope equal to R_g. V_p was calculated using Porod's Law, which states that $V = 2\pi^2 {I(0)}/{Q}$, where Q, the Porod invariant, is equal to $\int_0^\infty q^2 I(q) dq$ [81]. For compact particles at high values of q, the Porod approximation states that $I(q) = kq^{-4}$, where k is dependent on the surface volume of the scattering particle [81]. The Porod Plot of $I(q)q^4$ vs q^4 allowed for estimation of V_p at high values of q, where the plot was linear [81]. D_{max} was calculated from the distance distribution function, $p(r)$, which is the distribution of distances between all pairs of points within the particle (analogous to the Patterson function for X-ray crystallography) [80]. $p(r) = \frac{1}{2\pi^2}\int_0^\infty I(q)qrsin(qr)dq$, and is the Fourier Transform of $I(q) = 4\pi \int_0^{D_{max}} p(r) \frac{\sin(qr)}{qr} dr$ [81]. Intuitively, D_{max} is the position where $p(r)$ returns to 0 at large values of r. Though $p(r)$ cannot be determined analytically from the SAXS curve, as $I(q)$ is not known from 0 to ∞, D_{max} can be estimated by indirect Fourier transform [81]. Using ATSAS software, D_{max} was varied to produce a well-behaved $p(r)$ plot that was positive for $0 < r < D_{max}$ and gently sloped to $p(r) = 0$ at $r = 0$ and $r = D_{max}$ [82].

The ubiquitin ligase SspH1 from *Salmonella* uses a modular and dynamic E3 domain for Ub transfer

Matt Cook[1], Scott P. Delbecq[1#], Thomas P. Schweppe[1], Miklos Guttman[2], Rachel E. Klevit[1], and Peter S. Brzovic[1]*

From the [1]Department of Biochemistry, University of Washington, Seattle WA 98195; [2]Department of Medicinal Chemistry, University of Washington, Seattle WA 98195

Running title: *SspH1 uses a modular and dynamic E3 domain for Ub transfer*

[#]Present address: InBios International, Inc. 562 1st Ave S, Seattle WA 98104

*To whom correspondence should be addressed: Peter S. Brzovic: Department of Biochemistry, University of Washington, Seattle WA 98195; brzovic@uw.edu; Tel. (206) 685-1550.

Keywords: ubiquitylation, *Salmonella*, SspH1, PKN1, bacterial effector, E3 Ubiquitin-ligase, E2 Ubiquitin-conjugating enzyme, Ubiquitin, ubiquitin transfer

---

Abstract

SspH/IpaH bacterial effector E3 ubiquitin ligases are a family of prokaryotic E3s utilized by a variety of invasive gram-negative bacteria during pathogenesis. SspH/IpaH E3s are unrelated in sequence and structure to known eukaryotic E3s but must function in a eukaryotic environment and utilize host cell E2 ubiquitin-conjugating enzymes to target host proteins for ubiquitylation. Despite several crystal structures, details of E2~Ub recognition and the mechanism of ubiquitin transfer are poorly understood. Here we show that the catalytic E3 ligase domain of SspH1 can be divided into two subdomains; an N-terminal subdomain (NSD) that harbors the active site cysteine, and a C-terminal subdomain (CSD) that harbors an E2~Ub binding site. NMR experiments utilizing paramagnetic spin labels reveal the orientation of E2~Ub bound to SspH1 and how the E3 active site engages the active site of the E2~Ub conjugate. Unexpectedly, Hydrogen/Deuterium Exchange mass spectrometry reveals that the region of SspH1 that binds the E2~Ub conjugate is dynamic. Mutations designed to restrict motion within the SspH1 E3 domain during ubiquitin

transfer reveal that movement of SspH1 E3 subdomains is critical for catalysis. Our results support a model in which both the E2 and Ub subunits of an E2~Ub are used to clamp onto a dynamic region of SspH1, where it is then poised to react with a conformation of the E3 in which the active-site harboring NSD is proximal to the E2~Ub conjugate-harboring CSD.

Introduction

To promote infectivity and survival within a eukaryotic cell, numerous species of pathogenic bacteria utilize macromolecular secretion systems to translocate a cadre of effector proteins directly into the host cell cytoplasm. Within the host, the various effector proteins can function to alter the cytoskeleton to promote bacterial entry, affect vesicle maturation, transport, and fusion, and target pathways that regulate host innate immune responses (1). Ubiquitin (Ub) signaling pathways, found exclusively in eukaryotes, are targeted by various bacterial effector proteins from different pathogens (2,3). This is perhaps not surprising as Ub signaling affects nearly all aspects of eukaryotic cell biology. Post-translational modification of proteins by Ub is used to regulate numerous aspects of protein function including protein activity, localization, macromolecular interactions, and lifetime (4). To exploit this regulatory system, one strategy used by both viral and bacterial pathogens is to introduce effector proteins that function as E3 Ub ligases that target specific host proteins for ubiquitylation (5-6).

Protein ubiquitylation, in most cases, involves the formation of a stable isopeptide bond between the carboxyl-terminus of Ub and the ε-amino group of a lysine residue (7-9). The end-product can be a mono-ubiquitylated or multi-mono-ubiquitylated substrate. However, Ub also has lysine residues that can serve as a platform for building poly-Ub chains on a target protein. The best-characterized are K48-linked chains, a signal that targets a protein for destruction by the 26S

proteasome (4). Regardless of the end-product, protein ubiquitylation requires the successive action of three types of enzyme: an E1 Ub-Activating enzyme, an E2 Ub-Conjugating enzyme, and an E3 Ub-Ligase (7-9). The E1 activates Ub in an ATP-dependent reaction to form a covalent E1~Ub thioester species. Activated Ub is then transferred via a trans-thiolation reaction to an E2 to generate an E2~Ub thioester conjugate. E2~Ub then pairs with an E3 to transfer Ub to a substrate protein. Eukaryotic E3s are generally divided into two mechanistic classes. RING/U-box type E3s serve an activation and scaffolding role to facilitate the direct transfer of Ub from the E2~Ub conjugate to the target (9). In contrast, reactions catalyzed by HECT-type or RBR-type E3s require at least two stages for Ub transfer from E2~Ub to substrate. In Stage I, the E3 binds an activated E2~Ub and Ub is transferred from the E2 active site to the E3 to form an obligate E3~Ub thioester intermediate. In Stage II, Ub is transferred from an E3~Ub conjugate usually to a Lysine residue of a target protein or another Ub subunit to form a covalent isopeptide bond (7-9).

Members of the SspH/IpaH family of bacterial effectors function as HECT-type E3s but are unrelated in sequence and structure to any known eukaryotic E3s (10). They are well represented in strains of *Salmonella* and *Shigella* and are widely distributed in other gram-negative pathogens. The architecture of SspH/IpaH E3s consists of a variable N-terminal region required for translocation into the host via a Type 3 Secretion System, a leucine-rich repeat domain (LRR) responsible for substrate binding, and a C-terminal E3 domain that catalyzes Ub transfer (Fig. 1A, Fig. S1A) (10,11). Despite structural differences, SspH/IpaH E3s share important functional similarities with their eukaryotic HECT counterparts. Like HECT E3s, SspH/IpaH E3s form an obligate E3~Ub intermediately prior to substrate modification and must utilize specific host E2~Ubs and target specific host proteins for ubiquitylation (12-16).

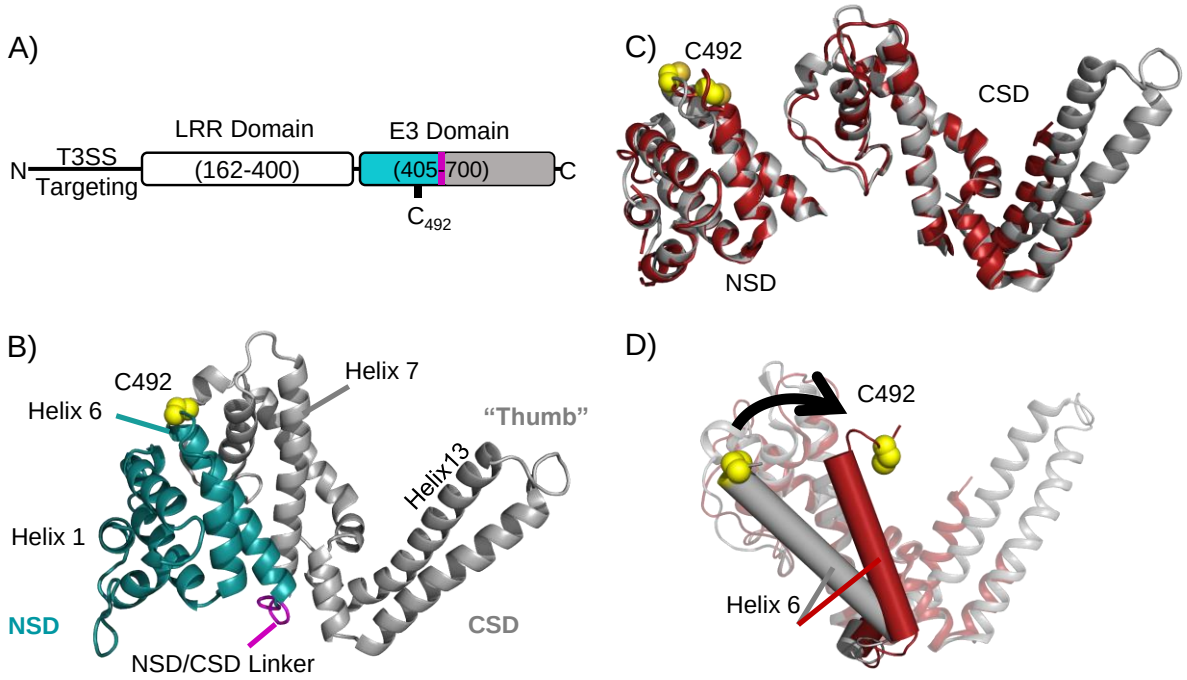

Figure 1. Domain architecture and topology of SspH1. **A)** A Type III Secretion System (T3SS) targeting sequence is present at the N-terminus of SspH1 followed by the substrate-binding leucine-rich repeat (LRR) domain and catalytic ubiquitin ligase (E3) domain. The E3 domain has a catalytic cysteine, C492, at the active site. **B)** The topology of SspH/IpaH E3 domains, based on the structure of SspH2 (77% identical to SspH1, PDB # 3G06 (14)), can be divided into an N-terminal subdomain (NSD, blue) and a C-terminal subdomain (CSD, grey), which are connected by a short linker (magenta). **C)** NSDs and CSDs from E3 domains of SspH2 (grey) and IpaH3 (red, PDB # 3CVR (12)) superimpose with backbone RMSDs < 1Å. **D)** Alignment of the SspH2 and IpaH3 E3 domains superposing only the CSDs, reveals a 20° difference in the position of NSD helix 6 relative to the CSD in the two structures.

Several studies have shown that SspH/IpaH E3s exclusively use E2s from the Ube2D (UbcH5) family as a source of activated Ub (12-17). Though Ube2D3~Ub (UbcH5c~Ub) is used by both eukaryotic and bacterial E3s, the differing topology of the SspH/IpaH E3 catalytic domain suggested that these bacterial E3s interact differently with Ube2D~Ub conjugates as compared to eukaryotic E3s. Using NMR spectroscopy, Levin et al. (2010) demonstrated that the E3 domain of SspH2 binds a surface of Ube2D3~Ub that is distinct from that recognized by eukaryotic HECT- and RING-type E3s (17). However, the profound differences in sequences and domain topology between SspH/IpaH E3s and eukaryotic E3s leaves unresolved the question as to how these E3s bind and orient Ube2D~Ub conjugates to catalyze Ub transfer.

A general feature shared by HECT-type E3s is their modular construction, and a key question concerning these E3 families is how individual domains work in concert to facilitate Ub transfer. Comparison of SspH/IpaH structures containing both LRR and E3 domains show that these domains can undergo a remarkable re-orientation in which the N-terminus of the LRR domain can move by as much as 100Å relative to the E3 domain (Fig. S1B) (12,14). Largely overshadowed by this large conformational change are potential structural changes within the E3 domain itself that may also be critical for Ub transfer. Conformational variation within the E3 domain was first observed in the crystal structure of the isolated E3 domain of IpaH1.4 in which two different conformations were observed in the asymmetric unit (13). As described below, we find that subsequent structures of other SspH/IpaH E3 domains adopt one of these two conformations (Fig. S2).

Understanding how the various domains and conformational states work in concert to promote Ub transfer is a key objective for deciphering the biological roles of E3s that function in eukaryotic cells. As part of this effort, we focused on the bacterial E3 SspH1 from *Salmonella*

which targets the eukaryotic kinase PKN1 for ubiquitylation. PKN1 is associated with regulating a number of pathways including NF-kB and Androgen Receptor signaling, both of which are involved in the cellular response to bacterial invasion (18-20). PKN1 can be activated by members of the Rho family of small G proteins, which bind to the HR domains in the N-terminal region of PKN1 (21). First identified using two-hybrid screens (19), PKN1 has been confirmed as an SspH1 substrate through *in vitro* ubiquitylation assays and *in vivo* infection assays (15,20). The minimal construct of PKN1 sufficient for binding and ubiquitylation is Homology Region b (HRb) (Fig. S1C), and a structure of the HRb region of PKN1 bound to the SspH1 LRR domain has been determined (20). Though the structure of the SspH1 E3 domain has not yet been solved, those of several closely related E3s, including SspH2 (77.6% identical in the E3 domain), are available. Thus, SspH1 is a structurally tractable system for studying interactions with the host ubiquitylation machinery and the bonafide substrate that allows for investigating protein interactions and domain motions that occur during substrate ubiquitylation.

Here, we show that the mobility of structural elements within the SspH1 E3 domain is critical for Ub transfer. We demonstrate that the SspH1 E3 domain can be divided into separate sub-domains, an N-terminal Sub-Domain (NSD) harboring the catalytic cysteine, and a C-terminal Sub-Domain (CSD) responsible for recruiting Ube2D~Ub. In contrast to E2~Ub binding sites that have been characterized in eukaryotic E3s, the CSD region we identify as necessary for Ube2D~Ub binding is dynamic in the absence of an E2~Ub conjugate. Selective use of spin labels in the SspH1 E3 domain reveals how Ube2D~Ub binds to SspH1 and how the E3 catalytic cysteine approaches the E2~Ub conjugate active site. The data presented support a mechanistic model in which both subunits of Ube2D3~Ub are needed to grasp onto the CSD, properly orienting the E2~Ub conjugate active site to react with the E3 catalytic cysteine. Finally, upon formation of an

E3~Ub intermediate, the NSD must move relative to the CSD in order to deliver activated Ub to the target substrate.

Results

SspH1 LRR-E3 is a monomeric protein

A previous study suggested that SspH/IpaH constructs containing both LRR and E3 domains form obligate dimers in solution (15). Such high molecular weight complexes could negatively impact NMR-based experiments and complicate data analysis. To determine the quaternary structure of SspH1 in solution, we examined the behavior of SspH1 LRR-E3 (residues 162-700, MW= 61.8kDa) in the presence and absence of the PKN1 HRb motif (residues 108-201) using analytical Size-Exclusion Chromatography (SEC). On SEC, both SspH1 and the SspH1/PKN1 complex eluted as single peaks at elution volumes consistent with monomeric SspH1 or a 1:1 SspH1:PKN1 complex, respectively. The isolated SspH1 E3 domain, which does not bind PKN1, also behaves as a monomeric species on SEC (Fig. S3A). Analysis of the SspH1 LRR-E3 elution peak by multi-angle light scattering yielded a molecular weight of ~63kDa in good agreement with the calculated molecular weight of this construct (Fig. S3B). Thus, under our experimental conditions, in both the absence and presence of substrate, purified SspH1 E3 and LRR-E3 constructs behave as monomeric proteins.

SspH/IpaH E3 domains can be divided into two distinct subdomains

As originally described by Singer et. al. (2008), the structure of SspH/IpaH E3 catalytic domains consists of three regions: an N-terminal lobe, a middle region, and a C-terminal lobe or "thumb region" that protrudes away from the rest of the E3 domain (Fig. 1B) (13). Several subsequent SspH/IpaH structures all exhibit the same overall α-helical fold of the E3 domain (12-14,22). Comparison of the various structures reveals conformational heterogeneity within the E3 Ub ligase domain. Superposition of structurally conserved Cα backbone atoms from IpaH3 (PDB

3CVR (12)) and SspH2 (PDB # 3G06 (14)) E3 domains yields an RMSD of ~3.8Å (Fig. S2A). However, if SspH/IpaH E3 domains are divided into two separate subdomains, an N-terminal SubDomain (NSD; helices 1-6 of the SspH2 E3 domain) and a C-terminal SubDomain (CSD; SspH2 helices 7-13), the individual regions have much higher structural similarity. The structurally conserved regions of the NSD and CSD from IpaH3 and SspH2 can be superposed with a backbone RMSD of less than ~1Å (Fig. 1C, Fig. S2B). Likewise, the corresponding NSD and CSD regions from the structures of IpaH1.4 (13), IpaH4 (PDB # 5HK1), IpaH9.8 (23), and SlrP (22) all superpose with similar backbone RMSDs. Within the CSD of the various E3 domains, additional structural diversity is observed in the tip segment of the Thumb region (Fig. S2A). As shown in Fig. 1D, superposition of the IpaH3 and SspH2 E3 CSD regions reveals an ~20° rotation of the relative orientation of NSD Helix 6, and therefore the entire NSD, between these structures. NSD Helix 6 harbors the catalytic Cys required to first accept Ub from an E2~Ub conjugate and then to transfer the activated Ub to a target substrate. This change in orientation alters the relative position of the catalytic Cys by more than 21Å (Cα-Cα distance). Intriguingly, comparison of IpaH3 and SspH2 with the available crystal structures of IpaH1.4, IpaH4, and SlrP, shows that each of these E3 domains adopts one or the other of these two different conformational states (Fig. S2C).

A short loop segment (Fig. 1B, magenta loop) connects E3 Helices 6 & 7 and links the NSD (cyan subdomain) to the CSD (gray subdomain). By introducing a stop codon into the loop segment, we were able to express and purify the NSD which is well-behaved and highly soluble. We initially attempted to generate an SspH1 CSD construct separated at this linker region but found that inclusion of helix 6 residues was needed to produce a soluble CSD construct. This suggests that at least a portion of helix 6 interacts with the CSD and these contacts aid in the stability and solubility of this subdomain. Purified NSD (residues 406-516) and CSD (residues

489-700) constructs yielded dispersed $^{1}H,^{15}N$-TROSY NMR spectra at 25°C (Fig. 2A,B). For each construct, the peak intensities are more uniform than in the E3 domain, and most of the expected number resonances are observed (~100 of the predicted 120 peaks for the NSD; ~200 of the predicted 210 peaks for the CSD). In comparison, only ~150 of the predicted 320 resonances are observed in the $^{1}H,^{15}N$-TROSY spectrum of the full SspH1 E3 domain and the intensities of the peaks are more variable (Fig. 2C). Though only a subset of resonances is observed for the E3 domain, those that are present overlay well with NSD and CSD resonances (Fig. 2D). This result indicates that residues in the isolated NSD and CSD constructs adopt similar environments and, therefore, tertiary structure as in the full E3 domain. As we have no evidence for non-specific association or dimerization of the E3 domain (see above), we propose that the variable intensities and absence of some peaks in the spectrum of the E3 domain is likely due to conformational exchange involving relative motions of the NSD and CSD, presumably between states observed in available crystal structures.

Identification of an E2~Ub Interaction Site in the SspH/IpaH E3 domain

Though neither subdomain exhibits E3 ligase activity on its own, the ability to separate and isolate E3 subdomains provided an opportunity to explore important E3 functional roles, particularly the interaction with activated E2~Ub. Substitution of the Ube2D3 active site Cys with Ser was used to generate a stable oxy-ester linked E2~Ub conjugate (Ube2D3-O-Ub) for NMR experiments. A second Ube2D3 mutation, S22R, was introduced into the β-sheet of the E2 to prevent additional non-covalent interactions of Ub with the E2 that could complicate analysis and interpretation of NMR spectra (24). This E2 backside mutation does not abrogate the ability of SspH1 to ubiquitylate PKN1 (Fig. S4A). As previously reported for free Ube2D3 and Ub binding

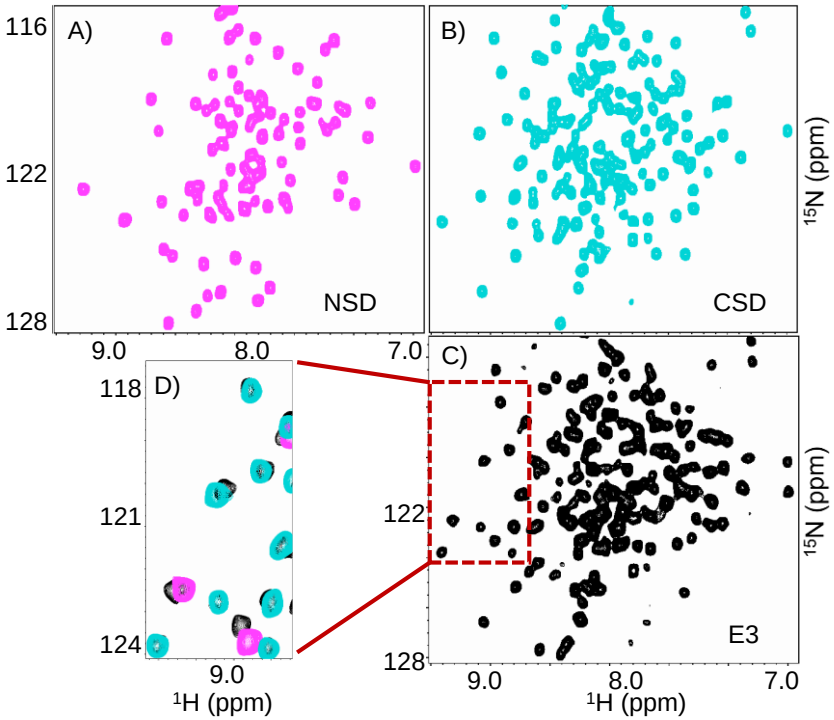

Figure 2. NMR spectra show that the SspH1 E3 can be divided into two separately-folded subdomains. SspH1 NSD (**A**, magenta spectrum) and CSD (**B**, cyan spectrum) yield dispersed ^{1}H, ^{15}N-TROSY NMR spectra. Comparison to the spectra of the E3 domain (**C**, black spectrum) show that resonances from the E3 domain overlay well with those from the NSD and CSD (**D**). NMR spectra were collected on 200 µM ^{15}N-labeled SspH1 NSD, CSD, or 100µM E3 domain at 25°C in 25mM sodium phosphate, 150mM sodium chloride, and 10% D_2O at pH 7.

to SspH2 (17), no significant chemical shift perturbations are observed in the $^{1}H,^{15}N$-TROSY spectrum of free Ube2D3 or Ub upon addition of SspH1 E3 (Fig. S4B). However, as observed for binding to SspH2, selective peak broadening/intensity loss is observed when the ^{15}N-labeled Ube2D3-O-Ub conjugate is added to SspH1. These results show that both subunits of the E2~Ub conjugate are required for binding SspH1. (Fig. 3A, Fig. S5A). Despite harboring the active site Cys, addition of the NSD had no effect on the spectrum of Ube2D3-O-Ub (Fig. 3B, Fig. S5B). In contrast, significant spectral changes are observed upon addition of the CSD (Fig. 3C, Fig. S5C). Mapping the most perturbed resonances onto a surface representation of Ube2D3~Ub reveals that the same Ube2E3-O-Ub resonances are perturbed upon addition of the CSD and the full E3 domain (Fig. 3D, Fig. S5).

Keszei and Sicheri (2017) demonstrated that mutation of residues in the Thumb region of the IpaH9.8 E3 domain (corresponding to SspH1 Y642 and R663), well removed from the catalytic cysteine, reduced binding of free Ube2D2 to IpaH9.8 and decreased the ability to form an IpaH9.8~Ub intermediate (16). We observe similar behavior for SspH1 and have further localized the region that binds Ube2D3~Ub using a combination of mutational analysis and paramagnetic spin-labels in NMR-based experiments. In SspH1, the tip segment of the Thumb is bounded by the conserved residues Y642 on the N-terminal side and G666 on the C-terminal side (Fig. 4A). Single point mutations within this region (L655A, A661Q, and G666A) abrogate the ability of the SspH1 E3 domain to synthesize unanchored poly-Ubiquitin chains (Fig. 4A,B). Thus, even a relatively conservative substitution of Ala for G666, a residue that shows >98% conservation within SspH/IpaH E3s, greatly reduced the ability of Ube2D3-O-Ub to interact with the SspH1 E3 domain (Fig. 4C). This behavior is not restricted to SspH1 as loss of E3 ligase activity was also observed when the corresponding mutation G754A was introduced into the SspH2 E3 domain

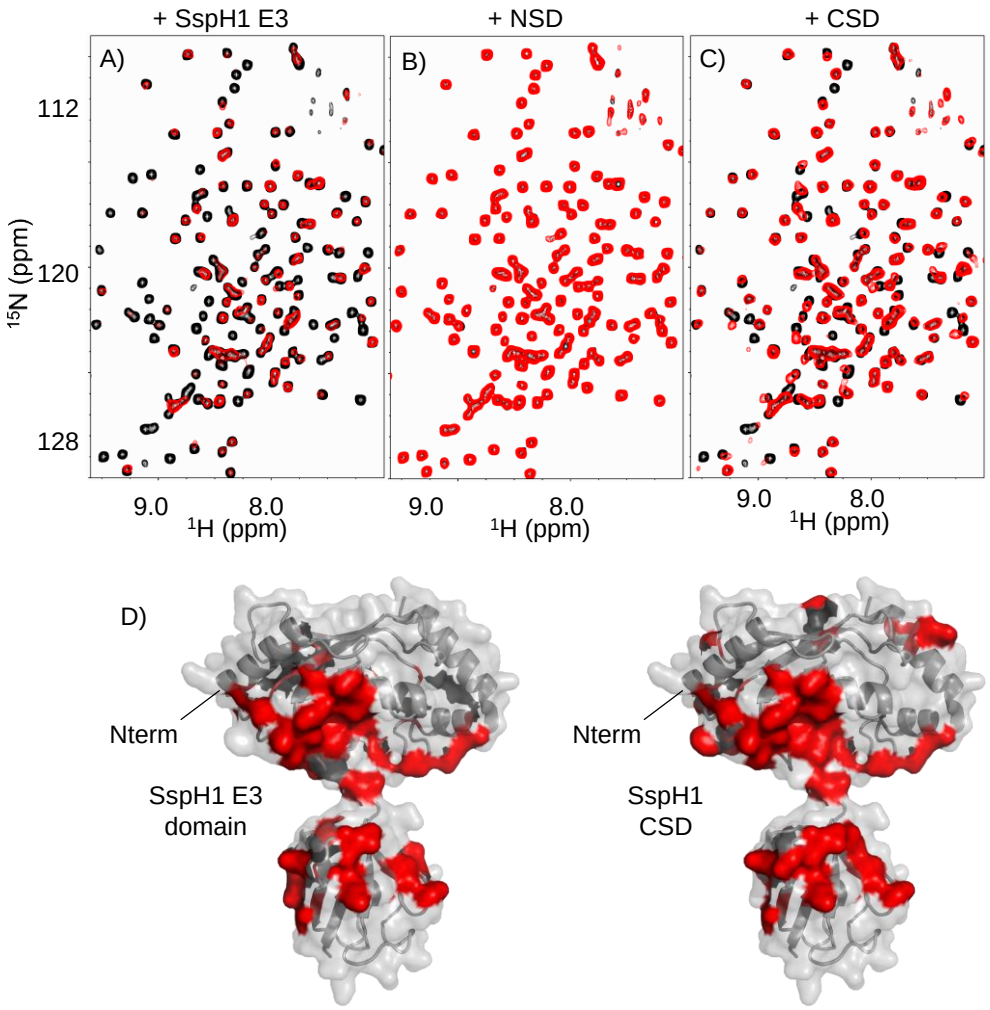

Figure 3. Ube2D3~Ub binding is localized to the SspH1 CSD. ^{1}H,^{15}N-TROSY NMR spectral overlays of ^{15}N-Ube2D3-O-Ub alone (black spectra) or in the presence (red spectra) of SspH1 E3 domain. A) 100µM Ube2D3-O-Ub +/- 50µM SspH1 E3 domain. **B**) 200µM Ube2D3-O-Ub +/- 200µM NSD. (**C**) 200µM Ube2D3-O-Ub +/- 200µM CSD . (**D**) Ube2D3-Ub residues whose resonances are perturbed upon binding to the SspH1 E3 domain or CSD are plotted on a surface structure representation of the Ube2D3~Ub conjugate (PDB # 3UGB (53)).

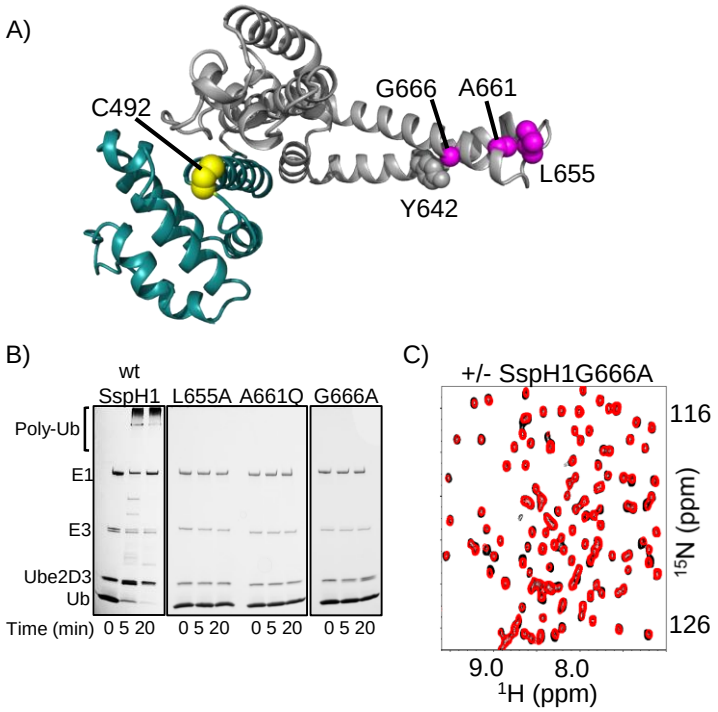

Figure 4. Tip segment of CSD Thumb region, bounded by Y642 and G666, is required for binding Ube2D3~Ub conjugate**. (A)** Structure of the SspH2 E3 domain (SspH1 numbering) showing the NSD (cyan) and catalytic C492 (yellow spheres) and the CSD (gray). Residues in the tip segment targeted for mutagenesis are shown as magenta spheres. **(B)** Single point mutants L655A, A661Q, and G666A abrogate the ability of SspH1 E3 domain to synthesize unanchored polyubiquitin chains. Assay conditions: 1μM E1, 5μM Ube2D3, 2μM SspH1, 50μM Ub, 5mM $MgCl_2$, 5mM ATP, pH7, 37°C. **(C)** $^{1}H,^{15}N$-TROSY NMR spectral overlay of 100μM ^{15}N-Ube2D3-O-Ub in the absence (black spectrum) and presence of 50μM G666A SspH1 E3 domain (red spectrum). Only minor perturbations of Ube2D3-O-Ub resonances are observed indicating reduced binding affinity.

(Fig. S4C). Overall, our mutagenesis results show that the integrity of the Thumb tip segment is critical for binding Ube2D3~Ub and, therefore, E3 activity.

To further characterize binding of Ube2D3~Ub to SspH1, we utilized paramagnetic spin labels incorporated at various positions in the SspH1 E3 domain. Iodoacetamido-TEMPO was used to covalently modify individual cysteine residues introduced at specific sites in the SspH1 E3 domain (Fig. 5A). The unpaired paramagnetic electron in TEMPO selectively broadens the NMR resonances of residues in proximity to the spin label. TEMPO-SspH1 was added to ^{15}N-labeled Ube2D3-O-Ub and ^{1}H,^{15}N-TROSY spectra were collected before (SL-active) and after (SL-quenched) addition of ascorbate (Fig. 5B), which eliminated the paramagnetic effect. Resonance perturbations specifically induced by paramagnetic TEMPO were quantified by analyzing peak intensities in the SL-active and SL-quenched spectra and the corresponding residues were mapped onto a surface representation of the Ube2D3~Ub conjugate (Fig. 5C). It should be noted that the intensities of Ube2D3-O-Ub resonances located at the E2~Ub conjugate/SspH1 interface are significantly reduced due to exchange broadening caused by binding to SspH1 (Fig. 3A, Fig. S5A). Therefore, weak resonances that fall below one standard deviation from the average intensity, as well as resonances that could not be adequately resolved, were omitted from the analysis.

The E3 domain has only a single cysteine residue, the active site C492. As the E3 active site must come into proximity of the Ube2D3~Ub active site, C492 provides a convenient location for incorporation of a spin-label (termed SL492). As shown in Figure 5, SL492 has a highly localized effect on Ube2D3-O-Ub resonances in the SspH1 E3/Ube2D3-O-Ub complex. SL492 results in selective perturbation of Ube2D3 residues 81, 83, 89, 92, 117, and 120-125 (Fig. 5B, Fig. S6A). These residues surround an entrance to the E2~Ub conjugate active site that is opposite the surface that makes direct contact to the CSD (compare Fig. 3D to Fig. 5C). Importantly, the

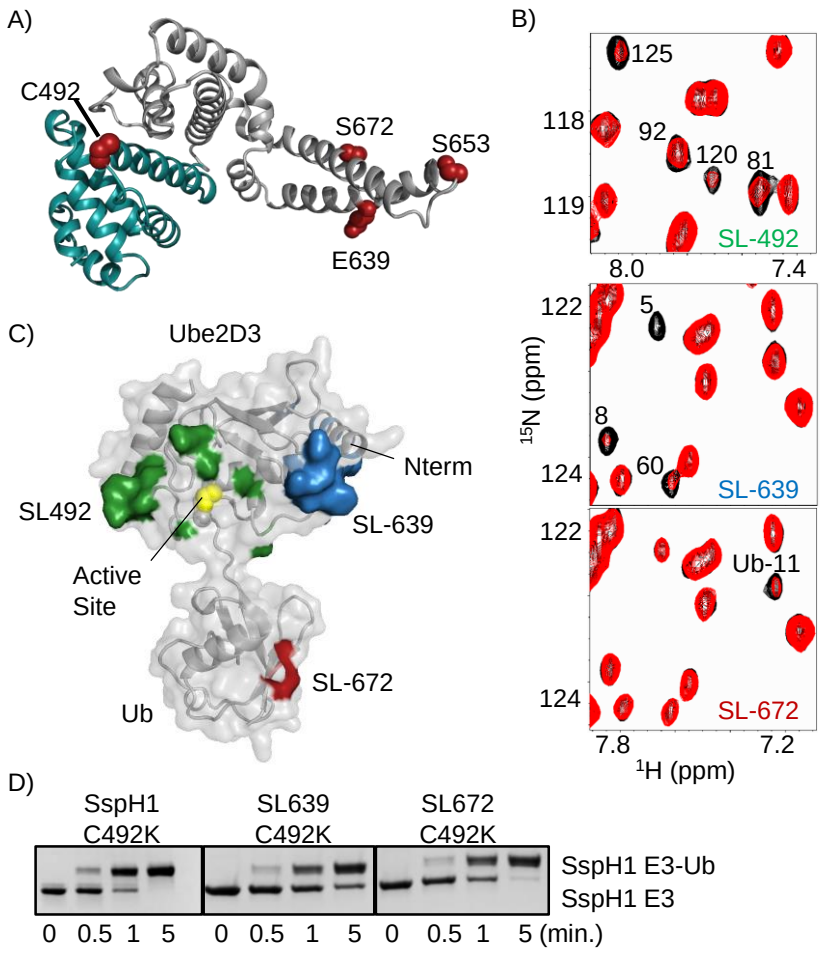

Figure 5. Ube2D3~Ub binding to CSD Thumb helices places the E2~Ub thioester bond in a reactive conformation. **(A)** Structure of the SspH2 E3 domain (SspH1 numbering) showing the locations of C492, E639, S653, and S672 (red spheres) where TEMPO spin labels were incorporated into the E3 domain. **(B)** ^{1}H-^{15}N-TROSY spectral overlays of 150μM ^{15}N-Ube2D3-O-Ub in the presence of SL-active (red spectra) and SL-quenched (black spectra) SspH1 E3 domains. **C)** Resonance perturbations specifically induced by spin labels mapped onto a surface representation of Ube2D3-O-Ub. SL639 preferentially broadens peaks corresponding to Ube2D3 (blue surface). SL672 preferentially broadens peaks in the Ub subunit (red surface). The surfaces defined by SL639 and SL672 are adjacent to the E2 and Ub binding surfaces the make direct contact with the E3 domain of Ssph1 (compare with **Fig. 3D**). SL492 (green surface) affects residues surrounding an entrance to the E2~Ub active site. **(D)** SL639 and SL672 form productive complexes with Ube2D3~Ub as shown by the ability to transfer Ub to the E3 active site of SspH1 C492K. Reaction conditions were 1μM E1, 2μM Ube2D3, 5μM SspH1, 100μM Ub, 5mM $MgCl_2$, 5mM ATP, pH7, 37°C

NMR data collected in solution reveal the direction from which the E3 catalytic cysteine approaches the E2~Ub conjugate active site as it is presented by the CSD (Fig. 5C, green surface).

TEMPO spin-labels were incorporated at three other sites in the SspH1 domain. In combination with an active site C492A mutation, E639, S653, or S672 were individually changed to Cys to allow for single-site labeling within the SspH1 Thumb region (Fig. 5A). SL653, located at the tip of the Thumb, effectively abrogated binding of Ube2D3-O-Ub, presumably due to steric interference with the incoming E2~Ub conjugate (Fig. S7A). In contrast, variants in which a bulky spin label was incorporated at positions SL639 and SL672, adjacent to SspH1 tip segment, do bind Ube2D3-O-Ub allowing their further characterization. Based on the structures of SspH2 and IpaH3, these two positions are located near the base of the thumb on opposite surfaces of the anti-parallel Thumb helices. In SspH2 and IpaH3, the α-carbons of the corresponding residues are separated by only 11.4Å or 14.5Å, respectively. Despite their proximity, SL639 and SL672 perturb distinct resonances in different subunits of the Ube2D3~Ub conjugate: SL639 affects E2 resonances (Ube2D3 residues 5, 8 and 9 in helix 1, residues 59, 60, 62 and 63 in loop 4, and residues 96, 98, 99 in loop 7) and SL672 affects only Ub resonances corresponding to residues 11, 12, and 44. (Fig. 5B, Fig. S6B,C). The results are mapped onto the surface of the Ube2D3~Ub conjugate in blue and red, respectively (Fig. 5C).

The pattern of chemical shift perturbations observed for ^{15}N-labeled Ube2D3-O-Ub in the presence of reduced SL639 and SL672, where the paramagnetic effect has been eliminated, is similar to that observed for binding to wild-type SspH1 E3 domain (Fig. S7B). These data show that Ube2D3-O-Ub interacts with SL639 and SL672 in much the same way as with wild-type SspH1. To further verify that SL639 and SL672 form productive complexes with Ube2D3~Ub, we developed a Ub transfer assay that is not dependent on an active site cysteine, C492, which

must be removed for selective introduction of spin labels at positions 632 and 672. We found that interaction of Ube2D3~Ub with the SspH1 E3 domain enhances the intrinsic lysine reactivity of the E2~Ub conjugate relative to Ube2D3~Ub alone (Fig. S9B). Building on this observation, we replaced the SspH1 active site Cys with a Lys (C492K) generating an SspH1 E3 construct that transfers Ub to the Lys residue at the active site position. The product is an E3-Ub species with Ub covalently linked to the E3 via an isopeptide bond. Analysis by reducing SDS-PAGE shows that addition of C492K SspH1 E3 to a ubiquitylation reaction mixture results in rapid formation of a stable E3-Ub species that does not form when using a C492A mutant (Fig. S7C). Using C492K SspH1, spin labels can be selectively introduced at positions 639 and 672. As shown in Fig. 5D, both C492K-SL639 and C492K-SL672 are functional in Ub transfer to the E3 active site forming a stable E3-Ub species. Therefore, Stage I of the Ub transfer reaction, from E2~Ub to the E3 active site residue, is still functional in the presence of these SspH1 modifications. The finding that spin label modifications adjacent to the tip segment of the Thumb region do not disrupt E2~Ub binding, combined with mutations within the tip segment that nearly eliminate the interaction, argue strongly that E2~Ub binding is localized to the tip segment of the Thumb region. Furthermore, the data obtained using selective spin labeling are consistent with a model in which the E2 subunit binds on one side of the Thumb region and the Ub subunit on the other.

The SspH1 E2~Ub binding site is dynamic

Available SspH/IpaH E3 structures exhibit conformational heterogeneity in the tip segment of the Thumb region that we show is required for E2~Ub binding. For instance, SspH2 contains two well-ordered anti-parallel helices, whereas IpaH1.4, IpaH4, IpaH9.8, and SlrP exhibit a pronounced kink in the penultimate helix of the thumb region, and the electron density for this

segment is absent in the structure of IpaH3 (Fig. S2). Which, if any, of the available SspH/IpaH E3 structures represents a conformation poised to bind Ube2D~Ub is not clear and the observed heterogeneity may be indicative of dynamics in this region. To characterize the behavior of the E2~Ub conjugate binding region, we performed hydrogen/deuterium exchange combined with mass spectrometry (HDX-MS) on the E3 domain of SspH1. HDX-MS provides insight into local protein conformation and dynamics (25).

Hydrogen/Deuterium exchange reactions were carried out for varying amounts of time by incubating the protein in buffered D_2O followed by quenching in ice-cold buffer at pH 2.5. Quenched solutions were processed using standard protocols (see methods) and the masses of peptides derived from the E3 domain were obtained by mass spectrometry. Three peptides arising from the Thumb region were identified and confirmed by MS-MS fragmentation. Time courses plotting peptide fractional deuteration with time are shown in Figure 6A (mass spectra in Fig. S8). The peptide segment that encompasses the region required for E2~Ub binding (SspH1 residues 651-668; shown in orange in panels A and B) undergoes rapid H/D exchange and is nearly completely exchanged at the earliest time point (3 sec). In contrast, flanking regions that are helical in all structures (shown in green and blue) undergo much slower exchange. The data are consistent with a model in which the SspH1 Ube2D~Ub binding region lacks higly ordered secondary structure allowing facile exchange of backbone amide protons in this region. Thus, the available crystal structures may each represent one of multiple possible conformational states. The dynamic behavior of the SspH1 E2~Ub binding region stands in stark contrast to the well-structured E2-binding regions that have been characterized for eukaryotic RING, RBR, and HECT E3s (26-30).

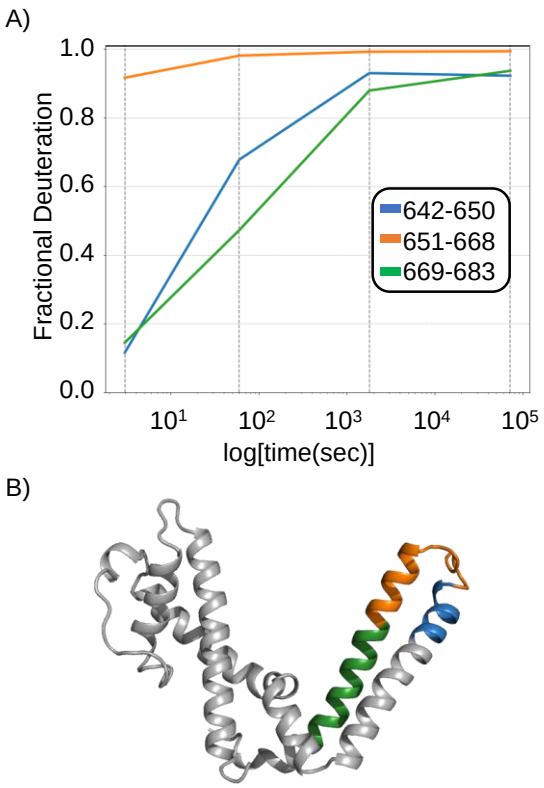

Figure 6. Hydrogen/deuterium exchange mass spectrometry (HDX-MS) reveals a dynamic Ube2D~Ub binding site. **(A)** HDX-MS curves for three peptides in the thumb region of the SspH1 CSD are shown for residues 642-650 (blue), 651-668 (orange) and 669-683 (green). Fractional deuteration of each peptide at 3s, 1m, 30m, and 20hr time points is plotted relative to each respective fully deuterated peptide. **(B)** The locations of the three peptides highlighted from HDX-MS data are depicted on the structure of SspH2.

Mutations designed to block NSD/CSD conformational changes inhibit Ub-transfer

The Ub transfer mechanism employed by HECT and SspH/IpaH E3s requires that the E3 active site Cys be positioned to react with the E2~Ub conjugate active site in the E3/E2~Ub complex. The identified E2~Ub binding site on SspH1 is distant from the E3 active site Cys, suggesting that the E3 must undergo a large conformational change for Ub transfer to occur. The different E3 domain conformations observed in SspH/IpaH crystal structures coupled with our finding that the SspH1 E3 domain can be partitioned into separate N-terminal and C-terminal subdomains led us to hypothesize that movements of the two domains may be required for coordinated Ub transfer. ConSurf analysis (31,32) of the SspH/IpaH family revealed a highly conserved Gly residue (G515) in the short linker connecting the NSD to the CSD at a position far removed both from the E3 active site and E2~Ub binding region (Fig. 7A). Substitution of Gly515 with a more conformationally constrained proline greatly reduces the ability of SspH1 to catalyze the ubiquitylation of PKN1 HRab (Fig. 7B). Though not as effective as the wild-type enzyme, G515P SspH1 still catalyzes the net hydrolysis of Ube2D3~Ub to free E2 and Ub as demonstrated in single turnover experiments, (Fig. 7C). The reaction is dependent on the SspH1 active site cysteine (Fig. S9A) and, therefore, formation of an E3~Ub intermediate. The results demonstrate that SspH1 G515P can still bind E2~Ub conjugate and form an E3~Ub thioester intermediate. Thus, it appears that flexibility in the linker between the NSD and CSD, far removed from the E3 catalytic site, is critical for Ub transfer to substrate.

To further investigate the role for inter-domain movement, we compared residues in the NSD/CSD interface in existing SspH/IpaH E3 structures to identify residues that are likely to be solvent exposed in one conformation and buried in the other. Our goal was to bias or trap SspH1 in one of the two E3 conformational states. To aid the identification of a target for mutagenesis,

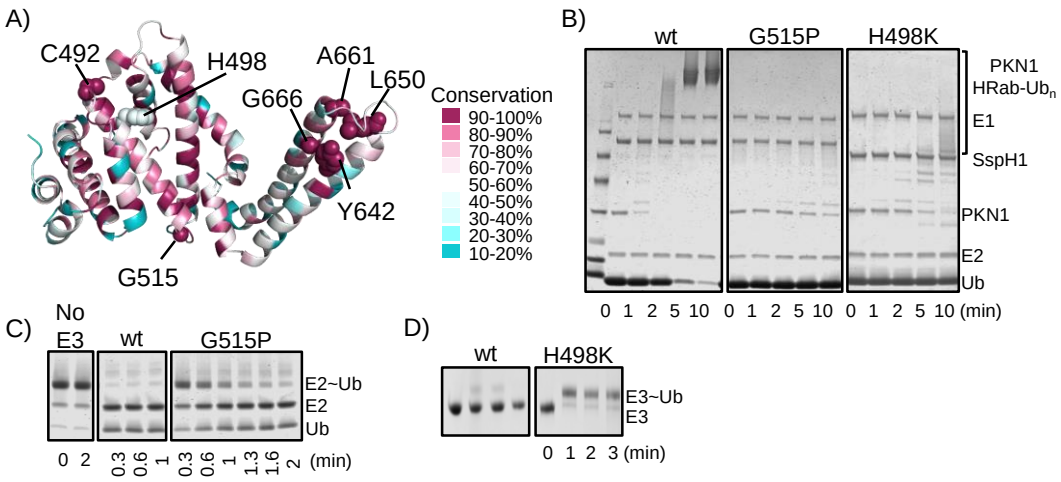

Figure 7. Mutations designed to restrict NSD and CSD conformations impair SspH1 ubiquitylation activity. **A)** Consurf analysis, comparing the amino sequences of 164 different SspH/IpaH E3 domains, showing the location of conserved residues in the SspH/IpaH family of E3s plotted onto a ribbon structure of the SspH2 E3 domain. Highly conserved residues are shown in dark magenta. The positions of active site C492 (SspH1 numbering) and other residues discussed in the text are shown as spheres. **B)** Ubiquitylation assays with G515P and H498K SspH1 E3 mutants show decreased ability of SspH1 to ubiquitylate the PKN1 substrate. Assays were performed using 1uM wheat E1, 5μM Ube2D3, 2μM SspH1, 5μM PKN1 1-201 (rHRab), 100μM Ub, 5mM $MgCl_2$, pH7, at 37°C. Reactions were initiated by the addition of 5mM ATP. **C)** Single turnover assays following wild-type and G515P SspH1 catalyzed net hydrolysis of the Ube2D3~Ub conjugate to free Ube2D3 and Ub. Assays were performed using 20μM Ube2D3~Ub and 8μM SspH1 at pH 7 and 37°C. Aliquots were quenched in non-reducing SDS sample buffer and analyzed by non-reducing SDS-PAGE. **D)** Ubiquitylation assays for wt and H498K SspH1, as described in panel B, analyzed by non-reducing SDS-Page. The results show the accumulation of high steady state levels of SspH1 H498K~Ub intermediates in the reaction mixture that persist long after the wild-type reaction is complete.

we generated two SspH1 homology models using the Swiss PDB webserver based on the structures of IpaH3 and SspH2 (Fig. S10A) (33). The model based on IpaH3 yields an SspH1 conformation in which the NSD catalytic residue C492 is closer to the Ube2D3~Ub binding region in the CSD and is referred to as the "proximal" conformation (see also Fig. S2C). The "distal" conformation is based on the structure of SspH2 in which the active site Cys is further from the E2~Ub conjugate binding site. Comparison of these models identified SspH1 H498 in Helix 6 of the NSD, downstream of the catalytic residue C492, as a residue predicted to be in different environments in the two different E3 conformational states; solvent exposed in the proximal model and buried in the distal model. H498 is not highly conserved within the E3 family: ConSurf analysis shows that Leu, His, and Phe residues all occur at this site (Fig. 7A). Therefore, any observed differences in activity assays of H498 mutants are unlikely to be due to mutation of a critical catalytic residue.

We chose to substitute His498 with Lys to disfavor the conformational state in which it would be buried and tested its ability to ubiquitylate the PKN1-HRab substrate. As predicted from our model, introduction of the H498K mutation into the SspH1 LRR-E3 construct substantially inhibits the ability of the enzyme to ubiquitylate PKN1. Under our assay conditions, the wild-type-catalyzed reaction was essentially complete after ~5 minutes with nearly all the free Ub in the reaction mixture depleted (Fig. 7B). In contrast, the H498K reaction shows synthesis of shorter poly-Ub chains and much slower ubiquitylation of PKN1 and depletion of free Ub (Fig. 7B). A variety of other mutations at this position were also tested to confirm that residues more similar to the wild-type histidine show greater ability to ubiquitylate substrate (Fig. S9C).

To ascertain what step(s) of the Ub transfer reaction are slower in the H498K mutant, we analyzed reaction mixtures by non-reducing SDS-PAGE to enable visualization of labile E2~Ub and E3~Ub species. After ~2 minutes, an E3~Ub intermediate is observed for both the wild-type

and H498K catalyzed reactions, though the steady-state level is much higher for the H498K mutant and persists much longer in the reaction mixture, well after the wild-type reaction is complete (Fig. 7D). Therefore, this mutant can efficiently carry out transfer of Ub from the E2~Ub conjugate to its own active site but is disabled in its ability to pass Ub to substrate. Importantly, NMR experiments confirm that the H498K mutation does not affect the interaction of the E3 domain with ^{15}N-labeled Ube2D3-O-Ub (Fig. S9D). Thus, the H498K mutation designed to bias the E3 domain toward a proximal conformation appears to have generated a form of SspH1 that can readily undergo the first step of the Ub transfer reaction in which E2~Ub binds the E3 and transfers the activated Ub to the E3 active site but is handicapped in its ability to perform the second Ub transfer step from its own active site to substrate.

Discussion

Eukaryotic E3 Ubiquitin Ligases are characterized by a diverse set of functional topologies that are typically classified into RING/U-box, HECT, and RBR E3s (8). Certain types of pathogenic bacteria, such as the gram-negative pathogens *Salmonella* and *Shigella*, add to this diversity utilizing topologically distinct E3s that are directly introduced into host cells during pathogenesis (2,3). These enzymes must operate and compete in the same environment with host E3s and other proteins for E2~Ub conjugates and host targets to generate specific Ub signals advantageous to the pathogen. Thus, like for their eukaryotic counterparts, it is necessary to understand the mechanism of Ub transfer catalyzed by bacterial E3s, how these enzymes recognize host proteins, and how they assemble multiple proteins into competent E3 Ub ligase complexes that catalyze regulated Ub transfer. As described herein, SspH/IpaH E3s share certain characteristics with their eukaryotic counterparts but have developed new mechanisms for

interacting with the host ubiquitylation machinery to exploit ubiquitin signaling in support of pathogenesis.

Much of the recent literature on SspH/IpaH E3s has focused on the large reorientation of the LRR and E3 domains observed in various crystal structures (16,22,34). Our further analysis of these structures revealed that multiple conformations are present in the E3 domains. The available structures tend to adopt one of two different conformations: a proximal conformation, in which the catalytic cysteine is closer to the Thumb region, and a distal conformation in which the catalytic cysteine is further away (Fig. 1D). Our analysis suggests that the two conformations can be interconverted by rigid-body rotation of the NSD (helices 1-6) ~20° relative to the CSD (helices 7-13). The different conformations alter the position of the catalytic cysteine relative to the CSD by at least 21Å.

Is a conformational change in the SspH1 E3 domain required for Ub transfer to substrate in solution? Three of our findings directly address this question. First, the pivot for this rotation resides in the loop linking the NSD and CSD. Mutation of a highly conserved Gly residue in the linker, located over 35Å away from the active site Cys, to a conformationally restricted Pro residue (SspH1 G515P) disrupts the ability of SspH1 to transfer Ub to substrate (Fig. 7A,B). Nonetheless, SspH1 G515P is still capable of catalyzing the breakdown of Ube2D3~Ub to free E2 and Ub (Fig. 7C), a reaction that requires the SspH1 catalytic Cys and formation of an E3~Ub intermediate (Fig. S9A). Therefore, the E3 active site can still access the E2~Ub conjugate active site in this mutant. Second, the non-conserved residue H498, ~10Å away from the active site C492, is predicted to be solvent exposed in the proximal conformation but buried in the distal conformation. Mutation to Lys (SspH1 H498K) also disrupts Ub transfer to substrate (Fig. 7A,B). An unexpected result obtained with SspH1 H498K is that we observe a high steady-state level of an SspH1~Ub

intermediate in solution (Fig. 7D). Third, the ability to physically separate the NSD and CSD into constructs that are soluble and retain tertiary structures similar to that found in the full E3 domain shows that the NSD and CSD can function semi-independently, consistent with the hypothesis that these domains can change position relative to each other. Our findings with SspH1 H498K and G515P demonstrate that formation of an E3~Ub intermediate is not sufficient for substrate ubiquitylation. An additional step is required. Based on our analysis of available crystal structures and the data presented herein, the additional step is consistent with a conformational change involving the NSD and CSD within the SspH1 E3 domain.

What are the roles of the individual SspH1 E3 subdomains and how do they coordinate to effect Ub transfer to substrate? Our NMR studies show that although the NSD harbors the active site Cys required for generating an E3~Ub intermediate, no interaction with Ube2D3~Ub was detected even at the high concentrations used in NMR experiments (Fig. S5B). Instead, E2~Ub binding is a function limited to the CSD. The Ube2D~Ub binding site appears to be localized to the tip of the Thumb segment bounded by the conserved residues Y642 in Helix12 and G666 in Helix13 of SspH1 (Fig. 4). Mutations introduced within this segment, including introduction of a spin label at position S653, negatively impact E2~Ub binding and SspH1 activity. Even a relatively conservative mutation (SspH1 G666A) can have a profound effect. In the structure of the SspH2 E3 domain, which is highly homologous to the SspH1 E3 domain and shares ~77% sequence identity, the structurally conserved Gly (> 98% conservation within the E3 family) is located in the middle of the long terminal helix that completes the Thumb region. Changing G666 to alanine, a residue with much higher helix propensity than Gly, would not be predicted to introduce any steric clashes with other residues or alter the conformation observed in the SspH2 crystal structure. Nonetheless, SspH1 G666A significantly disrupts binding of Ube2D3~Ub to SspH1 and,

therefore, Ub transfer to substrate (Fig. 4C). The same mutation introduced into SspH2, G754A, also perturbs the ability of the SspH2 E3 domain to synthesize unanchored poly-Ub chains (Fig. S4C). On the other hand, introduction of bulky spin-labels at sites immediately flanking the tip segment of the SspH1 Thumb (SL639 and SL672) still form productive complexes with Ube2D3~Ub (Fig. 5D, Fig. S7B). Therefore, a segment of SspH1 spanning ~22 residues in the tip segment of the Thumb region is necessary for binding Ube2D~Ub and SspH1 activity.

Canonical binding sites have been described for eukaryotic RING, HECT, and RBR E3s. All these families have recognizable topologies that interact with an E2 surface generally comprised of residues located in Helix1, Loop4, and Loop 7 of the E2 domain (9,35). This is not the case for SspH1 and the Ube2D~Ub binding site is not analogous to that described for any eukaryotic E3/E2~Ub interface. SspH1 (this work) and SspH2 (17) recognize a distinct surface of Ube2D3 that does not include Helix1 but involves a number of residues in Helix2. Among the family of human E2s that carry activated Ub, this region is variable (Fig. S10B,C). Thus, recognition of this Ube2D surface segment is consistent with the observed E2 selectivity of SspH/IpaH E3s. Furthermore, in solution, HDX-MS experiments show the Ube2D~Ub binding region of SspH1 is dynamic, a finding that contrasts with the stable E2 interfaces generally found in eukaryotic E3 Ub ligases. This behavior was not expected based on the highly homologous SspH2 crystal structure, but is consistent with the structural variability observed in this region in other SspH/IpaH E3 ligases. Structures of IpaH1.4, IpaH4, IpaH9.8, and SlrP show a defined kink in the penultimate helix of the Thumb region. Perhaps more pertinent, the electron density of the tip segment is absent in the structure of IpaH3 (Fig. S2). Thus, the various crystal structures may represent snapshots of possible Thumb E2~Ub binding site conformational states. Resonance assignments of CSD backbone atoms could further address this issue for the solution state of

SspH1. Unfortunately, though 2D $^{1}H,^{15}N$-TROSY spectra of the CSD show significant improvements over the spectra of the full E3 domain, we have so far been unable to collect a full suite of suitable 3D data to allow for complete backbone assignments. Thus, whether all family members harbor dynamic E2~Ub binding sites and which conformation recognizes Ube2D~Ub remain open questions.

How does Ube2D~Ub binding to the tip segment of the SspH1 Thumb region orient the E2~Ub conjugate and E3 active sites to accomplish the first step of Ub transfer? Our NMR mapping studies show that both Ube2D and Ub subunits are required for binding to the E3 (Fig. 3) and spin-labeling experiments are consistent with a mode of binding in which the Ube2D and Ub subunits of the conjugate grasp onto opposite sides of the tip segment of the SspH1 Thumb region. Using both the Ube2D3 and Ub subunits to grasp the Thumb would bring these subunits closer to each other, a model for binding that is consistent with the observed reactivity of the SspH1/Ube2D3~Ub complex. Interaction of Ube2D3~Ub with SspH1 enhances the intrinsic reactivity of the E2~Ub conjugate toward free Lys in solution and allows transfer Ub to a Lys substituted at the SspH1 active site (Fig. 5D, Fig. S9B). This is relevant to our binding model as recent work has shown that not all conformations of the Ube2D~Ub conjugate are equally reactive toward Lys, behavior that is particularly well documented for Ube2D~Ub (9,36-38). In solution, the free Ube2D~Ub conjugate is dynamic and, though tethered, the two subunits can move independently relative to each other (39). Interaction of Ube2D~Ub with several eukaryotic RING E3s has been shown to shift the population of conformational states toward a “closed” Ube2D~Ub conformation in which the Ub subunit can make direct contact with Helix 2 of the E2 subunit (29,36,40,41). This closed conformation is more reactive in aminolysis with the ε-amino group of a Lys residue. Transthiolation, however, is less dependent on the conformation of Ube2D~Ub.

Eukaryotic HECT-type E3s bind E2~Ub conjugates in a conformation that promotes transthiolation and disfavors aminolysis (38). The eukaryotic HECT E3 NEDD4L and RBR E3 HHARI have been shown to promote an "open" E2~Ub conformation in which the Ub subunit is held away from the E2 domain (27,37-38). As shown for Ube2D3~Ub stabilized in an open conformation, the conjugate can still undergo facile transthiolation, but reactivity towards Lys is greatly reduced (42). For the SspH1/Ube2D~Ub complex there does not appear to be a direct interaction between the E2 and Ub subunits outside of the E2~Ub conjugate active site. However, binding of Ube2D~Ub to opposite sides of the SspH1 Thumb would result in a "semi-closed" E2~Ub conformation, a conformation that must be more reactive toward Lys (Fig. 5D).

The way Ube2D~Ub binds SspH1 positions the E2~Ub conjugate thioester for a trans-thiolation reaction with the E3 active site Cys. A spin label attached to the E3 active site (SL-492) reveals the direction from which the E3 catalytic Cys enters the E2~Ub conjugate active site, approaching from the side defined by Ube2D residues 81, 83, 89, 92, 117, and 120-125. This direction of approach is similar to that captured in the structure of Ube2D2-O-Ub bound to the HECT E3 NEDD4L (27). HECT E3 domains like NEDD4L, can be divided into an N-Lobe subdomain, which binds activated E2~Ub, and a C-Lobe subdomain that harbors an active site cysteine residue. In the structure of the complex, the C-lobe of NEDD4L approaches the E2~Ub conjugate active site from the same direction as the SspH1 catalytic Cys. Intriguingly, this direction of approach was also observed for the substrate Lys of RanGAP1 modified with the ubiquitin-like protein SUMO in the Ubc9 active site (43,44). Thus, this approach into the E2~Ub conjugate active site is exploited by both prokaryotic and eukaryotic E3 ligases.

Overall, our results are consistent with a mechanism where Ube2D~Ub clamps onto the thumb region of the CSD positioned to react with the E3 active site Cys (Fig. 8B). We propose

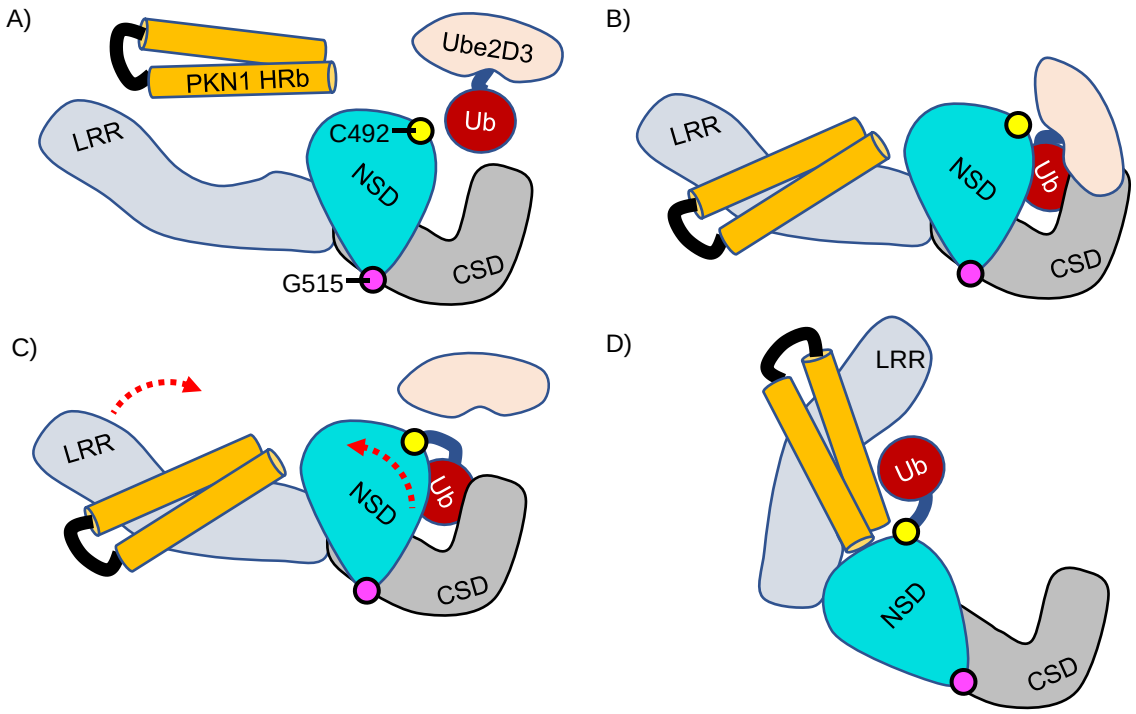

Figure 8. Proposed mechanism and domain motions for SspH/IpaH catalyzed Ub transfer. **A)** For Ub transfer, SspH1 must bind both substrate (PKN1 HRb domain) and an activated E2~Ub conjugate (Ube2D3~Ub). Though tethered, in solution the Ub and E2 subunits of Ube2D3~Ub can move independently of each other and primarily occupy an open conformation. **B)** Both subunits of the Ube2D3~Ub conjugate grasp onto the thumb region of the CSD adopting a semi-closed conformation. The resulting orientation positions the E2~Ub active site to react with the E3 active site cysteine when the NSD in the proximal conformation of the E3 domain. The trans-thiolation reaction could be further facilitated by the flexibility of the E2~Ub binding region. **C)** After Ub is transferred to the E3 active site, Ube2D3 dissociates from the complex. **D)** The E3 domain undergoes a conformational change to the distal conformation, with the NSD pivoting towards the substrate bound to the LRR domain. This motion is aided by the flexibility of the linker (magenta) connecting the NSD and CSD. This motion may occur in concert with a large conformational change involving a large conformational change in the relative position of the LRR and E3 domains. The result is that Ub is brought into proximity of the substrate, where it is transferred from the E3 active site to a substrate lysine.

that the proximal conformation in which the active site Cys is ~21Å closer to the thumb region is the most likely to react with the E2~Ub conjugate. Binding of Ube2D~Ub to the E3 and/or transfer of Ub to the catalytic Cys in the NSD may be further aided by the flexibility of the tip segment of the Thumb region. After formation of the SspH1~Ub activated intermediate, Ube2D dissociates from the enzyme (Fig. 8C). Subsequently, the E3 domain must undergo a conformational change to the distal conformation which brings the activated Ub now attached to the E3 active site Cys into position to react with substrate (Fig. 8D). We note that in the structure of SspH2 LRR-E3 (14), the E3 domain is in a distal conformation and the LRR domain is very close to the active site Cys, suggesting that this may be closer to the conformation that is poised to carry out the ultimate Ub transfer step. Therefore, it is possible that movements of the LRR domain and the proximal-to-distal conformational change within the E3 domain are closely coordinated. Though the topology of SspH/IpaH E3s is not shared by its eukaryotic counterparts, the formation of an obligate E3~Ub intermediate and modular domains that must coordinate to effect Ub transfer are characteristics shared with eukaryotic HECT-like E3s. Large domain re-orientations between HECT and RBR E3 sub-domains are required to facilitate Ub transfer. Thus, engaging the E2~Ub conjugate in a region distinct from the active site appears to be a universal property of mechanistic HECT-like E3s, and large conformational changes exist to facilitate Ub transfer amongst E2, E3 and substrate.

Experimental Procedures

Protein Expression, Purification, and Paramagnetic Spin-Label Conjugation.

DNA sequences for SspH1, SspH2 and PKN1 constructs were cloned into pET28 vectors in frame with an N-terminal hexahistidine tag followed by a thrombin-cleavage sequence; mutations were generated by the QuickChange protocol. His-tags were not removed unless

otherwise indicated. The DNA sequences for UbcH5c and UbcH5c C85S S22R ("CSSR") were cloned into pET28 vectors out of frame of tags. Proteins were expressed in *E. coli* BL21(DE3) cells in LB media. ^{15}N-labeled proteins were grown in minimal MOPS media supplemented with $^{15}NH_4Cl$. His-tagged proteins were purified by Ni^{2+} affinity purification; UbcH5c variants were purified by strong-cation exchange chromatography on an SP column (GE Healthcare) via a 0-1M salt gradient in 25mM MES pH 6 at 4°C. The final step of purification for all proteins was size exclusion chromatography over Superdex75 resin equilibrated in 25mM sodium phosphate, 150mM NaCl, pH 7 at 4°C or room temperature. Cloning and purification of human and wheat E1, ubiquitin, and generation of purified UbcH5c-O-Ub were performed as described previously (36-39). Cysteines on spin-labelled proteins were modified with spin label by incubation in 25mM sodium phosphate, 25mM sodium chloride, 1-2mM TCEP, pH 7 overnight at 4°C or 30 minutes at 37°C in the presence of 10X molar excess of iodoacetamide-TEMPO (Sigma-Aldrich) solubilized in DMSO. Excess spin label was removed by buffer exchange via centrifugal filtration.

SEC-MALS and Analytical SEC

For SEC-MALS, purified 50μM SspH1 was separated by size exclusion chromatography over Superdex200 resin equilibrated in 25mM sodium phosphate, 150mM sodium chloride, 1mM DTT, pH 7. Multi-angle light scattering was detected using a Wyatt mini-Dawn Treos and differential refractive index was detected using a Wyatt Optilab T-rEX. Molecular weight was determined using Wyatt Astra 6.1 software. For Analytical SEC, 50μM SspH1 E3 domain, 50μM LRR-E3 domain, or 50μM LRR-E3 domain in complex with 75μM PKN1 108-201 (HRb region) was eluted on a 24mL GE Superose6 10/300 GL equilibrated in 25mM sodium phosphate, 150mM sodium chloride, pH 7 at room temperature. Molecular weight standards were 1mg/mL alcohol

dehydrogenase (Sigma-Aldrich, 145kDa), 1mg/mL bovine serum albumin (New England Biolabs, 66kDa), and 100μM Ube2D3 (17kDa).

Ubiquitylation Assays

Ubiquitylation assays were performed in 25mM sodium phosphate, 150mM sodium chloride, pH 7 buffer at 37°C using 1μM human or wheat E1 (UBA1), 5μM E2 Ube2D3, 2μM E3, 50μM or 100μM Ub, 5μM PKN1 1-201 (HRab region) or 108-201 (HRb region), 5mM $MgCl_2$, and 5mM ATP. Reactions were initiated by addition of ATP. Sampled time points were taken by addition of 5μL reaction mixture to 5μL reducing or nonreducing SDS-PAGE load dye followed by boiling (for reduced samples) or incubation on ice (for nonreduced samples) prior to electrophoresis of 7.5μL final sample volume on a 4-20% gradient SDS-PAGE gel (Bio-Rad). Intrinsic Lys reactivity assays were performed with purified 40μM Ube2D3~Ub, 20μM SspH1 and 50mM Lysine at pH 7, 25°C. Gels were visualized by Coomassie staining and imaged on a Licor Odyssey CLx or Bio-Rad Gel Doc.

NMR Spectroscopy

NMR data were collected on a Bruker 500Mhz, or 600 MHz AVANCE with cryoprobe at 25°C. Data were processed using NMRPipe (45) and analyzed using NMRViewJ (46). NMR samples were prepared in standard buffer with the addition of 10% D_2O. Protein concentrations varied from 50-200μM. Paramagnetic spin labels were reduced by addition of 10mM sodium ascorbate in 25mM sodium phosphate, 150mM sodium chloride, pH 7 buffer. Surface structure representations of resonance perturbations were plotted using PyMOL (47) on molecular structures

deposited in the Protein Data Bank at rcsb.org (48). TROSY spectra peaks were assigned using standard three-dimensional sequential assignment techniques as previously described (49).

Hydrogen-Deuterium Exchange Mass Spectrometry.

Hydrogen-deuterium exchange for SspH1 E3 domain (residues 389-700) was initiated by incubating 1 mg/mL protein in deuterated 25mM sodium phosphate, 150mM NaCl pD 7 buffer for 3s, 1m, 30m, or 20hr at room temperature. Exchange was stopped by addition of ice-cold quench buffer (0.2% formic acid, 100mM TCEP, 2M GndCL, pH 2.5). Pepsin digestion was performed during quenching by addition of 3 mg/mL pepsin and incubation on ice for 5m. Undeuterated sample was prepared by incubation in non-deuterated 25mM sodium phosphate, 150mM NaCl pH 7 buffer. Fully deuterated sample was prepared by first preparing a stock of unfolded protein in 4M GndCl and boiling for 30m prior to initiation of exchange, followed by exchange in deuterated 25mM sodium phosphate, 150mM NaCl pD 7 buffer for 30m while boiling. Samples were flash frozen in liquid nitrogen following exchange, quenching and digestion, and stored at -80C. Prior to mass spectrometry, samples were thawed on ice and peptides were separated by liquid chromatography on a C18 column. Mass spectrometry was performed on a Waters Synapt G1. Mass spectra were analyzed by MassLynx software (Waters Corporation), and HX-Express2 (50,51). Peptides were identified using Protein Prospector (52).

Footnotes

Funding was provided by grants from the National Insitutes of Health: R01GM098503 (P.S.B.), R01GM088055 (R.E.K.), T32GM826827 (M.C.), and the University of Washington School of Medicine Hurd Fellowship (M.C.)

Acknowledgments: We would like to thank Katherine Reiter and Tobias Ritterhoff for critical reading of the manuscript.

Conflict of interest: The authors declare that they have no conflicts of interest with the contents of this article

References

1. Cui, J., and Shao, F. (2011) Biochemistry and cell signaling taught by bacterial effectors. *Trends in Biochemical Sciences*. **36**, 532–540
2. Perrett, C.A., Lin, D.Y., Zhou, D. (2011) Interactions of bacterial proteins with host eukaryotic ubiquitin pathways. *Front. Microbiol*. **4(2)**, 143
3. Ashida, H., Kim, M., Sasakawa, C. (2014) Exploitation of the host ubiquitin system by human bacterial pathogens. *Nat. Rev. Microbiol.* **12(6)**, 399-413
4. Komander, D., and Rape, M. (2012) The Ubiquitin Code. *Annu. Rev. Biochem.* **81**, 203–229
5. Huibregtse J, Rohde JR (2014) Hell's BELs: Bacterial E3 Ligases That Exploit the Eukaryotic Ubiquitin Machinery. *PLoS Pathog* **10(8)**, e1004255
6. Ashida, H., Sasakawa, C. (2017) Bacterial E3 ligase effectors exploit host ubiquitin systems. *Curr. Opin. Microbiol.* **35**,16-22
7. Pickart C.M. and Eddins, M.J., (2004) Ubiquitin: structures, functions, mechanisms. *Biochim. Biophys. Acta* **1695(1-3)**, 55-72.
8. Zheng N, Shabek N., (2017) Ubiquitin Ligases: Structure, Function, and Regulation. *Annu. Rev. Biochem.* **86**, 129-157.
9. Stewart M.D., Ritterhoff T., Klevit R.E., Brzovic P.S. (2016) E2 enzymes: more than just middle men. *Cell Res.* **26(4)**, 423-40.
10. Rohde, J. R., Breitkreutz, A., Chenal, A., Sansonetti, P. J., and Parsot, C. (2007) Type III Secretion Effectors of the IpaH Family Are E3 Ubiquitin Ligases. *Cell Host & Microbe*. **1**, 77–83
11. Tanner K., Brzovic P., Rohde J.R. (2015). The bacterial pathogen-ubiquitin interface: lessons learned from Shigella. *Cell Microbiol.* **17(1)**, 35-44.
12. Zhu, Y., Li, H., Hu, L., Wang, J., Zhou, Y., Pang, Z., Liu, L., and Shao, F. (2008) Structure of a Shigella effector reveals a new class of ubiquitin ligases. *Nat Struct Mol Biol.* **15**, 1302–1308
13. Singer, A. U., Rohde, J. R., Lam, R., Skarina, T., Kagan, O., Dileo, R., Chirgadze, N. Y., Cuff, M. E., Joachimiak, A., Tyers, M., Sansonetti, P. J., Parsot, C., and Savchenko, A. (2008) Structure of the Shigella T3SS effector IpaH defines a new class of E3 ubiquitin ligases. *Nat Struct Mol Biol*. **15**, 1293–1301
14. Quezada, C. M., Hicks, S. W., Galan, J. E., and Stebbins, C. E. (2009) A family of Salmonella virulence factors functions as a distinct class of autoregulated E3 ubiquitin ligases. *PNAS*. **106**, 4864–4869
15. Edwards, D. J., Streich, F. C., Ronchi, V. P., Todaro, D. R., and Haas, A. L. (2014) Convergent Evolution in the Assembly of Poly-Ubiquitin Degradation Signals by the Shigella flexneri IpaH9.8 Ligase. *J. Biol. Chem.* **289**, 34114–34128
16. Keszei, A.F., Sicheri, F. (2017) Mechanism of catalysis, E2 recognition, and autoinhibition for the IpaH family of bacterial E3 ubiquitin ligases. *PNAS*. **114(6)**, 1311-1316
17. Levin, I., Eakin, C., Blanc, M.-P., Klevit, R. E., Miller, S. I., and Brzovic, P. S. (2010) Identification of an unconventional E3 binding surface on the UbcH5~Ub conjugate recognized by a pathogenic bacterial E3 ligase. *PNAS*. **107**, 2848–2853
18. Haraga, A., and Miller, S. I. (2003) A Salmonella enterica Serovar Typhimurium Translocated Leucine-Rich Repeat Effector Protein Inhibits NF-kB-Dependent Gene Expression. *Infection and Immunity*. **71**, 4052–4058
19. Haraga, A., and Miller, S. I. (2006) A Salmonella type III secretion effector interacts with the mammalian serine/threonine protein kinase PKN1. *Cell Microbiol.* **8**, 837–846

20. Keszei, A. F. A., Tang, X., Mccormick, C., Zeqiraj, E., Rohde, J. R., Tyers, M., and Sicheri, F. (2013) Structure of an SspH1-PKN1 Complex Reveals the Basis for Host Substrate Recognition and Mechanism of Activation for a Bacterial E3 Ubiquitin Ligase. *Molecular and Cellular Biology*. **34**, 362–373
21. Maesaki R, Ihara K, Shimizu T, Kuroda S, Kaibuchi K, Hakoshima T., (1999). The structural basis of Rho effector recognition revealed by the crystal structure of human RhoA complexed with the effector domain of PKN/PRK1. *Mol. Cell.* **4(5)**, 793-803.
22. Zouhir, S., Bernal-Bayard, J., Cordero-Alba, M., Cardenal-Muñoz, E., Guimaraes, B., Lazar, N., Ramos-Morales, F., and Nessler, S. (2014) The structure of the Slrp–Trx1 complex sheds light on the autoinhibition mechanism of the type III secretion system effectors of the NEL family. *Biochem. J.* **464**, 135–144
23. Seyedarabi, A., Sullivan, J. A., Sasakawa, C., and Pickersgill, R. W. (2010) A disulfide driven domain swap switches off the activity of Shigella IpaH9.8 E3 ligase. *FEBS Letters*. **584**, 4163–4168
24. Brzovic, P. S., Lissounov, A., Christensen, D. E., Hoyt, D. W., and Klevit, R. E. (2006) A UbcH5/Ubiquitin Noncovalent Complex Is Required for Processive BRCA1-Directed Ubiquitination. *Molecular Cell*. **21**, 873–880
25. Guttman, M., Lee, K.K. (2016) Isotope labeling of biomolecules: structural analysis of viruses by HDX-MS. *Methods Enzymol*. **566**, 405-426
26. Huang, L., Kinnucan, E., Wang, G., Beaudenon, S., Howley, P.M., Huibregtse, J.M., Pavletich, N.P. (1999) Structure of an E6AP-UbcH7 complex: insights into ubiquitination by the E2-E3 enzyme cascade. *Science*. **286**, 1321-1326
27. Kamadurai, H. B., Souphron, J., Scott, D. C., Duda, D. M., Miller, D. J., Stringer, D., Piper, R. C., and Schulman, B. A. (2009) Insights into Ubiquitin Transfer Cascades from a Structure of a UbcH5B∼Ubiquitin-HECT NEDD4L Complex. *Molecular Cell*. **36**, 1095–1102.
28. Yuan L., Lv Z., Atkison J.H., Olsen S.K., (2017). Structural insights into the mechanism and E2 specificity of the RBR E3 ubiquitin ligase HHARI. *Nat. Commun.* 8(1): 211
29. Dou, H., Buetow, L., Sibbet, G. J., Cameron, K., and Huang, D. T. (2012) BIRC7–E2 ubiquitin conjugate structure reveals the mechanism of ubiquitin transfer by a RING dimer. *Nat Struct Mol Biol*. **19**, 876–883
30. Lin, D. Y.-W., Diao, J., and Chen, J. (2012) Crystal structures of two bacterial HECT-like E3 ligases in complex with a human E2 reveal atomic details of pathogen-host interactions. *PNAS*. **109**, 1925–1930
31. Landau M., Mayrose I., Rosenberg Y., Glaser F., Martz E., Pupko T., Ben-Tal N. (2005) ConSurf 2005: the projection of evolutionary conservation scores of residues on protein structures. *Nucl. Acids Res.* **33**, W299-W302.
32. Ashkenazy H., Abadi S., Martz E., Chay O., Mayrose I., Pupko T., and Ben-Tal N. (2016). ConSurf 2016: an improved methodology to estimate and visualize evolutionary conservation in macromolecules. *Nucl. Acids Res.* **44**, W344-350.
33. Guex, N., Peitsch, M.C. (1997) SWISS-MODEL and the Swiss-PdbViewer: An environment for comparative protein modeling. *Electrophoresis*. **18**, 2714-2723
34. Chou, Y.-C., Keszei, A. F. A., Rohde, J. R., Tyers, M., and Sicheri, F. (2011) Conserved Structural Mechanisms for Autoinhibition in IpaH Ubiquitin Ligases. *J. Biol. Chem.* **287**, 268–275
35. Wenzel, D. M., Stoll, K. E., and Klevit, R. E. (2011) E2s: structurally economical and functionally replete. *Biochem. J.* **433(1)**, 31-42
36. Pruneda, J.N., Littlefield, P.J., Soss, S.E., Nordquist, K.A., Chazin, W.J., Brzovic, P.S., Klevit, R.E. (2013) Structure of an E3:E2~Ub complex reveals an allosteric mechanism shared among RING/U-box ligases. *Mol. Cell.* **46(6)**, 933-942
37. Dove, K.K., Olszewski, J.L., Martino, L., Duda, D.M., Wu, X.S., Miller, D.J., Reiter, K.H., Rittinger, K., Schulman, B.A., Klevit, R.E. (2017) Structural studies of HHARI/UbcH7~Ub reveal unique E2~Ub conformational restriction by RBR RING 1. *Structure*. **6(6)**, 890-900
38. Dove, K.K., Stieglitz, B., Duncan, E.D., Rittinger, K., Klevit, R.E. (2016) Molecular insights into RBR E3 ligase ubiquitin transfer mechanisms. *EMBO Rep.* **17(8)**, 1221-1235
39. Pruneda, J.N., Stoll, K.E., Bolton, L.J., Brzovic, P.S., Klevit, R.E. (2011) Ubiquitin in motion: structural studies of the ubiquitin-conjugating enzyme~ubiquitin conjugate. *Biochemistry*. **50(10)**, 1624-1633
40. Saha A., Lewis S., Kleiger G., Kuhlman B., Deshaies R.J. (2011) Essential role for ubiquitin-ubiquitin-conjugating enzyme interaction in ubiquitin discharge from Cdc34 to substrate. *Mol. Cell* **42(1)**, 75-83.
41. Metzger, M.B., Pruneda, J.N., Klevit, R.E., Weissman, A.N. (2014) RING-type E3 ligases: master manipulators of E2 ubiquitin-conjugating enzymes and ubiquitination. *Biochim. Biophys. Acta.* **1843(1)**, 47-60

42. Pruneda, J.N., Smith, F.D., Daurie, A., Swaney, D.L., Villen, J., Scott, J.F., Stadnyk, A.W., Le Trong, I., Stenkamp, R.E., Klevit, R.E., Rohde, J.R., Brzovic, P.S. (2014) E2~Ub conjugates regulate the kinase activity of Shigella effector OspG during pathogenesis. *EMBO J.* **33(5)**, 437-449.
43. Bernier-Villamor, V., Sampson, D.A., Matunis, M.J., Lima, C.D. (2002) Structural basis for E2-mediated SUMO conjugation revealed by a complex between ubiquitin-conjugating enzyme Ubc9 and RanGAP1. *Cell.* **108(3)**, 345-56
44. Reverter, D., Lima, C.D. (2005) Insights into E3 ligase activity revealed by a SUMO-RanGAP1-Ubc9-Bup358 complex. *Nature*. **435(7042)**, 687-692
45. Delaglio, F., Grzesiek, S., Vuister, G.W., Zhu, G., Pfeifer, J., Bax, A. (1995) NMRPipe: a multidimensional spectral processing system based on UNIX pipes. *J. Biomol. NMR.* **6**, 277-293
46. Johnson, B.A., Blevins, R.A. (1994) NMR View: A computer program for the visualization and analysis of NMR data. *J. Biomol. NMR*. **4(5)**, 603-614
47. The PyMOL Molecular Graphics System, Version 1.7 Schrödinger, LLC.
48. Berman, H.M., Westbrook, J., Feng, Z., Gilliland, G., Bhat, T.N., Weissig, H., Shindyalov, I.N., Bourne, P.E. (2000) The Protein Data Bank. *Nucl. Acid Res.* **28**, 235-242
49. Sattler, M., Schleucher, J., Griesinger, C. (1999) Heteronuclear multidimensional NMR experiments for the structure determination of proteins in solution employing pulsed field gradients. *Prog. Nucl. Mag. Res. Sp.* **34(2)**, 93-158
50. Weis, D.D., Kass, I.J. & Engen, J.R. (2006). Semi-automated analysis of hydrogen exchange mass spectra using HX-Express. *J. Amer. Soc. Mass Spectrom.* **17(12)**, 1700-1703.
51. Guttman M., Weis, D.D., Engen, J.R. & Lee, K. K. (2013). Analysis of overlapped and noisy Hydrogen/Deuterium exchange data. *J. Amer. Soc. Mass Spectrom.* **24(12)**, 1906-1912.
52. 75, R.J., Baker, P.R., Huang, L., Hansen, K.C., Allen, N.P., Rexach, M., Burlingame, A.L. (2005) Comprehensive analysis of a multidimensional liquid chromatography mass spectrometry dataset acquired on a quadrupole selecting, quadrupole collision cell, time-of-flight mass spectrometer: II. New Developments in Protein Prospector allow for reliable and comprehensive automatic analysis of large datasets. *Mol. Cell. Proteomics.* **4(8)**, 1194-1204.
53. Page, R.C., Pruneda, J.N., Amick, J., Klevit, R.E., Misra, S. (2012) Structural insights into the conformation and oligomerization of E2~ubiquitin conjugates. *Biochemistry*. **51(20)**, 4175-4187

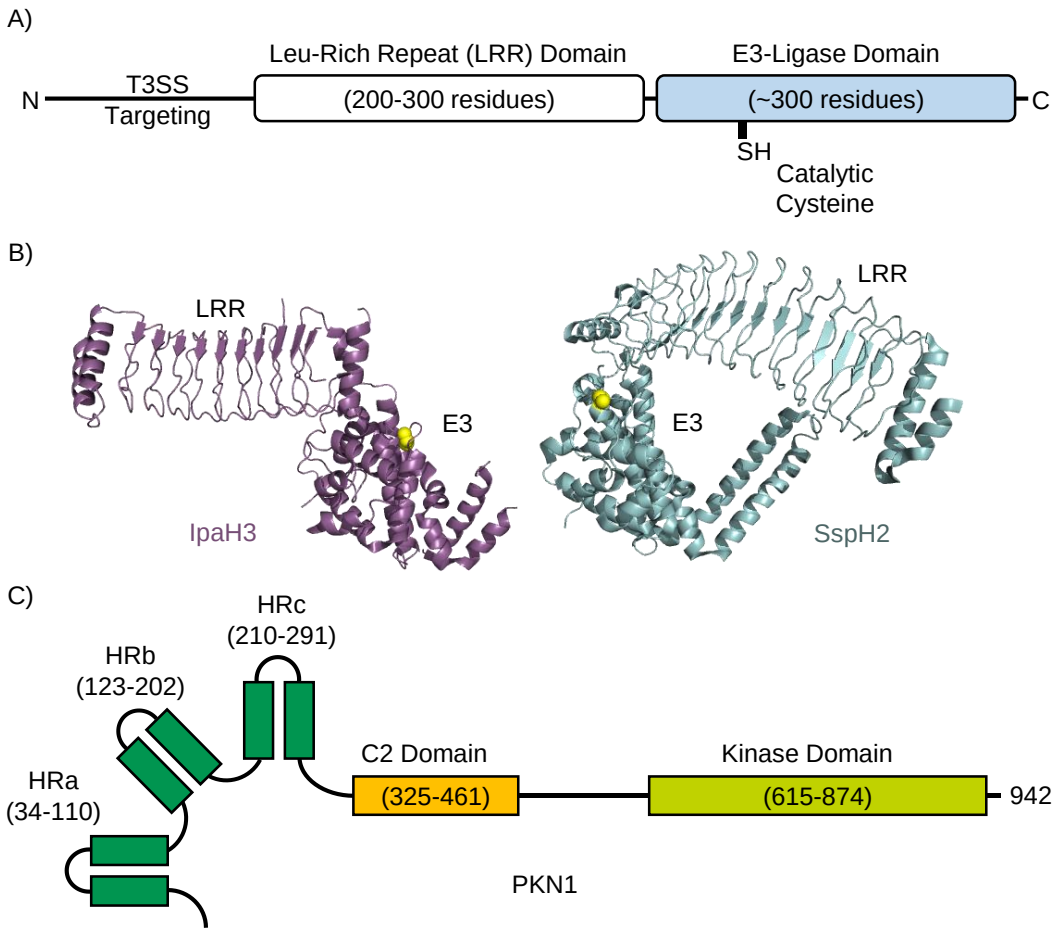

Figure S1. Architecture of SspH/IpaH E3s and Human PKN1, a substrate for SspH1. **A)** Conserved domain architecture of SspH/IpaH E3s. Each E3 in this family possesses an N-terminal Type III Secretion System (T3SS) targeting sequence, a substrate-binding leucine-rich repeat (LRR) domain of variable size, and a catalytic E3 ubiquitin ligase domain containing an active site cysteine that forms a thioester intermediate with the C-terminus of ubiquitin during transfer. **B)** Crystal structures of IpaH3 (purple, PDB # 3CVR (12)) and SspH2 (cyan, PDB # 3G06 (14)) containing LRR and E3 domains. The catalytic cysteines in the E3 domains are shown as yellow spheres. Structural comparison of IpaH3 and SspH2 shows a large reorientation of the LRR relative to the E3 domain between structures. **C)** Domain architecture of the human kinase PKN1, a cellular substrate of SspH1. SspH1 binds the two anti-parallel helices of the HRb region of PKN1 through its LRR (PDB # 4NKG (20)). PKN1 constructs for both the HRab and HRb regions are used as *in vitro* substrates for SspH1.

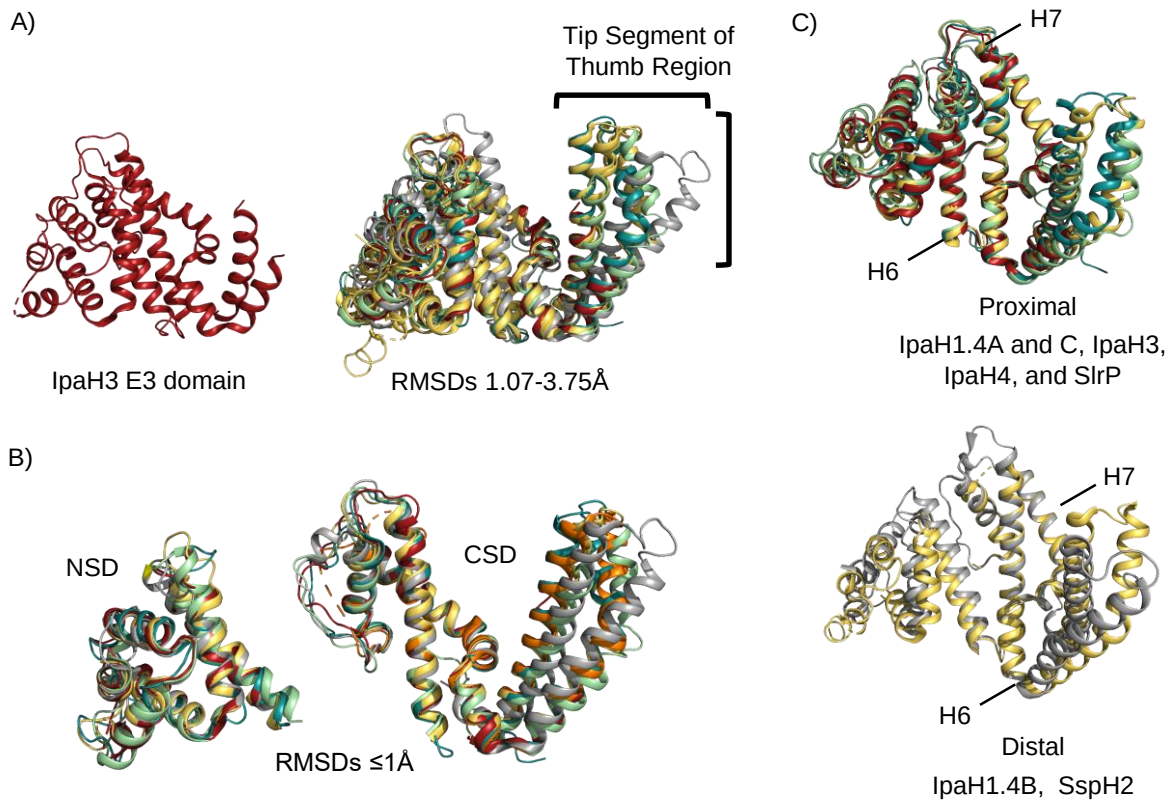

Figure S2. Comparison of SspH/IpaH family E3 domain topologies. **A)** Pairwise superposition of the E3 domains of IpaH1.4 chains A and C, IpaH4, SlrP, and SspH2 (PDB entries 3CKD, (13), 5KH1, 4PUF (22), and 3G06 (14), respectively) with IpaH3 (PDB # 3CVR (12)). The structure of the IpaH9.8 (PDB # 3L3P (23)) was not used for this panel as it exhibits a unique NSD domain swapped structure. IpaH3 was chosen as the basis for comparison as its structure exhibits the minimal number of structural elements common to all SspH/IpaH E3 domains. The various E3 domains superpose pairwise with backbone RMSDs of structurally conserved regions ranging from 1.07-3.75Å. **B)** Superposition of the NSD and CSD of IpaH1.4A and C, IpaH3, IpaH4, SlrP, and SspH2. The sub-domains superpose with backbone RMSDs of structurally conserved regions of <1Å. Comparison of CSD structures reveals additional structural heterogeneity in the tip segment of the Thumb region. **C)** Top Panel: Superposition of the E3 domains of IpaH1.4A and C, IpaH3, IpaH4, and SlrP. These structures adopt a "proximal" conformation. Bottom panel superposition of the E3 domains of IpaH1.4B and SspH2. These structures adopt a "distal" conformation. All E3 structures are oriented such that the first extended helix of the CSD (labeled H7) is positioned vertically. Comparison of the proximal and distal conformations show large changes in the position of the NSD relative to H7 and, therefore, the CSD. This is most easily observed by comparing the position of H6 relative to H7 in the proximal and distal conformations.

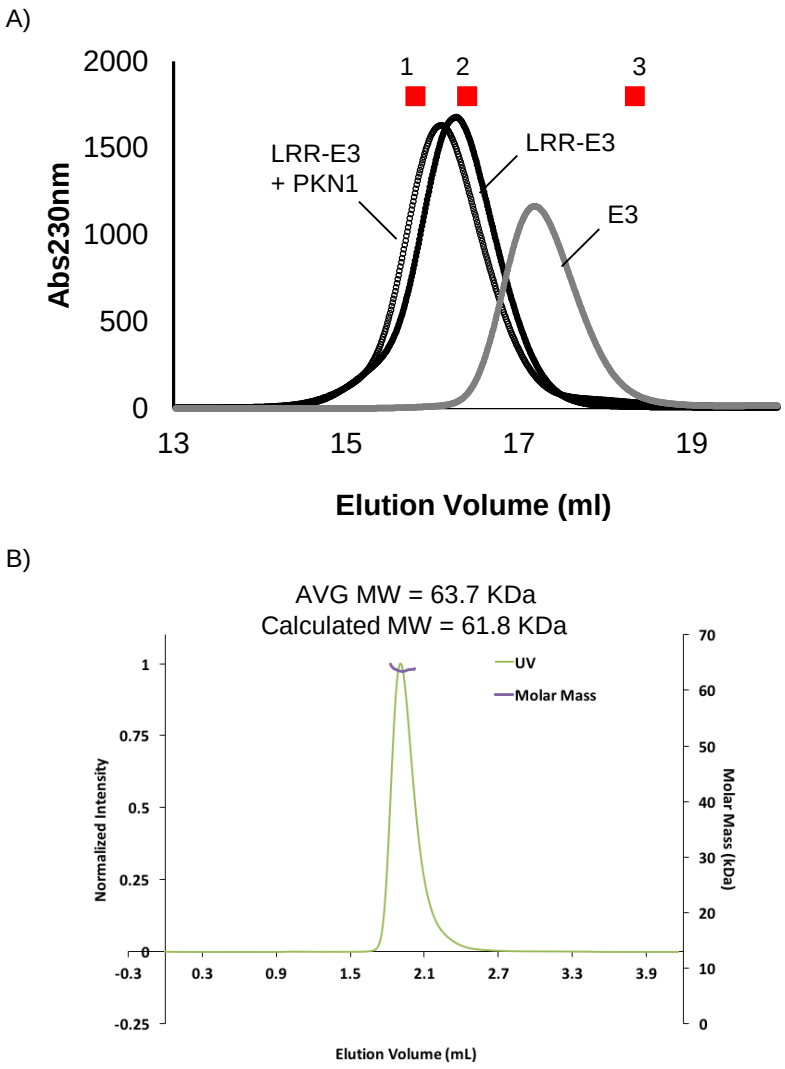

Figure S3. SspH1 constructs behave as monomers. **A)** Analytical SEC runs of 50µM SspH1 E3 domain, SspH1 LRR-E3 domain, or SspH1 LRR-E3 domain bound to PKN1 108-201 (HRb domain, 75mM) on a 24mL GE Superose6 10/300 GL equilibrated in 25mM sodium phosphate, 150mM sodium chloride, pH 7 at room temperature. The elution volumes for SEC standards are indicated as red squares: 1) ADH (~145kDa), 2) BSA (~66kDa) and 3) Ube2D3 (~17kDa). **B)** SEC-MALS analysis of 50 µM SspH1 LRR-E3 eluted on a 2.5mL Superdex200 equilibrated with 25mM sodium phosphate, 150mM sodium chloride, pH 7 at room temperature shows that SspH1 LRR-E3 is monomeric.

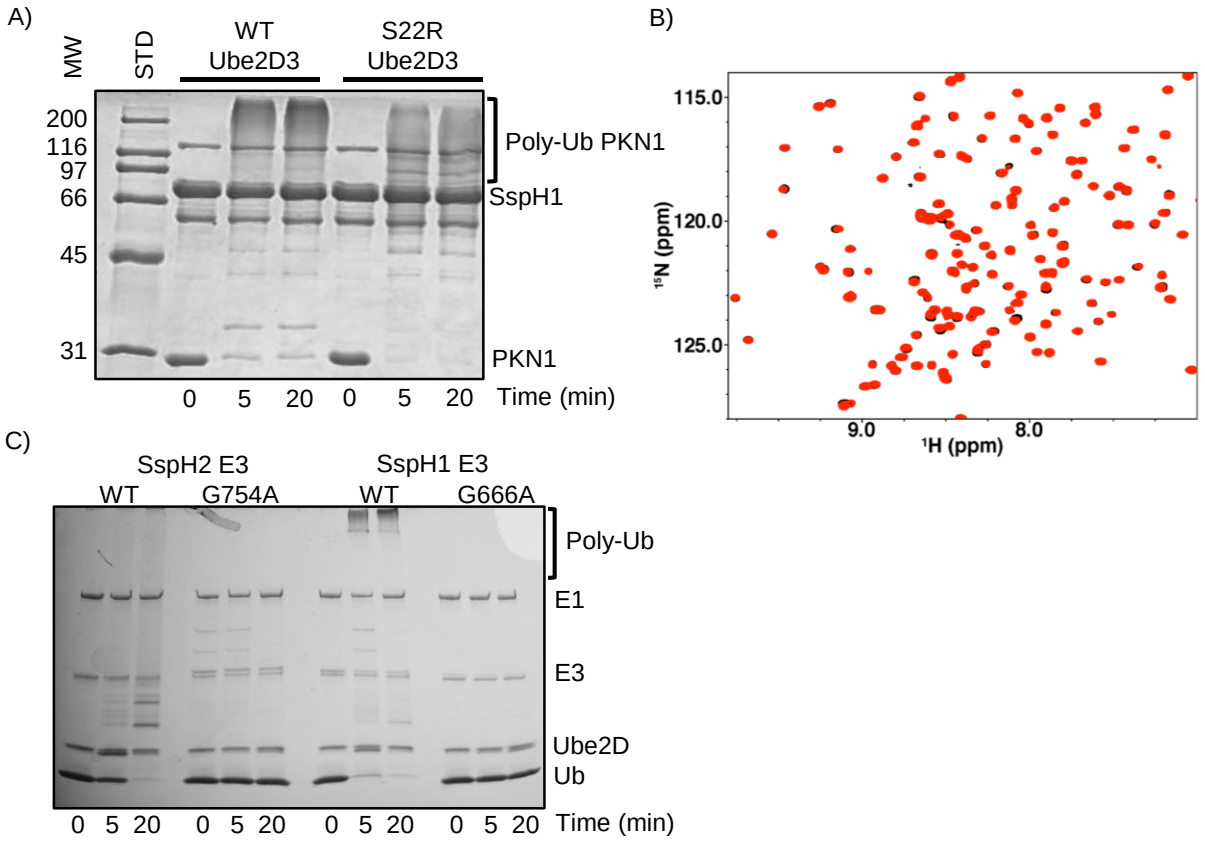

Figure S4. Assays for SspH1 catalyzed ubiquitylation of PKN1 HRab. Assay compare the activities of wild-type Ube2D3, S22R Ube2D3, SspH1 G666A E3 domain, and SspH2 G754A E3 domain. NMR spectra show that free Ube2D3 and free Ub do not interact with the SspH1 E3 domain. Only the Ube2D3~Ub conjugate binds to the SspH1 E3 domain. **A)** Ubiquitylation assays of SspH1 with either wild-type or S22R Ube2D3. S22R blocks non-covalent Ub binding to Ube2D3, but this interaction is not essential for SspH1 catalyzed ubiquitylation of PKN1. **B)** Overlay of $^{1}H,^{15}N$-TROSY NMR spectra of 150uM ^{15}N-Ube2D3 and ^{15}N-Ub in the absence (black) and presence (red) of 150uM SspH1 E3 domain. No significant chemical shift perturbations are observed (compare with **Fig. 3A**) showing that both E2 and Ub subunits present in the context of an Ube2D3~Ub conjugate are required for binding to the SspH1 E3 domain. **C)** Mutation of a conserved Gly residue (SspH2 G754A and SspH1 G666A) in the tip segment of the Thumb region of both SspH1 and SspH2 abrogates the ability of the E3 domains to synthesize unanchored poly-Ub chains. Assay conditions: 1µM E1, 5µM Ube2D3, 2µM SspH1, 50µM Ub, 5mM $MgCl_2$, 5mM ATP, pH7, 37°C.

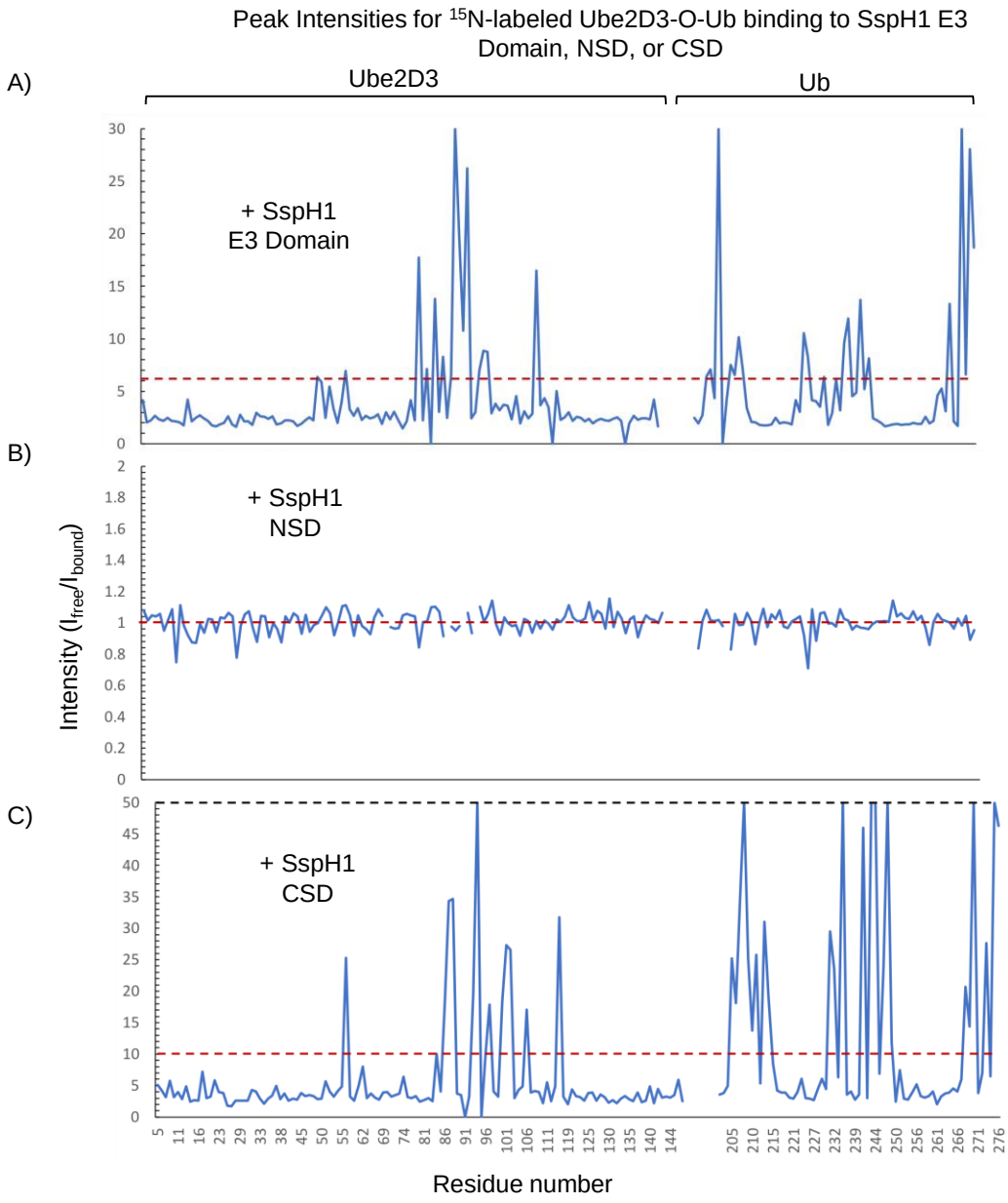

Figure S5. Analysis of Ube2D3-O-Ub binding to the SspH1 E3 domain, NSD, and CSD. NMR intensity analyses for 150uM ^{15}N-Ube2D3-O-Ub binding to 75uM SspH1 **A)** E3 domain, **B)** N-terminal subdomain (NSD), or **C)** C-terminal subdomain (CSD). ^{15}N-Ube2D3-O-Ub peak intensities were determined in the absence and presence of the SspH1 construct. The ratio of I_{free}/I_{bound} was plotted. This analysis highlights the perturbed residues but can lead to very large values for resonance that are completely disappear in the bound state due to exchange broadening. In these cases, a maximum value was assigned. The dotted red line indicates the average change in peak intensity for each experiment. Though the ratios vary, the same pattern of ^{15}N-Ube2D3-O-Ub resonances are perturbed upon addition of wild type SspH1 E3 domain and the SspH1 CSD. No interaction was observed with the SspH1 NSD.

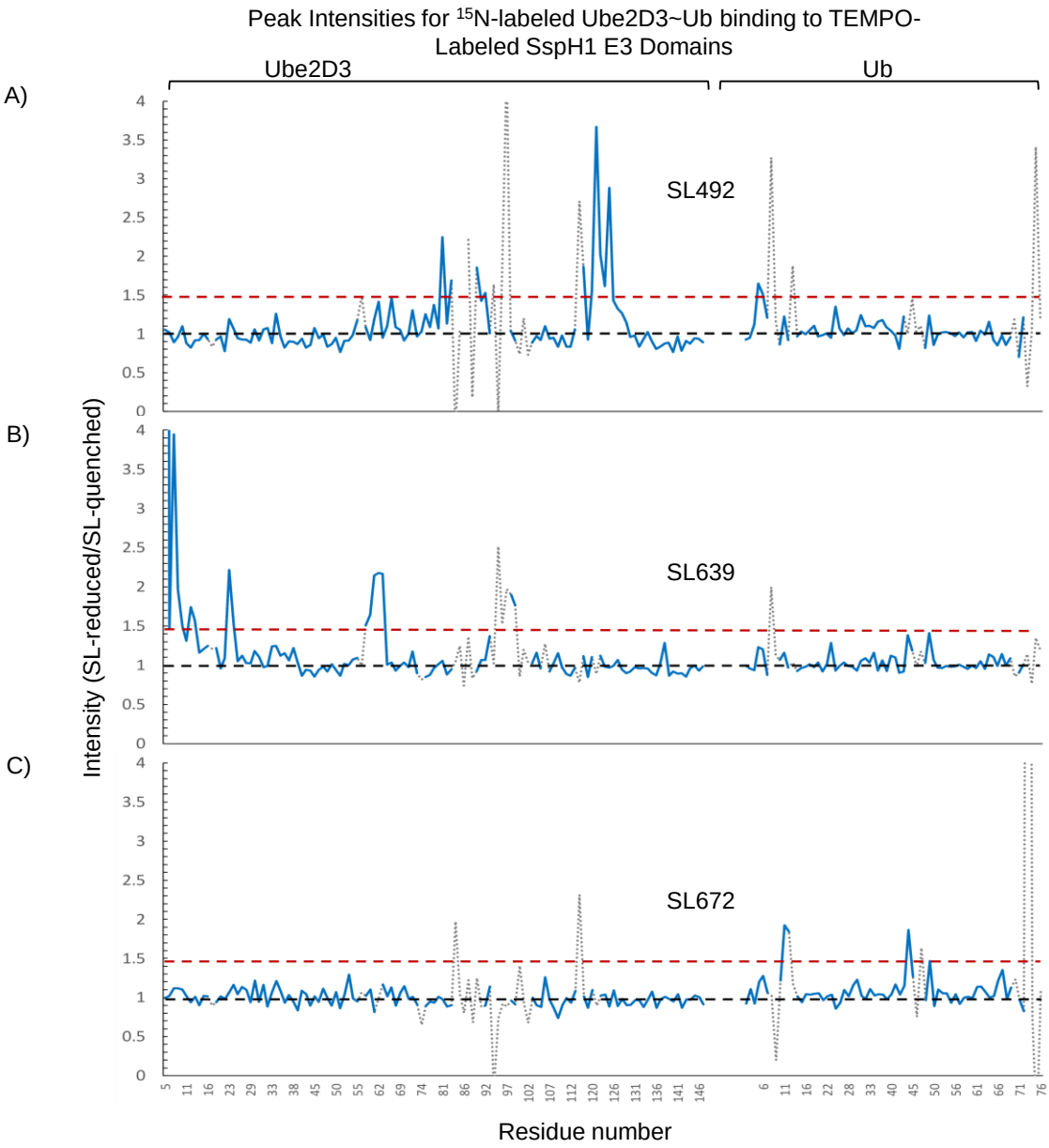

Figure S6. Binding of Ube2D3-O-Ub to SspH1 E3 domains modified with paramagnetic TEMPO spin labels. NMR intensity analyses for 150uM ^{15}N-Ube2D3-O-Ub binding to 75uM SspH1 E3 domain modified with TEMPO spin label incorporated at position **A)** C492 (SL492), **B)** E639 (SL639), or **C)** S672 (SL672). ^{1}H,^{15}N-TROSY spectra were collected for ^{15}N-labeled Ube2D3-O-Ub in the presence of TEMPO spin-labeled E3 domain in the absence (SL-active) and presence (SL-quenched) of ascorbate. Addition of ascorbate eliminates the paramagnetic effect of the unpaired electron. The ratio of peak intensities was calculated as $I_{quenched}/I_{unquenched}$ and graphed as a dotted line. Intensities of resonances of residues at the SspH1/E2~Ub interface that were reduced due to exchange broadening resulting from the binding interaction were eliminated from the analysis. The remaining values were graphed as a solid blue line.

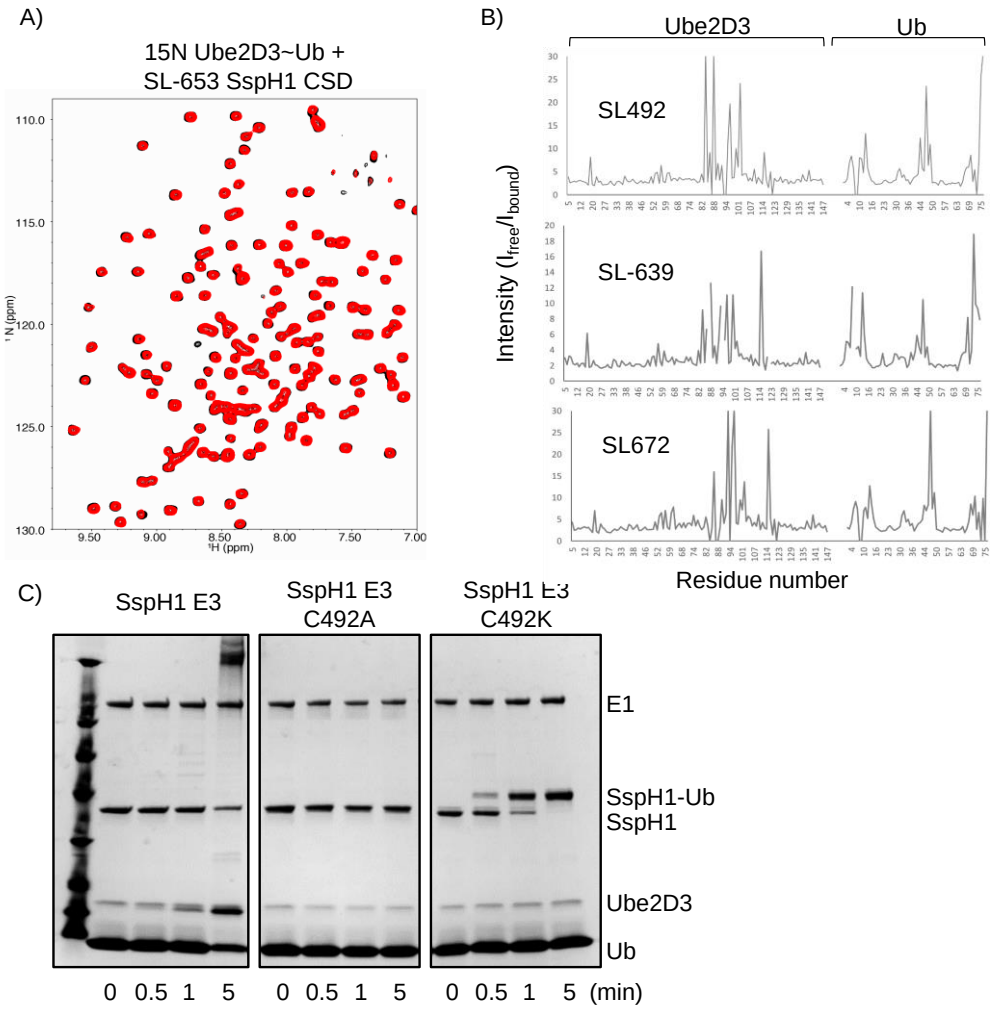

Figure S7. A) Loss of Ube2D3-O-Ub binding due to incorporation of a spin label at position 653 in the tip segment of the SspH1 Thumb region. Overlay of ^{1}H,^{15}N-TROSY NMR spectra of 150uM ^{15}N-Ube2D3-O-Ub in the absence (black spectrum) and presence of 150uM SspH1 E3 domain with a TEMPO spin label at position S653. No significant chemical shift perturbations are observed (compare with Fig. 3A) showing that a spin label introduced at this position abrogates binding of Ube2D3-O-Ub to SL653. **B)** Ube2D3~Ub forms productive complexes with SL492, SL639, and SL672. Resonance intensities of ^{15}N-Ube2D3-O-Ub in the presence of SL-quenched SspH1 constructs were compared with free ^{15}N-Ube2D3-O-Ub to determine which resonances were perturbed by binding to the various E3 constructs. Intensity ratios were calculated and plotted as described in Supp. Fig. 5. The pattern of perturbed resonances is similar in each case and is similar to that observed in the presence of the wild-type E3 domain (compare Supp. Fig. 5A), consistent with Ube2D3-O-Ub binding similarly to each SspH1 E3 construct. **C)** C492K SspH1 can be specifically modified with Ub at the SspH1 active site position, demonstrating that Ube2D3~Ub binds to SspH1 in a conformation that is active in aminolysis reactions. Reaction conditions: 1µM wheat E1, 2µM Ube2D3, 5µM SspH1, 100µM Ub, 5mM $MgCl_2$, 5mM ATP, pH 7, 37°C.

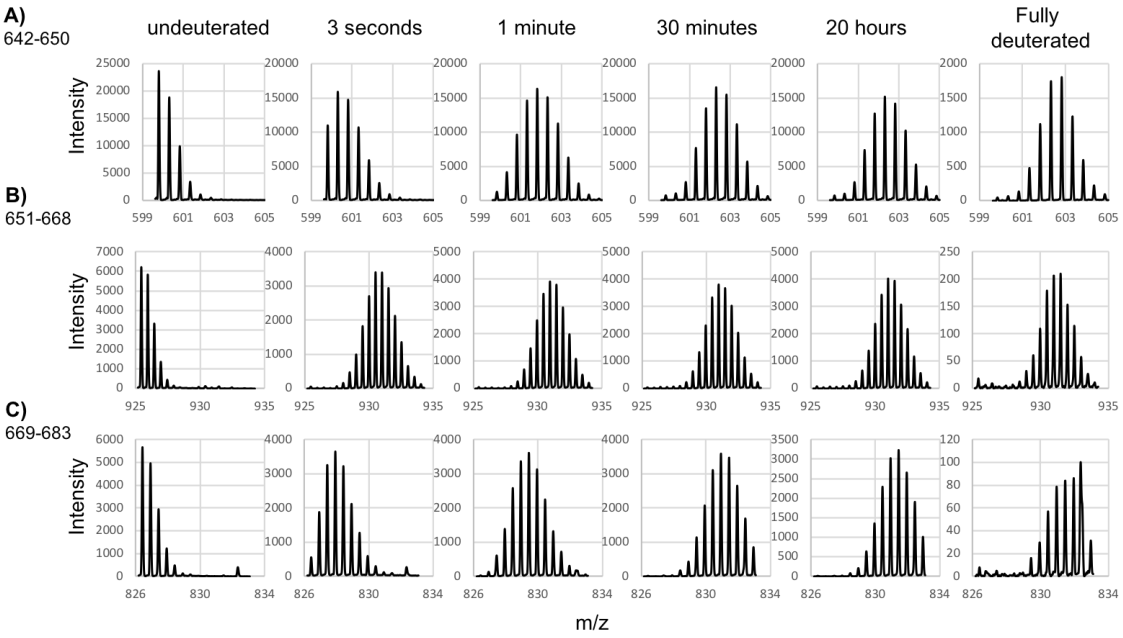

Figure S8. The tip segment of the SspH1 Thumb region that binds Ube2D3~Ub is dynamic. Hydrogen/deuterium exchange mass spectral envelopes for three consecutive peptides in the thumb helices of SspH1: **A)** residues 642-650, **B)** residues 651-668, and **C)** residues 669-683. A single binomial curve was fit to each envelope, and the mean of each fitted curve was used to calculate fractional deuteration of the 3 second, 1 minute, 30 minutes, and 20 hours timepoints relative to undeuterated and fully deuterated samples. Fractional deuteration as a function of time for each peptide is plotted in main text Figure 6A.

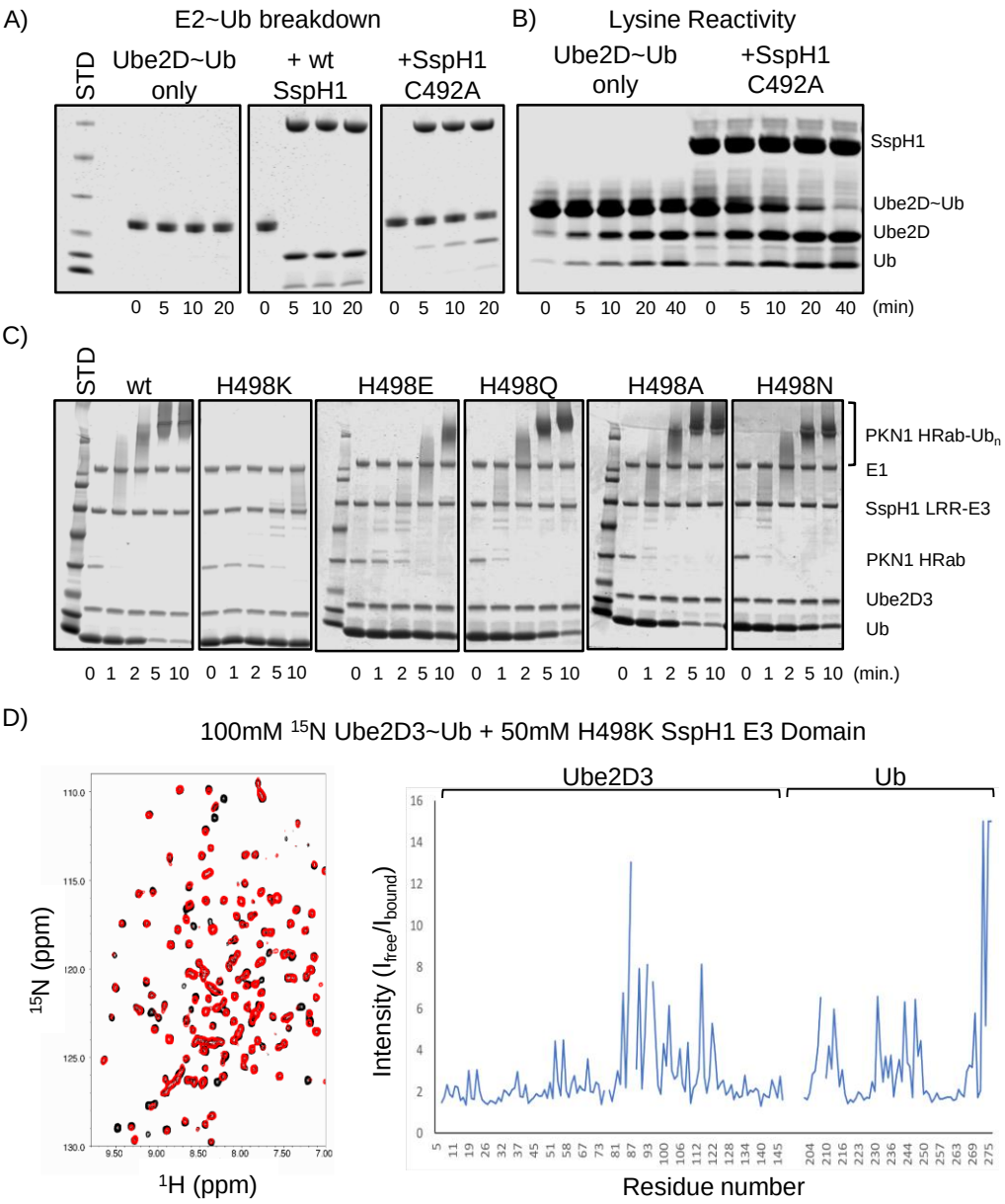

Figure S9. A) Net hydrolysis of Ube2D3~Ub to free Ube2D3 and Ub catalyzed by SspH1 is dependent on C492. **B)** Interaction of Ube2D3~Ub with SspH1 enhances intrinsic Lys reactivity of the E2~Ub conjugate. **C)** Ubiquitylation of PKN1 catalyzed by wt SspH1 and H498K mutants. **D)** Binding of 15N-labeled Ube2D3-O-Ub to H498K SspH1 E3 domain is similar to binding to the wt SspH1 E3 domain. Overlay of ^{1}H,^{15}N-TROSY NMR spectra of 150uM ^{15}N-Ube2D3-O-Ub in the absence (black spectrum) and presence of 75uM SspH1 H498K E3 domain (red spectrum). Changes in resonance intensities were calculated as described for Supp. Fig. 5. Ubiquitylation assays: 1µM wheat E1, 5µM Ube2D3, 2µM SspH1, 100µM Ub, 5mM $MgCl_2$, 5mM ATP, pH7, 37°C. E2~Ub hydrolysis conditions: 20µM E2~Ub, 8µM SspH1, pH7, 37 °C. Intrinsic Lys reactivity conditions: 40µM Ube2D3~Ub, 20µM SspH1, 50mM Lysine, pH 7, 25°C.

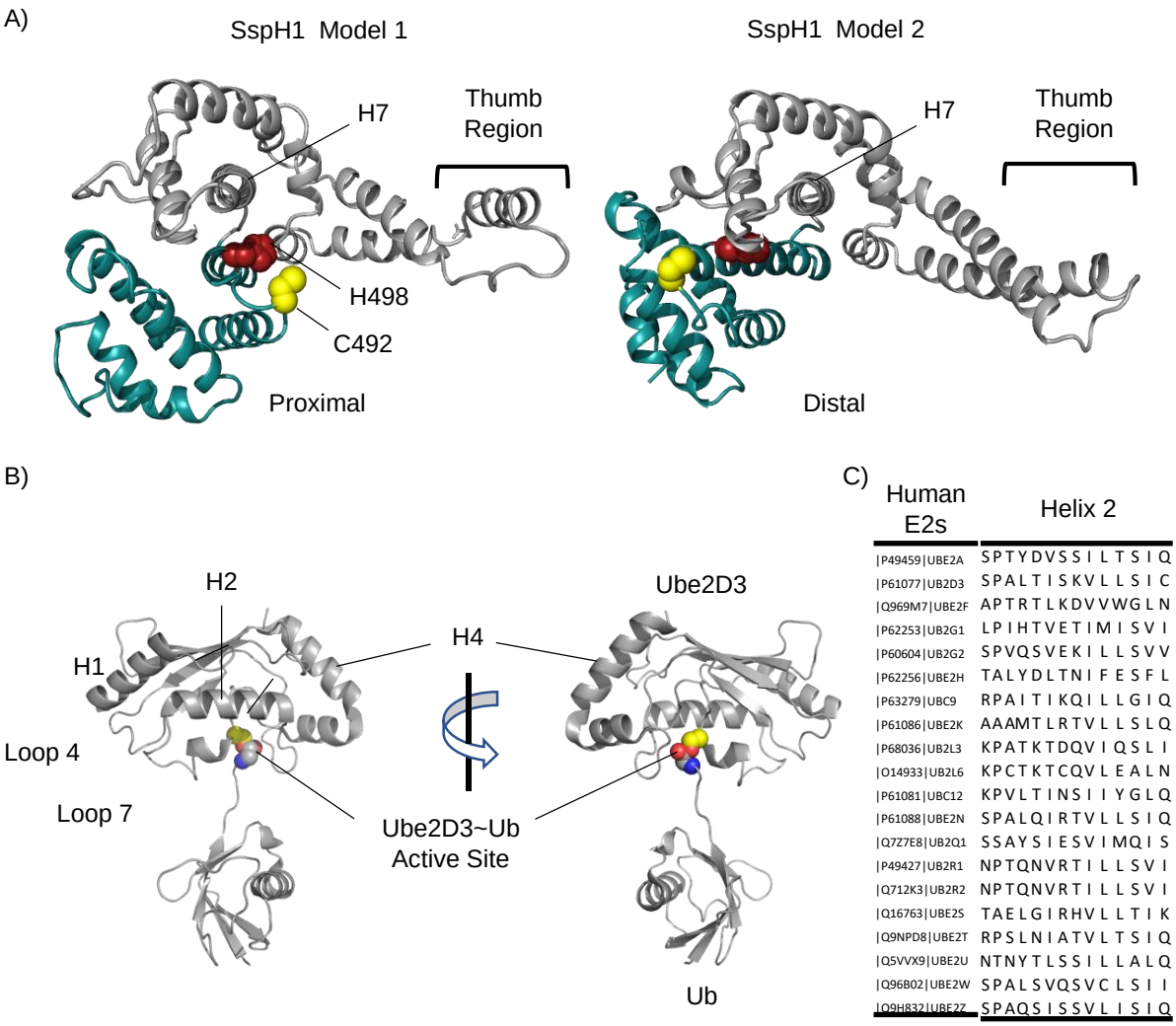

Figure S10 A) Homology models of SspH1 based on crystal structures of IpaH3 (proximal conformation) and SspH2 (distal conformation). The models predict large changes in the local environment of H498 (red) in the two conformational states. In the "proximal" position, with the active site Cys (yellow) closer to the Thumb region, H498 is solvent exposed. In the "distal" position, with the active site Cys further from the Thumb region, H498 is buried within the NSD/CSD interface. **B)** Ribbon representation of Ube2D3~Ub conjugate (from PDB # 4BVU (42)) identifying E2 structural elements described in the text. **C)** Sequence alignment of Helix 2 from multiple human E2s demonstrating the sequence variation in this region of the E2 core topology. As shown in Fig. 3D in the main text, the Ube2D residues that directly interact with the SspH1 E3 domain are primarily located in loop 7 and helix 2. These findings are consistent with the observed selectivity of SspH/IpaH E3s for the Ube2D family of E2s.

Part II: Roles of E2 and Substrate in the Second Stage of Ub Transfer

The mechanism of SspH1 entails two main stages of Ub transfer: 1) from E2~Ub to the SspH1 active site Cys, and 2) from SspH1 to a lysine residue on PKN1 or Ub. Part I focused on the first stage, identifying how SspH1 engages E2~Ub through the flexible thumb helices in the C-terminal subdomain prior to transfer to the active site Cys in the N-terminal subdomain. Parts II and III focus on the second transfer stage. The emphasis in Part II is on investigating the differential ubiquitylation activity of SspH1 with various E2s, leading to the discovery that the E2 also plays a critical role in driving Ub transfer from SspH1~Ub to substrate. The emphasis in Part III is structurally characterizing the role of the E2 in the second stage, as well as an analysis of the structural changes that occur in SspH1 upon activation with Ub and in the presence of substrate.

Previous work has shown that IpaH-SspH E3s are active with members of the Ube2D family of E2s [34, 35, 48, 49, Part I]. The Ube2D family consists of only a Ubc domain and has high sequence homology to the Ubc domain of the Ube2E family. The Ube2E family possess an additional unstructured N-terminal extension of ~60 residues. A construct of Ube2E3 lacking its N-terminal extension, ΔN-Ube2E3 (residues 61-207) is 65% identical and 82% similar to Ube2D3 **(Fig 1A)**. The crystal structures of Ube2D3 (PDB: 1X23), ΔN-Ube2E2 (PDB: 1Y6L, 97% identical to ΔN-Ube2E3) and Ube2L3 (PBD: 1C4Z) show that the topologies of these E2s are very similar **(Fig 1B)**. A preliminary crystal structure of ΔN-Ube2E3 was solved, revealing an identical topology to that of ΔN-Ube2E2. A summary and analysis of the structure is provided in **Appendix 2**. Intriguingly, the sequences of Ube2D3 and Ube2E3 in the regions shown to bind the SspH2 E3 domain in 48 and the SspH1 E3 domain in **Part I** are nearly completely conserved. The sequence of Ube2L3 in the SspH2 E3 binding region, however, is not similar to Ube2D3 or

A

```
Ube2E3  61-TSAKRIQKELAEITLDPPPNCSAGPKGDNIYEWRSTILGPPGSVYEGGVFFLDITFSSDY
Ube2D3   1-MALKRINKELSDLARDPPAQCSAGPVGDDMFHWQATIMGPNDSPYQGGVFFLTIHFPTDY
            : ***:***:::: *** :***** **::::.*::**:**  * *:****** * * :**

Ube2E3 121-PFKPPKVTFRTRIYHCNINSQGVICLDILKDNWSPALTISKVLLSICSLLTDCNPADPLV
Ube2D3  61-PFKPPKVAFTTRIYHPNINSNGSICLDILRSQWSPALTISKVLLSICSLLCDPNPDDPLV
           *******:* ***** ****:* ******:.:***************** * ** ****

Ube2E3 181-GSIATQYLTNRAEHDRIARQWTKRYAT
Ube2D3 121-PEIARIYKTDRDKYNRISREWTQKYAM
            .**  * *:* :::**:*:**::**
```

B

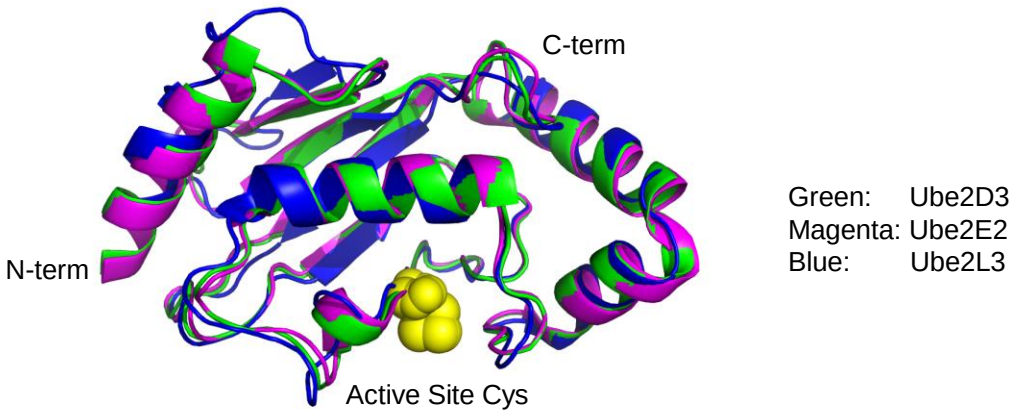

Figure 1. Comparison between Ube2D3 and ΔN-Ube2E3 (Ube2E3 61-207) by **(A)** pairwise sequence alignment shows that Ube2D3 and the UBC domain of Ube2E3 (residues 61-207) are 65% similar and 82% identical. Active site Cys is highlighted in yellow. **(B)** Structural alignment between Ube2D3 (PDB: 1X23), Ube2E2 54-201 (97% identical to Ube2E3 61-207), and Ube2L3 (PDB 1C4Z)

Ube2E3. Do Ube2E3 and Ube2L3 also bind and have ubiquitylation activity with SspH1 similar to Ube2D3? Even if they do not, the results could highlight other areas of the E2 that may be involved transferring Ub to SspH1.

Like SspH1, eukaryotic HECT and RBR E3s utilize a two-step Ub transfer mechanism and form an obligate E3~Ub via an active site cysteine. Both families of E3s can use Ube2D3 for Ub transfer, but they can also use a specialized E2, Ube2L3. Unlike Ube2D3, Ube2L3 is not lysine reactive, and does not have ubiquitylation activity with RING E3s. Thus, Ube2L3 has evolved to perform transthiolation reactions with E3s that utilize a HECT-type mechanism. IpaH-SspH effectors also utilize a HECT-type mechanism, so perhaps they also utilize the transthiolation-specific Ube2L3. To determine which E2s are active with SspH1, the ubiquitylation activity and structural interactions between SspH1 and Ube2D3, ΔN-Ube2E3, and Ube2L3 were systematically investigated.

Ubiquitylation activity of SspH1 with Ube2D3, ΔN-Ube2E3 and Ube2L3

To test if SspH1 is active with Ube2D3, ΔN-Ube2E3, or Ube2L3, ubiquitylation activity was assayed with three different constructs of SspH1 in the presence of a fragment of its substrate, PKN1. The three constructs of SspH1 tested were full-length, LRR-E3 domains (residues 162-700), and E3 domain (389-700). The fragment of PKN1 used was the HRb domain (108-201) that binds the LRR domain of SspH1. Poly-Ub chain synthesis was observed for all constructs of SspH1 when Ube2D3 was used as the E2 (**Fig 2**). No activity was observed when ΔN-Ube2E3 or Ube2L3 were used as the E2. For the full-length and LRR-E3 SspH1 constructs, free Ub and PKN1 were depleted within the first 5 minutes. The distribution of poly-Ub chains was similar in both, suggesting that the first 161 residues of SspH1 have little effect on ubiquitylation activity and the

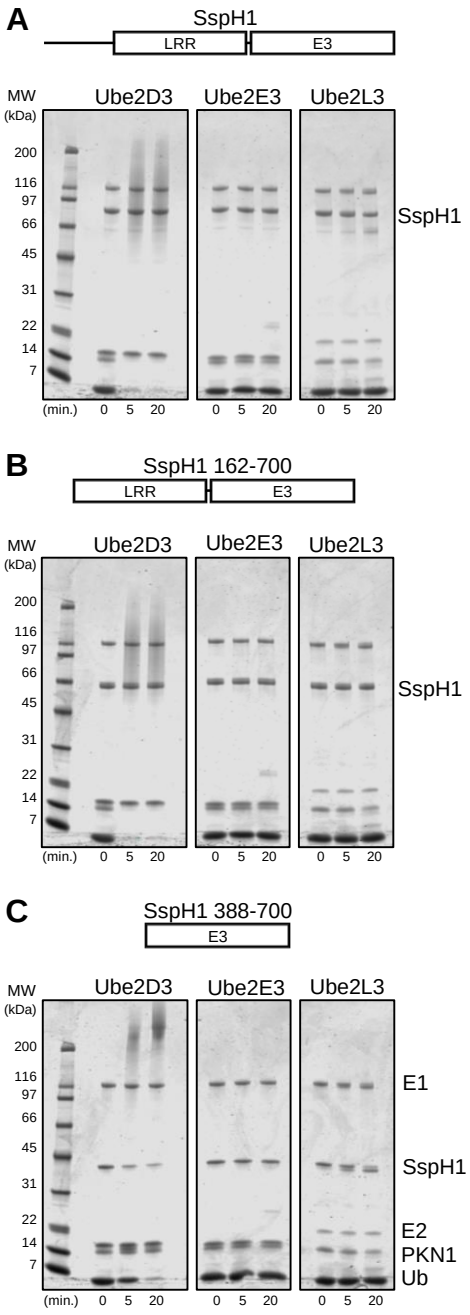

Figure 2. Substrate-based ubiquitination activity of three constructs of SspH1 with three different E2s: Ube2D3, ΔN-Ube2E3 (61-207) and Ube2L3. Ubiquitination assays for **(A)** full-length SspH1, **(B)** SspH1 162-700 (LRR-E3 domains), and **(C)** SspH1 389-700 (E3 domain). Reaction conditions: 1μM E1, 5μM E2, 2μM E3, 50μM Ub, 5μM His-PKN1 108-201, 5mM $MgCl_2$, 5mM ATP, PBS pH7, 37°C. Reducing gel samples taken at 0 min (before addition of ATP), 5 and 20 minutes, followed by 4-20% gradient SDS-PAGE and staining with Coomassie.

types of products synthesized under these conditions (**Fig 2A,B**). The isolated SspH1 E3 domain does not modify PKN1 but can synthesize unanchored poly-Ub chains. With this construct, free Ub was depleted from the reaction mixture within the first 20 minutes (**Fig 2C**). The depletion of free Ub in the reaction mixture was slower for the isolated E3 domain. The products formed in this reaction are unanchored poly-Ub chains and migrate at higher molecular weights at the 5 and 20-minute timepoints as compared to the PKN1-anchored poly-Ub chains formed by the full-length and LRR-E3 constructs.

Even though ΔN-Ube2E3 is highly homologous to Ube2D3 and is nearly 100% conserved in the SspH1 binding surface, it completely lacks ubiquitylation activity with SspH1. Similarly, the transthiolation-specific Ube2L3 also lacks activity with SspH1 even though SspH1 utilizes a HECT-type Ub transfer mechanism. From the multiple turnover ubiquitylation assays in **Fig 2**, it is not clear if the lack of poly-Ub chain forming activity with Ube2E3 and Ube2L3 results from an inability of the E2~Ub conjugate to perform Stage I transfer from E2~Ub to SspH1, or Stage II transfer from SspH1~Ub to substrate. To determine at which stage of Ub transfer Ube2E3 and Ube2L3 are non-functional with SspH1, E2~Ub single turnover ubiquitylation assays were performed, and the interactions between SspH1 and the various E2s were investigated by NMR.

E2~Ub single turnover activity of SspH1 with Ube2D3~Ub, ΔN-Ube2E3~Ub and Ube2L3~Ub

In the absence of substrate, IpaH-SspH effectors discharge ubiquitin from an E2~Ub in an active site-dependent manner without forming poly-Ub chains [44, 51]. Unlike the E3 domain alone, which can generate unanchored poly-Ub chains, in the context of the LRR domain, transfer of Ub to the active site Cys does not necessarily lead to ubiquitylation [Part I]. To test if SspH1 LRR-E3

can hydrolyze E2~Ub for the E2s used here in an active site dependent manner, Ube2D3~Ub, ΔN-Ube2E3~Ub, and Ube2L3~Ub were created by incubating each E2 with E1 and Ub, followed by separation by gel filtration. Purified E2~Ub was then incubated with SspH1 LRR-E3 harboring a wildtype active site cysteine (Cys492) or active site dead mutant Cys492Ala (**Fig 3**). As expected, SspH1 rapidly hydrolyzed Ube2D3~Ub in an active site-dependent manner (**Fig 3A**). Surprisingly, SspH1 was also able to hydrolyze ΔN-Ube2E3~Ub in an active site-dependent manner (**Fig 3B**), though at a slower rate than for Ube2D3~Ub. In contrast, Ube2L3~Ub was not hydrolyzed by SspH1 (**Fig 3C**).

The fact that Ube2D3~Ub and ΔN-Ube2E3~Ub can both transfer Ub to the SspH1 active site Cys, but poly-Ub chains are formed with Ube2D3 and not ΔN-Ube2E3 in multiple turnover ubiquitylation assays suggests there may be an additional role for the E2 beyond the first step of Ub transfer. However, the reaction conditions in the E2~Ub conjugate single turnover assay are different than that in the multiple turnover ubiquitylation assays. To test if PKN1 can still be ubiquitylated by SspH1 using Ube2D3 in the E2~Ub conjugate single turnover reaction conditions, a Western blot was performed against Flag-tagged PKN1 and Ub. (**Fig 3D**). In the absence of PKN1 no poly-Ub chains are observed, but in the presence of PKN1, an increase in molecular weight of Ub bands is observed with a concomitant increase in molecular weight of PKN1 bands. Therefore, in the E2~Ub conjugate single turnover reaction conditions, SspH1 can still build poly-Ub chains on substrate using Ube2D3~Ub, though Ube2E3 is still inactive.

Generating a non-reactive SspH1~Ub mimic

The reactive thioester bond between the SspH1 active site cysteine and the C-terminus of Ub is short-lived and difficult to trap because the thioester bond is quickly hydrolyzed by solvent.

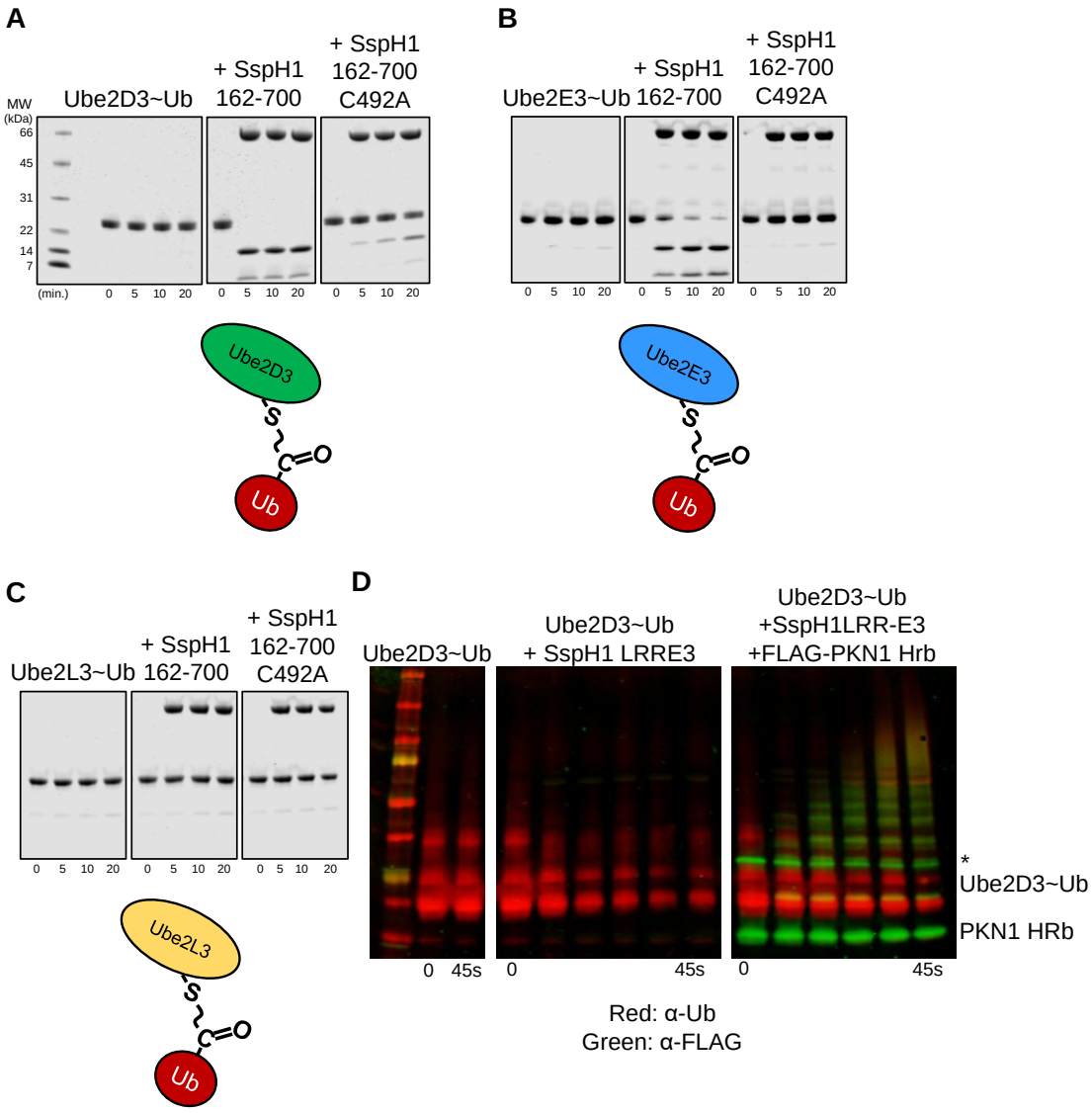

Figure 3. E2~Ub discharge assays for SspH1 162-700 (LRR-E3) wildtype active site and C492A for **(A)** Ube2D3, **(B)** ΔN-Ube2E3, and **(C)** Ube2L3. E2~Ub were charged with Ub by E1, purified by SEC, and incubated at 37°C with SspH1. Reaction conditions: 20μM E2~Ub, 8μM E3. Non-reducing gel samples taken at 0 min (before addition of E3), 5, 10 and 20 minutes, followed by 4-20% gradient SDS-PAGE and staining with Coomassie. **(D)** Western blot against Ub and FLAG-tagged PKN1 HRb performed similarly to **(A)** with timepoints taken from 0-45 seconds and with the addition of PKN1. *PKN1 has a Cys residue at position 120 which allows a small amount of PKN1 HRb to exist in the form of a disulfide linked dimer.

This is also true of thioester bonds in eukaryotic HECT~Ub or RBR~Ub. Thioester bonds in E2~Ub are longer-lived than E3~Ub (though there is variation across E2s) but are still reactive enough to make them unsuitable for extensive structural characterization using biophysical techniques such as NMR, HDX, SAXS, or crystallography. Past work to make E2~Ub more amenable to structural studies has shown that E1 can transfer Ub to an E2 in which the active site cysteine of has been mutated to serine or lysine, generating a less reactive oxyester bond or non-reactive isopeptide bond between the C-terminus of Ub and the active site Ser or Lys of the E2 [84].

The ability to generate an oxyester or isopeptide bond between Ub and an E2 active site Ser or Lys mutant is dependent on the inherent reactivity of the E2~Ub conjugate. Ube2D3, a highly reactive and promiscuous E3, readily forms oxyester or isopeptide Ub conjugates in typical ubiquitylation reaction conditions. Ube2L3, an E2 specialized for transthiolation reactions, does not form an oxyester or isopeptide Ub conjugate as readily as Ube2D3, and the ubiquitylation reactions generating stable Ube2L3-Ub require longer incubation times, larger amounts of E1 and Ub, and high pH to push the reaction to completion. Past attempts at generating stable mimics of HECT~Ub and RBR~Ub using a similar strategy of mutating the active site cysteine to Ser or Lys have not been successful primarily for two reasons: **1**) lack of reactivity of the E2~Ub conjugate with a Ser or Lys at the E3 active site, and **2**) off-target modifications of surrounding Lys residues by the E2~Ub conjugate.

In **Part I**, it was shown that SspH1 binds Ube2D3~Ub in a lysine-reactive conformation and that replacement of the SspH1 active site Cys with Lys allows for modification with Ub. To test the conditions in which a Lys active site mutant of SspH1 can be stably modified with Ub, SspH1 with a WT active site Cys, C492K, and C492A were incubated with E1, E2, and Ub. Two constructs of SspH1 were tested, LRR-E3 domains (residues 162-700) (**Fig 4A,B**) and E3 domain

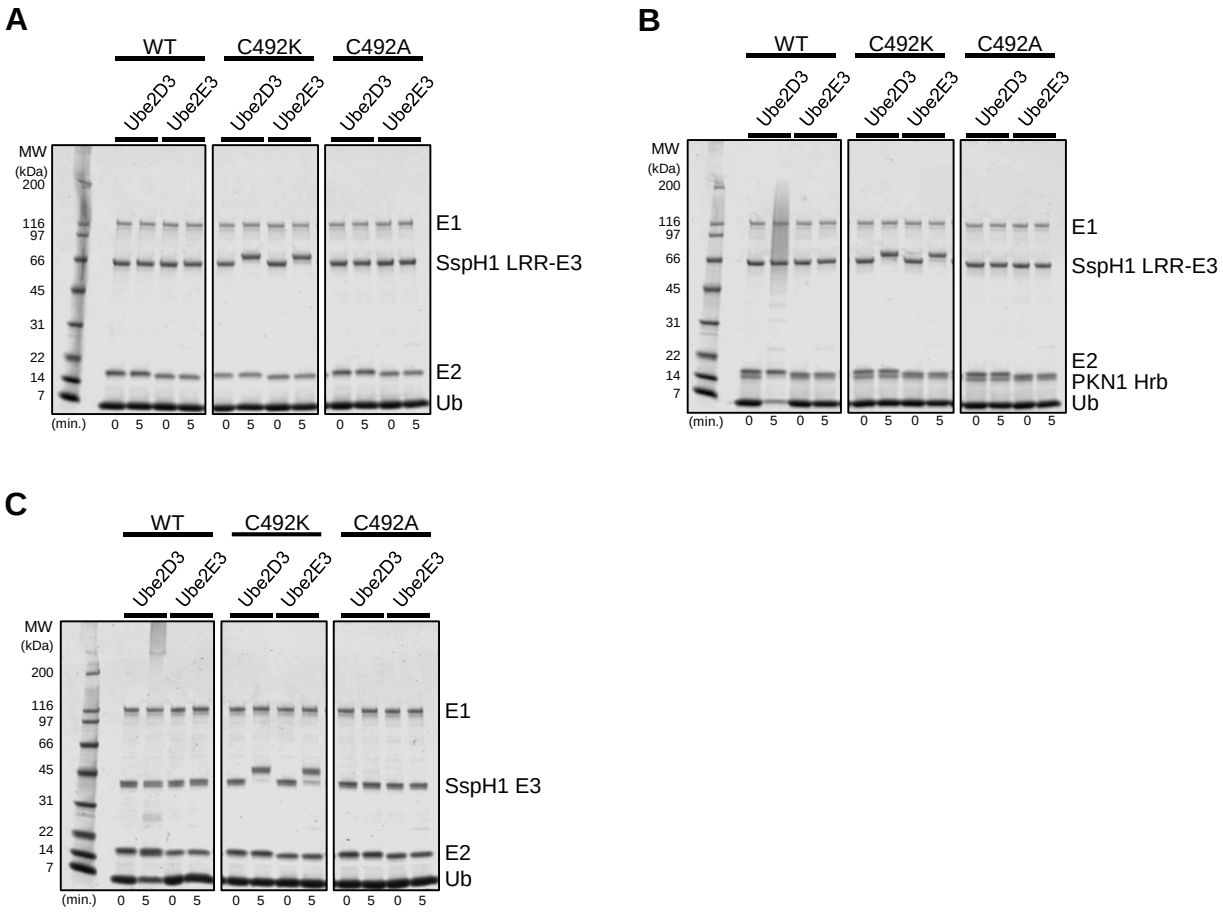

Figure 4. SspH1 lysine active site modification assays with two different E2s for **(A)** SspH1 LRR-E3 without substrate, **(B)** SspH1 LRR-E3 with substrate PKN1, and **(C)** SspH1 E3. Assays were performed with either Ube2D3 or ΔNUbe2E3 as the E2, and cysteine, lysine, or alanine residue at position 492 in SspH1. Reaction conditions: 1μM E1, 5μM E2, 2μM His-SspH1, 50μM Ub, 5μM His-PKN1 108-201, 5mM $MgCl_2$, 5mM ATP, PBS pH7, 37°C. Reducing gel samples taken at 0 min (before addition of ATP), and 5 min, followed by 4-20% gradient SDS-PAGE and staining with Coomassie.

alone (389-700) (**Fig 4C**). The LRR-E3 construct was tested in the absence (**Fig 4A**) and presence (**Fig 4B**) of substrate PKN1 HRb. Two E2s, Ube2D3 and ΔN-Ube2E3 were tested as they can both transfer Ub to the active site Cys of SspH1 (**Fig 3**). In all cases, SspH1 C492K was rapidly modified with a single Ub, with no modification observed for SspH1 C492A. As expected, poly-Ub chains were only observed for SspH1 WT in complex with PKN1, and SspH1 E3 WT. Therefore, a nonreactive mimic of SspH1~Ub, 'SspH1-NH-Ub' can be generated by using Ube2D3~Ub and ΔN-Ube2E3~Ub to selectively form an isopeptide bond between the C-terminus of Ub and a Lys residue at the position of the active site Cys.

The ability to generate SspH1-NH-Ub demonstrates four important features about the interaction between SspH1 and E2~Ub: **1)** SspH1 binds E2~Ub in a lysine-reactive conformation. As previously described, HECT and RBR E3s have been shown to bind E2~Ub in a conformation that reduces lysine reactivity to promote transthiolation with the E3 active site Cys [17, 22, 23]. Despite also having an active site Cys required for Ub transfer, SspH1 binds Ube2D3~Ub and ΔN-Ube2E3~Ub in a conformation that is lysine reactive. A lysine reactive conformation of E2~Ub requires an intact E2, but transthiolation does not (Brzovic, unpublished results). Thus, transthiolation reactions do not need to be catalyzed, and require only close proximity of thioester bonds. **2)** When bound to SspH1, E2~Ub is oriented to react specifically with the SspH1 active site Cys. There are 16 other Lys residues in the SspH1 E3 domain, 6 of which reside in the CSD 'thumb' helices that were shown to bind Ube2D3~Ub in **Part I**. The fact that the lysine-reactive conformations of Ube2D3~Ub and ΔN-Ube2E3~Ub do not transfer Ub to these residues suggests that the Ube2D3~Ub and ΔN-Ube2E3~Ub thioester bond is oriented to react specifically with the SspH1 active site Cys. Given that the E2~Ub conjugate binding site has been shown to be dynamic in the absence of bound E2~Ub, the presence of Ube2D3~Ub and ΔN-Ube2E3~Ub likely stabilizes

the structure of the SspH1 thumb helices to position the thioester bond specifically to react with the SspH1 active site Cys. **3)** Substrate does not affect the ability of SspH1 C492K to be modified with Ub. Comparison between **Fig 4A** and **Fig 4B** shows that the presence of PKN1 HRb does not affect the ability of SspH1 C492K to be modified. Further, PKN1 HRb is not itself modified. The fact that SspH1 binds E2~Ub in a lysine reactive conformation, but none of the 7 Lys residues in PKN1 HRb are modified with Ub is further evidence that E2~Ub binds specifically to react with the SspH1 active site Cys. **4)** Transfer of Ub to the active site of SspH1, even when not autoinhibited, does not necessarily lead to ubiquitylation. As previously demonstrated, both Ube2D3~Ub and ΔN-Ube2E3~Ub can be hydrolyzed by SspH1 in an active-site dependent manner, but ubiquitylation activity is only observed with Ube2D3. The results with SspH1 C492K demonstrate that SspH1 binds both Ube2D3~Ub and ΔN-Ube2E3~Ub in a lysine-reactive conformation, and both E2s can transfer Ub to the Lys at the SspH1 active site. Therefore, both Ube2D3~Ub and ΔN-Ube2E3~Ub can transfer Ub to a Cys or Lys residue at the active site of SspH1, but poly-Ub chains are only formed with Ube2D3~Ub.

SspH1-NH-Ub represents the first nonreactive E3~Ub mimic generated for any class of E3, and investigation of its structure and interaction with substrate and components of the ubiquitylation system will provide novel insights into the mechanism of ubiquitin transfer for E3s that utilize a two-step Ub transfer mechanism. In **Part III**, various constructs of SspH1 and SspH1~Ub in solution are structurally characterized by SAXS and HDX-MS, and the interactions between SspH1~Ub and E2, Ub, and E2~Ub characterized by NMR. Numerous attempts at crystallizing various constructs of SspH1 or SspH1~Ub in complex with PKN1, E2, or E2-O-Ub (using Ube2D3 or ΔN-Ube2E3) to obtain a high-resolution atomic structure have not yet been

successful. However, low resolution crystals which diffracted out to ~8Å were obtained for SspH1 LRR-E3 bound to PKN1 HRb.

Interactions between SspH1 and Ube2D3, Ube2E3, or Ube2L3

The results from the multiple turnover, E2~Ub single turnover, and active site Lys modification assays show that ΔN-Ube2E3 and Ube2D3 can both transfer Ub to the active site of SspH1, but only Ube2D3 can be utilized by SspH1 to ubiquitylate substrate. Why doesn't ΔN-Ube2E3 work to modify substrate? Perhaps the differences in activity come from the formation of non-productive complexes. A non-productive complex may result from weak interactions, binding of E2~Ub in the wrong orientation, or binding to the wrong surface of SspH1. To structurally characterize complex formation between SspH1 and E2~Ub, NMR was used to map the surfaces of free E2 and E2~Ub for Ube2D3, Ube2E3, and Ube2L3.

SspH1 does not bind free Ube2D3, ΔN-Ube2E3, Ube2L3, or Ube2L3~Ub

Structural studies of eukaryotic E3s have shown that they are able to bind free E2 as well as E2~Ub [16, 85, 86, 87]. This is not the case for IpaH-SspH effectors, as the SspH2 E3 domain was shown not to bind free Ube2D3 or Ub [48]. Since SspH1 possess differential ubiquitylation activity with Ube2D3, ΔN-Ube2E3, and Ube2L3, binding of the SspH1 E3 domain to free E2s was tested here. If ΔN-Ube2E3 has a high affinity to SspH1 that prevents productive complex formation with ΔN-Ube2E3~Ub, the lack of ubiquitylation activity could be explained by competitive inhibition.

To test if the SspH1 E3 domain binds free Ube2D3 or Ub, ^{1}H-^{15}N TROSY spectra of a mixture of unconjugated 200μM ^{15}N-Ube2D3 and 200μM ^{15}N-Ub were collected in the absence (black spectrum) and presence 200μM (blue spectrum) and 400μM (red spectrum) SspH1 E3

domain (**Fig 5**). In accordance with previous results, peaks corresponding to Ube2D3 residues did not shift upon addition of SspH1 E3 domain, even at a greater molar ratio than those used previously [48]. However, some weak shifting was observed for peaks corresponding to Ub residues, indicating that SspH1 has a higher affinity for Ub than for free Ube2D3. The implications of Ub binding will be discussed later.

To test if the SspH1 E3 domain can bind free ΔN-Ube2E3, ^{1}H-^{15}N TROSY spectra of 200μM ^{15}N-ΔN-Ube2E3 were collected in the absence (**Fig 6A**) and presence (**Fig 6B**) of 100μM SspH1 E3 domain. Resonance intensity analysis (**Fig 6C**) shows very little loss in resonance intensity in the presence of the SspH1 E3 domain, indicating that the SspH1 E3 domain does not bind free ΔN-Ube2E3. Therefore, ΔN-Ube2E3 does not act as a competitive inhibitor of ΔN-Ube2E3~Ub.

To check if the inability of SspH1 to hydrolyze Ube2L3~Ub is due to lack of productive complex formation between SspH1 and Ube2L3 or Ube2L3~Ub, ^{1}H-^{15}N TROSY spectra of 200μM ^{15}N-Ube2L3 was collected in the presence and absence of 55μM SspH1 E3 domain **(Fig 7A)**, and spectra of 210μM ^{15}N-Ube2L3-O-^{15}N-Ub was collected in the presence and absence of 56μM SspH1 E3 domain **(Fig 7B)**. Due to a limited amount of sample, the final concentration of ^{15}N-Ube2L3-O-^{15}N-Ub was diluted to 185μM instead of 210μM in the presence of SspH1 E3 domain. To correct for the decrease in resonance intensity as a result of lower sample concentration, a correction factor of 210μM/185μM=1.35 was applied to the calculated ratio of resonance intensities for that experiment **(Fig 7C,D)**. The addition of SspH1 E3 resulted in very little peak broadening or chemical shifts in the spectra of ^{15}N-Ube2L3 or ^{15}N-Ube2L3-O-^{15}N-Ub, suggesting that the lack of activity of SspH1 with Ube2L3 is due to an inability to form a productive SspH1/Ube2L3~Ub complex. Therefore, though Ube2L3 has evolved to be a

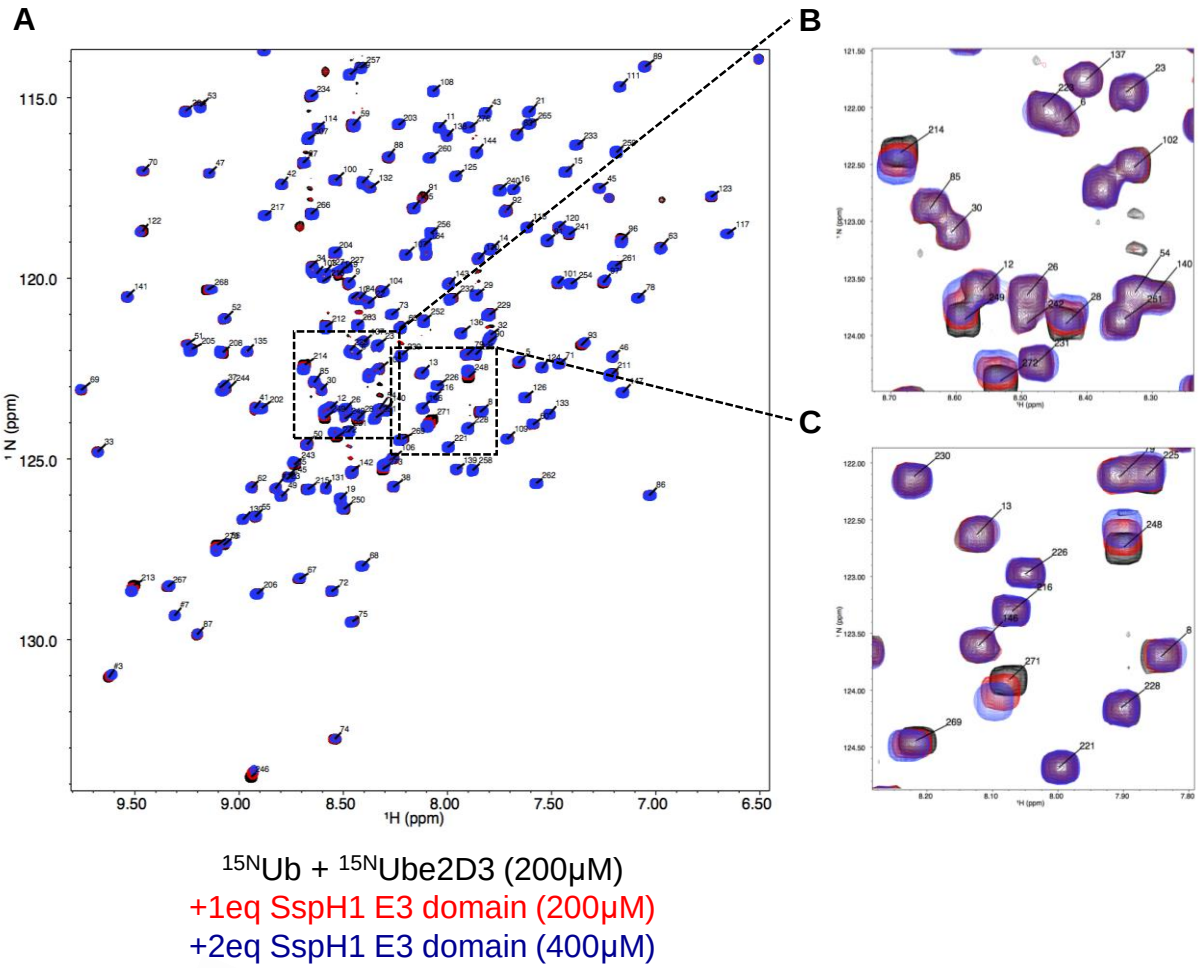

Figure 5. ^{1}H-^{15}N-TROSY spectra of **(A)** free 200µM 15N-Ub and free 200µM 15N-Ube2D3 alone (black spectrum) or in the presence of 200µM SspH1 E3 (red spectrum) or 400µM SspH1 E3 (blue spectrum). **(B)** and **(C)** close up of ^{1}H-^{15}N-TROSY resonances perturbed upon SspH1 E3 domain binding. Resonances labelled 201 and greater represent ubiquitin resonances, those labelled under 200 represent Ube2D3 resonances. **(D)** Close up view of residues on the hydrophobic patch of ubiquitin (PDB: 1UBQ).

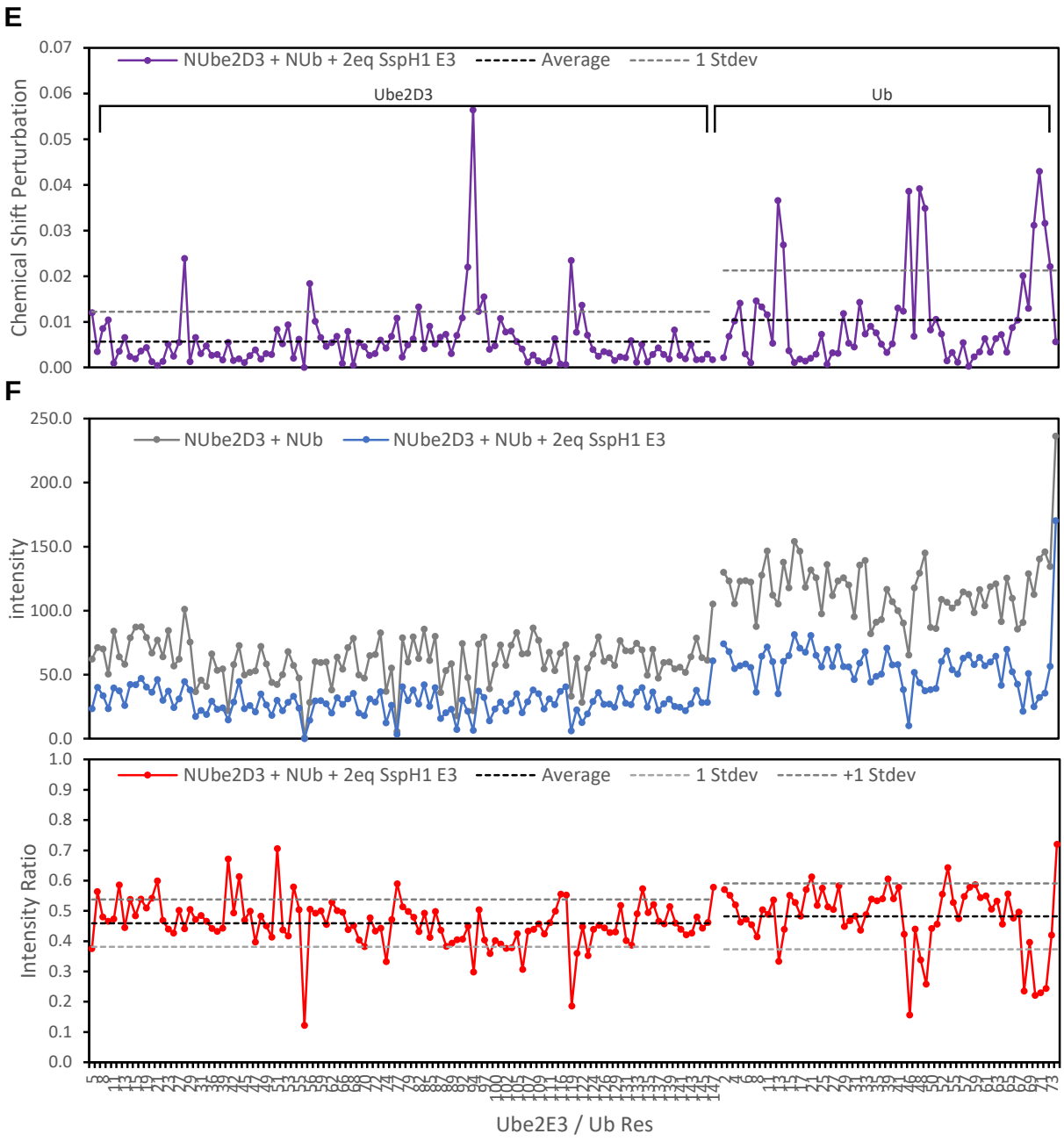

Figure 5. Resonance chemical shift perturbation analysis **(E)** and intensity analysis **(F)** for a mixture of unconjugated 200μM ^{15}N-Ube2D3 and 200μM ^{15}N-Ub in the presence of 600μM SspH1 E3 domain. Chemical shift perturbation calculated by $\sqrt{(\delta N/5)^2 + \delta H^2}$ where δN is the change in ^{15}N ppm and δH is the change in ^{1}H ppm for a particular resonance. Raw intensities in **(F)** top panel, intensity ratios of bound/free are in **(F)** bottom panel.

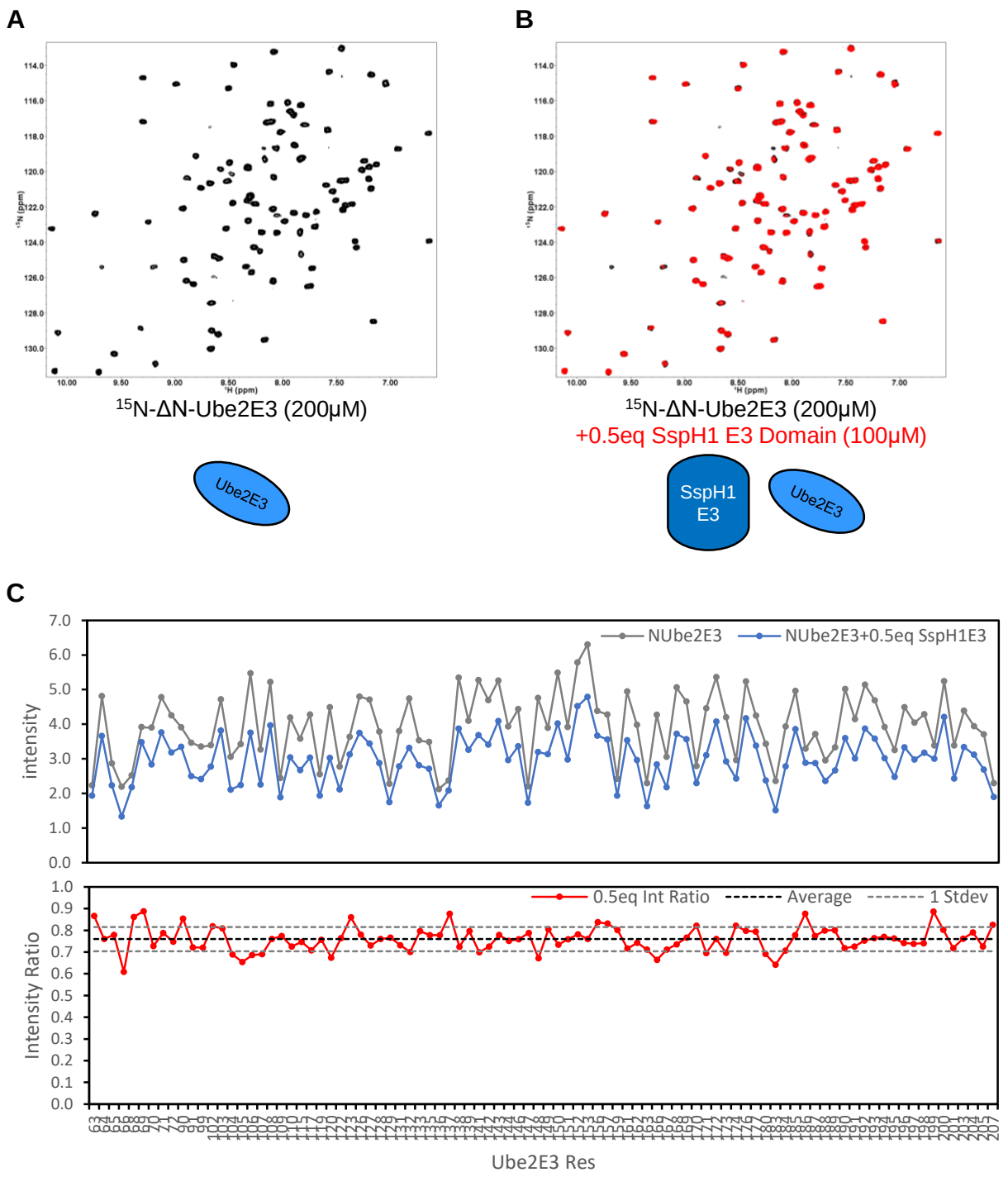

Figure 6. ^{1}H-^{15}N TROSY spectra of **(A)** 200μM ^{15}N-ΔN-Ube2E3 (black spectrum) alone and **(B)** in the presence of 100μM SspH1 E3 (red spectrum). **(C)** Resonance intensity analysis of ^{1}H-^{15}N TROSY spectra in **(A)**. Raw intensities in top panel, intensity ratios of bound/free are in bottom panel.

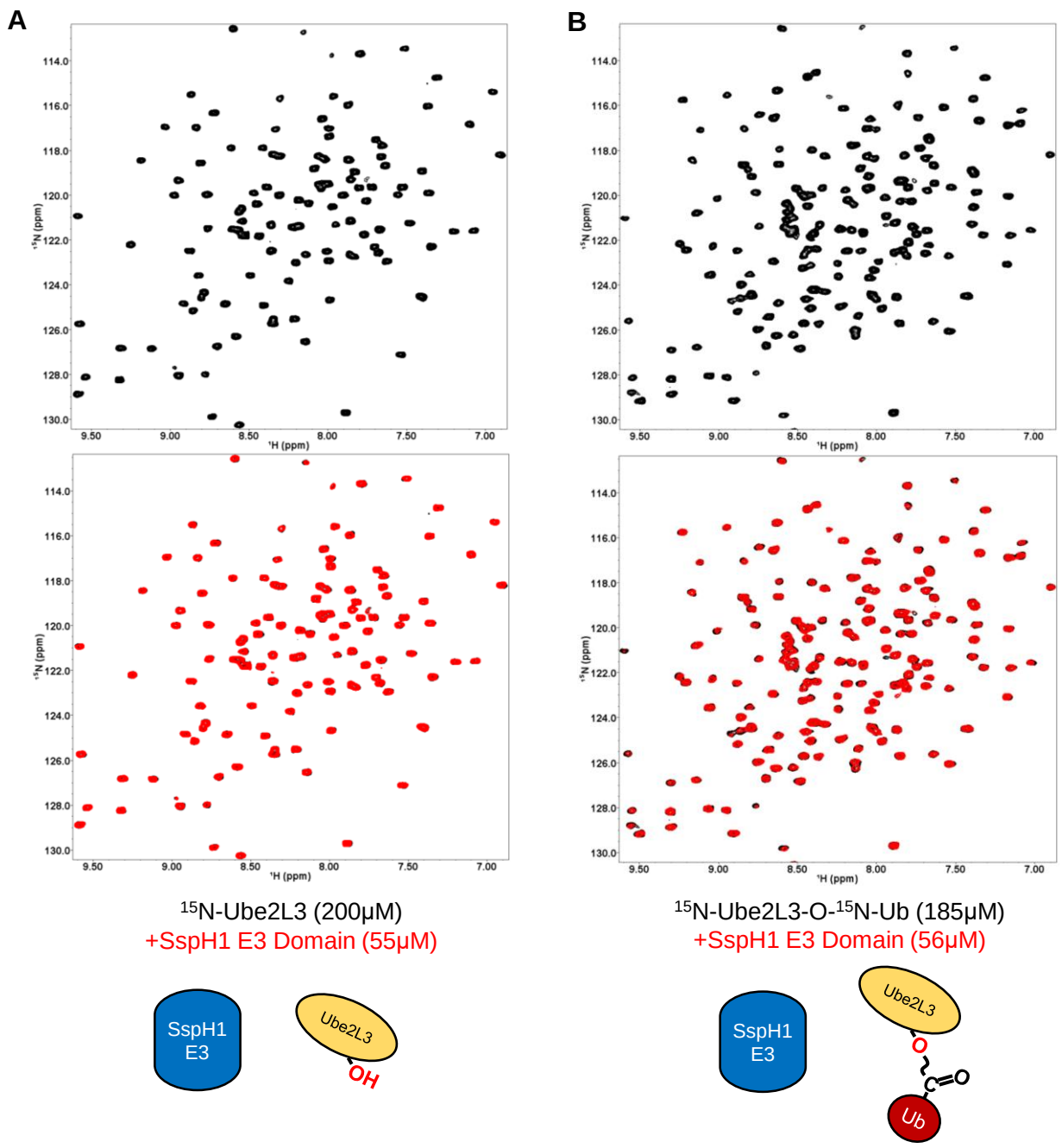

Figure 7. ^{1}H-^{15}N TROSY spectra of **(A)** 200μM ^{15}N-Ube2L3 (black spectrum) alone (top panel) and in the presence of 55μM SspH1 E3 (red spectrum, bottom panel). **(B)** ^{1}H-^{15}N TROSY spectra of 210μM ^{15}N-Ube2L3-O-^{15}N-Ub (black spectrum) alone (top panel) and 185μM ^{15}N-Ube2L3-O-^{15}N-Ub in the presence of 56μM SspH1 E3 (red spectrum, bottom panel).

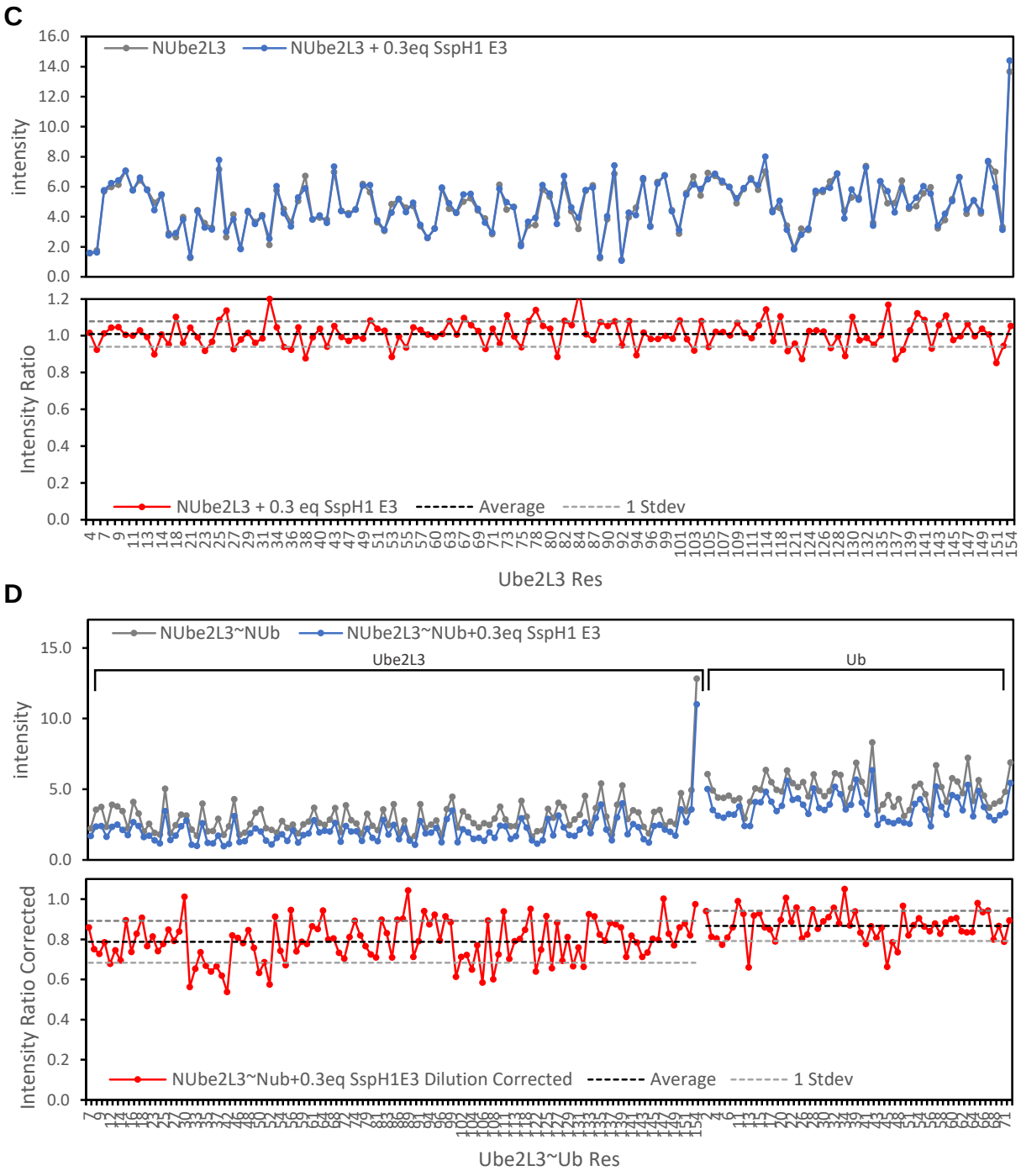

Figure 7. Resonance intensity analysis of ^{1}H-^{15}N TROSY spectra for **(C)** 200µM ^{15}N-Ube2L3 in the presence of 55µM SspH1 E3, and **(D)** 185µM ^{15}N-Ube2L3-O-^{15}N-Ub (black spectrum) in the presence of 56µM SspH1 E3. Raw intensities are in top panels, intensity ratios of bound/free are in bottom panels. For ^{15}N-Ube2L3-O-^{15}N-Ub, slight dilution in sample volume led to a correction factor of 210µM/185µM=1.35 to be applied to intensity ratios to correct for a decrease in resonance intensity due to dilution.

transthiolating E2 for eukaryotic E3s, its molecular surface is not readily recognized by SspH1. Since the sequence for Ube2L3 is quite different from that of Ube2D3 or Ube2E3 in the SspH1 binding region, it is not surprising that Ube2L3 does not bind SspH1.

SspH1-binding surfaces for Ube2D3~Ub, ΔN-Ube2E3~Ub and Ube2L3~Ub

To test if SspH1 binds Ube2D3~Ub and ΔN-Ube2E3~Ub similarly, ^{1}H-^{15}N TROSY spectra were obtained for 100μM ^{15}N-Ube2D3-O-^{15}N-Ub or ^{15}N-ΔN-Ube2E3-O-^{15}N-Ub in the presence and absence of 25μM SspH1 E3 domain **(Fig 8A,B)**. The residues corresponding to the resonances that are most perturbed upon addition of SspH1 are highlighted on structures of Ube2D3 (PDB: 1X23), Ube2E2 (PDB: 1Y6L), and Ub (PDB: 1UBQ) **(Fig 8C,D)**. The most perturbed resonances were identified by quantifying the intensity of each resonance and calculating the ratio of SspH1-bound versus free for each resonance **(Fig 8E,F)**. Since many resonances decreased in intensity for SspH1-bound constructs, ratios that fell below 1 standard deviation of the average were selected as most perturbed. ^{15}N-Ube2D3-O-^{15}N-Ub and ^{15}N-ΔN-Ube2E3-O-^{15}N-Ub show similarly perturbed surfaces in the presence of SspH1 E3 domain, including helix 2 and loop 7 of the E2 subunit, and the C-terminus and hydrophobic β-sheet patch of the Ub subunit. These surfaces align with those characterized in Levin (2010) and **Part I** of this work.

The work in Levin (2010) examined the E3 domain of SspH2 in the presence of Ube2D3~Ub. To test if the presence of the LRR domain alters interactions between the E3 domain and E2~Ub, ^{1}H-^{15}N TROSY spectra were obtained for 100μM ^{15}N-Ube2D3-O-^{15}N-Ub alone and in the presence of 25μM SspH1 LRR-E3 domain **(Fig 9A)**. The perturbed surface of ^{15}N-Ube2D3-O-^{15}N-Ub **(Fig 9B)** following resonance intensity analysis **(Fig 9C)** reveals a similar surface to

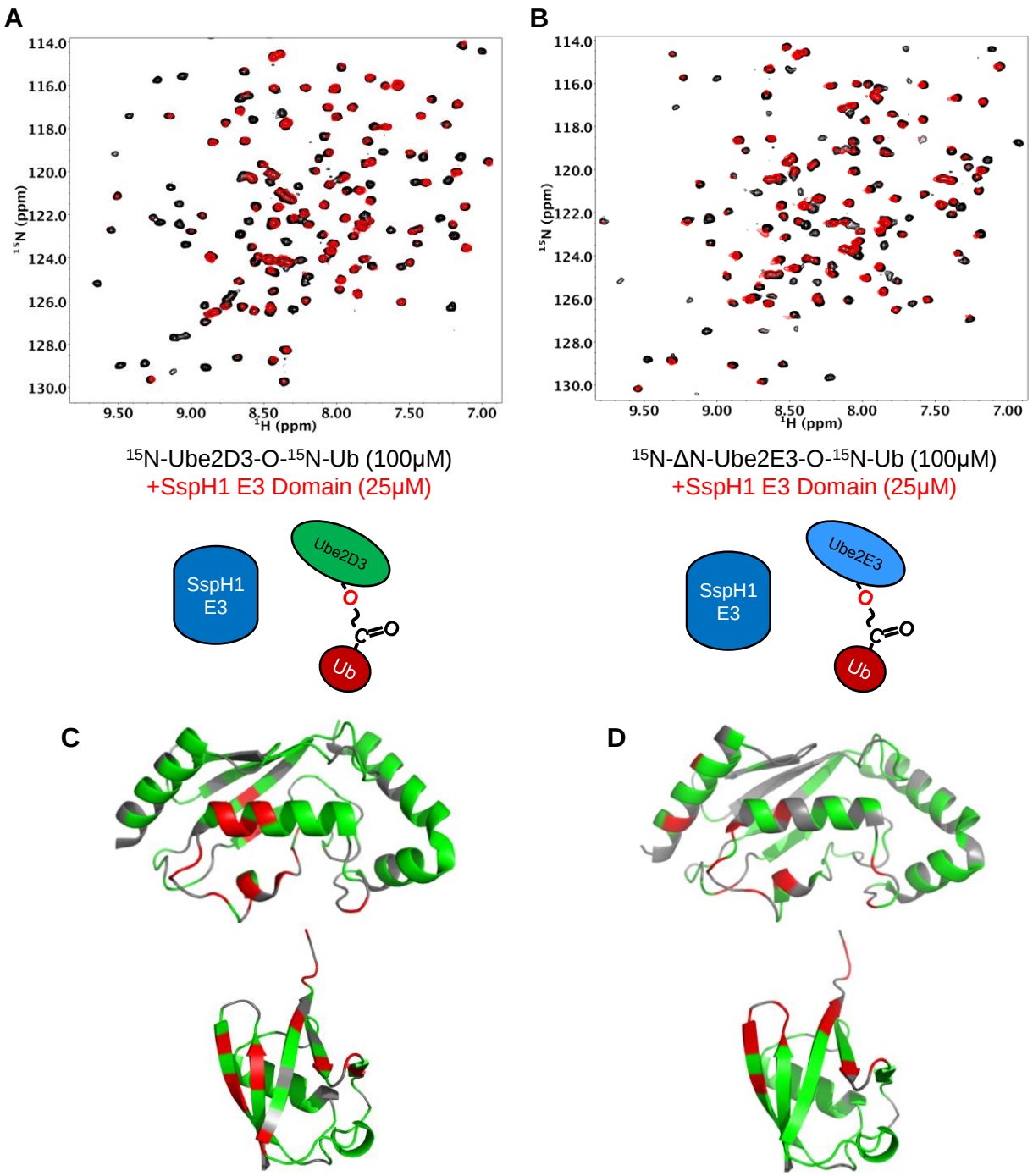

Figure 8. ^{1}H-^{15}N TROSY spectra of **(A)** 100μM ^{15}N-Ube2D3-O-^{15}N-Ub (black spectrum) in the presence of 25μM SspH1 E3 (red spectrum) and **(B)** 100μM ^{15}N-ΔN-Ube2E3-O-^{15}N-Ub (black spectrum) in the presence of 25μM SspH1 E3 (red spectrum). **(C)** Perturbed residues (red) on structures of Ube2D3 (PDB: 1X23) and ubiquitin (PDB: 1UBQ). **(D)** Perturbed residues (red) on structures of Ube2E2 (PDB: 1Y6L, 97% identical to Ube2E3) and ubiquitin (PDB: 1UBQ). Unresolved, unassigned, or low intensity residues in grey. Resonance intensity analysis identifying perturbed residues in **(E)** and **(F)** (next page).

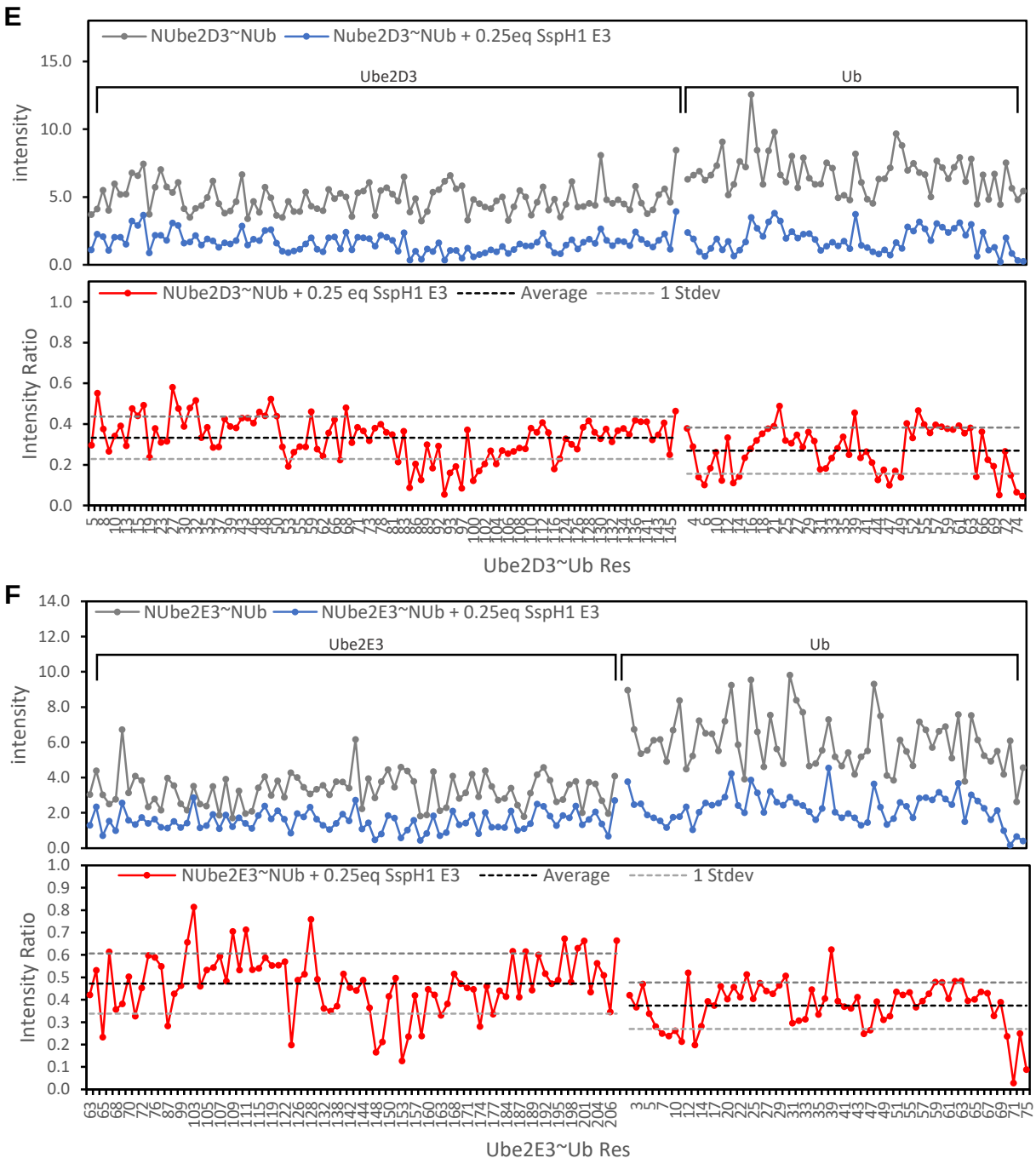

Figure 8. Resonance intensity analysis of ^{1}H-^{15}N TROSY spectra for **(E)** 100µM ^{15}N-Ube2D3-O-^{15}N-Ub in the presence of 25µM SspH1 E3 and **(F)** 100µM ^{15}N-ΔN-Ube2E3-O-^{15}N-Ub in the presence of 25µM SspH1 E3. Raw intensities are in top panels, intensity ratios of bound/free are in bottom panels. Perturbed resonances falling below 1 standard deviation are plotted on molecules structures in **(C)** and **(D)**

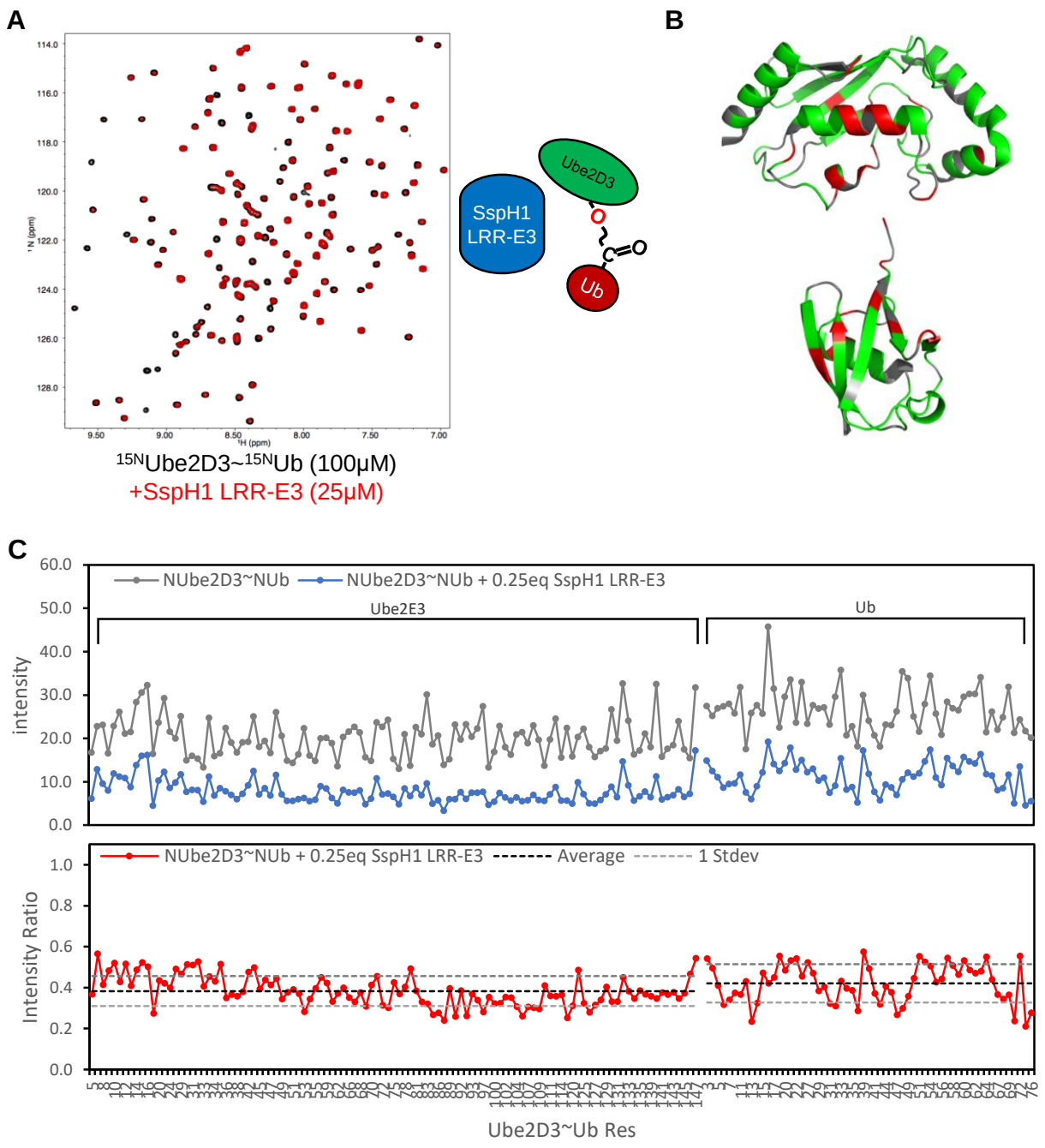

Figure 9. ^{1}H-^{15}N TROSY spectra of **(A)** 100μM ^{15}N-Ube2D3-O-^{15}N-Ub (black spectrum) in the presence of 25μM SspH1 LRR-E3 (red spectrum). **(B)** Perturbed residues (red) on structures of Ube2D3 (PDB: 1X23) and ubiquitin (PDB: 1UBQ). Unresolved, unassigned, or low intensity residues in grey. **(C)** Resonance intensity analysis of ^{1}H-^{15}N TROSY spectra in **(A)**. Raw intensities are in top panels, intensity ratios of bound/free are in bottom panels. Perturbed resonances falling below 1 standard deviation are plotted on molecules structures in **(B)**

that obtained with the SspH1 E3 domain, indicating that the LRR domain does not impact the ability of the E3 domain to engage E2~Ub.

Investigating the difference in reactivity between Ube2D3 and ΔN-Ube2E3 in SspH1 catalyzed reactions

If Ube2D3 and ΔN-Ube2E3 are so similar in sequence and structure (**Fig 1**), and both Ube2D3~Ub and ΔN-Ube2E3~Ub transfer Ub to the SspH1 active site cysteine (**Fig 3**), then why are poly-Ub chains only formed by SspH1 with Ube2D3? The surfaces of Ube2E3 and Ube2D3 that interacts with the thumb region of SspH1 are nearly completely conserved, and NMR shows that these surfaces for both E2~Ubs are perturbed upon binding SspH1 (**Fig 8**). Though the E2s function in Stage I, it is possible that one or more other surfaces of the E2s that are not conserved play a critical role in Stage II of the Ub transfer reaction. Previous studies have shown that single amino acid substitutions in these E2s can have a profound effect on ubiquitylation activity. Nuber and Scheffner (1999) showed that a Val in the active site of Ube2E1 (corresponding to Ser83 in Ube2D3) prevents ubiquitylation activity with HECT-type E3s E6-AP and Rsp5. Ube2D3 S83V recapitulated the lack of activity observed with Ube2E1 [88]. Wu *et al.* (2003) showed that Ube2D3 N77S disables isopeptide bond formation with RING-type E3s. Brzovic *et al.* (2006) showed that Ube2D3 S22R disables processive poly-Ub chain building building activity with the RING-type E3 BRCA1 [13]. Pruneda *et al.* (2012) showed that Ube2D3 L104Q disfavors the lysine-reactive "closed-state" for Ube2D3~Ub and hinders ubiquitylation activity with RING-type E3s. Therefore, there is a large body of evidence suggesting that single amino-acid substitutions in E2s designed to hinder ubiquitylation activity can lead to insights into Ub transfer mechanisms.

There are two methods of uncovering the differences between Ube2E3 and Ube2D3 through mutational analysis: mutating Ube2E3 residues to corresponding Ube2D3 residues to promote poly-Ub activity, or mutating Ube2D3 residues to corresponding Ube2E3 residues to inhibit poly-Ub activity. Given past work, it is reasonable to assume that it should be easier to inhibit an enzyme's activity through mutational analysis rather than give an enzyme new activity. Therefore, to determine if any specific set of amino acids in Ube2D3 are required for poly-Ub chain building activity with SspH1, a variety of mutations were made in Ube2D3 based on the sequence alignment with Ube2E3 (**Fig 1**) and previous literature. The various Ube2D3 mutants were tested for ubiquitylation activity with SspH1 domain (**Fig 10**, **Table 1**).

An example of the ubiquitylation assays performed is shown in **Fig 10**. The various Ube2D3 mutants or ΔN-Ube2E3 were incubated with SspH1 E3 domain or full-length SspH1 in complex with PKN1. Reactions were performed with WT SspH1 or a C492K mutant to assess lysine reactivity of the E2~Ub conjugate. Examples of Ube2D3 mutations chosen based on mutations uncovered in previous literature (S22R, L104Q) are shown in **Fig 10A,B**. Examples of mutations based on the sequence alignment between Ube2D3 and Ube2E3 (T53D/H55T, S83V) are shown in **Fig 10C,D**. The full results of these assays are presented in **Table 1**. No single amino acid substitution, or set of substitutions, disabled SspH1 poly-Ub chain activity for Ube2D3 completely. Ube2D3 N77S, which has previously been shown to inhibit lysine reactivity of Ube2D3~Ub, did have a small effect on lysine reactivity here [89], but did not completely inhibit lysine reactivity of Ube2D3 with Lys at the SspH1 active site. The S22R mutation did appear to slightly change the distribution of poly-Ub chains formed with the SspH1 E3 domain (**Fig 10B**), but the enzyme was still highly active and fully modified PKN1.

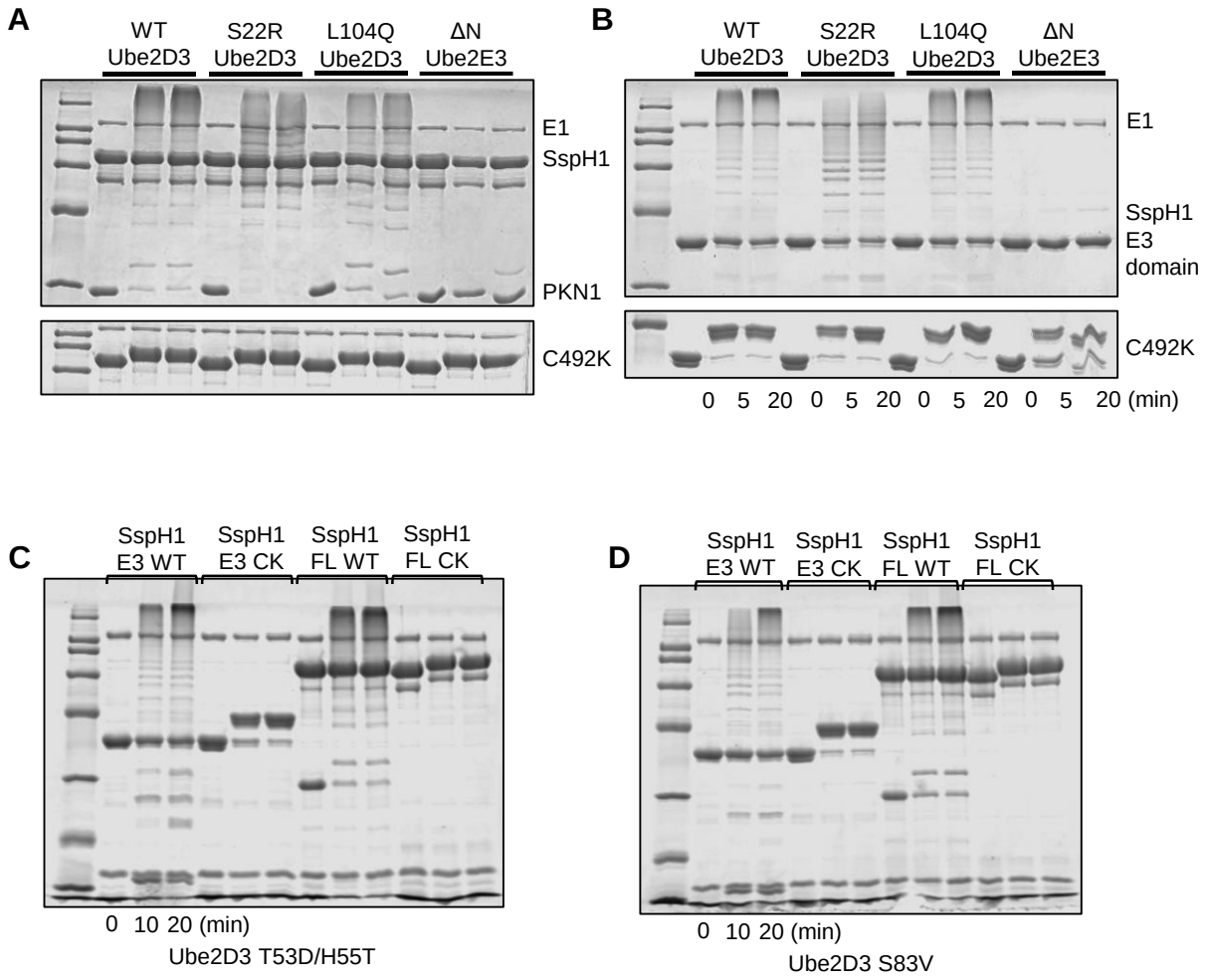

Figure 10. SspH1 ubiquitylation activity with Ube2D3 wildtype and mutants S22R, L104Q, UbcM2 for **(A)** full length SspH1 in complex with PKN1 HRb or **(B)** SspH1 E3 domain. SspH1 ubiquitylation assays for SspH1 E3 domain or full-length (FL) SspH1 with wildtype active site cysteine (WT) or Cys492Lys (CK) mutation for **(C)** Ube2D3 T53D/H55T mutant or **(D)** Ube2D3 S83V mutant. Ubiquitylation conditions: 1μM E1, 5μM E2, 10μM SspH1, 100μM Ub, 20μM PKN1 HRab (1-201), 5mM ATP, 5mM $MgCl_2$, 37°C. Reducing gel samples taken at 0 min (before addition of ATP), 10 and 20 min, followed by 4-20% gradient SDS-PAGE and staining with Coomassie.

Ube2D3 ➔ Ube2E3	SspH1 E3 WT	SspH1 E3 C492K
A19P/Q20N	✔	✔
$_{29}$DMFH$_{32}$->NIYE	✔	✔
V26K/$_{29}$DMFH$_{32}$->NIYE	✔	✔
Q34R	✔	✔
T53D	✔	✔
T53D/H55T	✔	✔
T70R	✔	✔
S83V	✔	✔
$_{90}$RSQ$_{92}$->KDN	✔	✔
D116A	✔	✔

HECT inactive →

RING polyUb →

LYS inactive →

Prevents closed state →

Other Mutants	SspH1 E3 WT	SspH1 E3 C492K
S22R	✔	✔
N77S	✔	slower
L104Q	✔	✔

Table 1. Summary of SspH1 ubiquitylation activity with Ube2D3 mutants. Examples of ubiquitylation reactions used to generate the table are shown in **Fig 10**.

Given that **1)** Ube2D3 and ΔN-Ube2E3 can both transfer Ub to the active site Cys of SspH1, **2)** SspH1 binds Ube2D3~Ub and ΔN-Ube2E3~Ub similarly, the lack of ubiquitylation activity with ΔN-Ube2E3 is puzzling. A screen of Ube2D3 → ΔN-Ube2E3 mutants to break the ubiquitylation activity of Ube2D3 did not uncover any single mutation or set of mutations that define a surface of Ube2D3 that is critical for Stage II of the SspH1 ubiquitin transfer reaction.

Ub drives E2~Ub binding to SspH1 via an L8-I44 hydrophobic patch

As described earlier, in the presence of large amounts of SspH1 E3, some weak shifting was observed for peaks corresponding to Ub residues, but not E2 residues. Enlarged views of the spectra in **Fig 5A** are shown in **Fig 5B** and **Fig 5C**, with peak labels above 200 corresponding to Ub residues (*i.e.* peak 48 corresponds to Ube2D3 residue 48 while peak 248 corresponds to Ub residue 48). Several Ub peaks clearly shift upon increasing additions of SspH1 E3 domain, and these peaks correspond to a hydrophobic patch on the β-sheet of Ub containing residues Ile44, Leu8, and Val70, and the C-terminal tail of Ub (**Fig 5D**). This surface is commonly used for protein-protein interactions in eukaryotic ubiquitin signaling. Chemical shift perturbation (CSP) analysis (**Fig 5E**) and resonance intensity analysis (**Fig 5F**) were performed to identify resonances most perturbed upon addition of SspH1 E3 domain. Chemical shift perturbation, an indicator of a change in the chemical environment of a residue, was calculated using the equation $\sqrt{(\delta N/5)^2 + \delta H^2}$, where δN is the change in location of a resonance in the ^{15}N dimension, and δH is the change in location of a resonance in the ^{1}H dimension.

To test if mutating the hydrophobic patch of Ub affects binding to the SspH1 E3 domain or ubiquitylation activity, mutations were made to Ub Ile44, Leu8, or Val70. Ubiquitylation activity of the SspH1 E3 domain was reduced dramatically by Ub Ile44Ala, Leu8Ala, and the

I44A/L8A double mutant (**Fig 11A**, top panel). Substrate-directed ubiquitylation was also reduced for SspH1 LRR-E3 in complex with PKN1 with the Ub I44A/L8A double mutant (**Fig 11B**, top panel). For Ub L8A and I44A/L8A mutants, modification of the Lys active site mutant was reduced for the SspH1 E3 domain and LRR-E3 domain in complex with PKN1 (**Fig 11A,B**, bottom panel). Ubiquitylation activity of the SspH1 E3 domain was also reduced by mutations to Val70, with a single non-conservative point mutant, Val70Asp, abolishing ubiquitylation activity (**Fig 11C**).

To test if mutation of the hydrophobic path of Ub abolishes binding to the SspH1 E3 domain, ^{1}H-^{15}N TROSY spectra of 150μM ^{15}N-Ub I44A/L8A were collected in the absence and presence of 450μM SspH1 E3 domain (**Fig 11D**). For wildtype Ub, peak shifts in the ^{1}H-^{15}N TROSY spectrum were observed in the presence of 1 and 2 molar equivalents of SspH1 E3 domain. A lack of peak shifting or broadening for Ub I44A/L8A in the presence of 3 molar equivalents of SspH1 E3 domain indicates that the hydrophobic patch is required for Ub binding to SspH1.

To test if the hydrophobic patch of Ub is required for E2~Ub binding, ^{1}H-^{15}N TROSY spectra of 150μM ^{15}N-Ube2D3-O-^{15}N-Ub I44A/L8A were collected in the absence (black spectrum) and presence (red spectrum) of 38μM SspH1 LRR-E3 (**Fig 11E**). Compared to the ^{1}H-^{15}N TROSY spectra for ^{15}N-Ube2D3-O-^{15}N-Ub in the presence of ¼ molar equivalents of SspH1 LRR-E3 (**Fig 9**), a lack of major peak shifting or intensity loss in the ^{1}H-^{15}N TROSY spectrum of ^{15}N-Ube2D3-O-^{15}N-Ub I44A/L8A in the presence of ¼ molar equivalents of SspH1 LRR-E3 indicates that the hydrophobic patch of Ub is critical for binding of E2~Ub. Therefore, the lack of ubiquitylation activity of SspH1 with Ub hydrophobic patch mutants can be attributed to a disruption of a competent E3-E2~Ub complex.

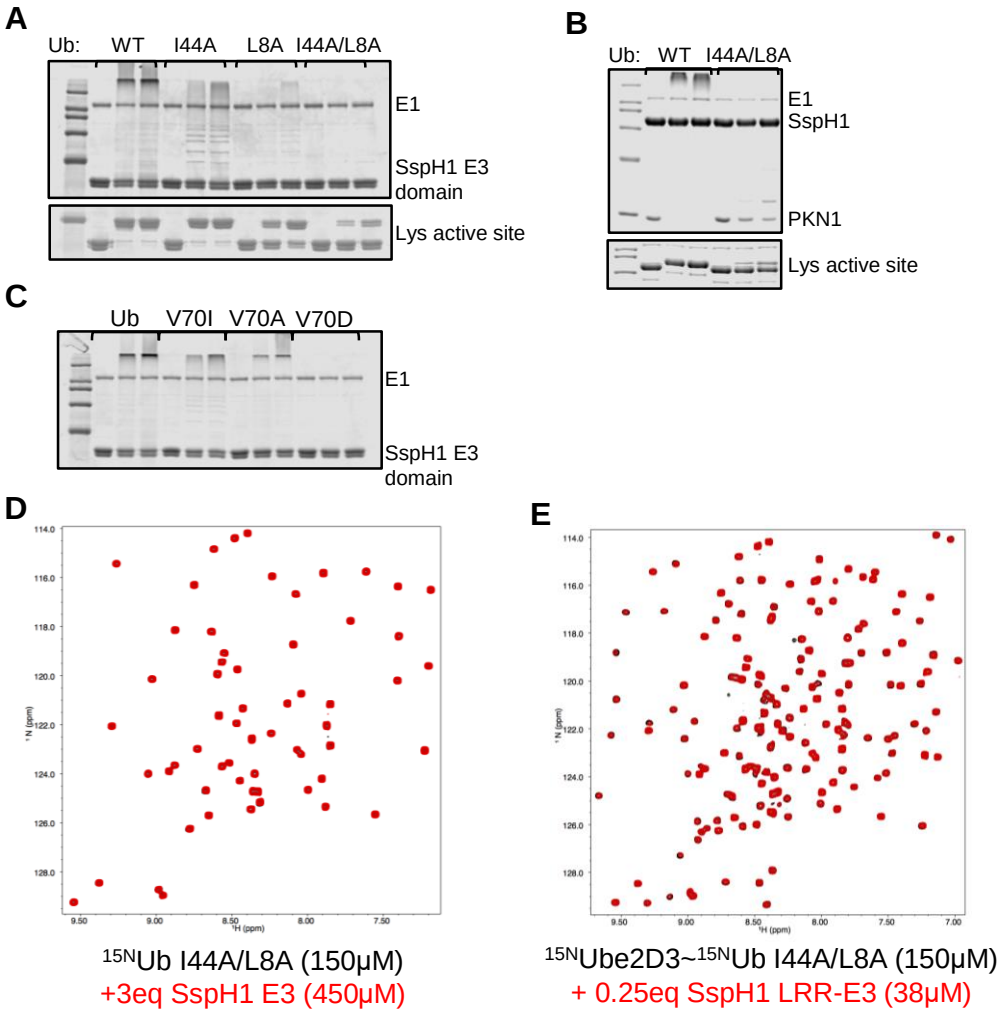

Figure 11. Hydrophobic patch on ubiquitin is required for SspH1 ubiquitylation activity and E2~Ub binding. **(A)** Ubiquitylation activity of SspH1 E3 domain with various ubiquitin mutants, from left-to-right: wildtype, I44A, L8A, and I44A/L8A double mutant. Top panel: wildtype cysteine active site, bottom panel: lysine mutant active site. **(B)** Ubiquitylation activity of SspH1 LRR-E3 in complex with PKN1 HRb and wildtype vs I44A/L8A ubiquitin. Top panel: wildtype cysteine active site, bottom panel: lysine mutant active site. **(C)** Ubiquitylation activity of SspH1 E3 domain and various V70 mutants of ubiquitin. **(D)** ^{1}H-^{15}N TROSY spectra 150μM ^{15}N-Ub I44A/L8A (black spectrum) alone and in the presence of 450μM SspH1 E3. **(E)** ^{1}H-^{15}N TROSY spectra of 150μM ^{15}N-Ube2D3-O-^{15}N-Ub I44A/L8A (black spectrum) alone and in the presence of 38μM SspH1 LRR-E3.

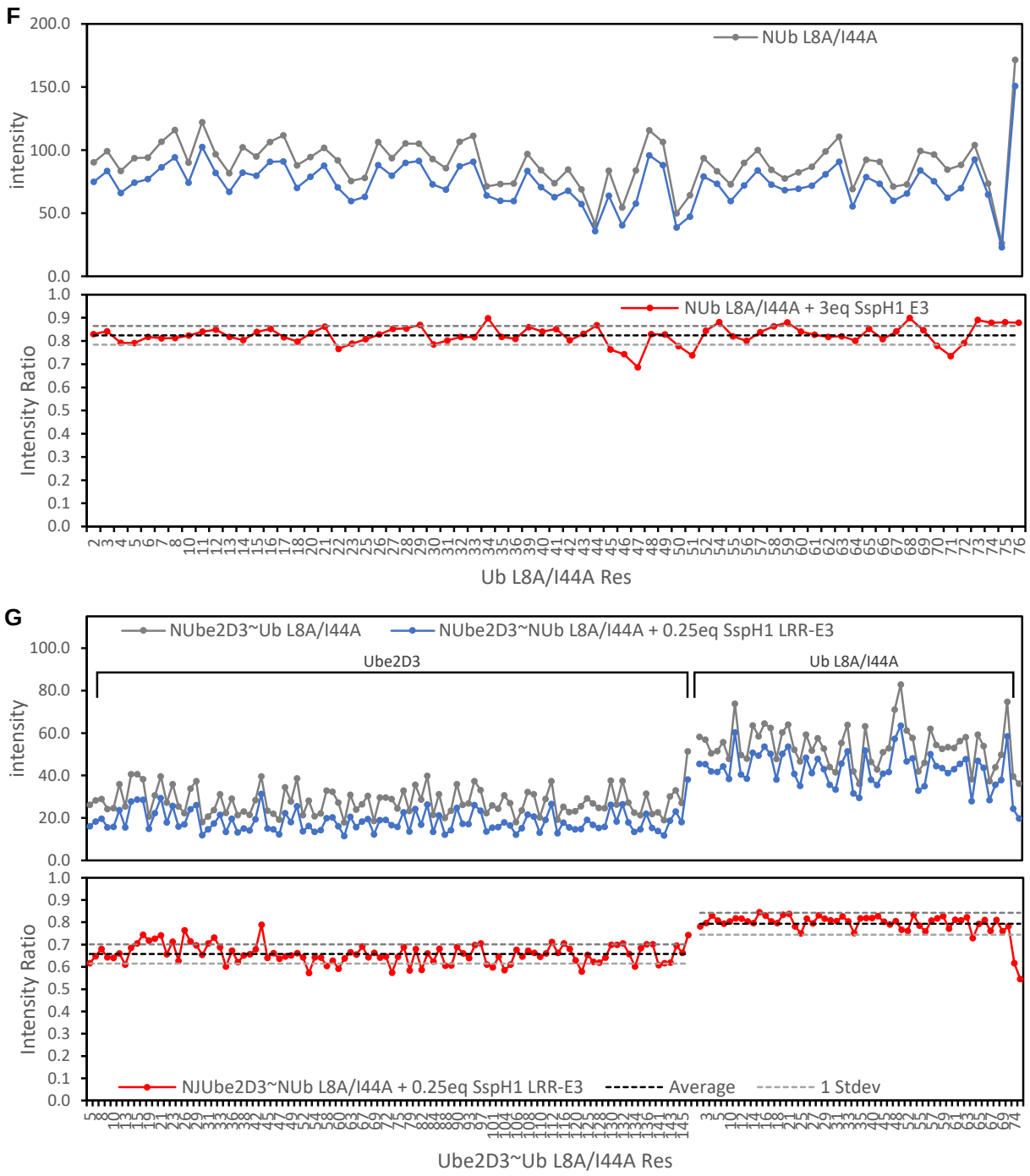

Figure 11. Resonance intensity analysis of ^{1}H-^{15}N TROSY spectra for **(F)** 150μM ^{15}N-Ub I44A/L8A in the presence of 450μM SspH1 E3 and **(G)** 150μM ^{15}N-Ube2D3-O-^{15}N-Ub I44A/L8A in the presence of 38μM SspH1 LRR-E3. Raw intensities in top panel, intensity ratios of bound/free are in bottom panel.

Most eukaryotic E3s characterized so far have detectable affinity for free E2. The affinity is high enough that crystal structures exist of the HECT-type E3 E6AP bound to free Ube2L3 (PDB 1C4Z [16]), the RBR-type E3 Parkin bound to free Ube2L3 (PDB 6DJX [87]), and RING-type E3 Bmi1/Ring1B bound to Ube2D3 (PDB 3RPG [85], PDB 4R8P [86]). However, SspH1 does not bind free Ube2D3 or ΔN-Ube2E3 with any noticeable affinity even though both can transfer Ub to the SspH1 active site. In fact, SspH1 binds free Ub with higher affinity than free E2, and even conservative mutations in L8 and I44 can drastically impact E2~Ub binding and ubiquitylation activity. The hydrophobic surface of Ub is widely used in eukaryotic Ub signaling and mediates protein-protein interactions with many types of proteins. Part I showed that E2~Ub binds SspH1 by clamping around the CSD thumb helices, with E2 located the near the first thumb helix and Ub located near the second thumb helix, near the C-terminus of the protein (**Part I Fig 5**). Therefore, it is likely that the hydrophobic surface of Ub is interacting with the second thumb helix of SspH1 to drive the interaction with E2~Ub.

Numerous non-conservative mutations in Ube2D3 near the active site and SspH1 binding surface did not affect ubiquitylation activity with SspH1 (**Table 1**). Conservative mutations in Ub, however, had drastic effects on Ube2D3-O-Ub binding and ubiquitylation activity with SspH1 (**Fig 11**). Ub also binds SspH1 with higher affinity than E2 (**Fig 5**). Therefore, it appears that the Ub subunit of E2~Ub drives the interaction with SspH1. Previous work with eukaryotic E3s has shown that different E2s hold Ub in different conformations in the E2~Ub conjugate, and that the conformation of the E2~Ub conjugate is important for reactivity with E3s (**Introduction**). It is possible that different conformations of Ube2D3~Ub and Ube2E3~Ub are responsible for very different ubiquitylation activities observed for both E2s. Both Ube2D3~Ub and Ube2E3~Ub bind SspH1 in similar ways to transfer Ub to the SspH1 active site Cys (**Fig 8**), so the differences in

catalytic activity between the E2s likely occurs during the second stage of Ub transfer, from SspH1~Ub to substrate. For eukaryotic E3s with a HECT-type mechanism, it has been assumed that the E3 directs ubiquitylation because it is the last enzyme in the ubiquitylation cascade holding Ub at an active site. Though this assumption has not been directly tested with eukaryotic E3s, the work in **Part II** shows that the assumption does not hold for SspH1. The work in **Part I** and **II** showed that it is possible to form a stable SspH1~Ub mimic by mutating the active site Cys to Lys, the first case that a stable E3~Ub has been formed for the IpaH-SspH family of E3s. This method is unlikely to work with eukaryotic HECT or RBR E3s because they do not bind E2~Ub in a lysine reactive conformation. In **Part III**, differences in the interactions with stable SspH1~Ub and Ube2D3 or Ube2E3 will be investigated by NMR to uncover the mechanism of SspH1 ubiquitylation, and the structural differences that occur in SspH1~Ub relative to SspH1 will be investigated by hydrogen-deuterium exchange mass-spectrometry and small-angle X-ray scattering.

SspH1 LRR-E3 forms unanchored poly-Ub chains in the presence of a substrate lacking lysine

The differential activity between Ube2D3 and Ube2E3 demonstrates that the E2 is critical for driving Ub transfer in Stage II of Ub transfer from SspH1~Ub to substrate. For SspH1 LRR-E3, substrate is also required for Stage II. Presented only with Ube2D3~Ub, SspH1 LRR-E3 will hydrolyze the E2~Ub conjugate, but unlike the E3 domain alone, does not build unanchored poly-Ub chains. Recent literature on the mechanism of IpaH-SspH1 E3s has focused on elucidating the role of the LRR domain in the mechanism of SspH1. Previous work has sought to explain the inhibitory effect of the LRR domain on poly-Ub chain building activity by close inspection of the

interface between LRR and E3 domains in the structures of IpaH3 (PDB: 3CVR [35]) and SspH2 (PDB: 3G06 [37]) (**Intro Fig 4B**) [42, 44]. Disruptive mutations at the interface of the LRR and E3 domains of IpaH9.8 and SspH1 relieved the inhibitory effect of the LRR domain with respect to poly-Ub chain synthesis, in effect unlinking the interaction between the domains [44]. Disrupting PKN1 binding by mutating its binding site on the LRR domain prevents the activating effect of PKN1, further confirming that substrate is required to activate the LRR-E3 domain for poly-Ub chain building activity [42].

Assuming that binding of substrate unlocks the LRR and E3 domains, a construct of PKN1 lacking Lys residues should activate SspH1 without building poly-Ub chains on PKN1. Since PKN1 would have no available Lys residues, the E3 domain should instead build unanchored poly-Ub chains similar to the free E3 domain alone. There are 7 Lys residues in PKN1 HRb at positions 133, 140, 142, 158, 161, 174, and 176. These residues were mutated to Arg, which is unable to form an isopeptide bond with the C-terminus of Ub. Used in ubiquitylation assays with SspH1 LRR-E3, rapid synthesis of unanchored poly-Ub chains was observed **(Fig 12)**. Thus, SspH1 was activated by lysine-less PKN1. However, the observed distribution of poly-Ub chains, their molecular weights, and their rate of formation differed greatly in reactions utilizing wildtype PKN1, lysine-less PKN1, and the unanchored chains generated by the SspH1 E3 domain alone. Comparing ubiquitylation activity of wildtype and lysine-less PKN1 in **Fig 12A** shows that both reactions are nearly complete by 5 minutes, but the molecular weight distribution of ubiquitin chains formed with lysine-less PKN1 is much higher. Comparing ubiquitylation activity at shorter timepoints **(Fig 12B)** shows that the rate of formation of ubiquitin chains is quite different between all three constructs. For SspH1 LRR-E3 in complex with wildtype PKN1 HRb and SspH1 E3 domain alone, poly-Ub chains are observable at the 30 second time point and steadily increase in

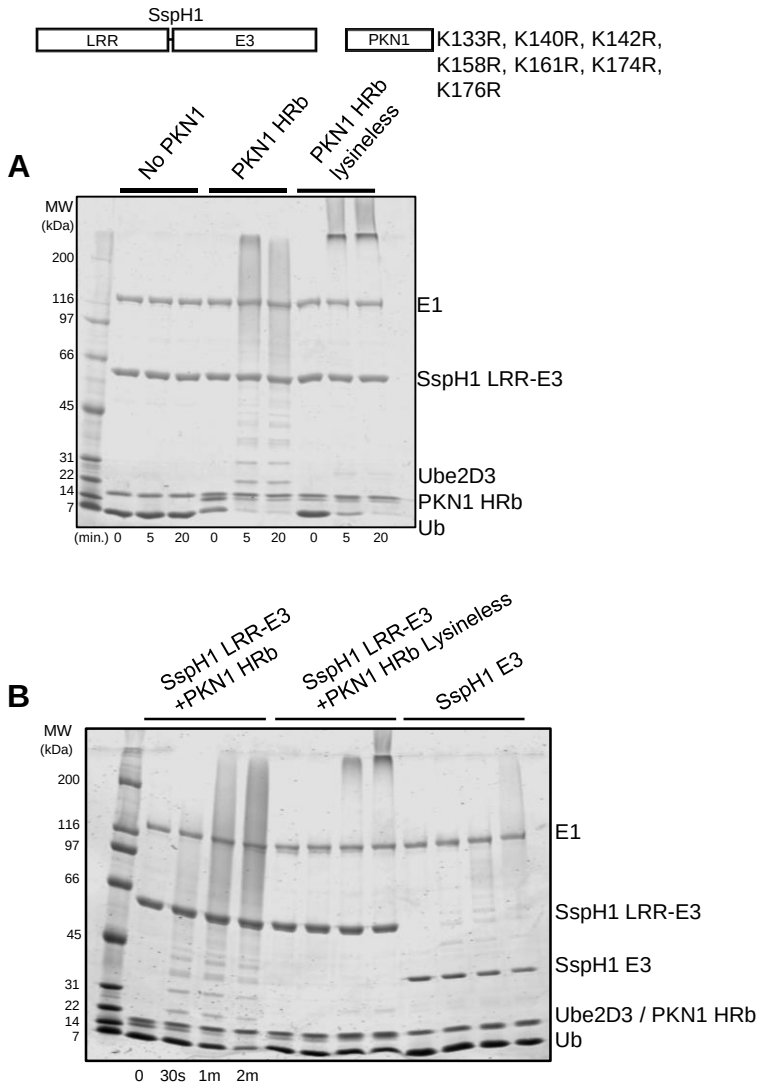

Figure 12. SspH1 ubiquitylation activity with lysineless substrate. **(A)** Ubiquitylation activity of SspH1 LRR-E3 with (from left-to-right) no substrate, substrate PKN1 HRb, and PKN1 HRb with all Lys residues mutated to Arg. Reaction conditions: 1μM E1, 5μM Ube2D3, 2μM SspH1, 50μM Ub, 5μM His-PKN1 108-201, 5mM $MgCl_2$, 5mM ATP, PBS pH7, 37°C. Reducing gel samples taken at 0 min (before addition of ATP), 5 and 20 min, followed by 4-20% gradient SDS-PAGE and staining with Coomassie. **(B)** Ubiquitylation activity of SspH1 LRR-E3 with (from left-to-right) PKN1 HRb, lysineless-PKN1 HRb, and SspH1 E3 domain alone. Reaction conditions as in **(A)**, but with shorter timepoints taken at 0 min (before addition of ATP), 30 seconds, 1, and 2 minutes.

band intensity and molecular weight over time. In contrast, for SspH1 LRR-E3 in complex with lysine-less PKN1 HRb, no poly-Ub chains are observable at the 30 second time point, but high molecular chains are observed by 1 minute. Also notable is the observation that SspH1 LRR-E3 with lysine-less PKN1 utilizes free ubiquitin faster than the E3 domain alone, suggesting that the LRR domain enhances the catalytic activity of the E3 domain.

Given the extensive interactions between LRR and E3 residues in the crystal structures of IpaH3 and SspH2, it is likely that the LRR domains of IpaH-SspH E3s are modulating the catalytic activity of the E3 domain through allosteric interactions induced by substrate binding. As shown in **Part I**, one way of modulating E3 activity is by altering the dynamic conformational states of the NSD and CSD that have been shown to be important for Ub transfer activity. It is possible that substrate binding alters LRR-E3 interactions to change the dynamic flexibility between the NSD and CSD, thereby modulating poly-Ub chain building activity. In **Part III**, differences in the structure of SspH1 that occur upon substrate binding will be investigated by hydrogen-deuterium exchange mass-spectrometry and small-angle X-ray scattering.

PART III: E2 Induces a Conformational Change in SspH1~Ub to Transfer Ub to Substrate

The Ub transfer mechanism of SspH1 consists of two stages: **1**) transfer of Ub from the active site cysteine of an E2~Ub conjugate to the active site cysteine of SspH1 forming an activated SspH1~Ub conjugate, and **2**) transfer of Ub from the active site cysteine of SspH1 to a lysine side chain on a substrate. In **Part II**, it was shown that Ube2D3~Ub and ΔN-Ube2E3~Ub can transfer Ub to the active site of SspH1 but poly-Ub chains are only formed with Ube2D3. This result demonstrates that the complex between SspH1~Ub and PKN1 is necessary but not sufficient for poly-Ub chain synthesis and suggests a continued role for Ube2D3 or Ube2D3~Ub in the second stage of Ub transfer.

An important finding described in **Part I** and **Part II** was that it is possible to generate a stable mimic of SspH1~Ub by replacing the active site Cys with Lys. Unlike other HECT-type E3s, SspH1 binds E2~Ub in a lysine-reactive conformation with the thioester bond oriented specifically to react with the active site Cys, and a Lys at this position is modified with a single Ub to form a stable SspH1-NH-Ub conjugate. This represents the first time a stable E3~Ub amenable for solution-state structural studies has been formed for the IpaH-SspH family of E3s. In **Part III**, as part of our effort to understand why an SspH1~Ub-PKN1 complex is not sufficient for poly-Ub chain synthesis and expand our understanding of Ub-transfer mechanism, SspH1-NH-Ub was used as a central species to investigate possible conformational changes that occur upon complex formation with PKN1, E2, Ub, and E2~Ub. This effort utilized a variety of biophysical methods including NMR, HDX-MS, and SAXS.

Interactions between SspH1~Ub and E2, and E2~Ub

In **Part II**, it was shown that SspH1 binds similar surfaces of Ube2D3~Ub and ΔN-Ube2E3~Ub, that both E2~Ubs bind SspH1 in a lysine-reactive conformation, and both E2~Ubs function in the transfer of Ub to the SspH1 active site. However, in Stage II of the Ub-transfer reaction, only Ube2D3 or Ube2D3~Ub appear to form a productive complex with SspH1~Ub. ΔN-Ube2E3 or ΔN-Ube2E3~Ub may not bind SspH1~Ub, or they bind but form a nonproductive complex. Therefore, ^{1}H-^{15}N TROSY spectra were collected to monitor potential interactions of E2, Ub, and E2~Ub species with SspH1 E3-NH-Ub intermediate.

The first set of experiments follow the addition of free ^{15}N-Ube2D3 S22R or ^{15}N-ΔN-Ube2E3 to SspH1. ^{1}H-^{15}N TROSY spectra collected in the absence (black spectra) and in the presence of 2 molar equivalents of SspH1 E3-NH-Ub (red spectra) are shown in **Figures 13A** and **13B**. Under these conditions, the observed resonance perturbations, both chemical shifts and intensity changes, in the E2s are relatively small. Analysis of chemical shift perturbations (CSPs) for ^{15}N-Ube2D3 (**Fig 13C**) reveal that resonances corresponding to residues near the active site, loop 7, and helix 2 shift in the presence of SspH1 E3-NH-Ub. Smaller shifts were also observed for residues in helix 1 and helix 3. For comparison, only 4 of ^{15}N-Ube2D3 resonances, all in loop 7, exhibited very weak CSPs upon addition to 2 molar equivalents of free SspH1 E3 (**Fig 5**). Under identical conditions, no clear chemical shifts were observed in the spectrum of ^{15}N-ΔN-Ube2E3 upon addition of SspH1-NH-Ub. Resonance intensities were also analyzed for both ^{15}N-Ube2D3 (**Fig 13D**) and ^{15}N-ΔN-Ube2E3 (**Fig 13E**) and reveal that general spectral broadening occurs in the E2 spectra upon addition of SspH1 E3-NH-Ub, indicating that both E2s do interact in some fashion with the E3-NH-Ub mimic. The average intensity ratio (bound/free ^{15}N-UbeD3) for Ube2D3 was 0.43 whereas that for ΔN-Ube2E3 was 0.64. These values suggest that Ube2D3 may

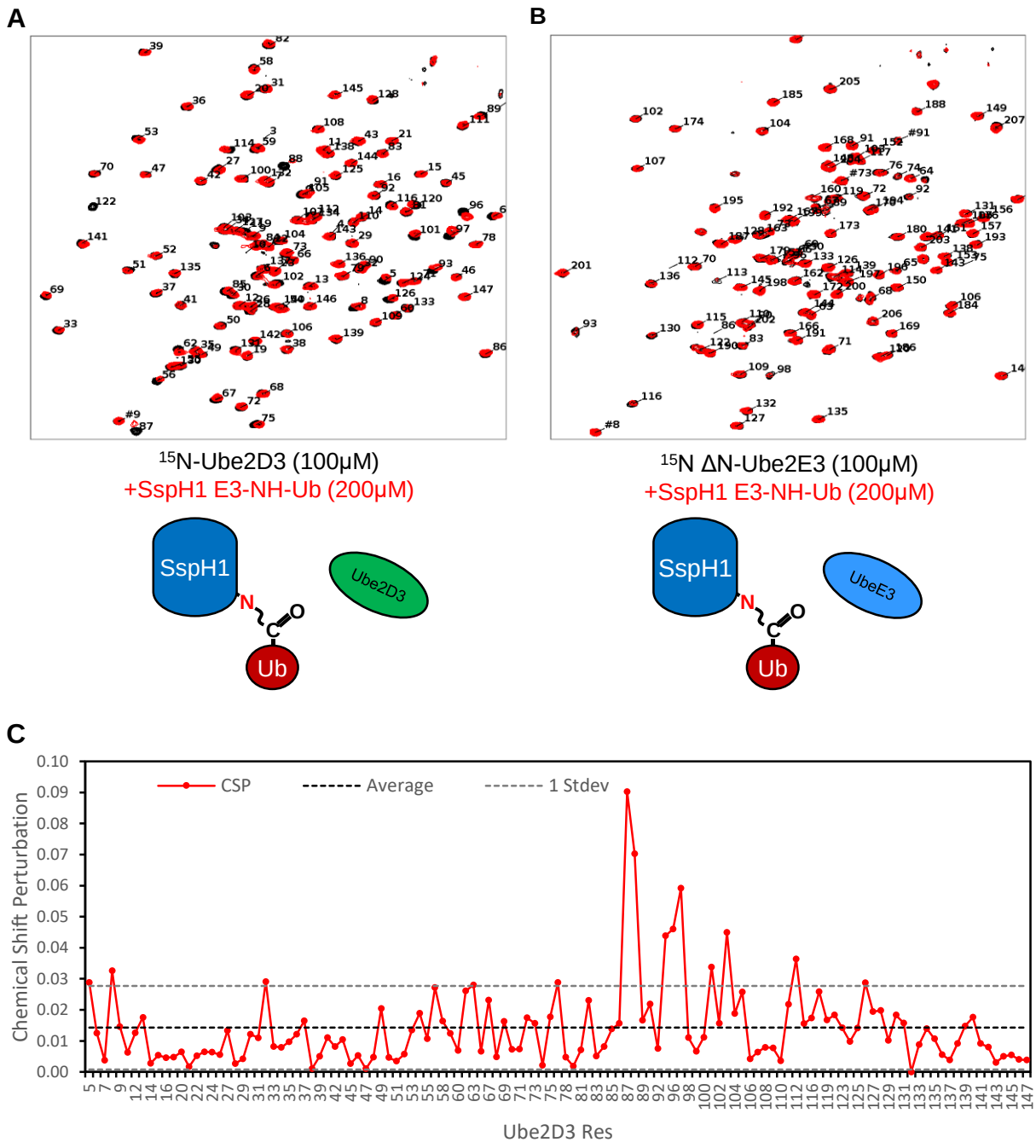

Figure 13. ^{1}H-^{15}N TROSY spectra of **(A)** 100μM ^{15}N-Ube2D3 S22R or **(B)** 100μM ^{15}N-ΔN-Ube2E3 in the absence (black spectra) and presence of 200μM SspH1 E3-NH-Ub (red spectra). **(C)** Chemical shift perturbations for ^{15}N-Ube2D3 resonances in the presence of 200μM SspH1 E3-NH-Ub. Raw intensities in top panel, intensity ratios of bound/free are in bottom panel.

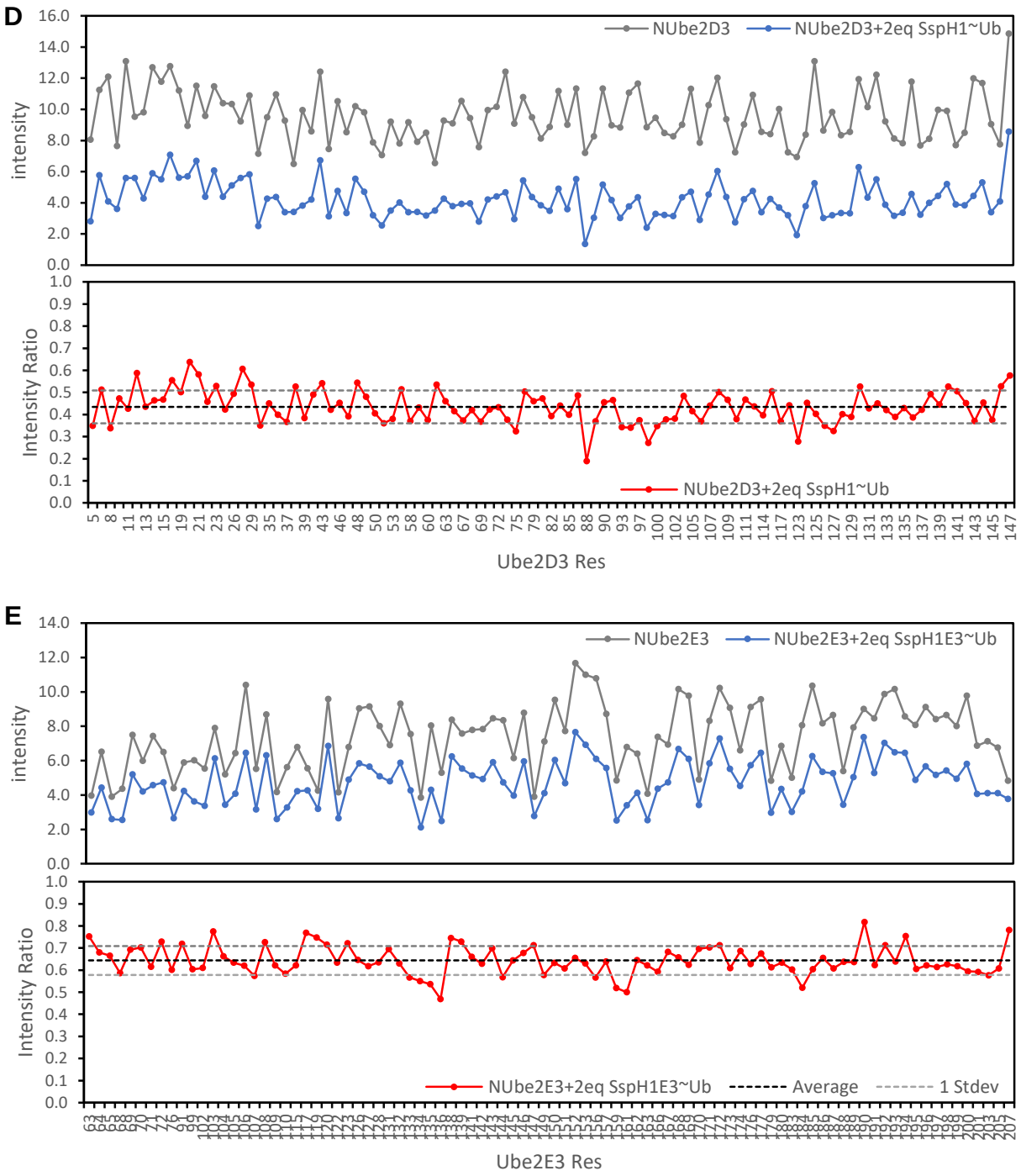

Figure 13. Resonance intensity analysis of ^{1}H-^{15}N TROSY spectra for **(D)** 100μM ^{15}N-Ube2D3 and **(E)** 100μM ^{15}N-ΔN-Ube2E3 in the presence of 200μM SspH1 E3-NH-Ub. Raw intensities are in top panels, intensity ratios of bound/free are in bottom panels

interact with SspH1-NH-Ub with higher affinity than ΔN-Ube2E3, though in both cases binding is very weak. For comparison, the average intensity ratio calculated for ^{15}N-Ube2D3 in the presence of 2 molar equivalents of free SspH1 E3 was 0.46 (**Fig 5**). Overall, these results suggest that SspH1 E3-NH-Ub, like free SspH1, does not bind free E2 well. However, SspH1 E3-NH-Ub does bind Ube2D3 differently than SspH1 E3, as evidenced by the observable chemical shifts. This difference cannot be attributed to noncovalent "backside" interactions between Ube2D3 and Ub, as the construct here included the Ube2D3 S22R mutation that blocks the interaction. It is possible that the presence of Ub at the active site of SspH1 changes the conformation of SspH1 E2~Ub binding site in the thumb region such that Ube2D3 can bind with slightly higher affinity to SspH1~Ub than SspH1. Alternatively, Ube2D3 could interact with a different or modified E2~Ub binding site only present in the E3~Ub intermediate.

Next, the interactions of ^{15}N-labeled E2~Ub conjugates with SspH1-NH-Ub were examined, ^{1}H-^{15}N TROSY spectra were obtained for 100μM ^{15}N-Ube2D3-O-^{15}N-Ub (**Fig 14A**) and 100μM ^{15}N-ΔN-Ube2E3-O-^{15}N-Ub (**Fig 14B**) in the absence (black spectra) and presence of 25μM (red spectra) or 50μM SspH1 E3-NH-Ub (green spectra). In contrast to free E2, general broadening of the spectra in the presence of SspH1-NH-Ub indicates that SspH1~Ub does bind E2~Ub. The most perturbed resonances were mapped onto structures of Ub and Ube2D3 (**Fig 14C**) or Ube2E2 (**Fig 14D**) as identified by intensity analysis (**Fig 14E,F**). The set of perturbed resonances are very similar to those found for ^{15}N-Ube2D3-O-^{15}N-Ub and ^{15}N-ΔN-Ube2E3-O-^{15}N-Ub binding to free SspH1 (**Fig 8**), suggesting that E2~Ub can bind to the thumb region in the SspH1~Ub intermediate in a similar manner as during Stage I of the Ub-transfer mechanism.

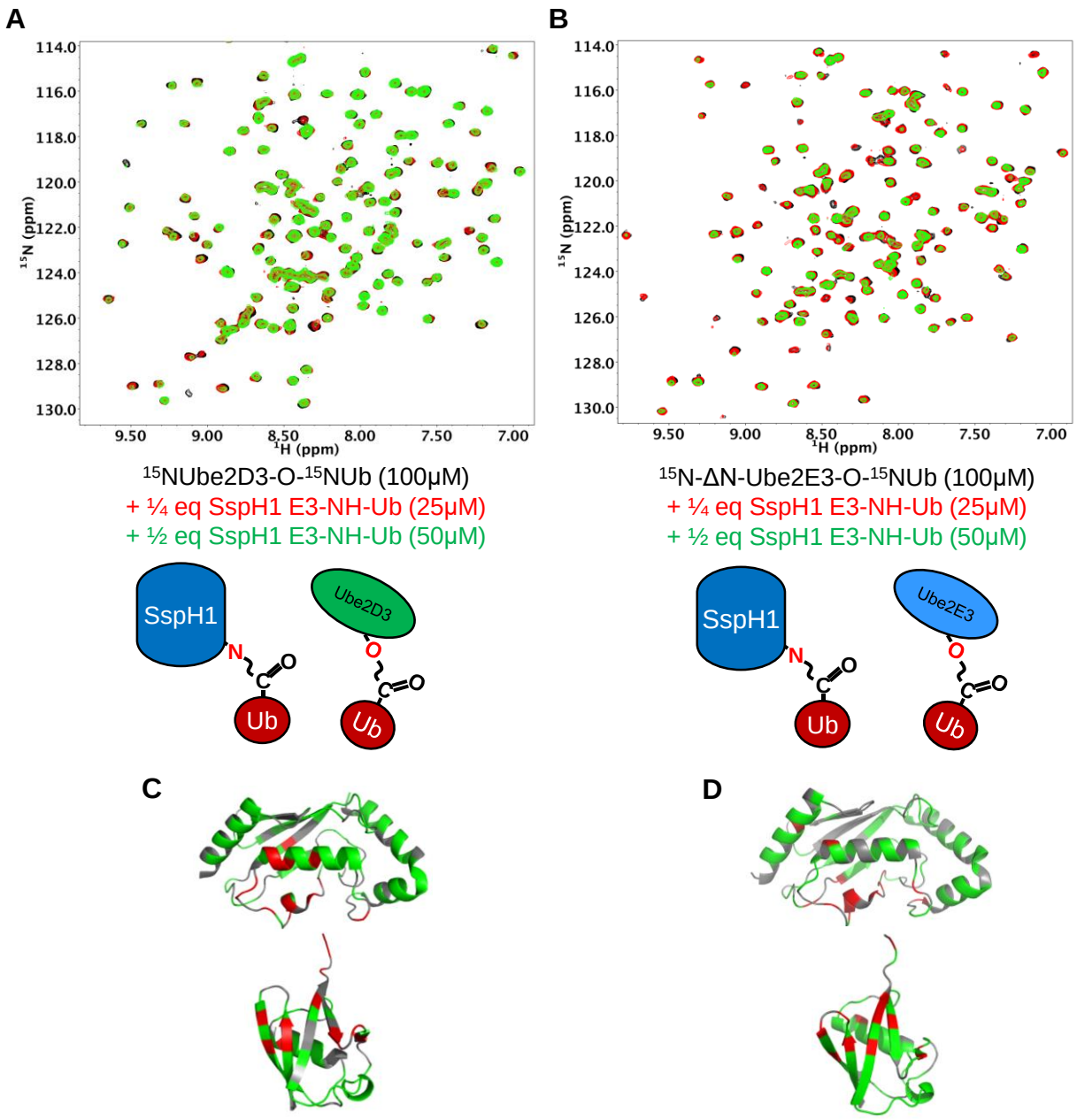

Figure 14. ^{1}H-^{15}N TROSY spectra of **(A)** 100μM 15N-Ube2D3-O-Ub or **(B)** 100μM 15N-ΔN-Ube2E3-O-^{15}N-Ub alone (black spectra) or in the presence of 25μM (red spectra) or 50μM SspH1 E3-NH-Ub (green spectra). Perturbed residues (red) are plotted on structures of **(C)** Ube2D3 (PDB: 1X23) and Ub (PDB: 1UBQ) or **(D)** Ube2E2 (PDB: 1Y6L) and Ub (PDB: 1UBQ).

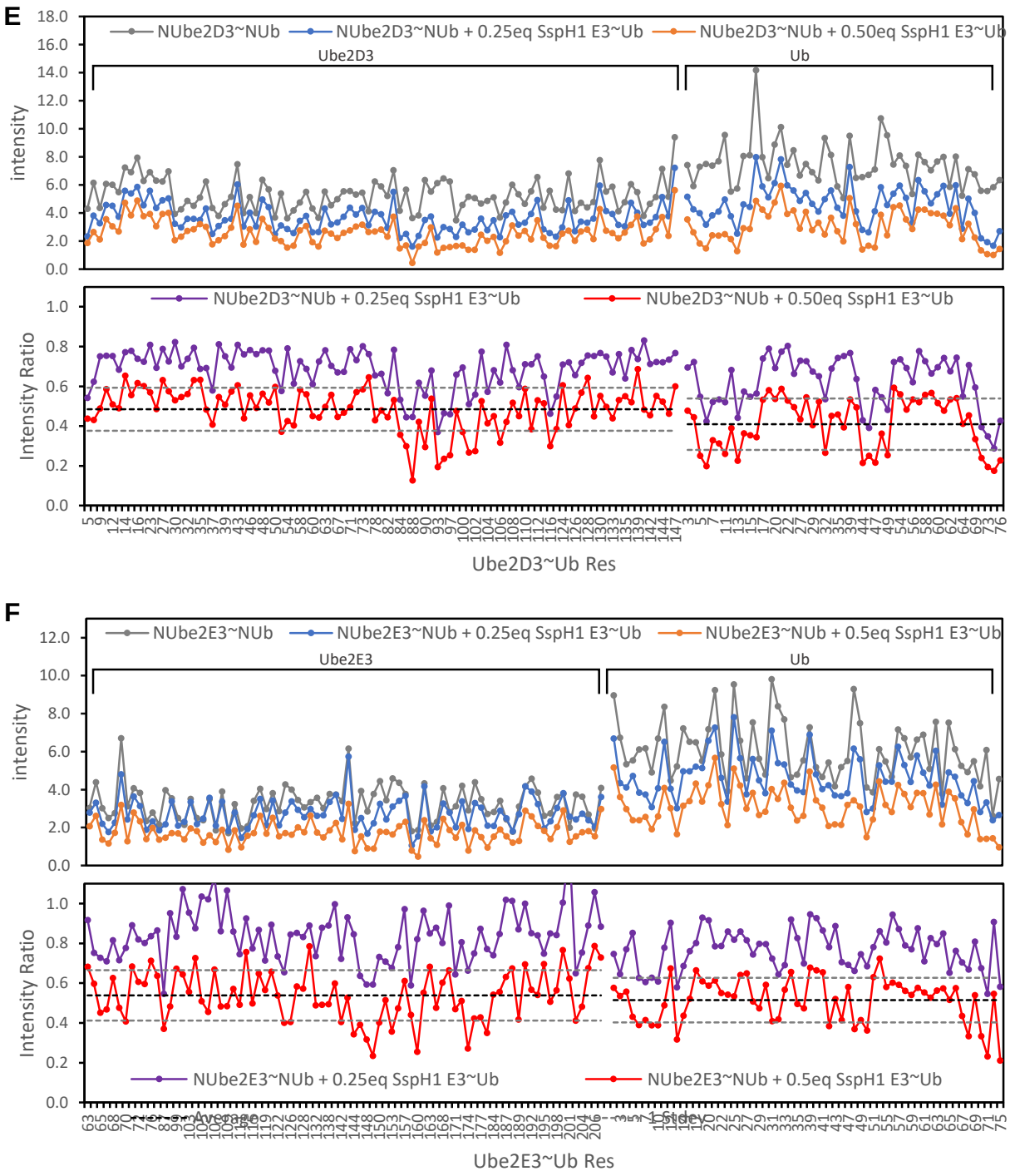

Figure 14. Resonance intensity analysis of ^{1}H-^{15}N TROSY spectra for **(E)** 100μM ^{15}N-Ube2D3 and **(F)** 100μM ^{15}N-ΔN-Ube2E3 in the presence of 25μM or 50μM SspH1 E3-NH-Ub. Raw intensities are in top panels, intensity ratios of bound/free are in bottom panels. Perturbed resonances falling below 1 standard deviation are plotted on molecules structures in **(C,D)**

$^{2}H^{15}N$-Ub-SspH1 as a probe for substrate interactions and protein conformational changes

To probe the chemical environment of Ub at the active site of SspH1 by NMR, $^{2}H^{15}N$-Ub was conjugated to SspH1 C492K generating $^{2}H^{15}N$-Ub-NH-SspH1, and ^{1}H-^{15}N TROSY were collected for $^{2}H^{15}N$-Ub alone (**Fig 15A**) and for the SspH1 LRR-E3-NH-$^{2}H^{15}N$-Ub conjugate (**Fig 15B**). SspH1 LRR-E3-NH-$^{2}H^{15}N$-Ub is a large protein by NMR standards (86kDa), and rapid relaxation of resonances make NMR studies impractical. However, protein deuteration of non-exchangeable protons reduces the high density of protons and potential relaxation pathways allowing for observations of signals and analysis of larger protein complexes. Purification of the isotopically labeled proteins in aqueous buffer allows protons to be incorporated into exchange sites such as backbone amides. Therefore, ^{1}H-^{15}N TROSY spectra can be collected on these samples, though in this case use of a high-field strength (800MHz) magnet with cryoprobe was required for obtaining high-quality spectra. Many Ub resonances displayed small chemical shift perturbations relative to free Ub, and it was straightforward to assign the SspH1 LRR-E3-NH-$^{2}H^{15}N$-Ub spectrum by inspection. Chemical shift perturbations compared to free $^{2}H^{15}N$-Ub were calculated for each of the resonances in the SspH1 LRR-E3-NH-$^{2}H^{15}N$-Ub spectrum (**Fig 15C**) and mapped onto a structure of Ub (**Fig 15D**). The results reveal that the most highly perturbed resonances (red and orange surfaces) define specific regions of the Ub subunit. The most highly perturbed resonances correspond to residues in the hydrophobic patch surrounding Ub residue I44 and in the C-terminal tail of Ub. This surface in free Ub was also affected upon addition of a large excess of SspH1 (**Fig 5**) and in E2~Ub (**Fig 8**) upon binding to free SspH1. Other surfaces of Ub perturbed in the SspH1-Ub conjugate, though to a lesser extent, correspond to a patch of residues on the other side of the Ub C-terminus and hydrophobic patch (green and yellow surfaces). The

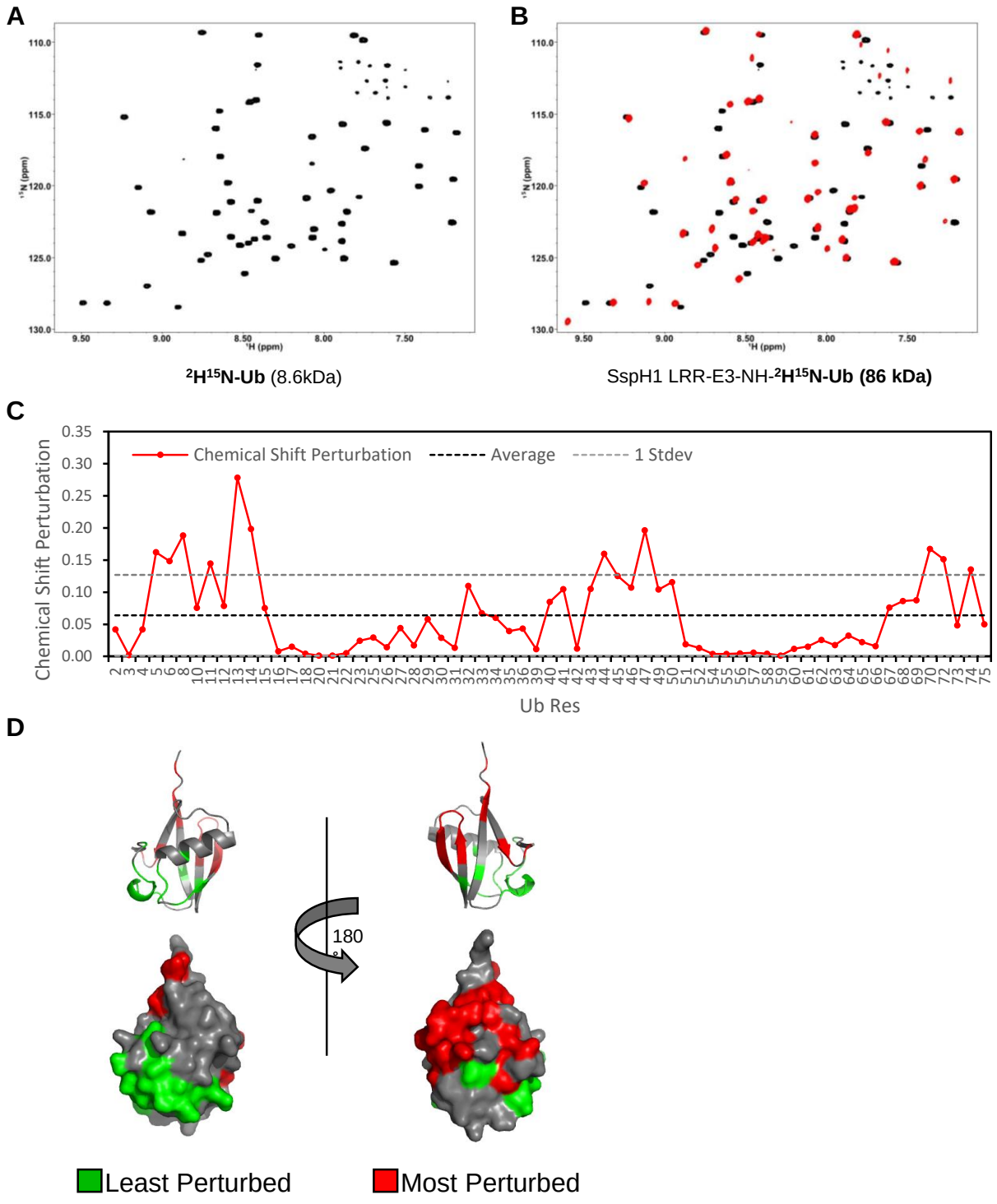

Figure 15. ^{1}H-^{15}N TROSY spectral overlays of **(A)** 100μM $^{2}H^{15}N$-ubiquitin (black spectrum) and **(B)** 150μM SspH1~$^{2}H^{15}N$-ubiquitin (red spectrum). **(C)** Chemical shift perturbations (CSP) of SspH1~$^{2}H^{15}N$-ubiquitin compared to that of $^{2}H^{15}N$-Ubiquitin normalized to the largest CSP. **(D)** Major CSPs plotted on a surface representation of the crystal structure of ubiquitin (PDB: 1UBQ). Red: perturbed resonance. Green: unperturbed resonance.

ability to obtain a high-quality ^{1}H-^{15}N TROSY spectrum of SspH1 LRR-E3-NH-$^{2}H^{15}N$-Ub indicates that Ub has some degree of freedom while conjugated to the SspH1 active site, as it is expected that a tightly docked Ub subunit in LRR-E3-NH-Ub would still exhibit a significant degree of spectral resonance broadening even with deuteration of the Ub subunit.

Influence of the substrate PKN1 on the SspH1-NH-Ub complex

Ultimately, a Lys residue of PKN1 must make intimate contact with the reactive thioester bond of the SspH1~Ub intermediate to achieve Ub transfer to substrate. It may be possible to observe these interactions by NMR utilizing ^{15}N-labeled PKN1 HRb or SspH1-NH-$^{2}H^{15}N$-Ub. Starting with labeled PKN1, ^{1}H-^{15}N TROSY spectra were collected for ^{15}N-PKN1 HRb alone (**Fig 16A**) and in complex with SspH1 LRR-E3 (**Fig 16B**) to first examine the CSPs that occur in PKN1 upon binding. The spectrum of free ^{15}N-PKN1 HRb reveals a dispersed spectrum with well-resolved resonances, indicating that the construct would be good for NMR studies. However, the spectra of ^{15}N-PKN1 HRb bound to SspH1 LRR domain (**Fig 16B**) and LRR-E3 (**Fig 16C**) show general broadening of the spectrum, and loss of most dispersed resonances even at low molar equivalents of SspH1. General broadening was also observed for ^{1}H-^{15}N TROSY spectra collected for the deuterated species, $^{2}H^{15}N$-PKN1, in the presence of SspH1 LRR-E3-NH-Ub using a high field magnet. This is likely due to the large molecular weight of the complex couple with the high affinity between SspH1 and PKN1 and the fact that the complex behaves as a unit. Therefore, ^{15}N-PKN1 HRb is not suitable for studying the addition of SspH1-NH-Ub and E2-O-Ub, which would form complexes of higher molecular weight than the ones shown here.

^{15}N-PKN1 HRb was also added to the free SspH1 E3 domain (no LRR domain present) to see if any weak interactions could be observed. A small amount of general broadening is observed

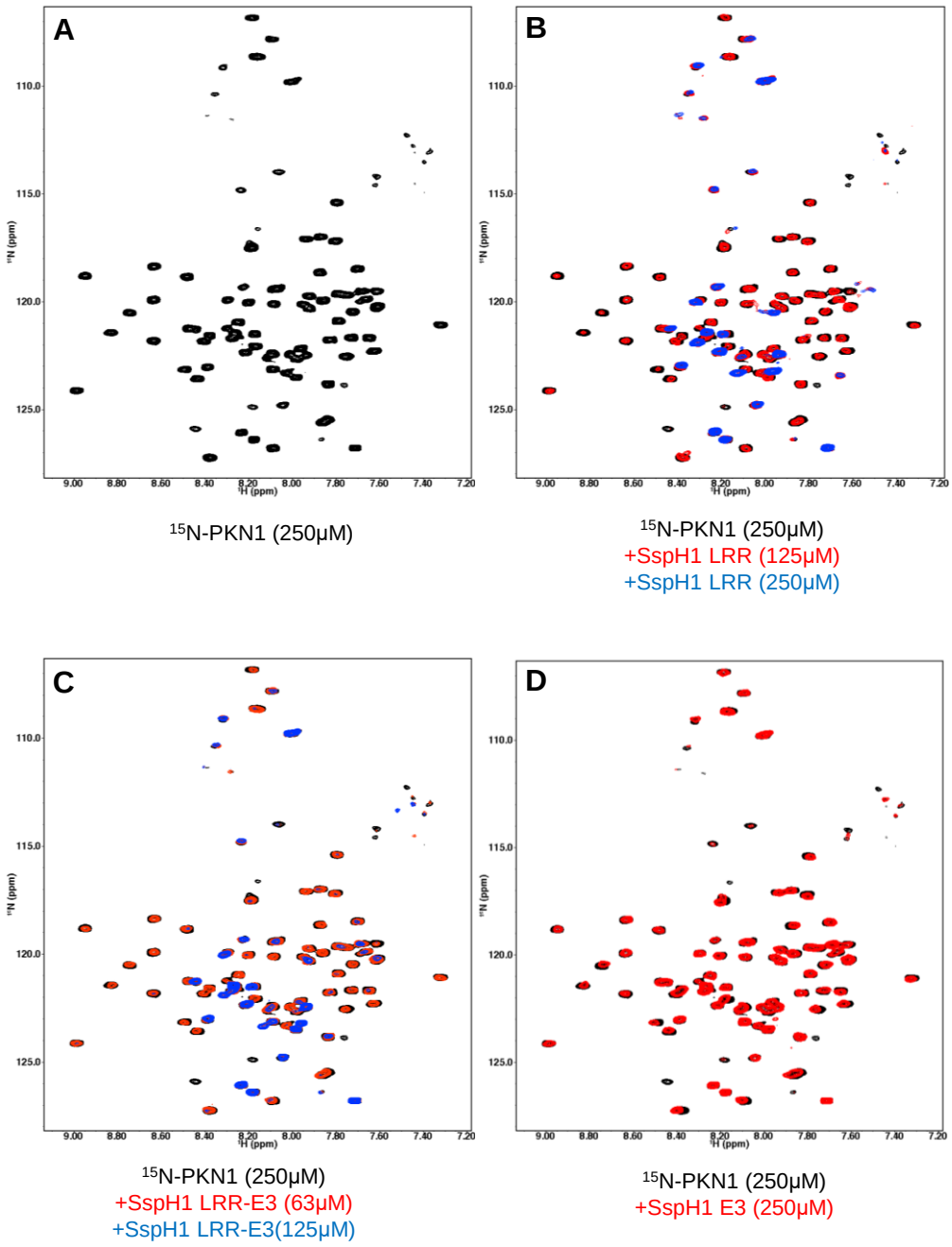

Figure 16. ^{1}H-^{15}N TROSY spectra of 250μM ^{15}N-PKN1 HRb (108-201) (black spectrum) **(A)** alone or **(B)** in the presence of 125μM (red spectrum) or 250μM (blue spectrum) SspH1 LRR domain (162-388). **(C)** in the presence of 63μM (red spectrum) or 125μM SspH1 LRR-E3 (blue spectrum), or **(D)** 250μM SspH1 E3 domain.

for ^{15}N-PKN1 HRb in the presence of SspH1 E3 domain (**Fig 16D**), indicating there may be some weak interaction between PKN1 and the E3 domain. Structures of SspH2 and IpaH4 show extensive interactions between LRR and E3 domains (**Intro Fig 4**). The structure of SspH1 LRR domain bound to PKN1 HRb places PKN1 close to the end of the LRR domain that interacts with the E3 domain (**Intro Fig 4**). At some point during Ub transfer, the SspH1 active site Cys must come near a Lys residue on PKN1, so it is likely that PKN1 does make some contacts with the E3 domain, though free in solution the affinity is very weak.

Though unable to directly observe PKN1 resonances in the SspH1-NH-Ub/PKN1 complex, the Ub subunit provides a useful reporter group for interactions in the complex. **Figure 17** shows ^{1}H-^{15}N TROSY spectra for **A)** SspH1 LRR-E3-NH-^{2}H^{15}N-Ub (black spectrum) and **B)** SspH1 LRR-E3-NH-^{2}H^{15}N-Ub in complex with PKN1 HRb (blue spectrum). As previously described, many resonances in the ^{2}H^{15}N-Ub spectrum shift upon conjugation to the SspH1 active site. In the presence of PKN1 no resonances in the SspH1 LRR-E3-NH-^{2}H^{15}N-Ub shift, and there is only some general broadening of the spectrum due to an increase in molecular weight of the complex from 86kDa to 100kDa. That fact that Ub resonances do not shift upon addition of PKN1 indicates that PKN1 does not directly contact Ub in the SspH1~Ub/PKN1 complex. Though initially unexpected, it is consistent with results that show formation of an SspH1~Ub/PKN1 complex is necessary but not sufficient for PKN1 ubiquitylation. Additional binding partners or interactions may be required to drive the interaction between Ub and PKN1.

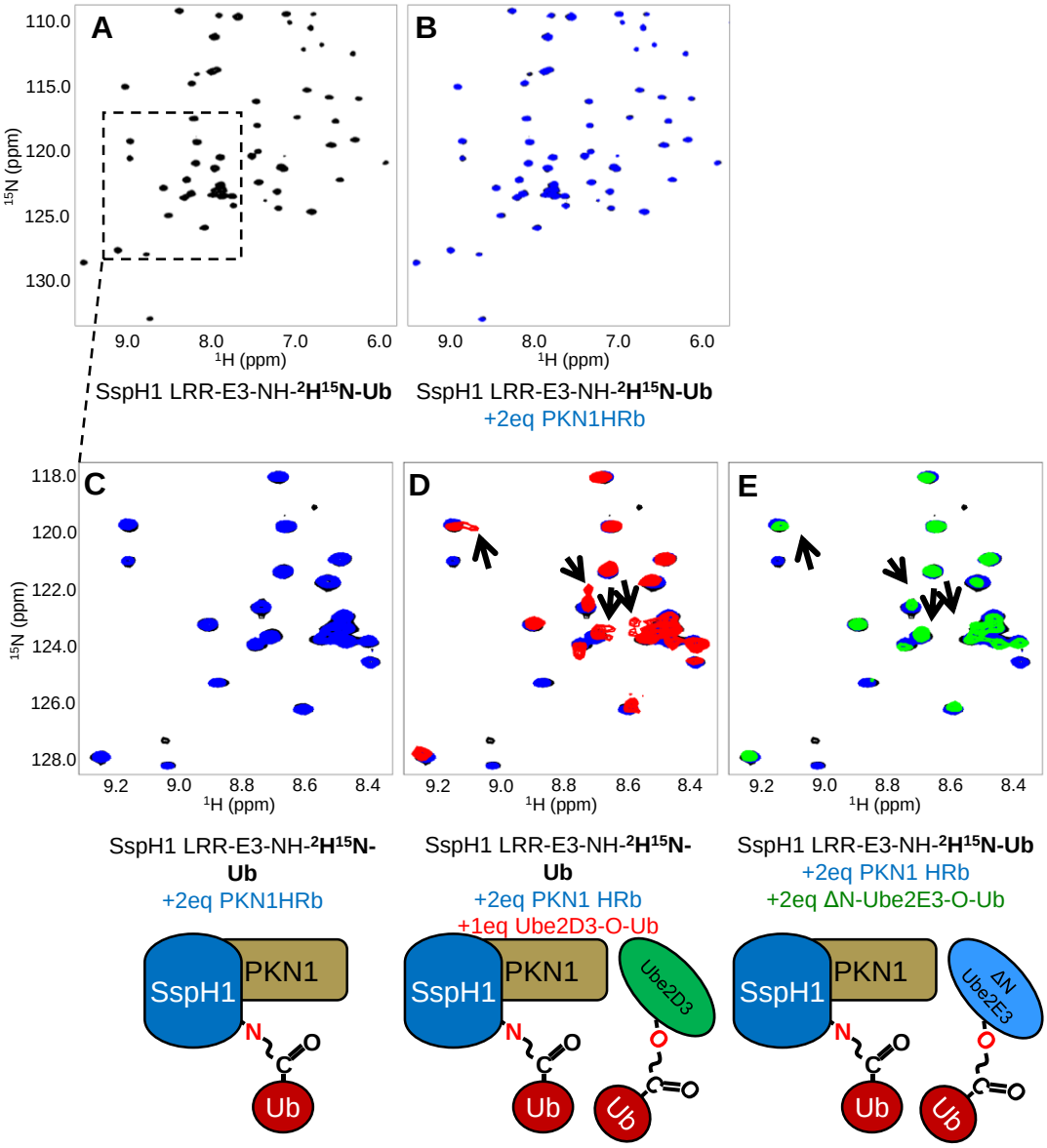

Figure 17. ^{1}H-^{15}N TROSY spectra of **(A)** 150µM SspH1 LRR-E3 C492K~$^{2}H^{15}N$-ubiquitin (black spectrum), and **(B)** 150µM SspH1 LRR-E3 C492K~$^{2}H^{15}N$-ubiquitin in complex with 300µM His-PKN1 108-201. Dotted box in **(A)** indicates close-up of ^{1}H-^{15}N TROSY spectral overlays **(C)** 150µM SspH1 LRR-E3 C492K~$^{2}H^{15}N$-ubiquitin in complex with 300µM His-PKN1 108-201 and upon addition of **(D)** 150µM Ube2D3-O-Ub or **(E)** 300µM ΔN-Ube2E3-O-Ub.

Ube2D3-O-Ub induces a conformational change in the SspH1~Ub-PKN1 complex

Ubiquitylation assays show that E2 or E2~Ub is required for the Stage II transfer of Ub from SspH1~Ub to substrate (**Part II**). Previous NMR results show that Ube2D3-O-Ub and ΔN-Ube2E3-O-Ub can both bind SspH1-NH-Ub (**Fig 14**). Using the $^{2}H^{15}N$-Ub subunit of SspH1-NH-Ub as a probe, E2~Ub was added to the SspH1-NH-$^{2}H^{15}N$-Ub/PKN1 complex and ^{1}H-^{15}N TROSY spectra were collected (**Fig 17**). Upon addition of Ube2D3-O-Ub, several Ub resonances shift, and new resonances appear (**Fig 17D**). Most of the new peaks are adjacent to existing peaks. This suggests that some Ub residues in the complex give rise to more than one resonance, or 'peak doubling.' This can occur when a single resonance experiences more than one chemical environment and the exchange between the two environments is slow enough to generate two separate NMR peaks. These results suggest that a conformational change is occurring in SspH1-NH-Ub, generating two separate environments for the Ub subunit. Interestingly, peak doubling or shifting is not observed upon addition of ΔN-Ube2E3-O-Ub (**Fig 17E**), though in both cases, general broadening is observed, likely a result of complex formation. General broadening of Ub resonances is not surprising as the molecular weight of the SspH1 LRR-E3~Ub/PKN1/E2~Ub complex approaches ~125kDa, a very large complex for NMR studies. The fact that peak doubling and shifting occurs in the presence of Ube2D3-O-Ub but not ΔN-Ube2E3-O-Ub indicates that Ube2D3-O-Ub induces a conformational change in SspH1-NH-Ub that ΔN-Ube2E3-O-Ub does not. This is the first demonstration of a structural difference between the SspH1-Ube2D3 and SspH1-Ube2E3 complexes that could explain SspH1's lack of ubiquitylation activity with Ube2E3.

The locations of most new SspH1-NH-$^{2}H^{15}N$-Ub resonances correspond to free $^{2}H^{15}N$-Ub

The presence of new resonances in the ^{1}H-^{15}N TROSY spectrum indicates a conformational change in SspH1-NH-$^{2}H^{15}N$-Ub. Surprisingly, a comparison between the spectra of free $^{2}H^{15}N$-Ub SspH1-NH-$^{2}H^{15}N$-Ub in complex with PKN1 and Ube2D3-O-Ub reveals that the locations of the new resonances largely correspond to the locations of resonances in free $^{2}H^{15}N$-Ub. However, several resonances appear in a location that does not correspond to free $^{2}H^{15}N$-Ub. These effects can be observed in **Fig 18** for the overlaid ^{1}H-^{15}N TROSY spectra of free $^{2}H^{15}N$-Ub (pink), SspH1 LRR-E3-NH-^{2}H-^{15}N-Ub (grey), SspH1 LRR-E3-NH-^{2}H-^{15}N-Ub in complex with PKN1 (blue), and SspH1 LRR-E3-NH-^{2}H-^{15}N-Ub in complex with PKN1 and Ube2D3-O-Ub (green).

The fact that peak doubling occurs makes quantitative intensity analysis of the previously-described spectra difficult to interpret, as only a subset of resonances have multiple intensities. Further, the broadness of resonances and differences in morphology of resonances in many cases make single intensity values of limited use. To gain insight into the behavior of resonances affected by the addition of Ube2D3-O-Ub, each resonance in the spectrum of SspH1 LRR-E3-NH-^{2}H-^{15}N-Ub in complex with PKN1 and Ube2D3-O-Ub was annotated as **1)** not doubling, **2)** doubling to a location corresponding to free Ub, or **3)** doubling to a new location. This qualitative analysis is plotted on a surface of Ub in **Fig 18E**: the green surface represents resonances that do not double, the red surface represents resonances that double to a location corresponding to free Ub, and the orange surface represents resonances that double to a new location. These surfaces show that the C-terminus and hydrophobic patch of Ub are responsible for resonances that double upon addition of Ube2D3-O-Ub. The hydrophobic patch of Ub was the surface most perturbed upon conjugation

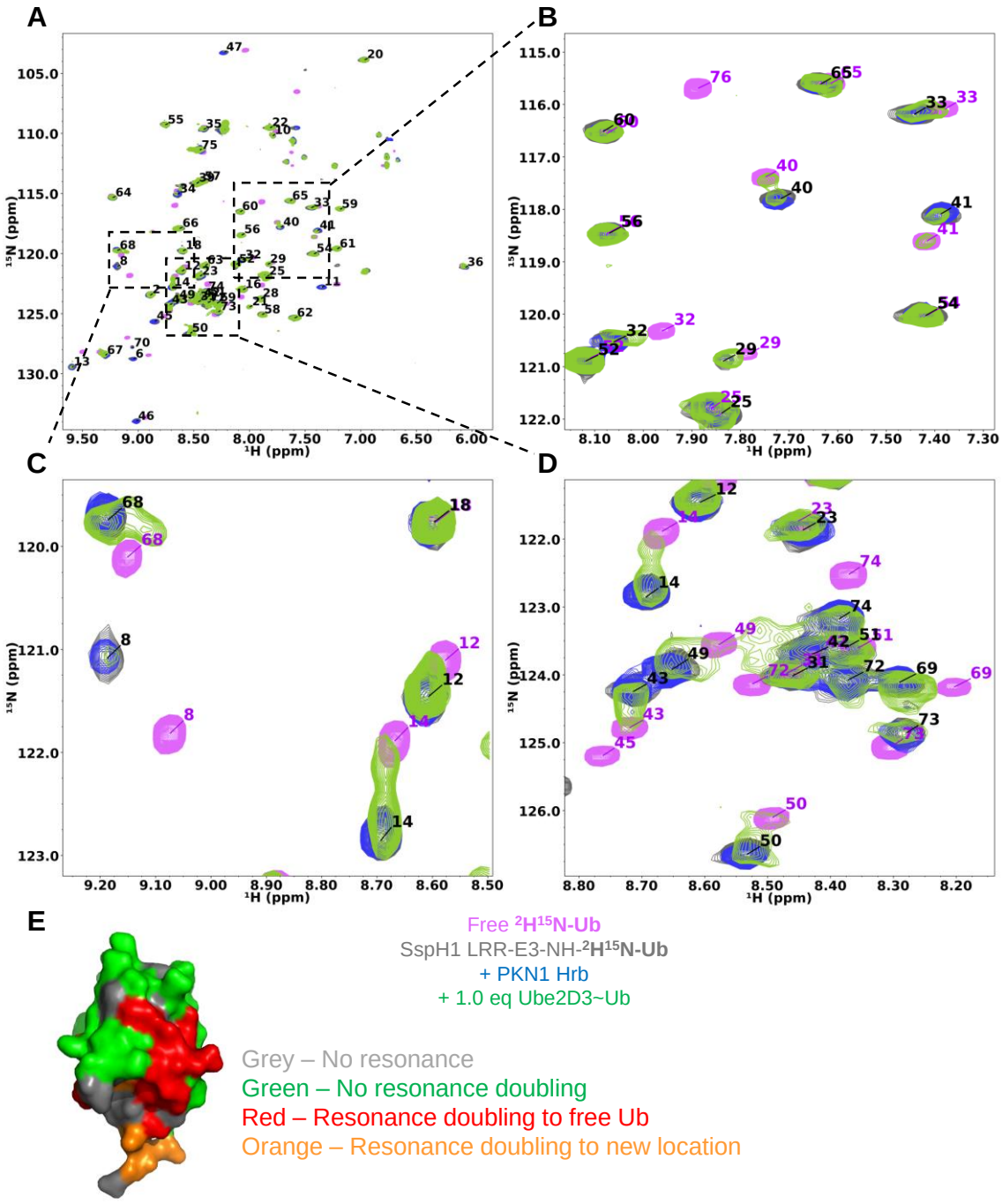

Figure 18. ^{1}H-^{15}N TROSY spectrum of 100μM ^{2}H^{15}N-ubiquitin (pink spectrum), and 150μM SspH1 LRR-E3~^{2}H^{15}N-ubiquitin alone (black spectrum) or in complex with 300μM His-PKN1 108-201 (blue spectrum) and 150μM Ube2D3~Ub (green spectrum). Full spectrum shown in **(A)** with zoomed in regions shown in **(B)** **(C)** and **(D)**. **(E)** Ubiquitin resonances perturbed in SspH1~Ub upon addition of Ube2D3~Ub plotted on a surface representation of ubiquitin (PDB: ID). Grey: resonance corresponding to residue not observed. Red: resonance doubles to chemical space corresponding to free ubiquitin resonances. Orange: resonance doubles to chemical space corresponding to non-free ubiquitin resonances.

to the SspH1 active site (**Fig 15**) and mediates interactions between E2~Ub and SspH1 (**Fig 8**). Intriguingly, residues in the C-terminal tail of Ub are responsible for resonances that double to a new location not corresponding to free Ub resonances. These observations suggest a model in which Ube2D3~Ub plays a role in transfer of Ub from the SspH1 active site Cys to a substrate lysine by inducing a conformational change in SspH1~Ub that moves Ub out of the SspH1 active site towards substrate. Ub residues that interact with SspH1 at the active site are displaced from their binding interface, and their resonances experience a new chemical environment similar to that of free Ub. Residues at the C-terminus of Ub experience a different change in chemical environment as they are moved from the SspH1 active site towards substrate, possibly poised to form an isopeptide bond between Ub Gly76 and a substrate lysine.

Effects of Ube2D3 S22R upon new SspH1-NH-$^{2}H^{15}N$-Ub resonances

As mentioned previously, Ube2D3 has a β-sheet surface that can interact non-covalently with Ub. This interaction is much weaker or absent in Ube2E3. It is possible that this "backside surface" opposite the Ube2D3 active site interacts with Ub at the E3 active site and plays a role in the formation of a PKN1/E3~Ub/E2~Ub complex that is poised for Ub transfer. The previous experiments, which revealed new SspH1 LRR-E3-NH-$^{2}H^{15}N$-Ub resonances in the presence of Ube2D3-O-Ub, did not contain the S22R mutation in the Ube2D3 subunit that blocks the noncovalent Ube2D3-Ub interaction between the backside β-sheet of Ube2D3 and the hydrophobic patch of Ub. As previously described, the S22R mutation does not critically impair the ability of SspH1 to ubiquitylate substrate but does have a minor effect on the distribution of poly-Ub chains formed. To test if the S22R mutation affects the NMR results presented in the previous section, similar experiments were performed using Ube2D3 S22R-O-Ub. While the

results were the same, some differences in the morphologies of resonances were observed, indicating that the backside of Ube2D3 may have some minor interactions with SspH1~Ub. To better visualize these differences, enlarged views of spectra for two resonances, corresponding to Ub residues Thr14 and Leu8, are presented here.

Effects of Ube2D3 S22R – A closer look at Ub resonances for Thr14 and Leu8

Fig 19 shows the resonance for SspH1 LRR-E3-NH-$^{2}H^{15}N$-Ub Thr14 in complex with PKN1 upon addition of Ube2D3-O-Ub or ΔN-Ube2E3-O-Ub. Also overlaid are spectra of free $^{2}H^{15}N$-Ub (pink spectrum) and SspH1 LRR-E3-NH-$^{2}H^{15}N$-Ub (grey spectrum). Upon addition of Ube2D3-O-Ub, the Thr14 peak doubles towards the location of the free $^{2}H^{15}N$-Ub peak. Upon addition of ΔN-Ube2E3-O-Ub, the Thr14 resonance does not shift or double. **Fig 20** shows the same Thr14 resonance, but upon addition of free Ube2D3 S22R or Ube2D3 S22R-O-Ub. Peak doubling is observed upon addition of Ube2D3 S22R-O-Ub, but not unconjugated Ube2D3 S22R. The morphology of the Thr14 resonance upon addition of Ube2D3 S22R-O-Ub differs from that upon addition of Ube2D3-O-Ub (**Fig 19**). Upon addition of Ube2D3-O-Ub, there is considerable overlap between the two peaks of the doubled Thr14 resonance, but upon addition of Ube2D3 S22R-O-Ub there is little overlap.

Fig 21 shows the SspH1 LRR-E3-NH-$^{2}H^{15}N$-Ub Leu8 resonance upon addition of Ube2D3 S22R, Ube2D3 S22R-O-Ub, or Ube2D3-O-Ub. Upon addition of Ube2D3 S22R, the Leu8 resonance does not shift or double, and decreases in intensity. Upon addition of Ube2D3 S22R-O-Ub, the Leu8 resonance doubles to a location corresponding to free Ub and increases in intensity with increasing amounts of Ube2D3 S22R-O-Ub. Upon addition of Ube2D3-O-Ub, the Leu8 resonance doubles to a new location on a trajectory near free Ub and increases in intensity with

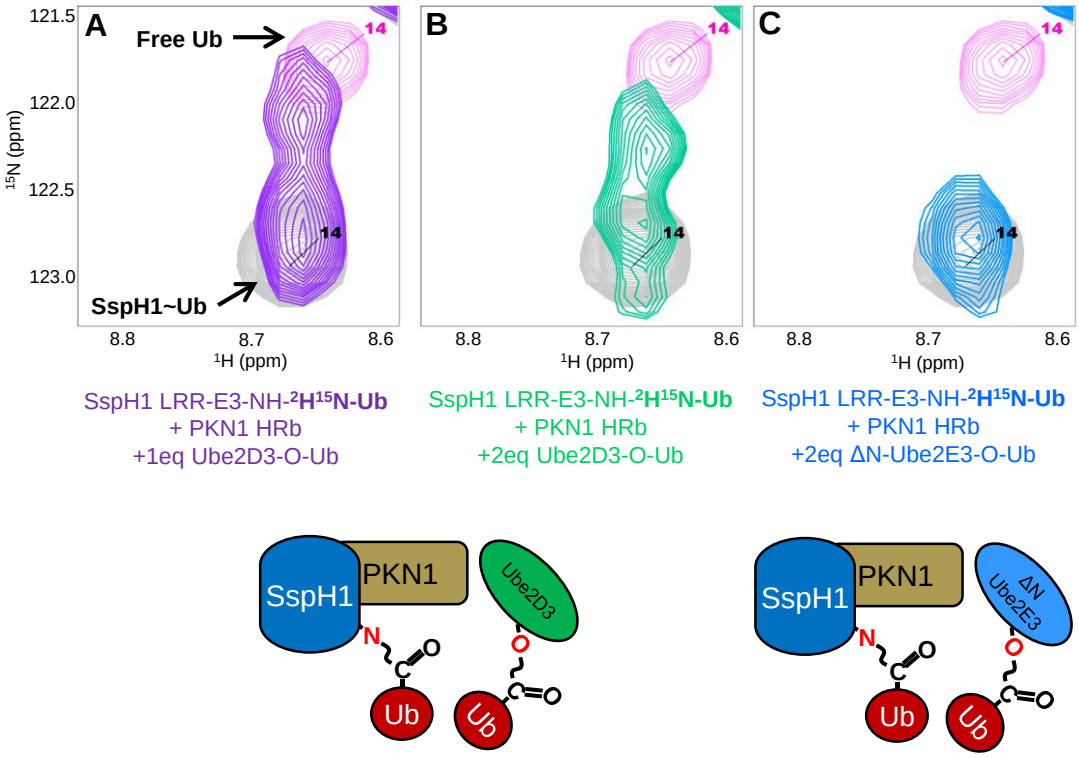

Figure 19. Close-up of the resonances belonging to ubiquitin Thr 14 in the ^{1}H-^{15}N TROSY spectra of 100µM $^{2}H^{15}N$-ubiquitin (pink spectrum), and 150µM SspH1 LRR-E3~$^{2}H^{15}N$-ubiquitin alone (black spectrum) or in complex with **(A)** 300µM His-PKN1 108-201 and 150µM Ube2D3-O-Ub (violet spectrum) **(B)** 300µM Ube2D3-O-Ub (light green spectrum) or **(C)** 300µM ΔN-Ube2E3-O-Ub (light blue spectrum)

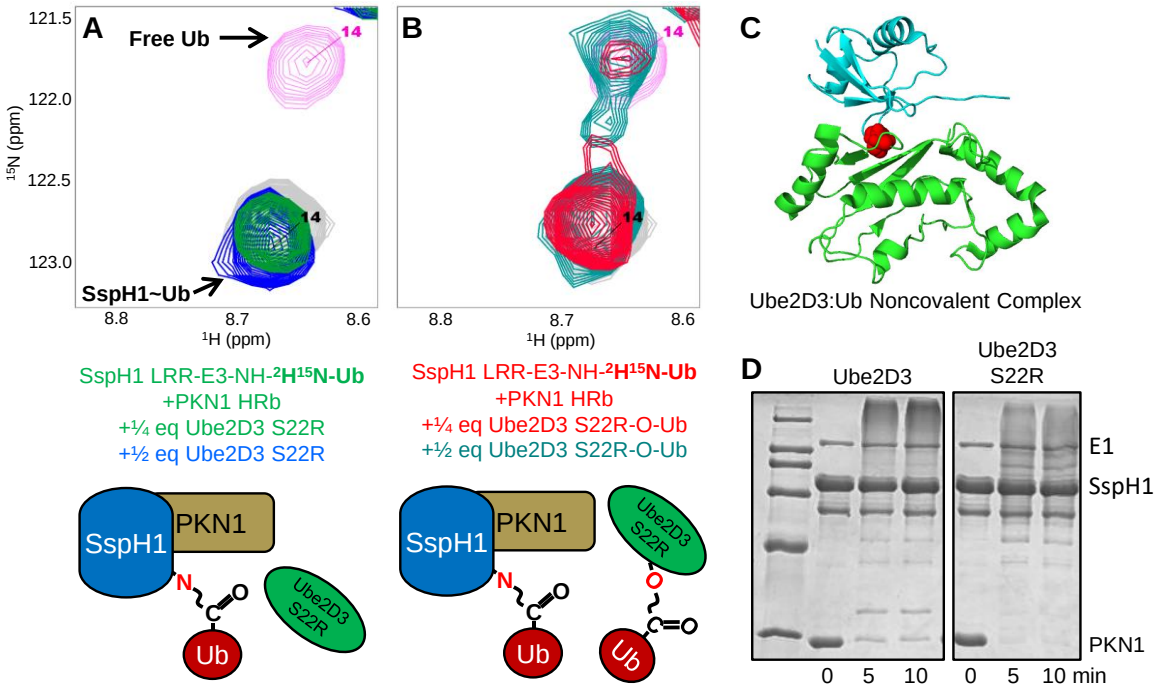

Figure 20. Close-up of the resonances belonging to ubiquitin Thr 14 in the ^{1}H-^{15}N TROSY spectra of 100μM $^{2}H^{15}N$-ubiquitin (pink spectrum), and 200μM SspH1 LRR-E3~$^{2}H^{15}N$-ubiquitin alone (black spectrum) or in complex with **(A)** 200μM His-PKN1 108-201 and 50μM (green spectrum) or 100μM Ube2D3 S22R (blue spectrum), and **(B)** 50μM (red spectrum) or 100μM Ube2D3 S22R-O-Ub (teal spectrum). **(C)** Structure of Ube2D3 bound to the Ile44 hydrophobic patch of ubiquitin via Ser22 (red spheres). PDB ID: 2FUH. **(D)** Ubiquitylation activity of SspH1 with wildtype-Ube2D3 or noncovalent ubiquitin binding site-disrupting S22R-Ube2D3 from **Part I**. Reaction conditions: 1μM E1, 5μM Ube2D3, 5μM SspH1, 100μM Ub, 5μM His-PKN1 1-201, 5mM $MgCl_2$, 5mM ATP, PBS pH7, 37°C. Reducing gel samples taken at 0 min (before addition of ATP), 5 and 20 min, followed by 4-20% gradient SDS-PAGE and staining with Coomassie.

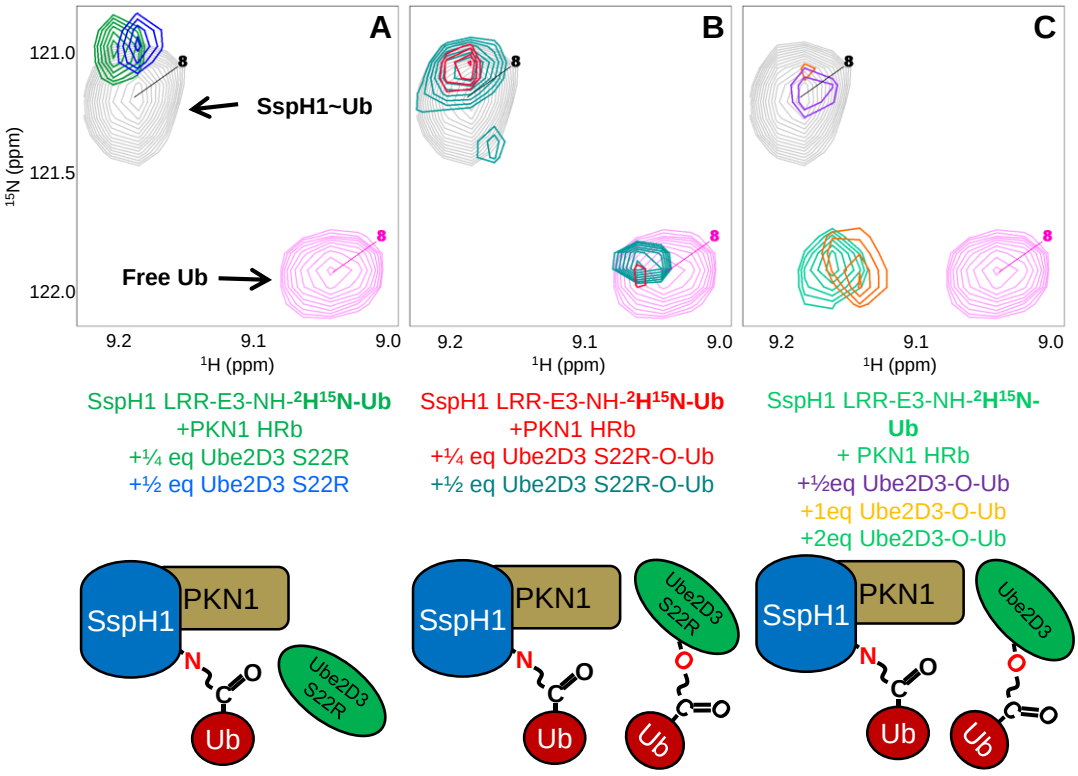

Figure 21. Close-up of the resonances belonging to ubiquitin Leu 8 in the ^{1}H-^{15}N TROSY spectra of 100µM $^{2}H^{15}N$-ubiquitin (pink spectrum), and 200µM SspH1 LRR-E3~$^{2}H^{15}N$-ubiquitin alone (black spectrum) or in complex with **(A)** 25µM (green spectrum) or 50µM Ube2D3 S22R (blue spectrum), **(B)** 25µM (red spectrum) or 50µM Ube2D3 S22R-O-Ub (teal spectrum), or **(C)** 100µM (purple spectrum), 140µM (orange spectrum) or 200µM Ube2D3~Ub (light green spectrum). **Note:** the Leu 8 resonance broadened out completely upon addition of 2eq ΔN-Ube2E3-O-Ub.

increasing amounts of Ube2D-O-Ub. Addition of ΔN-Ube2E3-O-Ub caused the resonance to broaden out completely.

Why is it the case that the Leu8 resonance increases in intensity upon addition of Ube2D3-O-Ub when the molecular weight of the PKN1/SspH1~Ub complex is increasing? For most resonances, an increase in molecular weight results in a decrease in intensity. For resonances directly involved in the SspH1~Ub binding interface, such as Leu8, movement towards a new environment may increase resonance intensity by moving the residue out of the interface. Upon addition of unconjugated Ube2D3 or ΔN-Ube2E3-O-Ub, which don't move Ub out of the interface, the resonance intensity of Leu8 decreases. The observation that Ube2D3-O-Ub and Ube2D3 S22R-O-Ub cause the resonance to move to different locations suggests that the backside of Ube2D3 may have minor interactions with SspH1~Ub, but ubiquitylation assays show that it is not important to the catalytic mechanism.

New Ub C-terminal resonances observed in the SspH1-NH-$^{2}H^{15}N$-Ub/Ube2D3-Ub complex

Resonances at the C-terminus of Ub are particularly interesting as they are closest to the E3 active site. Upon addition of Ube2D3-O-Ub and PKN1, the Ub C-terminal resonances also double but, in contrast to resonances in other regions of the Ub subunit, they shift to locations that do not correspond to those of free Ub. Presumably, this is because Ub is being moved into a position where its C-terminus is poised to form an isopeptide bond with a Lys residue on PKN1. To visualize these differences, enlarged views of spectra for two resonances, His68 (**Fig 22**) and Gly75 (**Fig 23**), are examined in detail. For His68, addition of Ube2D3 S22R-O-Ub induces resonance doubling in both the absence (**Fig 22A**) and presence of PKN1 (**Fig 22B**). The

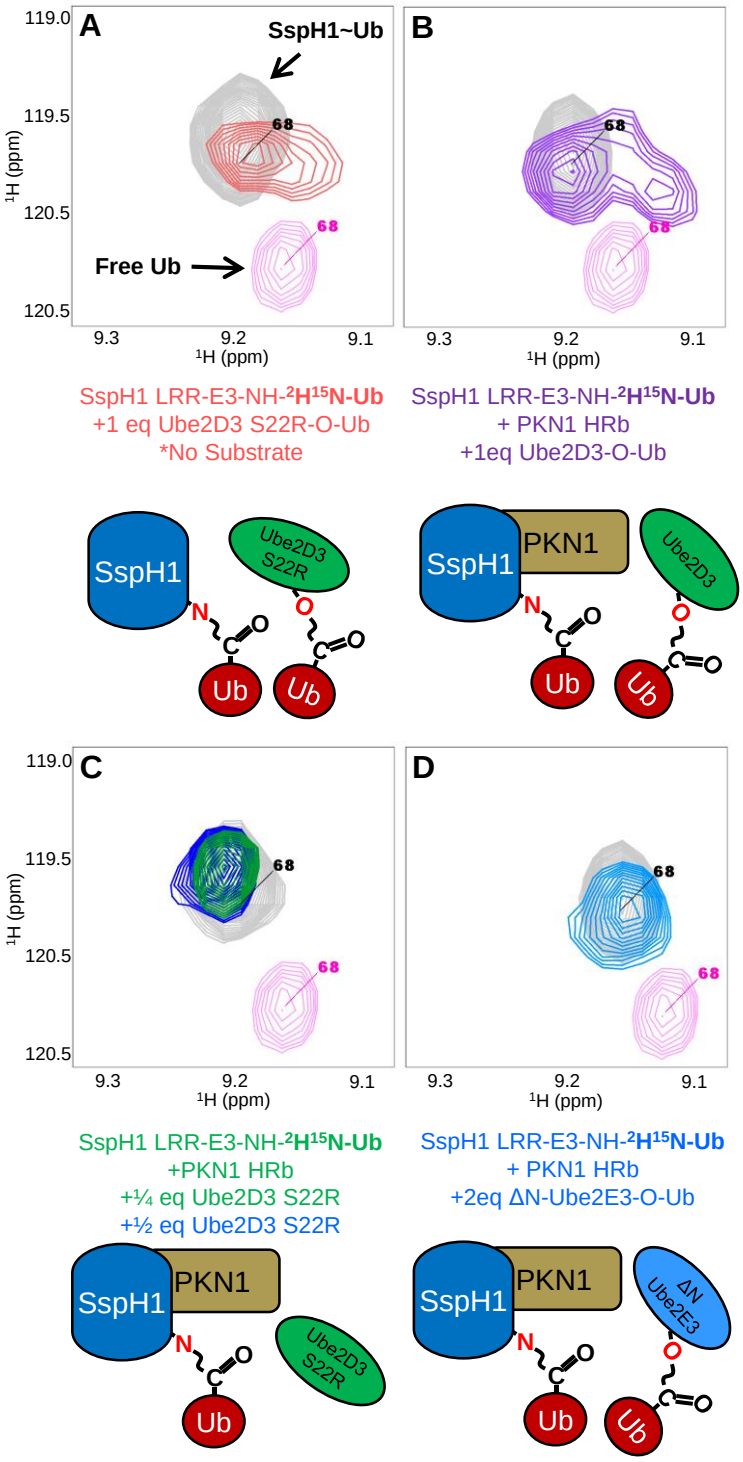

Figure 22. Close-up of the resonances belonging to ubiquitin His 68 in the ^{1}H-^{15}N TROSY spectra of $^{2}H^{15}N$-ubiquitin (pink spectrum), and SspH1 LRR-E3~$^{2}H^{15}N$-ubiquitin alone (black spectrum) or in complex with **(A)** 1 molar equivalent Ube2D3 S22R-O-Ub lacking substrate, **(B)** 1 eq Ube2D3-O-Ub and His-PKN1 108-201, **(C)** ¼ and ½ eq Ube2D3 S22R, or **(D)** 2 eq ΔN-Ube2E3-O-Ub and His-PKN1 108-201.

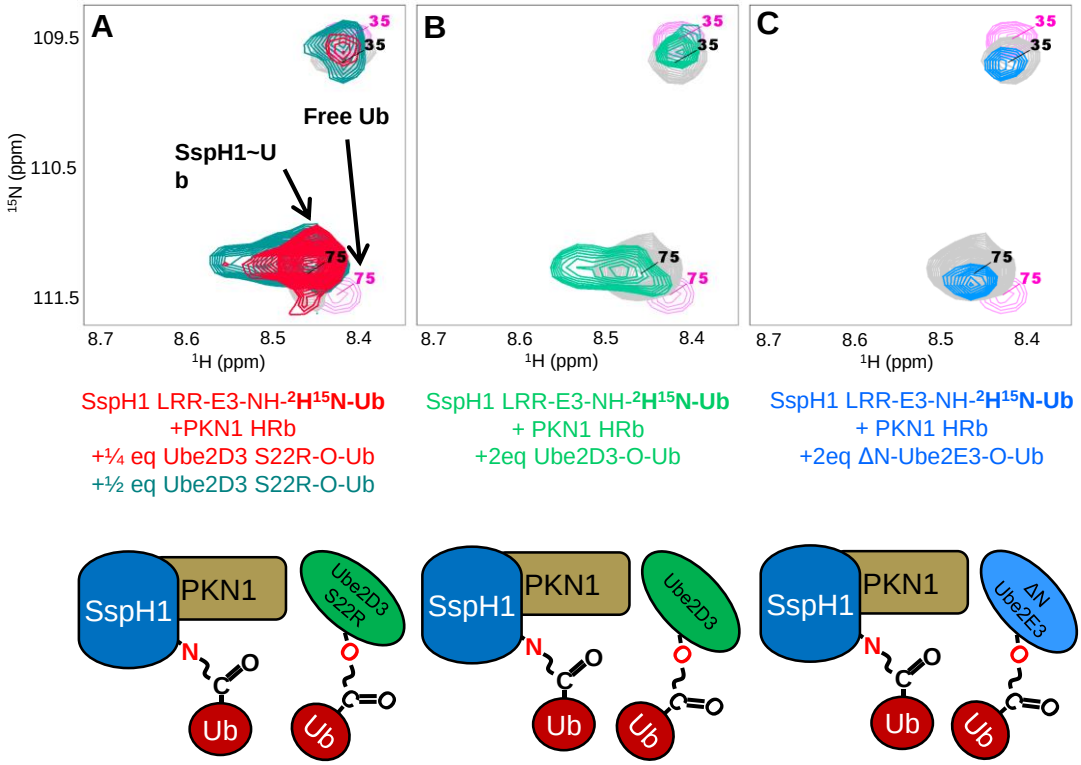

Figure 23. Close-up of the resonances belonging to ubiquitin Gly 75 in the ^{1}H-^{15}N TROSY spectra of 100µM $^{2}H^{15}N$-ubiquitin (pink spectrum), and 200µM SspH1 LRR-E3~$^{2}H^{15}N$-ubiquitin alone (black spectrum) or in complex with **(A)** 200µM His-PKN1 108-201 and 50µM (red spectrum) or 100µM Ube2D3 S22R-O-Ub (teal spectrum), or **(B)** 400µM His-PKN1 108-201 and 400µM Ube2D3~Ub (light green spectrum), or **(C)** 400µM His-PKN1 108-201 and 400µM ΔN-Ube2E3-O-Ub (light blue spectrum).

morphology of this resonance differs depending on the presence of substrate. In the absence of substrate, the resonance is very broad, while in the presence of substrate it appears to further shift equilibrium towards the new environment. The new resonance location is close to, but does not overlap, the location corresponding to the free Ub resonance. Few changes are observed upon addition of free E2 (**Fig 22C** or ΔN-Ube2E3-O-Ub (**Fig 22D**). The resonance for Gly75 shows similar, but more pronounced behavior (**Fig 23**). In SspH1-NH-$^{2}H^{15}N$-Ub (gray spectrum) the Gly75 resonance does not shift much from that of free $^{2}H^{15}N$-Ub (pink spectrum). Upon addition of Ube2D3 S22R-O-Ub (**Fig 23A**) or Ube2D3-O-Ub (**Fig 23B**), the resonance doubles to a new location that is clearly away from the location corresponding to free Ub. Upon addition of ΔN-Ube2E3-O-Ub (**Fig 23C**), the resonance decreases in intensity and does not double. These results show that the conformational change induced by the addition of Ube2D3-O-Ub moves Ub to a new chemical environment, presumably in close proximity to a substrate Lys residue.

The SspH1-NH-$^{2}H^{15}N$-Ub conformational change moves Ub towards substrate

For PKN1 to be modified by Ub, the SspH1~Ub active site must make direct contact with a substrate lysine. To test if Ube2D3-O-Ub does in fact move Ub towards substrate, a paramagnetic spin label, 4-acetamido-TEMPO, was conjugated to cysteine residues on PKN1 bound to SspH1 LRR-E3-NH-$^{2}H^{15}N$-Ub, and Ube2D3-O-Ub was added to induce broadening of the spectrum as Ub is moved out of the active site towards spin-labelled substrate (**Fig 24**,**25**). The PKN1 HRb construct used here possess one natural Cys residue at position 120 which was mutated to serine. Two of the seven lysine residues on PKN1 HRb, at positions 140 and 174, were separately mutated to cysteine to allow for spin label conjugation ("SL-140" and "SL-174") at sites where the C-terminus of Ub would be expected to be conjugated. Both of these sites can be modified by Ub *in*

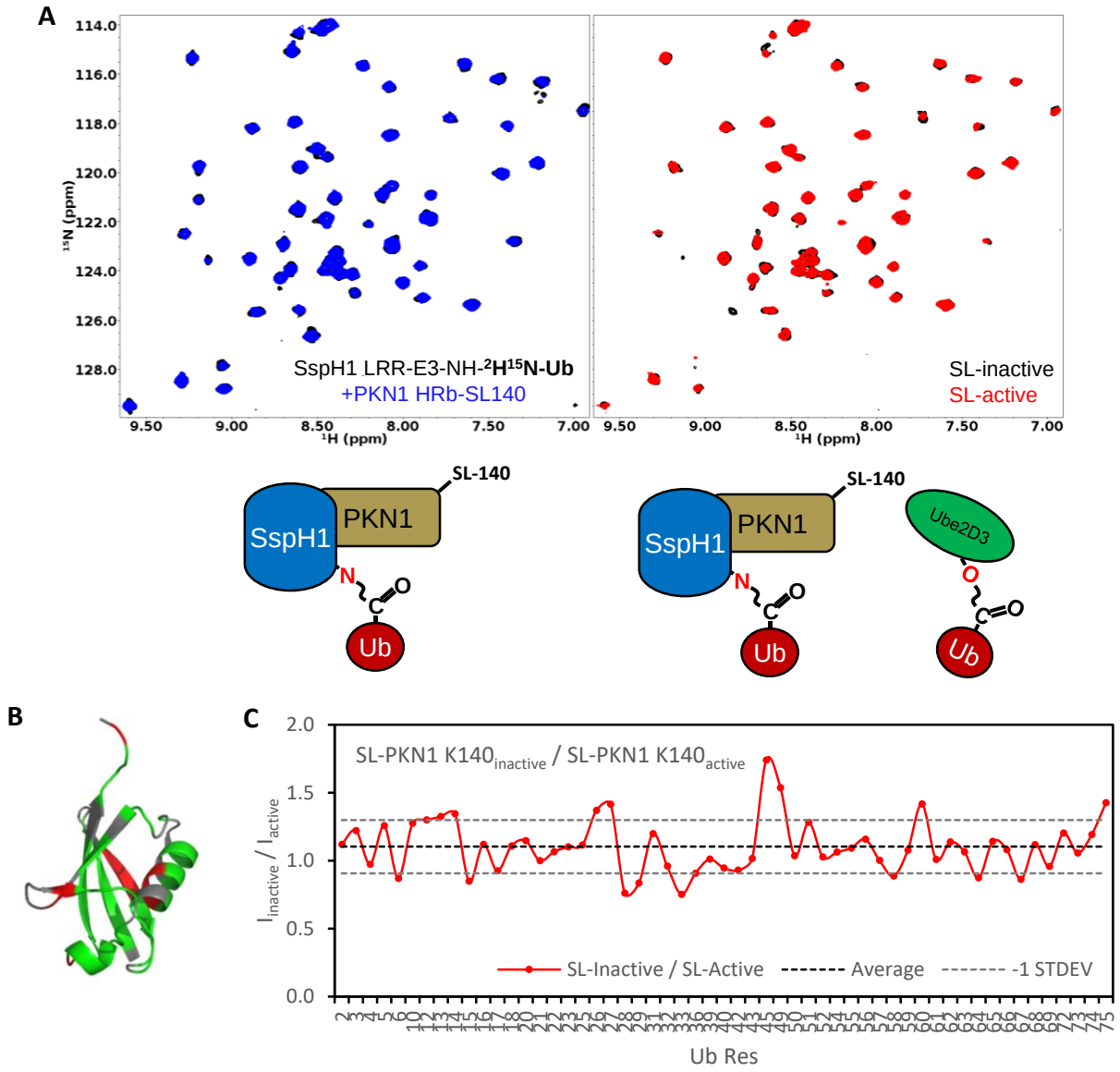

Figure 24. Paramagnetic spin label effect of iodoacetamido-TEMPO conjugated to PKN1 HRb K140C. **(A)** ^{1}H-^{15}N TROSY spectra of 100μM SspH1 LRR-E3-NH-$^{2}H^{15}N$-Ub (black spectrum) in complex with PKN1 HRb SL-140 (blue spectrum) in left panel, and upon addition of 50μM Ube2D3-O-Ub (red spectrum) and subsequent addition of 5mM sodium ascorbate (black spectrum) in right panel. **(B)** Residues most perturbed by spin label effect mapped on surface of Ub (PDB: 1UBQ). **(C)** Resonance intensity ratios of SL-inactive / SL-active. Perturbed resonances above 1 standard deviation are plotted in **(B)**

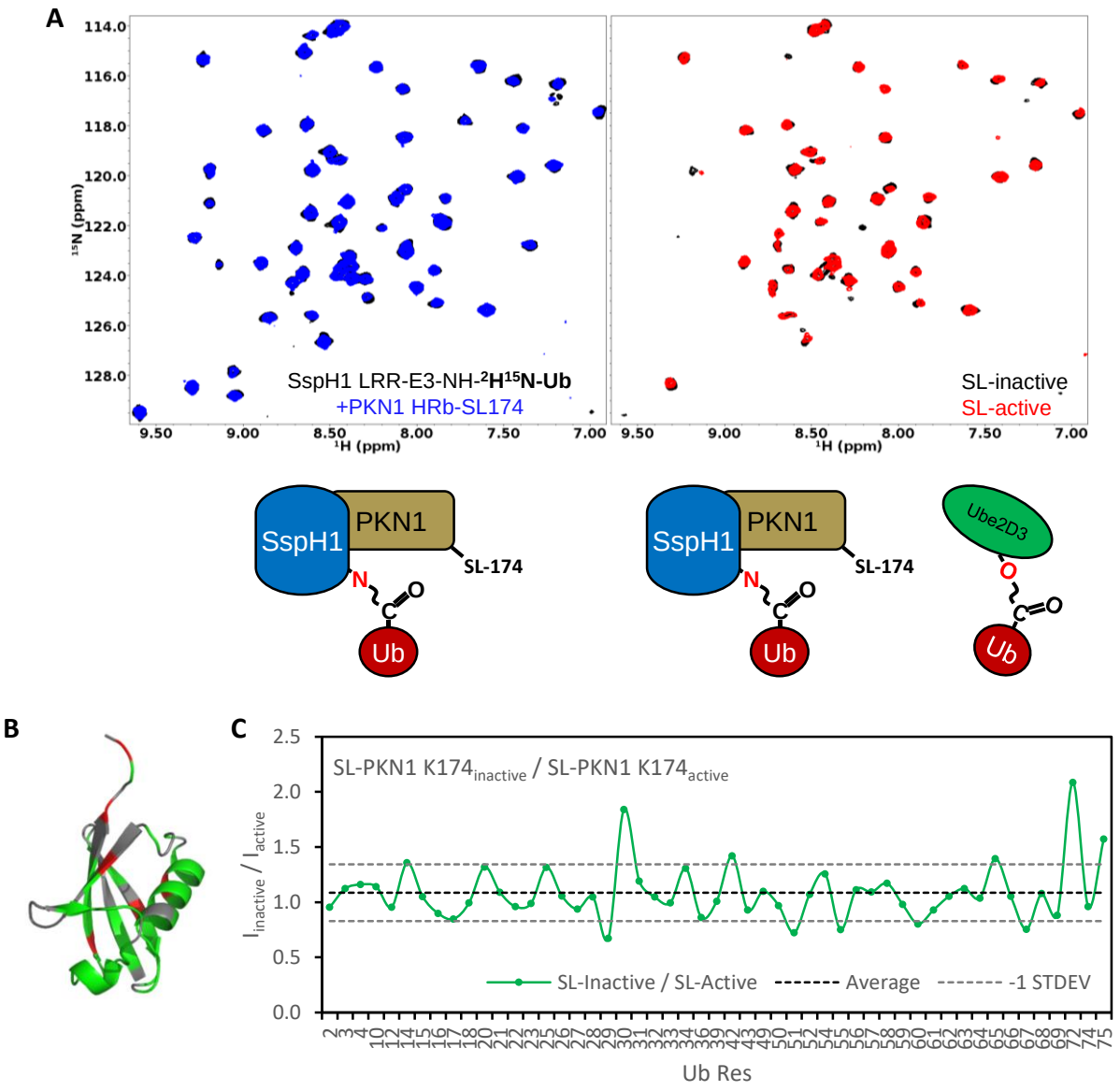

Figure 25 . Paramagnetic spin label effect of iodoacetamido-TEMPO conjugated to PKN1 HRb K174C. **(A)** ^{1}H-^{15}N TROSY spectra of 100µM SspH1 LRR-E3-NH-$^{2}H^{15}N$-Ub (black spectrum) in complex with PKN1 HRb SL-174 (blue spectrum) in left panel, and upon addition of 100µM Ube2D3-O-Ub (red spectrum) and subsequent addition of 15mM sodium ascorbate (black spectrum) in right panel. **(B)** Residues most perturbed by spin label effect mapped on surface of Ub (PDB: 1UBQ). **(C)** Resonance intensity ratios of SL-inactive / SL-active. Perturbed resonances above 1 standard deviation are plotted in **(B)**

vitro but exist on different helices in PKN1 HRb. **Fig 24** shows the spectra and intensity analysis collected for PKN1 HRb SL-140 and **Fig 25** shows the spectra and intensity analysis for PKN1 HRb SL-174. ^{1}H-^{15}N TROSY spectra in the left panels were obtained for SspH1 LRR-E3-NH-$^{2}H^{15}N$-Ub (black spectra) in complex with PKN1 HRb SL-140 or SL-174 (blue spectra). ^{1}H-^{15}N TROSY spectra in the right panels show the PKN1-spin label effect upon addition of Ube2D3-O-Ub to the SspH1~Ub/PKN1 complex. The spectrum for inactive spin label (after addition of sodium ascorbate) is shown in black, and the spectrum for active spin label is shown in red. Resonances that appear in the inactive spin label spectrum, but not the active spin label spectrum, are broadened by the spin label on PKN1 after formation of the SspH1-Ub/PKN1/Ube2D3-Ub complex. The residues corresponding to resonances most affected by spin label are shown mapped on a structure of Ub. As described earlier, some residues broaden extensively upon addition of Ube2D3-O-Ub, and these weak resonances were exempted from analysis.

Both SL-140 and SL-174 affect the average resonance intensity of the Ub subunit upon addition of Ube2D3-O-Ub. Multiple resonances increased in intensity when spin label was reduced, showing that the Ub subunit of SspH1-Ub moves closer to the spin label on PKN1 upon addition of Ube2D3-O-Ub. Several resonances experienced a large spin-label effect, corresponding to residues 13, 14, 26, 27, 45, 49, 60, 75 for PKN1 HRb SL-140, and residues 30, 42, 65, 72, 75 for PKN1 HRb SL-174. These results confirm that the conformational change in SspH1-NH-Ub-PKN1 induced by Ube2D3-O-Ub moves Ub towards PKN1.

How is this conformational change achieved? It was shown in **Part I** that the SspH1 E3 domain is composed of two subdomains, the N-terminal subdomain (NSD) which harbors the active site Cys, and the C-terminal subdomain (CSD) which harbors the E2~Ub conjugate binding site. Comparison of crystal structures of various SspH/IpaH effector E3 domains show that the

E2~Ub conjugate binding site is far from the active site Cys, and mutations in the linker region between the NSD and CSD designed to limit flexibility inhibits Ub transfer. Those results suggest that movement between the NSD and CSD are critical for catalysis. The results presented here suggest that binding of PKN1 and E2~Ub is required to induce the conformational change in SspH1.

In the absence of Ub at the active site, binding of E2~Ub to the SspH1 thumb helices orients the E2~Ub conjugate thioester bond for attack by the SspH1 active site Cys. After transfer of Ub from E2 to SspH1, free E2 leaves the complex, but SspH1~Ub is still not competent for Ub transfer, even in the presence of substrate. Binding of another E2~Ub induces a conformational change in SspH1, but this time there is a Ub conjugated to the active site Cys. Instead of moving the SspH1 active site Cys towards the incoming E2~Ub thioester bond, Ub at the active site of SspH1~Ub is moved towards bound substrate. The E2 subunit of the second incoming E2~Ub must be largely responsible for the second conformation change, as Ube2D3~Ub can move SspH1~Ub towards substrate but Ube2E3~Ub cannot.

It is still not clear what the exact structural difference is between Ube2D3 and Ube2E3 that defines the ability to induce the second conformational change. As described above, a variety of screening mutations were attempted (**Table 1**), but there was no Ube2D3 → Ube2E3 residue substitution that led to an inability of Ube2D3 to perform the second step of the reaction. Perhaps it is not the E2 itself, but the relative orientation of the subunits in E2~Ub that defines the ability to perform the second step of the reaction. Previous studies have shown that the E2 and Ub subunits for Ube2D3~Ub and Ube2L3~Ub can exist in different conformational states relative to each other (*eg.* distribution of open and closed conformations of the E2~Ub conjugates), but a similar analysis has not yet been performed for Ube2E3~Ub. It is unlikely that there is only a single residue or

series of residues in the E2 subunit that defines the set of possible conformational states for E2~Ub, which may explain the failure of the mutational screen.

A high-resolution structure of SspH1-NH-Ub could shed light on how the SspH1 active site changes with Ub covalently bound in the active site. Many attempts were made to crystallize various constructs of SspH1 or SspH1-NH-Ub alone or in complex with PKN1, E2 or E2-O-Ub, with both Ube2D3 and Ube2E3 used as the E2. The observation that the ^{1}H-^{15}N TROSY spectrum of SspH1-NH-$^{2}H^{15}N$-Ub is of high quality even in a large (>125kDa) complex suggests that Ub is not tightly docked to SspH1 while it is tethered at the active site. If Ub is dynamic at the active site, crystallization of SspH1-NH-Ub may ultimately prove difficult or impossible. A particular conformation of SspH1-NH-Ub may be stabilized by adding E2-O-Ub; however, the binding affinity between SspH1~Ub and E2~Ub is low enough that a 1:1 complex does not coelute by size exclusion chromatography, further complicating efforts towards crystallization. Although SspH1 is too large to obtain high-quality NMR data for the full E3 domain, lower-resolution biophysical methods can be used to study to the structure of SspH1-NH-Ub in solution. The next sections will present hydrogen-deuterium exchange and small-angle X-ray scattering analyses of various constructs of SspH1 and SspH1-NH-Ub alone and in complex with PKN1.

SAXS Analysis of SspH1

The crystal structures of IpaH4 and SspH2 (**Intro Fig 4B**) show a large difference in the conformations of the LRR and E3 domains relative to each other. From these crystal structures alone, it's not clear what the primary conformation of SspH1 is in solution, or how the conformation changes upon addition of substrate. To understand the overall shape of SspH1 in solution, the 6 constructs analyzed in the second round of HDX were also characterized by small-

angle X-ray scattering (SAXS). SAXS is a low-resolution structural method that provides information on the shapes and sizes of particles at low resolution. For each construct, ~10 mg/mL protein, with N-terminal affinity tag removed, was applied to a gel filtration column in-line with the SAXS beamline, and SAXS curves were recorded as proteins eluted off the column (See **Methods** for full details). The intensity (I_0) and radius of gyration (R_g) calculated for each SAXS curve are plotted in **Fig 26** and resemble A_{280} and R_g curves for proteins eluting off a gel filtration column in size-exclusion chromatography multi-angle light scattering experiments. In all constructs, a single I_0 peak was observed, and the R_g curve under the I_0 peak was flat, indicative of non-aggregating, well-behaved particles. For each construct, the SAXS curves collected from the first half of the peak (red curves) and second half of the peak (blue curves) were averaged and treated separately to determine how R_g, D_{max}, and V_p vary across the peak (See **Methods** for full details). R_g is the mass-weighted average distance from the center of the protein to every other point in the protein. D_{max} is the maximum distance between any two points in the protein. V_p (Porod Volume) is the volume of the particle. In all cases, analysis averaged SAXS curves from the red and blue regions of the curve yielded similar results, further demonstrating that all the constructs are well-behaved. A list of the R_g and D_{max} values calculated for each of the constructs in **Table 2**.

SAXS Analysis of the free SspH1 E3 domain yielded an R_g and D_{max} of ~25Å and ~86Å, respectively (**Fig 26A**). The presence of the LRR domain increased R_g and D_{max} values to ~35Å and ~119Å (**Fig 26B**). To determine if the shape of SspH1 LRR-E3 is similar to one of the conformations of LRR-E3 domains observed in the crystal structures of SspH2 or IpaH4 (**Intro Fig 4**), R_g and D_{max} was calculated for SspH1 homology models based upon the SspH2 and IpaH4 structures. Homology models were used for comparisons because the LRR domains for SspH1,

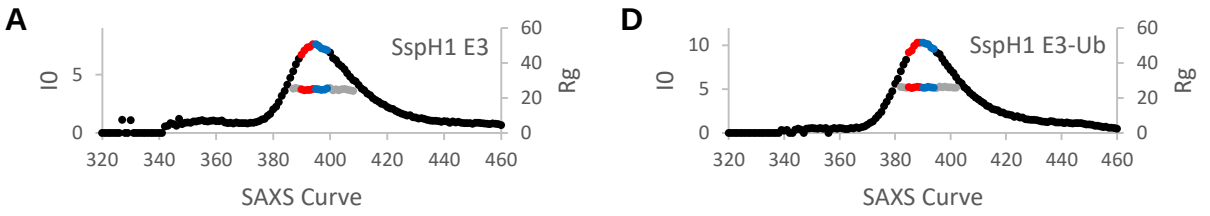

SspH1 E3	390-394 (red)	395-399 (blue)
Guinier Rg (Å)	24.56 +/- 0.26	24.97 +/- 0.92
P(r) Rg (Å)	24.94	25.27
P(r) Dmax (Å)	85.96	87.39
P(r) Vp (Å^3)	52600	53400

SspH1 E3-Ub	385-389 (red)	390-394 (blue)
Guinier Rg	26.08 +/- 0.15	26.07 +/- 0.90
P(r) Rg	26.15	26.13
P(r) Dmax	85.41	89.29
P(r) Vp	64700	63800

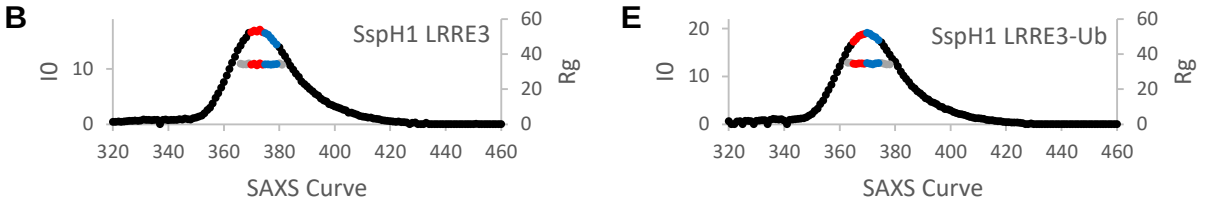

SspH1 LRRE3	370-374 (red)	375-379 (blue)
Guinier Rg	33.99 +/- 0.99	34.00 +/- 1.86
P(r) Rg	35.17	35.05
P(r) Dmax	118.97	119.00
P(r) Vp	88500	88100

SspH1 LRRE3-Ub	365-369 (red)	370-374 (blue)
Guinier Rg	34.53 +/- 0.78	34.53 +/- 2.40
P(r) Rg	35.37	35.20
P(r) Dmax	120.86	120.86
P(r) Vp	105000	104000

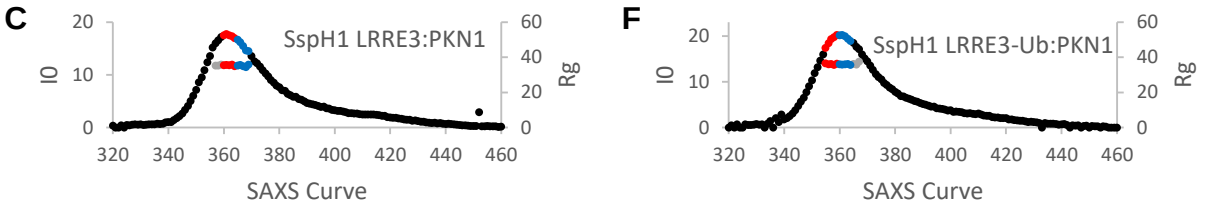

SspH1 LRRE3:PKN1	360-364 (red)	365-369 (blue)
Guinier Rg	35.46 +/- 0.18	35.27 +/- 0.95
P(r) Rg	36.78	35.99
P(r) Dmax	124.11	123.45
P(r) Vp	114000	112000

SspH1 LRRE3-Ub:PKN1	355-359 (red)	360-364 (blue)
Guinier Rg	35.97 +/- 0.46	35.77 +/- 0.21
P(r) Rg	36.43	36.40
P(r) Dmax	125.90	125.20
P(r) Vp	134000	133000

Figure 26. SAXS Analysis of **(A)** SspH1 E3 domain, **(B)**, SspH1 LRR-E3, **(C)** SspH1 LRR-E3/PKN1 HRb, **(D)**, SspH1 E3-Ub, **(E)** SspH1 LRR-E3-Ub, and **(F)** SspH1 LRR-E3-Ub:PKN1 HRb. Curves represent I_0 and R_g calculated from SAXS curves recorded for each protein eluting off a gel filtration column. SAXS curves for the first and second halves of the I0 peaks (red and blue, respectively) were treated separately for later analysis. Later analysis included Guinier Rg calculated from Guinier analysis, and Rg, Dmax, and Vp calculated from transformations of the real-space P(r) curves (see **Methods**).

Construct	R_g (Å)	D_{max} (Å)
SspH1 E3	25	86
SspH1 E3-Ub	26	87
SspH1 LRR-E3	35	119
SspH1 LRR-E3-Ub	35	121
SspH1 LRR-E3/PKN1 HRb	36	124
SspH1 LRR-E3-Ub/PKN1 HRb	36	126
SspH1 LRR-E3 Homology Model (SspH2 structure)	28.7	93.1
SspH1 LRR-E3 Homology Model (IpaH4 structure)	33.7	124.2
SspH1 LRR-E3/PKN1 Homology Model (IpaH4 structure)	33.5	124.3

Table 2. R_g and D_{max} values derived from SAXS analysis for the various SspH1 constructs and SspH1 homology models based on the structures of IpaH4 and SspH2.

SspH2, and IpaH4 are different sizes, and thus would be expected to give different results. The program CRYSOL from the ATSAS software package for SAXS analysis was used to calculate R_g and D_{max} [82]. The homology model of SspH1 based on the structure of SspH2 gave an R_g of 28.7Å and a D_{max} of 93.1Å. The model based on the structure of IpaH4 gave an R_g of 33.7Å and a D_{max} of 124.2Å. The experimental data for SspH1 gives an R_g of ~35Å and a D_{max} of ~119Å (**Fig 26B**). Though the R_g and D_{max} values do not fit either homology model conformations perfectly, they are much more similar to the conformation observed in the structure of IpaH4, suggesting that the LRR and E3 domains in solution accommodate a more open conformation with respect to each other. This is important as it suggests that overall the PKN1 binding site is readily accessible, in contrast to the competitive displacement model described in **Part II** of the dissertation.

Upon binding PKN1, the R_g of the SspH1 LRR-E3/PKN1 complex increased by ~1Å to ~36Å, and D_{max} increased by ~5Å to ~124Å (**Fig 26C**). These small changes suggest that substrate binding alone does not trigger a large re-orientation of LRR and E3 domains. Using the structure of the PKN1-HRb repeat bound to the SspH1 LRR domain (PDB 4NKG), a homology model was generated of the SspH1/PKN1 complex. Using CRYSOL, this model was calculated to have an R_g of 33.5Å and a D_{max} of 124.3Å, which are similar to the experimental values.

Ub at the active site did not have a major impact on the overall shape of SspH1. Analysis of SspH1 E3~Ub yielded an R_g of ~26Å and D_{max} of ~87Å, respectively (**Fig 26D**). Analysis of SspH1 LRR-E3~Ub yielded an R_g of ~35Å and D_{max} of ~121Å, respectively (**Fig 26E**). Compared to free enzyme, R_g and D_{max} increased only by ~1Å between for Ub-conjugated species, indicating that Ub is not inducing large reorientations of the LRR and E3 domains. The presence of Ub is observable in the SAXS data, as V_p increases in all cases. The most likely explanation for these

results is that Ub is being held in the active site of SspH1 in each of these constructs but is not inducing large conformational changes.

Though the R_g and D_{max} values calculated from SAXS curves are compatible with a SspH1 conformation similar to the IpaH4 structure, other conformations of the LRR and E3 domains could possibly yield similar values. SAXS curves can be used to generate low-resolution *ab initio* molecular envelopes in order to visualize various conformational states of a protein that are compatible with the curve. Two programs, GASBOR and DAMMIF [82] were used to generate *ab initio* molecular envelopes for each of the SspH1 constructs, but unfortunately none of the resulting envelopes were of high enough resolution to conclusively fit different orientations of the LRR and E3 domains. The resolution of *ab initio* envelopes in all cases was calculated to be only ~40Å by Fourier shell correlation [83] Ideally, Ube2D3-O-Ub would be added in complex with the various SspH1 constructs to probe conformational changes induced by addition of E2~Ub. However, the affinity of SspH1 and E2~Ub is low enough that the complex does not coelute on a gel filtration column, and it is unlikely that a monodisperse sample of SspH1 bound to Ube2D3-O-Ub could be prepared. SAXS is not a good method for studying conformational changes in polydisperse samples, so data was not collected for SspH1 in the presence of Ube2D3-O-Ub.

Structural changes in SspH1 Identified by Hydrogen-Deuterium Exchange Mass-Spectrometry

NMR experiments and ubiquitylation assays in **Part I** and **Part III** provided evidence that structural changes in SspH1 are critical for its Ub transfer mechanism. Another method for structurally characterizing proteins in solution and investigating different conformational states is

hydrogen-deuterium exchange followed mass-spectrometry (HDX-MS). HDX-MS monitors the exchange of labile hydrogens, such as polypeptide backbone amide hydrogens, with deuterium upon introduction of the protein into a deuterated solvent. The hydrogen-deuterium exchange process for a single site is characterized by a monoexponential function, $1 - e^{-k_{ex}t}$, where k_{ex} is the hydrogen-deuterium exchange (HDX) rate for the site. For a folded protein, k_{ex} is highly dependent on solvent accessibility and the presence of stabile hydrogen bonding interactions or salt bridges which are generally dependent on protein secondary-structure. The power of HDX-MS analysis lies in the ability to compare identical peptides in different states of the protein. Peptides that become more protected from HD-exchange can reveal the presence of the stabilization of protein secondary structure or new protein domain interactions. Alternatively, regions that lose protection become more solvent exposed and can indicate loss of secondary structure or exposure of new protein surfaces due to changes in domain interactions. Therefore, knowledge of HDX rates can provide structural information about a protein and domain rearrangements.

HDX-MS involves the following workflow: **1)** Initiating HDX by incubating a protein in deuterated solvent for varying amounts of time. **2)** Quenching the HDX reaction in acidic buffer. HDX is highly pH dependent and the rate is minimal at low pH. **3)** Generating small peptides amenable for mass spectrometry by pepsin digestion. These small peptides give region-specific information on exchange rates, and thus the structure of the protein. **4)** Reverse-phase liquid chromatography to separate peptides prior to mass spectrometry. **5)** Mass spectrometry and subsequent data analysis (see **Methods** for details).

The results of the HDX-MS experiments are a series of HDX curves that show the uptake of deuterium over time for each identified peptide. HDX curves for a peptide are enlightening

because they can be compared to a known crystal structure and to other regions of the protein to gain insights into the overall structure and dynamics of the protein. HDX curves are most instructive when comparing the exchange rate of the same peptide from different constructs, complexes, or at different stages in a pathway. One way of comparing the HD-exchange profiles for two proteins is by constructing *butterfly plots* (see **Methods** for full details). For Round 1 HDX experiments, butterfly plots were constructed for comparing SspH1 E3 domain to SspH1 E3-Ub, and full-length SspH1 to full-length SspH1-Ub to identify structural changes that occur in SspH1 when Ub is at the active site. **Fig 27** shows one-half of the butterfly plot, for the SspH1 E3 domain alone. The secondary structure of the SspH1 E3 is diagrammed above the butterfly plot in **Fig 27A**, with the colors of the secondary structure diagram corresponding to the colors in a homology model of the SspH1 E3 domain shown in **Fig 27B**.

Fig 28A shows the butterfly plot comparing SspH1 E3 to SspH1 E3-Ub. The half-butterfly plot in **Fig 27A** has more data points than the butterfly plot in **Fig 28A** because greater coverage from pepsin digestion was obtained for free SspH1. Since the purpose of the full butterfly plot is to compare constructs, data points not shared by both constructs were eliminated from analysis in the full butterfly plot. A powerful attribute of HDX analysis is revealed when comparing two closely related structures of SspH1, as differences in conformational states can be observed by changes in exchange rates of specific peptides. This is readily visualized by creating summation plots as shown in **Fig 28B**. For regions where the HDX curves for each construct are similar, the value in the summation plot is close to zero. A peak occurs in the summation plot for regions where the HDX curves for each construct are different. Peaks in the summation plot highlight regions in the protein that are structurally different between the two constructs. The summation plot in **Fig 28B** shows several peaks less than zero, indicating regions that are more structured in SspH1 E3-

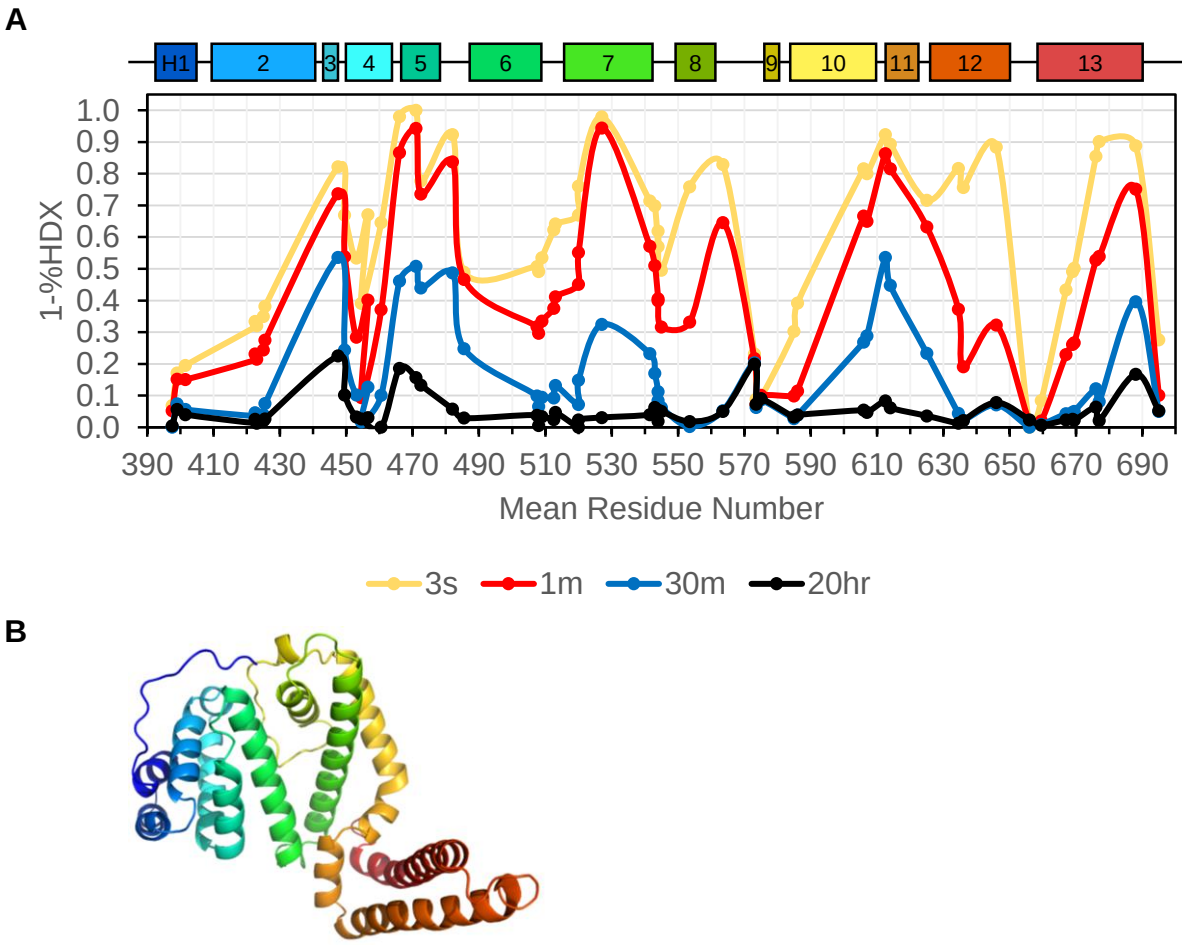

Figure 27. (A) One-half of a butterfly plot, for the SspH1 E3 domain. Each point corresponds to a different peptide. Each colored curve corresponds to the HDX values at the 3s, 1m, 30m, and 20hr timepoints, plotted as the value (1-% HDX). The secondary structure diagram for SspH1 is shown above the butterfly blot. Colors in the secondary structure diagram correspond to those on a homology model of the SspH1 E3 down shown in **(B)**. The homology model was generated from the crystal structure of SspH1 (PDB: 3G06)

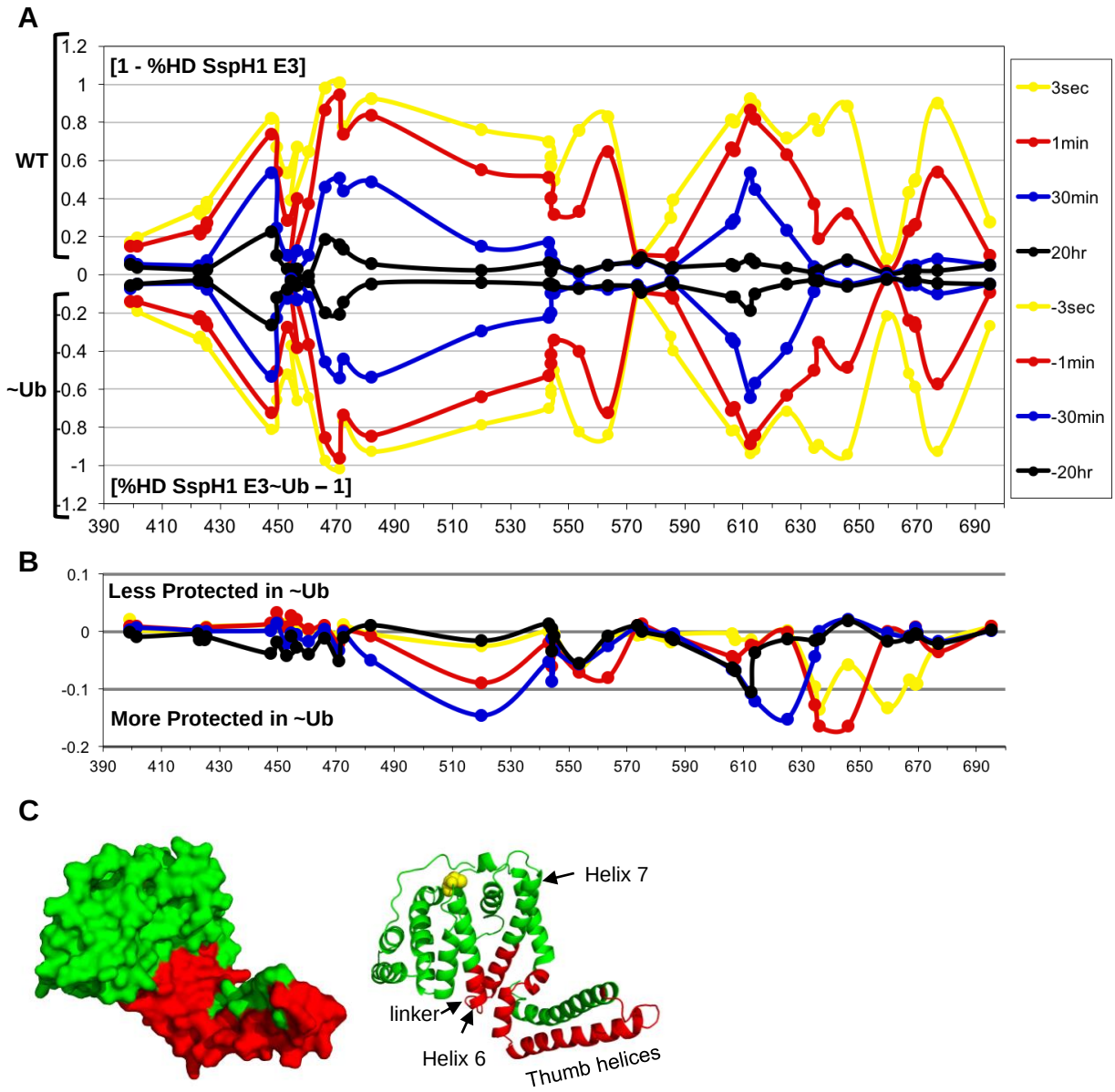

Figure 28. (A) Butterfly plots comparing the HDX percent deuteration patterns between SspH1 E3 domain and SspH1 E3-Ub. For each peptide processed as described in **Fig 31**, (1 - %HDX) for the E3 construct and (%HDX – 1) for the E3~Ub construct were plotted as a function of mean residue number. Deuteration profiles plotted for each sampled time point: 3 sec (yellow), 1 min (red), 30 min (blue), and 20 hr (black). The sum of the values in **(A)** are plotted in **(B)** to highlight areas of different between the deuteration profiles. **(C)** Differences in HDX exchange between E3 and E3~Ub shown in **(B)** are plotted in red on the SspH1 E3 homology model.

Ub than in the free E3 domain. The peaks correspond to peptides comprising residues 508-532 and 605-660. To visualize these regions structurally, peptides appearing as peaks in the summation plot are highlighted in red on surface and cartoon structures of the SspH1 E3 homology model (**Fig 28C**). These peptides comprise a continuous surface of the E3 domain, including one of the thumb helices in the CSD as well as portions of helices 6 and 7 that interact with the base of the thumb helices. In **Part I**, it was shown that E2~Ub clamps around the tip of the thumb helices prior to transferring Ub to the SspH1 active site cysteine. It was also shown that flexibility between the NSD and CSD is critical for ubiquitylation activity. The flexible linker between the NSD and CSD resides between helices 6 and 7, close to the base of the thumb helices. These two regions are also the regions stabilized by Ub when it is present at the SspH1 active site, suggesting that the flexibility of the thumb and NSD-CSD linker region is more constrained when Ub is at the active site.

Shown in **Fig 29A** is the butterfly plot comparing full-length SspH1 to full-length SspH1~Ub. Here, the different domains of SspH1 are labelled above the plot, revealing that the domain architecture of full-length SspH1 is reflected in the shape of the butterfly plot. The linkers between domains are unstructured and have fast HDX rates, thus appearing as nodes in the butterfly plot. Looking at the butterfly plot, the first structured region, from residues ~25-125, corresponds to an N-terminal domain of unknown function. The second structured region, from residues ~175-400 corresponds to the LRR domain. The third structured region, from residues ~425-700 residues, corresponds to the E3 domain, which can be further subdivided into N-terminal and C-terminal subdomains, as well as the E2~Ub conjugate-binding thumb helices. The summation plot is shown in **Fig 29B**, and shows peaks corresponding to protection from HDX in the thumb helices similar to that observed for the SspH1 E3 domain in **Fig 28B**. Therefore, the

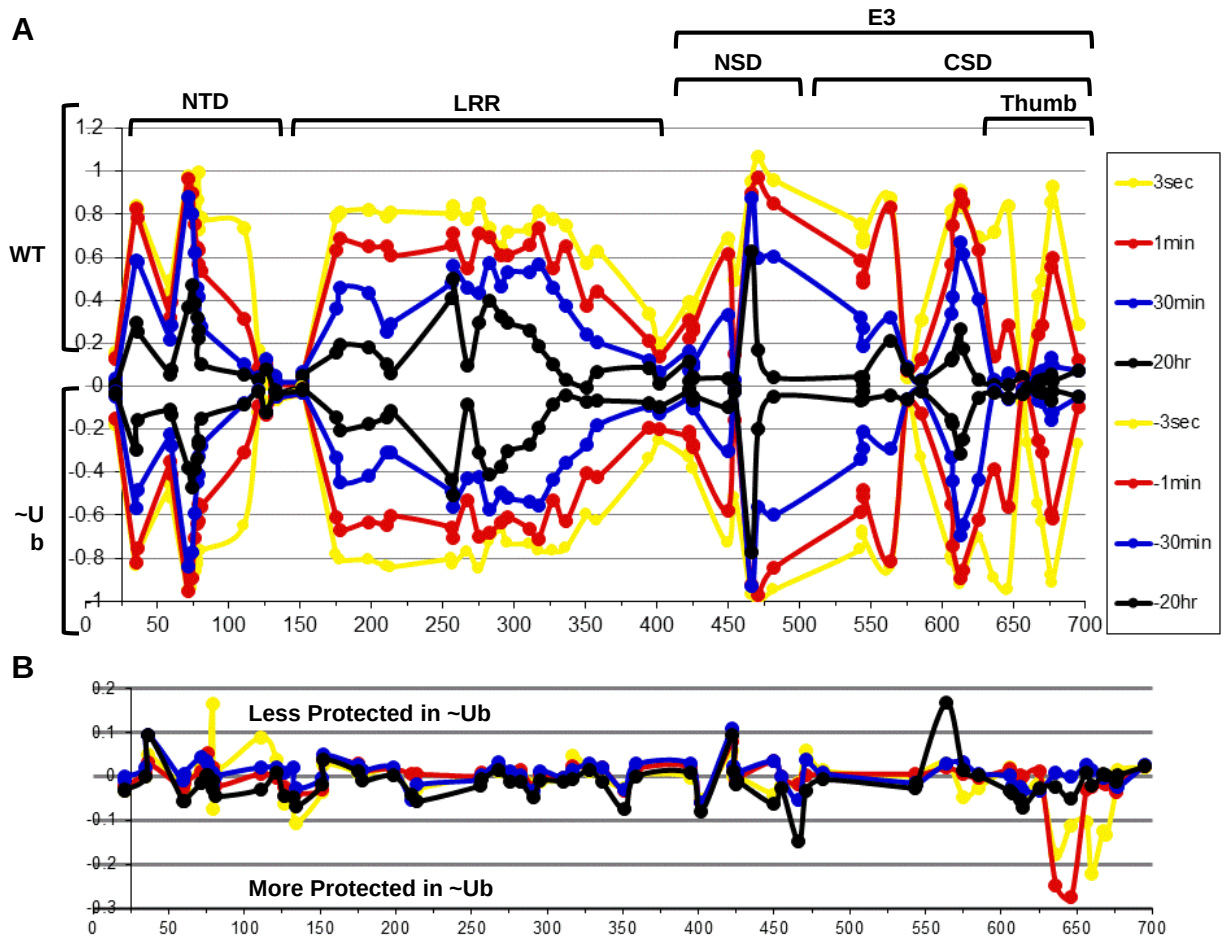

Figure 29. (A) and **(B)** Butterfly plots comparing the HDX percent deuteration patterns between His-SspH1 and His-SspH1 C492K-Ub prepared similarly as in Figure 28. NTD: N-terminal domain. LRR: leucine-rich repeat. NSD: N-terminal subdomain. CSD: C-terminal subdomain. Thumb: E2~Ub-binding terminal helices of the CSD.

presence of Ub at the active site in full-length SspH1 has a similar stabilizing effect on the thumb region as in the E3 domain alone.

The high degree of protection found for residues 25-125 in SspH1 reveals a previously unrecognized structured region of SspH1. This region is not shared by all members of the SspH-IpaH family, and sequence alignments show that *Salmonella* SspH and *Shigella* IpaH effectors differ in this N-terminal region. IpaH effectors from *Shigella* have a relatively short sequence prior to the LRR domain (~30 residues), and primary sequence analysis predicts it to be intrinsically disordered. However, sequence analysis revealed that a subset of other *Salmonella* effectors, including SspH2, share this motif [(39)], and a structure of the homologous domain from the *Salmonella* effector SifA has been determined (**Fig 30**). In the structure of SifA, which induces endosomal tubulation in the generation of *Salmonella*-containing vacuoles, this domain mediates interactions with the eukaryotic protein, SKIP, a regulator of microtubule growth [(90)]. It is possible that the N-terminal domain of SspH1 is also responsible for interacting with host proteins, perhaps as a mechanism for localization. Preliminary yeast two-hybrid screens with the SspH1 N-terminal domain in collaboration with Sam Miller's lab in the Microbiology Department of the University of Washington indicate that it may interact with Prp6, a component of the eukaryotic spliceosome, but this interaction has not been verified *in vitro*.

Besides intracellular localization, it is possible that the new N-terminal domain may play a role in the ubiquitin transfer reaction. To test if the N-terminal domain of SspH1 can interact in trans with other domains of SspH1, ^{1}H-^{15}N TROSY spectra were obtained for 250μM SspH1 1-127 alone (**Fig 30A**) or in the presence of 175μM SspH1 LRR-E3 or 175μM SspH1 E3. There was no noticeable resonance shifting or loss in resonance intensity for the SspH1 N-terminal domain in the presence of other SspH1 domains, suggesting that it is independent of the LRR or E3

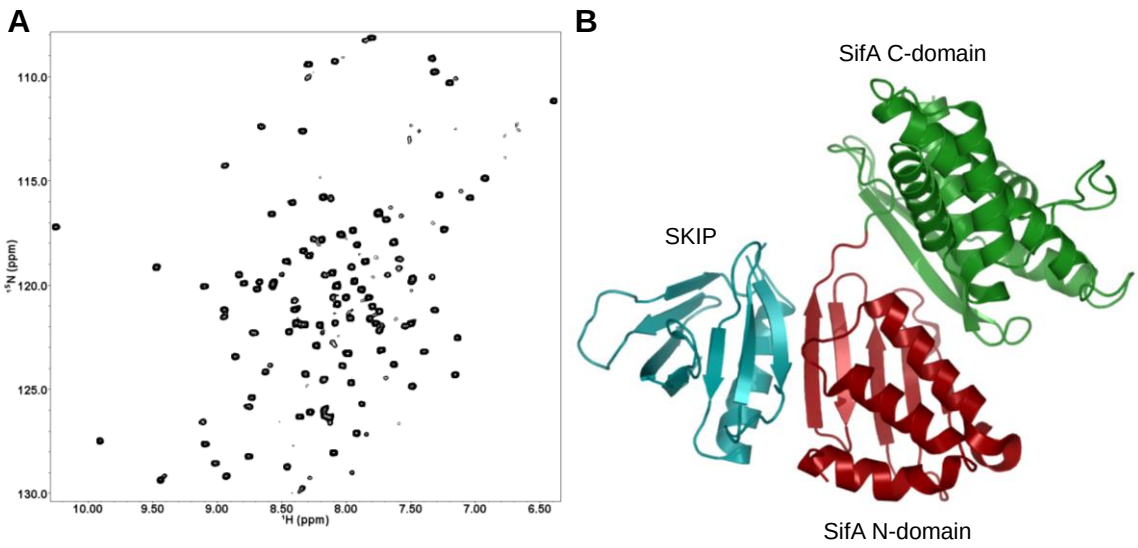

Figure 30. (A) ^{1}H-^{15}N TROSY spectrum of 250µM His-SspH1 1-127 alone (black spectrum) and in the presence of **(B)** Crystal structure of *Salmonella* SifA bound to human protein SKIP through it's N-terminal domain, which is 40% similar and 23% identical to the N-terminal sequence of SspH1. (PDB: 3CXB Ohlson 2008)

domains. It was also shown in **Fig 2** that the N-terminal domain does not affect ubiquitylation activity of SspH1. Therefore, the most likely role for the N-terminal domain is to mediate interactions with host cell proteins, similar to the function of the N-terminal domain in SifA.

One caveat with the data collected for full-length SspH1 and full-length SspH1-Ub was that it suffered from overall poor signal to noise, and mass spectra for peptides often overlapped. Noise in the mass spectra carried over to the summation graph (**Fig 29B**), which was not as high quality as that obtained for the E3 domain alone in (**Fig 28B**). Since the N-terminal domain does not interact with the LRR or E3 domains, and does not impact ubiquitylation activity, it was removed from SspH1 constructs in the second round of HDX experiments to reduce the number of potential peptides that could lead to overlap in the mass spectra. Thus, HDX analysis for SspH1 and various constructs was repeated, eliminating the SspH1 N-terminal domain, and employing an updated mass spectrometry pipeline was used that reduced spectral overlap (see Methods for details).

Second round of HDX-MS Experiments

In addition to repeating previous HDX experiments, additional data collected in a second round of HDX experiments sought to understand the role of the substrate PKN1 in driving SspH1 conformational changes. To analyze and visualize more than one pairwise comparison at a time, a new approach was adopted in addition to generating butterfly plots. Protection Factors were calculated comparing the various SspH1 constructs using the computational methods described in 79 (see **Methods** for additional discussion and details). Protection factors quantify the change in exchange rates between two experimental conditions [(79)]. After generating HDX curves using the procedure outlined in **Methods Fig 1**, custom Python scripts were written to implement the

algorithm described in 79 (see **Methods** for source code). The results from calculating directional protection factors are shown in **Figs 31-33**. Protection factors greater than 1 indicate greater protection from HDX, and thus a stabilization of secondary structure. Protection factors between 0 and 1 indicate less protection from HDX, and thus a destabilization of secondary structure. A value of 1 indicates no change, whereas a value of -1 indicates a protection factor could not be calculated due to an insufficient number of sampled points between the two conditions (see Methods for full details). This analysis focuses on structural changes in the E3 domain, so for all constructs, protection factors are only presented for peptides originating from the E3 domain.

Effects of LRR domain on SspH1 HDX

Fig 31 shows protection factors calculated for SspH1 E3 vs LRR-E3 (**Fig 31A**). Overall, the LRR domain has a highly stabilizing effect on the E3 domain, with the highest protection factors occurring at the interface between the LRR and E3 domains as predicted by a homology model of SspH1 LRR-E3 based on the structure of IpaH4 (**Fig 31D**). The highest protection factor occurs for a peptide comprising residues 449-460 (**Fig 31C**, top left red box). In the structure of IpaH4, which SspH1 appears to resemble in solution, contacts are observed between residues in this region, especially E333 in the NSD and S255 and S256 in the LRR domain (**Fig 31D**, top), observations consistent with our SAXS analysis. Other IpaH structures in the open conformation exhibit additional contacts and more helical structure in this region. No contacts are observed between these regions in the SspH2 structure. Significant protection is also observed in residues 551-570, corresponding to CSD α-helix 8 in the SspH1 homology model. In the SspH1 open conformation based on IpaH4, this helix is part of the NSD/CSD interface in the E3 domain and positioned next to residues 449-460 in the proximal conformation of the E3 domain described in

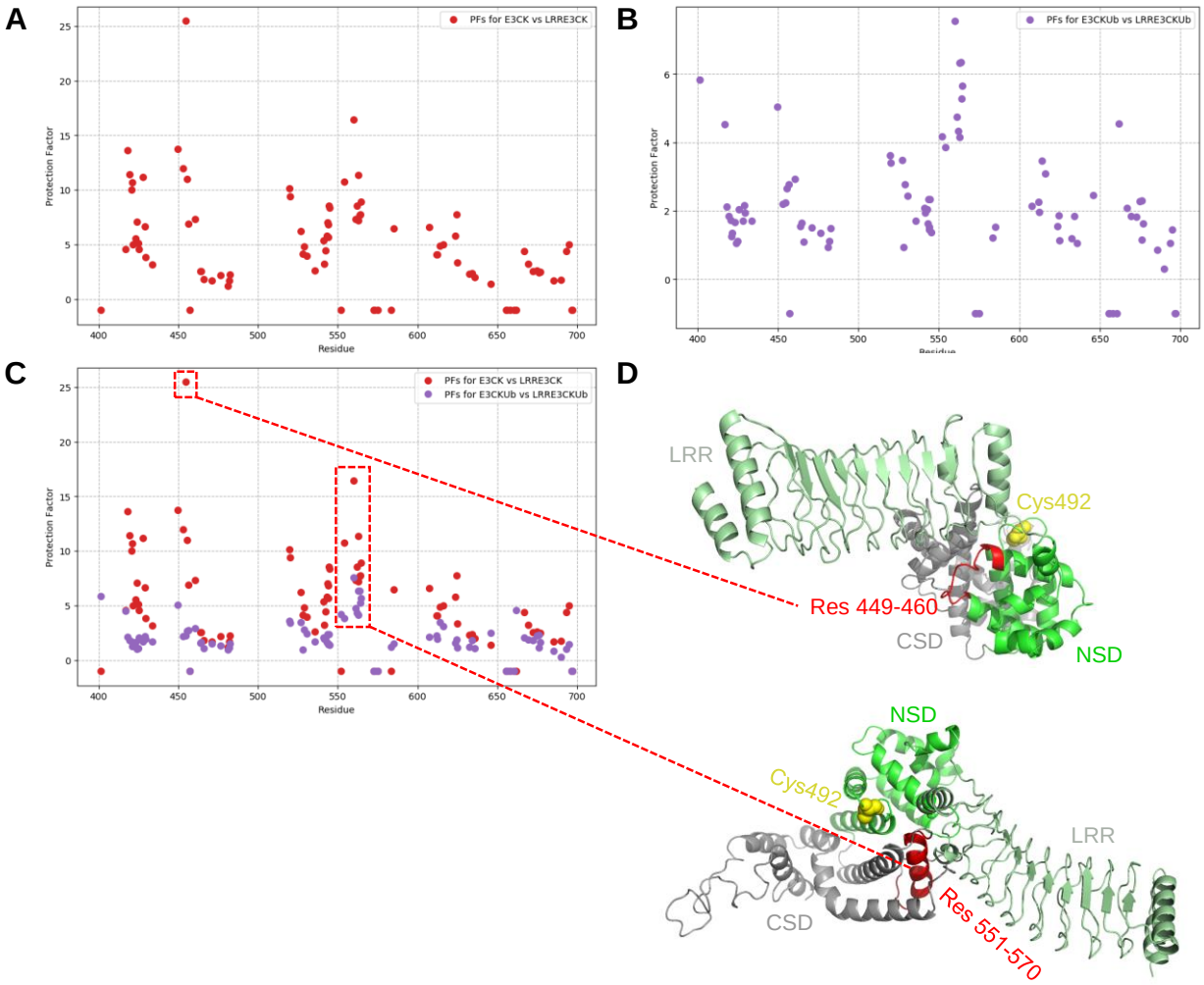

Figure 31. Impact of LRR domain. Protection factors were calculated for **(A)** SspH1 E3 vs SspH1 LRR-E3, and **(B)** SspH1 E3-Ub vs SspH1 LRR-E3-Ub. **(C)** Overlay of both comparisons between SspH1 between LRR-E3 or E3 domain alone constructs. **(D)** Homology model of SspH1 LRR-E3 based of structures of IpaH3 LRR-E3 (PDB 3CVR) and SspH1 LRR (PDB 4NKH). The peptides corresponding to residues 449-460 or 551-570, which have high protection factors in the presence of the LRR domain, are shown in red. LRR is shown in light green, the N-terminal subdomain (NSD) of the SspH1 E3 domain is shown in green, the C-terminal subdomain (CSD) of the SspH1 E3 domain is shown in gray, and the active site Cys492 is shown in yellow.

Part I. In the absence of the LRR domain, the SspH1 E3 domain is more dynamic, consistent with NMR data on the isolated E3 domain described in **Part I**. Thus, the high level of protection observed for residues 449-460 and 551-570 in the presence of the LRR domain are consistent with a more open conformation between the LRR and E3 domains in solution and suggests that the LRR domain may stabilize the proximal conformation of the E3 domain.

Changes in SspH1 structure in the SspH1~Ub intermediate

Fig 32 shows protection factors calculated for pairwise comparisons of SspH1 E3 vs E3-Ub (**Fig 32A**), SspH1 LRR-E3 vs LRR-E3-Ub (**Fig 32B**) and SspH1 LRR-E3:PKN1 HRb vs SspH1 LRR-E3-Ub:PKN1 HRb (**Fig 32C**). The difference between each of these comparisons is the presence of Ub at the active site of SspH1, and the overlay of each of the comparisons is shown in **Fig 32D**. For SspH1 E3 vs E3-Ub, Ub at the active site appears to generally stabilize the overall E3 domain, except for the first two helices, comprising residues 394-440 of the NSD, which have much lower protection factors (**Fig 32E**, blue surface). The overall stabilization of SspH1-Ub complex suggests that the free E3 is dynamic and Ub tethered to the active site may stabilize one conformation of the E3 domain. The highest protection factors occur in the first thumb helix, comprising residues 628-641 (**Fig 32E**, red surface). These residues were also shown to be most protected in the presence of Ub in the first round of HDX experiments (**Figs 28,29**). High protection factors were also calculated for residues 540-550 and 577-590 in the CSD, which are near the active site Cys492 in the homology model of SspH1 E3 (**Fig 32E**, orange surface). Protection in the thumb region could be due to 1) direct interactions between Ub tethered to the active site and the thumb helices, or 2) new interactions between the thumb regions and the NSD or CSD, or some combination of both. The changes in segments 540-550 and 577-590 are

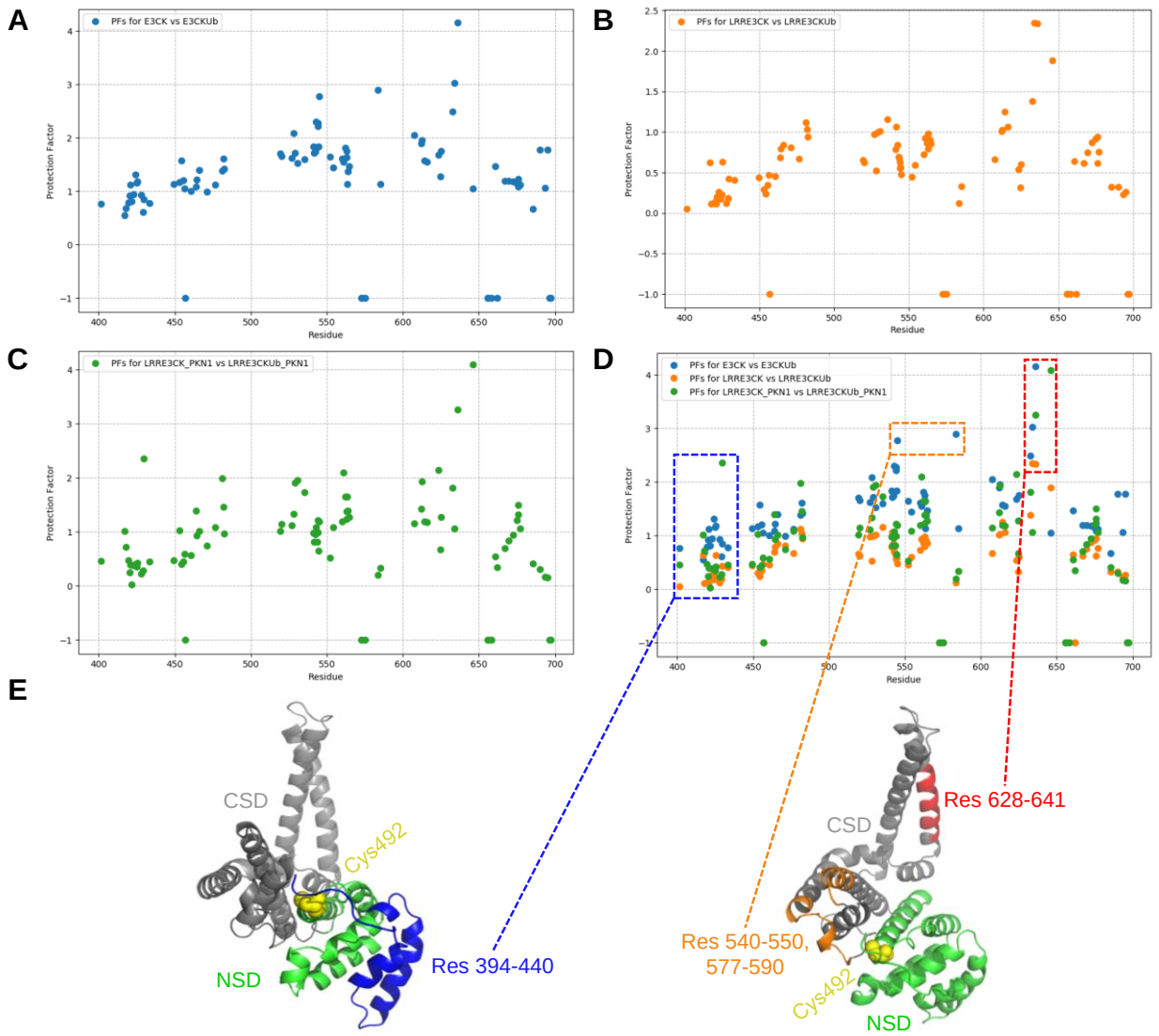

Figure 32. Impact of Ub at the active site. Protection factors were calculated for **(A)** SspH1 E3 vs SspH1 E3-Ub, **(B)** SspH1 LRR-E3 vs SspH1 LRR-E3~Ub, and **(C)** SspH1 LRR-E3:PKN1 HRb vs SspH1 LRR-E3-Ub:PKN1 HRb. **(D)** Overlay of all comparisons between SspH1 with a wildtype vs ubiquitin-conjugated active site. **(E)** Homology model of SspH1 E3 based on structure of SspH1 (PDB 3G06). The peptides corresponding to residues 394-440 (blue), 540-550, 577-590, (orange) and 628-641 (red), which have low (blue) or high (red/orange) protection factors in the presence of the Ub at the active site. The N-terminal subdomain (NSD) of the SspH1 E3 domain is shown in green, the C-terminal subdomain (CSD) of the SspH1 E3 domain is shown in gray, and the active site Cys492 is shown in yellow.

consistent with a conformational change, but it is not clear from these results whether Ub at the SspH1 active site favors the proximal or distal conformation of the E3 domain.

Comparison of SspH1 LRR-E3 and LRR-E3-Ub protection factors show that Ub stabilizes the thumb helices as previously described for SspH1 E3 and E3-Ub. Unexpectedly, the presence of Ub appears to reduce protection factors for the E3 domain as most protection factors calculated were between 0 and 1. SAXS and HDX-MS data are consistent with the SspH1 LRR-E3 preferring an open conformation similar to the IpaH4 structure. Transfer of Ub to the SspH1 active site could allow more conformational freedom between the LRR domain and the NSD and CSD E3 subdomains.

Effects of PKN1 on SspH1 HDX

Binding of PKN1 to SspH1 LRR-E3 results in overall deprotection of residues 400-450 in the NSD of the E3 domain and mild protection in certain segments of the CSD (**Fig 33**). When Ub is present at the SspH1 active site, similar overall trends are observed with modest increases to no change in protection observed throughout the E3 domain. However, one peptide comprising residues 410-425 shows very high protection in both comparisons (**Fig 33C**, red box). Since the comparisons are between two sets of separately-prepared protein samples, it is unlikely this result is a handling or systematic error. Highlighted on a homology model of SspH1 LRR-E3 bound to PKN1 HRb, this peptide resides in the N-terminal subdomain of the E3 domain near PKN1 HRb bound to the SspH1 LRR domain (**Fig 33D**). Therefore, the presence of bound PKN1 does effect structural changes in the SspH1 E3 domain, either by directly contacting the NSD, or through allosteric interactions that may involve the LRR domain or the region that links the LRR and E3 domains. For SspH1, though the E3 domain alone can build unanchored poly-Ub chains, the LRR-

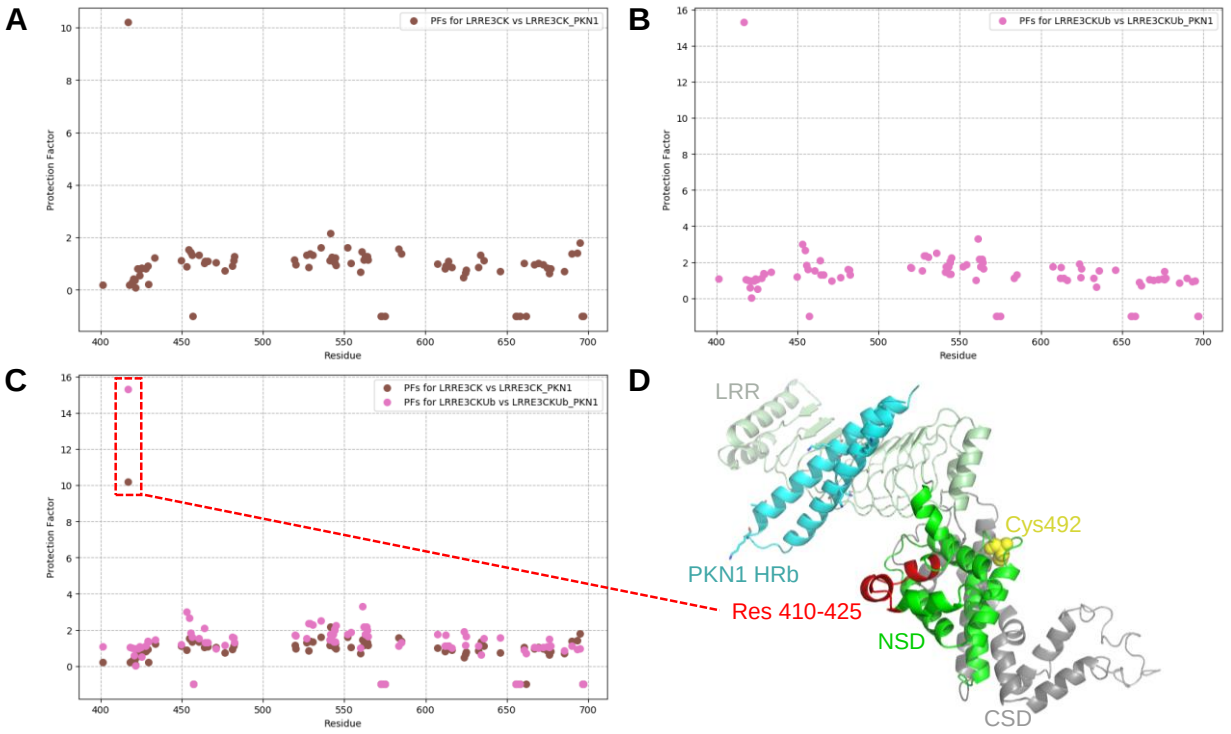

Figure 33. Impact of substrate binding. Protection factors were calculated for **(A)** SspH1 LRR-E3 vs SspH1 LRR-E3:PKN1 Hrb, and **(B)** SspH1 LRR-E3-Ub vs SspH1 LRR-E3-Ub:PKN1 Hrb. **(C)** Overlay of both comparisons between SspH1 LRR-E3 constructs in the absence and presence of bound PKN1 Hrb. **(D)** Homology model of SspH1 LRR-E3 bound to PKN1 HRb based of structures of IpaH3 LRR-E3 (PDB 3CVR) and SspH1 LRR:PKN1 HRb (PDB 4NKG). The peptide corresponding to residues 410-425, which has very high protection factors in the presence of PKN1, is shown in red. LRR is shown in light green, PKN1 HRb is shown in cyan, the N-terminal subdomain (NSD) of the SspH1 E3 domain is shown in green, the C-terminal subdomain (CSD) of the SspH1 E3 domain is shown in gray, and the active site Cys492 is shown in yellow.

E3 construct can only synthesize ubiquitin chains in the presence of PKN1, even though the E3 domain alone possess intrinsic ubiquitylation activity (**Fig 2**). This is not a result of occlusion of the active site or E2~Ub binding site, as E2~Ub can transfer Ub to the active site Cys of SspH1 in the absence of bound PKN1 (**Fig 3**). NMR results show that in this complex, PKN1 does not contact the Ub subunit at the active site. Instead, the HDX results here suggest that PKN1 modulates the conformation of SspH1 by stabilizing the first two helices in the NSD, which occur immediately after the LRR-E3 linker.

Summary

The work presented here uncovers important and novel features of the Ub transfer mechanism for the IpaH-SspH class of bacterial effector ubiquitin ligases. Though they are not structurally similar to eukaryotic E3s, IpaH-SspH E3s hijack the ubiquitylation machinery of a eukaryotic host cell to mark host proteins for degradation at the proteasome. The result is a reduced ability of the host to respond to bacterial invasion through cellular innate immunity pathways. To catalyze Ub transfer, IpaH-SspH E3s engage with host E2~Ubs as the source of activated Ub and target host substrate proteins for Ub modification. IpaH-SspH E3s contain two domains for ubiquitylating substrates: an LRR domain that binds substrate, and an E3 domain that catalyzes Ub transfer. The E3 domain contains an active site Cys that forms an obligate thioester intermediate with the C-terminus of Ub (E3~Ub). This makes the mechanism of IpaH-SspH E3s conceptually similar to eukaryotic HECT and RBR E3s, which also form an obligate E3~Ub via an active site Cys. E3s that utilize this type of mechanism must perform two Ub transfers, from E2~Ub to the E3 active site, and from E3~Ub to substrate. The prevailing view in the Ub field has been that the last enzyme in the pathway holding Ub at an active site governs Ub transfer. In this work, I show that this view is overly simplified for IpaH-SspH E3s given that E2~Ub is required to successfully perform both Ub transfer steps. This discovery was made by biochemically and structurally characterizing the complexes and conformational changes required to perform Ub transfer, using SspH1 as a model for the IpaH-SspH family. The properties of these bacterial E3s allow for detailed investigation into mechanisms of Ub transfer and serve as a foundation for understanding mechanisms important to both bacterial and eukaryotic Ub transfer and signaling. It is possible that some eukaryotic E3s that employ a HECT-like mechanism may use a similar

mechanism, and the strategy presented here of treating HECT-like mechanisms as two separate stages of Ub transfer could also be applied to eukaryotic E3s.

Part I describes the first step of Ub transfer, from E2~Ub to the SspH1 active site Cys. The E3 domain is composed of two subdomains, the NSD and CSD. The NSD harbors the active site Cys that forms an obligate thioester intermediate with Ub while the CSD contains the binding site for E2~Ub. The NSD and CSD are connected by a flexible linker, and movements of the NSD and CSD relative to each other are required for catalysis. Mutations that limit the flexibility of the linker or block movement at the NSD-CSD interface disrupt ubiquitylation activity. This is analogous to eukaryotic HECT and RBR E3s, which are also composed of different domains separating the E2~Ub conjugate binding site and the E3 active site, with movement of domains critical for Ub transfer.

The E2~Ub conjugate binding site in the CSD is composed of two dynamic thumb helices. E2~Ub clamps around the thumb helices, placing the E2 and Ub subunits in a conformation in which the thioester bond is oriented to react with the E3 active site Cys. The dynamic nature of the E2~Ub conjugate binding site is important for catalysis. Conservative mutations in the disordered region of the E2~Ub conjugate binding site, or that increase the helical propensity of the thumb helices, disrupt E2~Ub binding and ubiquitylation activity.

Part II demonstrates that the E2 also plays a role in the second step of Ub transfer. This is a novel finding and demonstrates that the previous assumption that E3s with a HECT-like mechanism are solely responsible for the second step of Ub transfer is incorrect. Two highly homologous E2s, Ube2D3 and Ube2E3, both bind SspH1 through an identical surface and transfer Ub to the E3 active site Cys. However, substrate is only ubiquitylated when Ube2D3 is used as the source of activated E2, whereas the closely related E2 Ube2E3 is only active in Stage I of the Ub

transfer mechanism. Extensive amino acid mutations in Ube2D3 to the respective amino acid in Ube2E3 failed to uncover residues that selectively inhibit Stage II transfer with Ube2D3. No simple explanation for the lack of Ube2E3 ubiquitylation activity has been uncovered, though, as described below, utilization of various biophysical approaches has begun to reveal differences between Ube2E3 and Ube2D3 in promoting conformational changes that may be used to develop further tests of the Ub-transfer mechanism.

Both Ube2D3~Ub and Ube2E3~Ub are oriented in a lysine-reactive confirmation while bound to the thumb helices, and replacement of the SspH1 active site Cys with Lys allows for modification with a single Ub at the active site position by either Ube2D3 or Ube2E3. This finding was unexpected, as only transthiolation is needed to transfer Ub to the SspH1 active site Cys. Ub modification at a SspH1 active site Lys is selective, and none of the other 16 Lys residues in SspH1 (6 in the thumb helices) are modified with Ub in ubiquitylation assays. The native thioester bond in SspH1~Ub is highly reactive, and stable SspH1-NH-Ub represents the first E3~Ub for the IpaH-SspH class of E3s that is amenable for structural studies. Eukaryotic HECT and RBR E3s do not bind E2~Ub in a Lys-reactive conformation, so it is unlikely that this same approach will work for generating stable HECT or RBR E3~Ub.

Part III uncovers a conformational change in SspH1 that is critical for the second step of Ub transfer. Ube2D3~Ub, but not Ube2E3~Ub, is able to induce this conformational change. The conformational change results in the Ub subunit of SspH1~Ub moving from the SspH1 active site in the E3 domain towards substrate bound to the LRR domain, where it is poised to form an isopeptide bond with a substrate Lys residue. The structural reason for the inability of Ube2E3~Ub to induce the conformational change is unclear. HDX-MS experiments comparing SspH1 to SspH1~Ub reveal that the E2~Ub conjugate binding site is stabilized when Ub is present at the E3

active site. Ube2D3~Ub and Ube2E3~Ub can both bind SspH1~Ub using similar surfaces of the E2~Ub conjugate, but since the E2~Ub conjugate binding site is structurally different in SspH1~Ub, the mode of E2~Ub binding may also be different. It is possible that a subtle difference in the structure of Ube2E3, or the orientation between the Ube2E3 and Ub subunits in Ube2E3~Ub, alters the binding mode in the reorganized E2~Ub binding site in SspH1~Ub that prevents it from inducing a conformational change.

In **Part II**, it was shown that substrate binding alters the interactions between the LRR and E3 domain. For SspH1 LRR-E3, substrate is required for Stage II. Presented only with E2~Ub, SspH1 LRR-E3 will hydrolyze the E2~Ub conjugate, but unlike the E3 domain alone, does not build unanchored poly-Ub chains. In the presence of a construct of substrate lacking Lys residues, SspH1 LRR-E3 builds unanchored poly-Ub chains similarly to the E3 domain alone. These results demonstrate that both the LRR domain and substrate binding modulate the activity of the E3 domain. The HDX-MS data in **Part III** reveals that the LRR allosterically stabilizes much of the structure of the E3 domain. Addition of PKN1, on the other hand, only stabilizes one small fragment of the NSD, close to the LRR interface. This fragment may be the critical region of the E3 domain that responds to substrate activation and determines if Ub is hydrolyzed from the active site or is transferred to a Lys residue. SAXS analysis suggests that addition of substrate does not induce large conformational changes between the LRR and E3 domains, so the mechanism of substrate activation likely occurs through the structural rearrangements in the NSD revealed by HDX-MS.

Key questions remain concerning the mechanism of SspH1. What are the structural differences between Ube2D3~Ub and Ube2E3~Ub that determine if a conformational change in SspH1 will occur? The difference is not trivial to uncover, but considering the high homology

between the E2s, the problem is likely tractable. What, precisely, are the rearrangements that SspH1 undergoes during the second stage of Ub transfer? Motion between the NSD and CSD is required for ubiquitylation transfer, and it was shown in **Part I** that limiting the flexibility between the NSD and CSD does not abolish the first stage of Ub transfer. Flexibility must also be important during the second stage, and movement of the NSD towards substrate is most likely responsible for transferring Ub towards substrate. Ultimately, high-resolution structures will be required to understand the atomic details of all the structural rearrangements that SspH1 undergoes during its catalytic cycle. Though crystal structures exist of IpaH-SspH proteins alone and in complex with substrate, atomic details are still not available concerning interactions with E2~Ub. Despite our attempts to crystallize numerous constructs of SspH1 or SspH1~Ub in complex with E2 or E2~Ub, crystals viable for high resolution structures were not obtained. The affinity between IpaH-SspH proteins and E2~Ub is low. One approach that may yield more successful results would be to physically tether the E2 to SspH1 via a flexible linker at the C-terminus, placing the E2 in close proximity to its binding site on SspH1. The E2~Ub conjugate binding site comprises the last two structured helices of SspH1, so this construct would place E2 very close to its binding site. Since the affinity between E2 and SspH1 is much lower than that of E2~Ub, it is likely that E1 could modify an E2 active site Ser of Lys to form stable E2~Ub in cis with SspH1. High resolution structures of E2~Ub bound to SspH1 and SspH1~Ub would reveal the precise details of the conformational changes SspH1 undergoes and may reveal the differences between Ube2D3 and Ube2E3 that result in striking differences in ubiquitylation activity.

References

1. Miao, E. A., Brittnacher, M., Haraga, A., Jeng, R. L., Welch, M. D., and Miller, S. I. (2003) Salmonella effectors translocated across the vacuolar membrane interact with the actin cytoskeleton. *Mol Microbiol*. **48**, 401–415
2. Perrett, C.A., Lin, D.Y., Zhou, D. (2011) Interactions of bacterial proteins with host eukaryotic ubiquitin pathways. *Front. Microbiol*. **2**:143
3. Ashida, H., Kim, M., Sasakawa, C. (2014) Exploitation of the host ubiquitin system by human bacterial pathogens. *Nat. Rev. Microbiol.* **12(6)**:399-413
4. Kim, M., Otsubo, R., Morikawa, H., Nishide, A., Takagi, K., Saskawa, C., Mizushima, T. (2014) Bacterial effectors and their functions in the ubiquitin-proteasome system: insights from the modes of substrate recognition. *Cells*. **3(3)**: 848-64
5. Wenzel, D.M., Stoll, K.E., Klevit, R.E. (2011) E2s: structurally economical and functionally replete. *Biochem J* **433(1):** 31-42.
6. Rape, M. (2009) Ubiquitin, infinitely seductive: symposium on the many faces of ubiquitin. *EMBO Rep*. **10(6)**:558-62
7. Komander, D., and Rape, M. (2012) The Ubiquitin Code. *Annu. Rev. Biochem.* **81**, 203–229
8. Hutchins, A.P., Liu, S., Diez, D., Miranda-Saavedra, D. (2013) The repertoires of ubiquitinating and deubiquitinating enzymes in eukaryotic genomes. *Mol. Biol. Evol.* **30(5)**: 1172-1187
9. Sacco, F., Perfetto, L., Castagnoli, L., Cesareni, G. (2012) The human phosphatase interactome: An intricate family portrait. *FEBS Lett.* **586(17)**: 2732-2739
10. Grabbe, C., Husnjak, K., Dikic, I. (2011) The spatial and temporal organization of ubiquitin networks. *Nat Rev Mol Cell Biol.* **12(5)**: 295-307
11. Brzovic, P.S., Klevit, R.E. (2006) Ubiquitin transfer from the E2 perspective: why is UbcH5 so promiscuous? *Cell Cycle.* **5(24)**:2867-73
12. Nguyen, L., Plafker, K.S., Starnes, A., Cook, M., Klevit, R.E., Plafker, S.M. (2014) The ubiquitin-conjugating enzyme, UbcM2, is restricted to monoubiquitylation by a two-fold mechanism that involves backside residues of E2 and Lys48 of ubiquitin. *Biochemistry*. **53(24)**: 4004-14
13. Brzovic, P. S., Keeffe, J. R., Nishikawa, H., Miyamoto, K., Fox, D., Fukuda, M., Ohta, T., and Klevit, R. (2003) Binding and recognition in the assembly of an active BRCA1/BARD1 ubiquitin-ligase complex. *PNAS*. **100**, 5646–5651
14. Dou, H., Buetow, L., Sibbet, G.J., Cameron, K., Huang, D.T. (2012) BIRC7-E2 ubiquitin conjugate structure reveals the mechanism of ubiquitin transfer by a RING dimer. *Nat Struct Mol Biol*. **19(9)**: 876-83
15. Scheffner, M., Nuber, U., and Huibregtse, J. M. (1995) Protein ubiquitination involving an E1–E2–E3 enzyme ubiquitin thioester cascade. *Nature*. **373**, 81–83
16. Huang, L., Kinnucan, E., Wang, G., Beaudenon, S., Howley, P.M., Huibregtse, J.M., Pavletich, N.P. (1999) Structure of an E6AP-UbcH7 complex: insights into ubiquitination by the E2-E3 enzyme cascade. *Science*. **286**, 1321-1326
17. Kamadurai, H.B., Souphron, J., Scott, D.C., Duda, D.M., Miller, D.J., Stringer, D., Piper, R.C., Schulman, B.A. (2009) Insights into ubiquitin transfer cascades from a structure of a UbcH5B~ ubiquitin-HECT(NEDD4L) complex. *Mol Cell*. **36(6)**: 1095-102

18. Trempe J.F., Sauve, V., Grenier, K., Seirafi, M., Tang, M.Y., Menade, M., Al-Abdul-Wahid, S., Krett, J., Wong, K., Kozlov, G., Nager, B., Fon, E.A., Gehring, K. (2013) Structure of parkin reveals mechanisms for ubiquitin ligase activation. *Science*. **340(6139)**: 1451-5
19. Dove, KK., Klevit, R.E. (2013) Structural biology: Parkin's serpentine shape revealed in the year of the snake. *Curr Biol.* **23(16)**: 692-3
20. Pruneda, J.N., Stoll, K.E., Bolton, L.J., Brzovic, P.S., Klevit, R.E. (2011) Ubiquitin in motion: structural studies of the ubiquitin-conjugating enzyme~ubiquitin conjugate. *Biochemistry*. **50(10)**, 1624-1633
21. Saha, A., Lewis, S., Kleiger, G., Kuhlman, B., Deshaies, R.J. (2011) Essential role for ubiquitin-ubiquitin-conjugating enzyme interaction in ubiquitin discharge from Cdc34 to substrate. *Mol. Cell* **42**: 75-83
22. Dove, K.K., Stieglitz, B., Duncan, E.D., Rittinger, K., Klevit, R.E. (2016) Molecular insights into RBR E3 ligase ubiquitin transfer mechanisms. *EMBO Rep.* **17(8)**: 1221-1235
23. Dove, K.K., Olszewski, J.L., Martino, L., Duda, D.M., Wu, X.S., Miller, D.J., Reiter, K.H., Rittinger, K., Schulman, B.A., Klevit, R.E. (2017) Structural studies of HHARI/UbcH7~Ub reveal unique E2~Ub conformational restriction by RBR RING 1. *Structure*. **6(6)**: 890-900
24. Lin, D. Y.-W., Diao, J., and Chen, J. (2012) Crystal structures of two bacterial HECT-like E3 ligases in complex with a human E2 reveal atomic details of pathogen-host interactions. *PNAS*. **109**, 1925–1930
25. Huibregtse J, Rohde JR (2014) Hell's BELs: Bacterial E3 Ligases That Exploit the Eukaryotic Ubiquitin Machinery. *PLoS Pathog* 10(8): e1004255. doi:10.1371/journal.ppat.1004255
26. Ashida, H., Sasakawa, C. (2017) Bacterial E3 ligase effectors exploit host ubiquitin systems. *Curr. Opin. Microbiol.* **35**:16-22
27. Lin D.Y., Diao, J., Zhou, D., Chen, J. (2011) Biochemical and structural studies of a HECT-like ubiquitin ligase from Escherichia coli O157:H7. *J Biol Chem*. **286(1)**:441-9
28. Diao, K., Zhang, Y., Huibregtse, J.M., Zhou, D., Chen, J. (2007) Crystal structure of SopA, a Salmonella effector protein mimicking a eukaryotic ubiquitin ligase. *Nat Struct Mol Biol.* **15(1)**: 65-70
29. Wu, B., Skarina, T., Yee, A., Jobin, M.C., Dileo, R., Semesi, A., Fares, C., Lemak, A., Coombes, B.K., Arrowsmith, C.H., Singer, A.U., Savchenko, A. (2010) NleG type 3 effectors from enterohaemorrhagiv Escherichia coli are U-box E3 ubiquitin ligases. *PLoS Pathog.* **6(6)**: e1000960
30. Kubori, T., Hyakutake, A., Nagai, H. (2008) Legionella translocates an E3 ubiquitin ligase that has multiple U-boxes with distinct functions. *Mol Microbiol.* **67(6)**: 1307-19
31. Rosebrock, T.R., Zeng, L., Brady, J.J., Abramovitch, R.B., Xiao, F., Martin, G.B. (2007) A bacterial E3 ubiquitin ligase targets a host protein kinase to disrupt plant immunity. *Nature*. **448(7151)**:370-4
32. Sanada, T., Kim, M., Mimuro, H., Suzuki, M., Ogawa, M., Oyama, A., Ashida, H., Kobayashi, T., Koyama, T., Nagai, S., Shibata, Y., Gohda, J., Inoue, J., Mizushima, T., Sasakawa, C. (2012) The Shigella flexneri effector OspI deamidates UBC13 to dampen the inflammatory response. *Nature*. **483(7391)**: 623-6
33. Cui, J., Yao, Q., Li, S., Ding, X., Lu, Q., Mao, H., Liu, L., Zheng, N., Chen, S., Shao, F. (2010) Glutamine deamidation and dysfunction of ubiquitin/NEDD8 induced by a bacterial effector family. *Science*. **329(5996)**: 1215-8
34. Rohde, J.R., Breitkreutz, A., Chenal, A., Sansonetti, P.J., Parsot, C. (2007) *Cell Host Microbe*. **1(1)**: 77-83

35. Zhu, Y., Li, H., Hu, L., Wang, J., Zhou, Y., Pang, Z., Liu, L., Shao, F. (2008) Structure of a Shigella effector reveals a new class of ubiquitin ligase. *Nat Struct Mol Biol*. **15(12)**: 1302-8
36. Singer, A.U., Rohde, J.R., Lam, R., Skarina, T., Kagan, O., Dileo, R., Chirgadze, N.Y., Cuff, M.E., Joachimiak, A., Tyers, M., Sansonetti, P.J., Parsot, C., Savchenko, A. (2008) Structure of the Shigella T3SS effector IpaH defines a new class of E3 ubiquitin ligases. *Nat Struct Mol Biol*. **15(12)**: 1293-301
37. Quezada, C.M., Hicks, S.W., Galan, J.E., Stebbins, C.E. (2009) A family of a Salmonella virulence factors functions as a distinct class of autoregulated E3 ubiquitin ligases. *PNAS*. **106(12)**: 4864-9
38. Miao, E. A., Scherer, C. A., Tsolis, R. M., Kingsley, R. A., Adams, L. G., Baumler, A. J., and Miller, S. I. (1999) Salmonella typhimurium leucine-rich repeat proteins are targeted to the SPI1 and SPI2 type III secretion systems. *Mol Microbiol*. **34**, 850–864
39. Miao, E.A., Miller, S.I. (2000) A conserved amino acid sequence directing intracellular type III secretion by Salmonella typhimurium. *PNAS*. **97(13)**: 7539-44
40. Seyedarabi, A., Sullivan, J.A., Sasakawa, C., Pickersgill, R.W. (2010) A disulfide driven domain swap switches off the activity of Shigella IpaH9.8 E3 ligase. *FEBS Lett.* **584(19)**: 4163-8
41. Takagi, K., Kim, M., Sasakawa, C., Mizushima, T. (2016) Crystal structure of the substrate-recognition domain of the *Shigella* E3 ligase IpaH9.8. *Acta. Crystallogr. F Struct. Biol. Commun.* **72(4)**:269-275
42. Keszei, A.F., Tang, X., McCormick, C., Zeqiraj, E., Rohde, J.R., Tyers, M., Sicheri, F. (2014) Structure of an SspH1-PKN1 complex reveals the basis for host substrate recognition and mechanism of activation for a bacterial E3 ubiquitin ligase. *Mol Cell Biol*. **34(3)**: 362-73
43. Zouhir, S., Bernal-Bayard, J., Cordero-Alba, M., Cardenal-Munoz, Z., Guimaraes, B., Lazar, N., Ramos-Morales, F., Nessler, S. (2014) The structure of the Slrp-Trx1 complex sheds light on the autoinhibition mechanism of the type III secretion system effectors of the NEL family. *Biochem J*. **464(1)**: 135-44
44. Chou, Y.C., Keszei, A. F. A., Rohde, J. R., Tyers, M., and Sicheri, F. (2012) Conserved Structural Mechanisms for Autoinhibition in IpaH Ubiquitin Ligases. *J. Biol. Chem.* **287**, 268–275
45. Haraga, A., Miller, S.I. (2006) A Salmonella type III secretion effector interacts with the mammalian serine/threonine protein kinase PKN1. *Cell Microbiol*. **8(5)**: 837-46
46. Fiskin, E., Bionda, T., Dikic, I., Behrends, C. (2016) Global analysis of host and bacterial ubiquitinome in response to *Salmonella* Typhimurium infection. *Mol. Cell*. **62(6)**: 967-981
47. Maculins, T., Fiskin, E., Bhogaraju, S., Dikic, I. (2016) Bacteria-host relationship: ubiquitin ligases as weapons of invasion. *Cell Res.* **26(4)**:499-510
48. Levin, I., Eakin, C., Blanc, M.P., Klevit, R.E., Miller, S.I., Brzovic, P.S. (2010) Identification of an unconventional E3 binding surface on the UbcH5~Ub conjugate recognized by a pathogenic bacterial E3 ligase. *PNAS*. **107(7)**: 2848-53
49. Edwards, D.J., Streich, F.C. Jr., Ronchi, V.P., Todaro, D.R., Haas, A.L. (2014) Convergent evolution in the assembly of poly-Ubiquitin degradation signals by the Shigella flexneri IpaH9.8 ligase. *J Biol Chem*. Epub Oct. 23, 2014
50. Haraga, A., and Miller, S. I. (2003) A Salmonella enterica Serovar Typhimurium Translocated Leucine-Rich Repeat Effector Protein Inhibits NF- B-Dependent Gene Expression. *Infection and Immunity*. **71**, 4052–4058

51. Keszei, A.F., Sicheri, F. (2017) Mechanism of catalysis, E2 recognition, and autoinhibition for the IpaH family of bacterial E3 ubiquitin ligases. *PNAS*. **114(6)**, 1311-1316
52. Taniguchi, T., Kawamata, T., Mukai, H., Hasegawa, H., Isagawa, T., Yasuda, M., Hashimoto, T., Terashima, A., Nakai, M., Mori, H., Ono, Y., Tanaka, C. (2001) Phosphorylation of tau is regulated by PKN. *J. Biol. Chem.* **276(13)**: 10025-31
53. Lachmann, S., Jevons, A., De Rycker, M., Casamassima, A., Radtke, S., Collazos, A., Parker, P.J. (2011) Regulatory domain selectivity in the cell-type specific PKN-dependence of cell migration. *PLoS One.* **6(7)**:e21732
54. Metzger, E., Muller, J.M., Ferrari, S., Buettner, R., Schule, R. (2003) A novel inducible transactivation domain in the androgen receptor: implications for PRK in prostate cancer. *EMBO J.* **22(2)**:270-280
55. Metzger, E., Yin, N., Wissmann, M., Kunowska, N., Fischer, K., Friedrichs, N., Patnaik, D., Higgins, J.M., Potier, N., Scheidtmann, K.H., Buettner, R., Schule, R. (2008) Prosphorylation of histone H3 at threonine 11 establishes a novel chromatin mark for transcriptional regulation. *Nat. Cell Biol.* **10(1)**:53-60
56. Watanabe, G., Saito, Y., Madaule, P., Ishizaki, T., Fujisawa, K., Morii, N., Mukai, H., Ono, Y., Kakizuka, A., Narumiya, S. (1996) Protein kinase N (PKN) and PKN-related protein rhophilin as targets of small GTPase Rho. *Science*. **271(5249)**:645-648
57. Modha, R., Campbell, L.J., Nietlispach, D., Buhecha, H.R., Owen, D., Mott, H.R. (2008) the Rac1 polybasic region is required for interaction with its effector PRK1. *J. Biol. Chem.* **283(3)**:1492-1500
58. Rabi, I.I., Zacharias, J.R., Millman, S., Kusch, P. (1938) A new method of measuring nuclear magnetic moment. *Phys. Rev*. 53:318
59. Purcell, E.M., Torrey, H.C., Pound, R.V. (1946) Resonance absorption by nuclear magnetic moments in a solid. *Phys. Rev*. 69:37-38
60. Bloch, F., Hansen, W.W., Packard, M. (1946) Nuclear induction. *Phys. Rev.* 69:127
61. Bloch, F. (1946) Nuclear induction. *Phys. Rev.* 70:460-474
62. Bloch, F., Hansen, W.W., Packard, M. (1946) The nuclear induction experiment. *Phys. Rev.* 70:474-485
63. Saunders, M., Wishnia, A., Kirkwood, J.G. (1957) The nuclear magnetic resonance spectrum of ribonuclease. *J. Am. Chem. Soc*. 79:3289-3290
64. Ernst, R.R. (1992) Nuclear magnetic resonance Fourier transform spectroscopy (Nobel lecture). *Angew. Chem., Int. Eng. Ed.* 31:805-930
65. Wuthrich, K. (2003) NMR studies of structure and function of biological macromolecules (Nobel lecture). *Angew. Chem., Int. Eng. Ed.* 42:3340-3363
66. Ernst, R.R., Anderson, W.A. (1966) Application of Fourier transform spectroscopy to magnetic resonance. *Rev. Sci. Instrum.* 37:93-102
67. Overhauser, A.W. (1953) Polarization of nuclei in metals. *Phys. Rev*. 92:411-415
68. Jeener, J. (1971) Ampere International Summer School, Basko Polje, Yugoslavia
69. Aue, W.P., Bartholdi, E., Ernst, R.R. (1976) Two-dimensional spectroscopy. Application to nuclear magnetic resonance. *J. Chem. Phys.* 64:2229-2246
70. Cavanagh, J., Fairbrother W.J., Palmer, A.G., Rance, M., Skelton, N.J. (2007) Protein NMR Spectroscopy Principles and Practice Second Edition. *Academic Press*
71. Hoch, J.C., Stern, A.S. (1996) NMR Data Processing. *Wiley-Liss*

72. Ikura, M., Kay, L.E., Bax, A. (1990) A novel approach for sequential assignment of proton, carbon-13, and nitogen-15 spectra of larger proteins: heteronuclear triple-resonance three-dimensional NMR spectroscopy. Application to calmodulin. *Biochemistry* 29(19):4659-4667
73. Katta, V., Chait, B.T. (1991) Conformational changes in proteins probed by hydrogen-exchange electrospray-ionization mass spectrometry. *Rapid Commun. Mass Spectrom*. **5**:214-217
74. Guttman, M., Lee, K.K. (2016) Isotope labeling of biomolecules: structural analysis of viruses by HDX-MS. *Methods Enzymol*. **566**, 405-426
75. Chalkley, R.J., Baker, P.R., Huang, L., Hansen, K.C., Allen, N.P., Rexach, M., Burlingame, A.L. (2005) Comprehensive analysis of a multidimensional liquid chromatography mass spectrometry dataset acquired on a quadrupole selecting, quadrupole collision cell, time-of-flight mass spectrometer: II. New Developments in Protein Prospector allow for reliable and comprehensive automatic analysis of large datasets. *Mol. Cell. Proteomics.* **4(8)**:1194-1204
76. Li, G.Z., Vissers, J.P., Silva, J.C., Golick, D., Gorenstein, M.V., Geromanos, S.J. (2009) Database searching and accounting of multiplexed precursor and product ion spectra from the data independent analysis of simple and complex peptide mixtures. *Proteomics*. **9(6)**:1696-1719
77. Weis, D.D., Kass, I.J. & Engen, J.R. (2006). Semi-automated analysis of hydrogen exchange mass spectra using HX-Express. *J. Amer. Soc. Mass Spectrom.* **17(12)**, 1700-1703.
78. Guttman M., Weis, D.D., Engen, J.R. & Lee, K. K. (2013). Analysis of overlapped and noisy Hydrogen/Deuterium exchange data. *J. Amer. Soc. Mass Spectrom.* **24(12)**, 1906-1912.
79. Walters, B.T. (2017) Empirical method to accurately determine peptide-averaged protection factors from hydrogen exchange MS data. *Anal. Chem.* **89(2)**, 1049-1053
80. Jacques, D.A., Trewhella, J. (2010) Small-angle scattering for structural biology – Expanding the frontier while avoiding the pitfalls. *Prot. Sci.* **19**:642-657
81. Svergun, D., Koch, M.H.J., Timmins, P.A., May, R.P. (2013) Small angle X-ray and neutron scattering from solutions of biological macromolecules. *Oxford University Press*
82. Franke, D., Petoukhov, M.V., Konarev, P.V., Panjkovich, A., Tuukkanen, A., Mertens, H.D.T., Kikhney, A.G., Hajizadeh, N.R., Franklin, J.M., Jeffries, C.M. and Svergun, D.I. (2017) ATSAS 2.8: a comprehensive data analysis suite for small-angle scattering from macromolecular solutions. *J. Appl. Cryst.* **50**:1212-1225
83. Tuukkanen, A.T., Kleywegt, G.J., Svergun, D.I. (2016) Resolution of *ab initio* shapes determined from small-angle scattering. *IUCrJ*. **3(6)**:440-447
84. Plechanovova, A., Jaffray, E.G., Tatham, M.H., Naismithm J.H., Hay, R.T. (2012) Structure of a RING E3 ligase and ubiquitin-loaded E2 primed for catalysis. *Nature*. **489(7414)**:115-120
85. Bentley, M.L., Corn, J.E., Dong, K.C., Phung, Q., Cheung, T.K., Cochran, A.G. (2011) Recognition of UbcH5c and the nucleosome by the Bmi1/Ring1b ubiquitin ligase complex. *EMBO J.* **30(16)**:3285-3297
86. McGinty, R.K., Henrici, R.C., Tan, S. (2014) Crystal structure of the PRC1 ubiquitylation module bound to the nucleosome. *Nature*. **514(7524)**:591-596
87. Sauve, V., Sung, G., Soya, N., Kozlov, G., Blaimschein, N., Miotto, L.S., Trempe, J.F., Lukacs, G.L., Gehring, K. (2018) Mechanism of parkin activation by phosphorylation. *Nat. Struct. Mol. Biol.* doi:10.1038/s41594-018-0088-7
88. Nuber, U., Scheffner, M. (1999) Identification of determinants in E2 ubiquitin-conjugating enzymes required for hect E3 ubiquitin-protein ligase interaction. *J. Biol. Chem.* **274(11)**:7576-7582

89. Wu, P.Y., Hanlon, M., Eddins, M., Tsui, C., Rogers, R.S., Jensen, J.P., Matunis, M.J., Weissman, A.M., Wolberger, C., Pickart, C.M. (2003) A conserved catalytic residue in the ubiquitin-conjugating enzyme family. *EMBO J.* **22(19)**: 5241-5250
90. Ohlson, M.B., Huang, Z., Alto, N.M., Blanc, M.P., Dixon, J.E., Chai, J., Miller, S.I. (2008) Structure and function of Salmonella SifA indicate that its interactions with SKIP, SseJ, and RhoA family GTPases induce endosomal tubulation. *Cell Host Microbe*. **4(5)**: 434-446

Appendix I: Python source code for calculating protection factors for various SspH1 constructs

```
##############################################################################
####################
from os import sys
import math
import numpy as np
import pandas as pd
from scipy import stats
from scipy import interpolate

### Global Variables
time = np.array([3.0,60.0,1800.0,72000.0])      # Array of sampled timepoints
in seconds
###

### Get the real residue numbers of a given peptide within the SspH1 sequence
###  Since peptide coverage is based on the E3CK construct MSMS data, that is
the sequence used here
def E3CK_get_bounds(s):

seq='GSHMASIRIHFDMAGPSVPREARALHLAVADWLTSAREGEAAQADRWQAFGLEDNAAAFSLVLDRLRETENF
KKDAGFKAQISSWLTQLAEDAALRAKTFAMATEATSTCEDRVTHALHQMNNVQLVHNAEKGEYDNNLQGLVSTGREM
FRLATLEQIAREKAGTLALVDDVEVYLAFQNKLKESLELTSVTSEMRFFDVSGVTVSDLQAAELQVKTAENSGFSKW
ILQWGPLHSVLERKVPERFNALREKQISDYEDTYRKLYDEVLKSSGLVDDTDAERTIGVSAMDSAKKEFLDGLRALV
DEVLGSYLTARWRLN'
    l=seq.find(s)+383
    h=l+len(s)-1
    return (np.array([l,h]))
###

### Calculate protection factor
def calc_pf(t, d1_in, d2_in, seq):

    d1 = np.copy(d1_in)
    d2 = np.copy(d2_in)
    error_return_default = [[0,0],[0,0],[0,0],[0,0],-1.0]

    # Calculate range of uptake values shared between d1 and d2
    r = min(max(d1),max(d2))-max(min(d1),min(d2))
    if (r < 0):
        print("uptake range error with {:}".format(seq))
        return error_return_default

    # If a sampled HDX point has lower fractional deuteration than that
preceding point, raise the deuteration point to the value
    #   of the preceding point. This ensures proper sampling points for
interpolation. This does not change the raw data, it is only
    #  for picking sampling points (see examples)
    for i in range(0,len(d1)-1):
        if (d1[i+1] < d1[i]):
            d1[i+1] = d1[i]
        if (d2[i+1] < d2[i]):
            d2[i+1] = d2[i]
```

```
    # Pick sampling times and perform log-linear interpolation to obtain HDX
values, Algorithm from Walters et al. 2017
    d_prime = np.linspace(max(min(d1),min(d2)) + 0.001, min(max(d1),max(d2)) -
0.001,10*r)
    if (len(d_prime) < 10):
      print("number of sampled points error with {:}".format(seq))
      return error_return_default

    # Log-linear interpolation from scipy
    f1 = interpolate.interp1d(d1, np.log10(time))
    f2 = interpolate.interp1d(d2, np.log10(time))
    try:
      t1_prime = 10**f1(d_prime)
      t2_prime = 10**f2(d_prime)
    except:
      print("interpolation error with {:}".format(seq))
      return error_return_default

    # Calculate the protection factor
    quotient = t2_prime / t1_prime
    pf = stats.gmean(quotient)
    if (np.isnan(pf)):
      print("pf calculation returns NAN error with {:}".format(seq))
      pf = -1.0

    return [d_prime, t1_prime, t2_prime, quotient, pf]
###

### Get HDX in ActiveBook format from CSV files ###
def get_data():
      # Read in a Pandas dataframe for each construct CSV saved from Activebook
    E3CK = pd.read_csv('./Activebooks/HDX_ActiveBook_E3CK_V2.csv')
    E3CKUb = pd.read_csv('./Activebooks/HDX_ActiveBook_E3CKUb_V2.csv')
    LRRE3CK = pd.read_csv('./Activebooks/HDX_ActiveBook_LRRE3CK_V2.csv')
    LRRE3CKUb = pd.read_csv('./Activebooks/HDX_ActiveBook_LRRE3CKUb_V2.csv')
    LRRE3CK_PKN1                                                              =
pd.read_csv('./Activebooks/HDX_ActiveBook_LRRE3CK_PKN1_V2.csv')
    LRRE3CKUb_PKN1                                                            =
pd.read_csv('./Activebooks/HDX_ActiveBook_LRRE3CKUb_PKN1_V2.csv')
    # Make lists of construct names and Pandas dataframe names
    names_list = ["E3CK", "E3CKUb", "LRRE3CK", "LRRE3CKUb", "LRRE3CK_PKN1",
"LRRE3CKUb_PKN1"]
    filename_list   =   [E3CK,   E3CKUb,   LRRE3CK,   LRRE3CKUb,   LRRE3CK_PKN1,
LRRE3CKUb_PKN1]
    # Make a dictionary for each construct
    d_E3CK={}
    d_E3CKUb={}
    d_LRRE3CK={}
    d_LRRE3CKUb={}
    d_LRRE3CK_PKN1={}
    d_LRRE3CKUb_PKN1={}
    # Make a list of the construct dictionaries
    file_dict_list = [d_E3CK, d_E3CKUb, d_LRRE3CK, d_LRRE3CKUb, d_LRRE3CK_PKN1,
d_LRRE3CKUb_PKN1]
    # Loop through each construct
    for file in range(len(filename_list)):
        curr = filename_list[file]
```

```
        # Loop through each peptide within the construct
        for i in range(0, len(curr)):
            #Peptide name
            peptide = curr.iloc[i,6]
            # Mean of each sampled timepoint
            values = [(curr.iloc[i,14]+curr.iloc[i,15])/2.0,
                      (curr.iloc[i,16]+curr.iloc[i,17])/2.0,
                      (curr.iloc[i,18]+curr.iloc[i,19])/2.0,
                      (curr.iloc[i,20]+curr.iloc[i,21])/2.0]
            # Error of each sampled timepoint
            errors = [curr.iloc[i,14]-values[0],
                      curr.iloc[i,16]-values[1],
                      curr.iloc[i,18]-values[2],
                      curr.iloc[i,20]-values[3]]
            # For the current construct and peptide, add that peptide's HDX
data to the dictionary
            #  for the construct in the list of constructs
            file_dict_list[file][peptide]=[values,    values_corr,    errors,
errors_corr]

    # Get the list of total peptides, 'keys'
    keys = []
    for entry in file_dict_list[file]:
        keys.append(entry)

    # Make list of peptides containing HDX data
    peptides = []
    for i in range(0, len(E3CK)):
        data = []
        # Make a list of HDX data for each construct
        for file in range(len(filename_list)):
            peptide = file_dict_list[file][keys[i]]
            data.append(peptide)
        peptides.append(data)

    return keys, names_list, peptides
###

### Calculate Protection Factors ###
def SspH1_PF_Analysis():

      # Get data from helper function
    keys, constructs, peptides = get_data()

    # Arrays of protection factors for given comparisons
    #  There are 15 possible unique pairwise Protection Factor comparisons for
the six constructs of SspH1
    #  Starting off with 5 interesting comparisons: Ub conjugation (3), addition
of LRR, addition of PKN1 to LRR
    PF_E3CK_E3CKUb = []
    PF_LRRE3CK_LRRE3CKUb = []
    PF_LRRE3CK_PKN1_LRRE3CKUb_PKN1 = []
    PF_E3CK_LRRE3CK = []
    PF_E3CKUb_LRRE3CKUb = []
    PF_LRRE3CK_LRRE3CK_PKN1 = []
    PF_LRRE3CKUb_LRRE3CKUb_PKN1 = []
```

```
    # Arrays of all of the results of data analysis for the protection factors
    all_E3CK_E3CKUb = []
    all_LRRE3CK_LRRE3CKUb = []
    all_LRRE3CK_PKN1_LRRE3CKUb_PKN1 = []
    all_E3CK_LRRE3CK = []
    all_E3CKUb_LRRE3CKUb = []
    all_LRRE3CK_LRRE3CK_PKN1 = []
    all_LRRE3CKUb_LRRE3CKUb_PKN1 = []

    # Loop through each peptide and get data
    for key in range(0,len(keys)):
      # Peptide sequence
        pep_name = keys[key]

        E3CK_name=constructs[0]
        E3CK_val=peptides[key][0][0]
        E3CK_err=peptides[key][0][2]
        E3CKUb_name=constructs[1]
        E3CKUb_val=peptides[key][1][0]
        E3CKUb_err=peptides[key][1][2]
        LRRE3CK_name=constructs[2]
        LRRE3CK_val=peptides[key][2][0]
        LRRE3CK_err=peptides[key][2][2]
        LRRE3CKUb_name=constructs[3]
        LRRE3CKUb_val=peptides[key][3][0]
        LRRE3CKUb_err=peptides[key][3][2]
        LRRE3CK_PKN1_name=constructs[4]
        LRRE3CK_PKN1_val=peptides[key][4][0]
        LRRE3CK_PKN1_err=peptides[key][4][2]
        LRRE3CKUb_PKN1_name=constructs[5]
        LRRE3CKUb_PKN1_val=peptides[key][5][0]
        LRRE3CKUb_PKN1_err=peptides[key][5][2]

        # Calculate protection factors for E3CK vs E3CKUb
        d_prime, t1_prime, t2_prime, quotient, pf = calc_pf(time, E3CK_val,
E3CKUb_val, pep_name)
        PF_E3CK_E3CKUb.append(pf)
        all_E3CK_E3CKUb.append([d_prime, t1_prime, t2_prime, quotient, pf])

        # Calculate protection factors for LRRE3CK vs LRRE3CKUb
        d_prime, t1_prime, t2_prime, quotient, pf = calc_pf(time, LRRE3CK_val,
LRRE3CKUb_val, pep_name)
        PF_LRRE3CK_LRRE3CKUb.append(pf)
        all_LRRE3CK_LRRE3CKUb.append([d_prime, t1_prime, t2_prime, quotient,
pf])

        # Calculate protection factors for LRRE3CK_PKN1 vs LRRE3CKUb_PKN1
        d_prime, t1_prime, t2_prime, quotient, pf = calc_pf(time,
LRRE3CK_PKN1_val, LRRE3CKUb_PKN1_val, pep_name)
        PF_LRRE3CK_PKN1_LRRE3CKUb_PKN1.append(pf)
        all_LRRE3CK_PKN1_LRRE3CKUb_PKN1.append([d_prime, t1_prime, t2_prime,
quotient, pf])

        # Calculate protection factors for E3CK vs LRRE3CK
        d_prime, t1_prime, t2_prime, quotient, pf = calc_pf(time, E3CK_val,
LRRE3CK_val, pep_name)
        PF_E3CK_LRRE3CK.append(pf)
```

```
        all_E3CK_LRRE3CK.append([d_prime, t1_prime, t2_prime, quotient, pf])

        # Calculate protection factors for E3CKUb vs LRRE3CKUb
        d_prime, t1_prime, t2_prime, quotient, pf = calc_pf(time, E3CKUb_val,
LRRE3CKUb_val, pep_name)
        PF_E3CKUb_LRRE3CKUb.append(pf)
        all_E3CKUb_LRRE3CKUb.append([d_prime,  t1_prime,  t2_prime,  quotient,
pf])

        # Calculate protection factors for LRRE3CK vs LRRE3CK_PKN1
        d_prime, t1_prime, t2_prime, quotient, pf = calc_pf(time, LRRE3CK_val,
LRRE3CK_PKN1_val, pep_name)
        PF_LRRE3CK_LRRE3CK_PKN1.append(pf)
        all_LRRE3CK_LRRE3CK_PKN1.append([d_prime,     t1_prime,     t2_prime,
quotient, pf])

        # Calculate protection factors for LRRE3CKUb vs LRRE3CKUb_PKN1
        d_prime,   t1_prime,   t2_prime,   quotient,   pf   =   calc_pf(time,
LRRE3CKUb_val, LRRE3CKUb_PKN1_val, pep_name)
        PF_LRRE3CKUb_LRRE3CKUb_PKN1.append(pf)
        all_LRRE3CKUb_LRRE3CKUb_PKN1.append([d_prime,   t1_prime,   t2_prime,
quotient, pf])
##########################################################################
####################
```

Appendix II: Crystal Structure of ΔN-Ube2E3

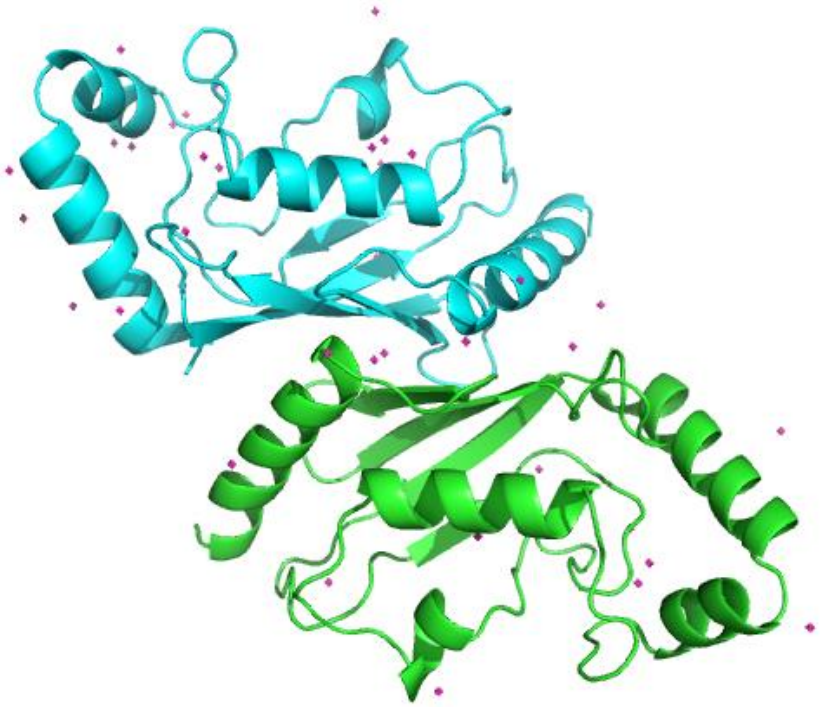

Appendix II Fig 1. Preliminary Crystal Structure of ΔN-Ube2E3 after initial refinement and model building. 10mg/mL ΔN-Ube2E3 was crystallized via sitting-drop vapor diffusion in in 0.8 lithium chloride, 0.1M Tris pH 8.5, and 32%(w/v) PEG 4000.

Data Collection	
Wavelength (Å)	1.54Å
Space group	$P12_11$
Unit cell (Å)	a = 47.56, b = 62.82, c = 51.57 α = 90°, β = 95.46°, γ = 90°
Resolution (Å)	23.83 - 2.15 (2.23 - 2.15)
Unique reflections	16083 (1570)
Completeness (%)	97
Wilson b-factor	17.91
Refinement	
Reflections used in refinement	16083 (1570)
Reflecitons used for R-free	779 (76)
R_{work}	0.1529 (0.1534)
R_{free}	0.2031 (0.2230)
Number of non-hydrogen atoms	2666
Protein residues	296
RMS (bonds)	0.012
RMS (angles)	1.15
Ramachandran favored (%)	98.3
Ramachandran allowed (%)	1.7
Ramachandran outliers (%)	0
Rotamer outliers (%)	1.9
Clashscore	3.88
Average B-factor	21.8

Appendix II Table 1. Preliminary crystallographic data and refinement statistics.